Synthesis and Performance Evaluation of a Novel Natural Surfactant–Polymer Assembly for Enhanced Oil Recovery

Thesis submitted in partial fulfillment of the requirements for the degree of

Doctor of Philosophy

by

Jinesh Subhash Machale

Department of Chemical Engineering
Indian Institute of Technology Guwahati

Western Australia School of Mines: Minerals, Energy, and Chemical Engineering
Curtin University

March 2022

Synthesis and Performance Evaluation of a Novel Natural Surfactant–Polymer Assembly for Enhanced Oil Recovery

Thesis submitted in partial fulfillment of the requirements for the degree of

Doctor of Philosophy

by

Jinesh Subhash Machale

Department of Chemical Engineering
Indian Institute of Technology Guwahati

Western Australia School of Mines: Minerals, Energy, and Chemical Engineering
Curtin University

March 2022

Dedicated to my

Family and Friends

THESIS CERTIFICATE

It is certified that the work described in this thesis titled **"Synthesis and Performance Evaluation of a Novel Natural Surfactant–Polymer Assembly for Enhanced Oil Recovery"** by Mr. Jinesh Subhash Machale for the award of the degree of Doctor of Philosophy is an authentic record of the results obtained from research work carried out under our supervision at the Department of Chemical Engineering, Indian Institute of Technology Guwahati (India) and Western Australia School of Mines: Minerals, Energy, and Chemical Engineering, Curtin University (Australia). To the best of our knowledge, this work is not submitted elsewhere for the award of any other degree or diploma.

Prof. Pallab Ghosh
Professor
Department of Chemical Engineering
IIT Guwahati, Guwahati–781039, Assam, India

Prof. Subrata Kumar Majumder
Professor
Department of Chemical Engineering
IIT Guwahati, Guwahati–781039, Assam, India

Dr. Tushar Kanti Sen
Adjunct Associate Professor
Chemical Engineering, WASM: Minerals, Energy and Chemical Engineering, Curtin University, Perth, WA–6845, Australia

Dr. Ali Saeedi
Associate Professor
Petroleum Engineering, WASM: Minerals, Energy and Chemical Engineering, Curtin University, Perth, WA–6845, Australia

Acknowledgments

I would like to express my sincere gratitude to several people who helped me to finish my Ph.D. by contributing in some manner to work outlined in my thesis.

To begin, I would like to express my heartfelt gratitude to my supervisors, Prof. Pallab Ghosh and Prof. Subrata Kumar Majumder, Department of Chemical Engineering, Indian Institute of Technology (IIT) Guwahati, as well as Dr. Tushar Kanti Sen and Dr. Ali Saeedi, Western Australia School of Mines (WASM): Mineral, Energy and Chemical Engineering, Curtin University for their constant supervision, support, and encouragement during my Ph.D. tenure at IIT Guwahati and Curtin University. Their unwavering support has pushed me to implement my ideas, resulting in the successful completion of my project. I would also like to thank them for creating a really healthy and welcoming work environment. They were always available for a discussion at any moment, which is essential for fruitful work. I am grateful for the opportunity to work under their guidance and will be eternally thankful to them.

I am also thankful to my honorable doctoral committee members, Prof. Anugrah Singh and Dr. Pankaj Tiwari, Department of Chemical Engineering, and Dr. Dipankar Narayan Basu, Department of Mechanical Engineering, IIT Guwahati, for providing valuable suggestions, relevant insights, and thought-provoking ideas during the seminars that helped me to significantly improve my research work. I would like to take this opportunity to thank my master's advisor Mr. Suresh Kumar Yatirajula (Assistant Professor, Department of Chemical Engineering, IIT Dhanbad), for his research-oriented teaching during my master's; his teaching helped me to extend my research interest.

I am also grateful to Prof. Anugrah Singh, Head of the Department of Chemical Engineering, IIT Guwahati, Prof. Bishnupada Mandal, former Head of the Department of Chemical Engineering, IIT Guwahati, and Prof. Hongwei Wu, Head of the Department of

Chemical Engineering, Curtin University, for allowing me to pursue my Ph.D. in these esteemed departments.

The acknowledgment would not be complete without appreciating the support received from Mr. Harsaraj Biswanath, Mr. Pankaj Kumar, and all the technical officers of the Department of Chemical Engineering, IIT Guwahati. I sincerely express gratitude to Dr. Roshanak Doroushi (Technical officer), Dr. Beng Chua (Manager of the Life Sciences Facility), and Mr. Mohsen Ghasemi (Technical officer) for their generous help and unlimited support during my stay at Curtin University. I also thank the Central Instruments Facility (CIF), IIT Guwahati, and John de Laeter Research Centre, Curtin University, for providing me the facility of high-end and sophisticated instruments necessary for this research work.

I would like to thank my lab mates Awadh, Dr. Shailesh, Mukesh, Dr. Badri, Herald, Dr. Eugene, Dr. Duraid Al-Bayati, and Mohamed for their assistance on various occasions. I am eternally grateful to my beloved friends Kajal, Krushna, Sushma, Piyal, Nilanjana, Sutapa, Siddharth. Surabhi, Prateek, Sakshi, Bharat, Tanmay, Shankar, Anant, Barsha, Rohit, and Sukrit for their unwavering and unending support. They were always there for me during my highs and lows, making my time at IIT Guwahati and Curtin University more enjoyable, memorable, and homely. I extend my distinct gratitude to Kajal and Krushna for their immense support, encouragement, affection, and care.

I am forever grateful to my parents, Mr. Subhash Machale and Mrs. Savita Machale; my sister, Mrs. Ashwini Awathankar; my brother-in-law, Mr. Pawan Awathankar; and my nephews, Aarav and (Late) Devansh for their love, prayers, uncountable sacrifices, and patience. They have always pushed me to put in extra effort and sincerity in all I do.

Last but not least, I want to express my gratitude to everyone who has been directly or indirectly involved in my work over the years.

Jinesh Machale

Abstract

A significant amount of oil (i.e., 60–70%) remains trapped in the reservoirs after the conventional primary and secondary methods of oil recovery. Enhanced oil recovery (EOR) is, therefore, necessary to recover the major fraction of unrecovered trapped oil from the reservoir to meet the present-day energy demands. The chemical method of EOR involves the injection of alkali, surfactant, polymer, and a combination of alkali–surfactants–polymer solution in the reservoir with the objective of achieving a reduction in interfacial tension and matching the mobility between oil and water for more recovery of oil. The success of this method depends on the effective synergy between the chemical additives. Every oil field has different conditions, which imposes new challenges towards an alternative but more effective EOR techniques.

Polymers are commonly used as mobility control agents for a better recovery of oil. Mostly, synthetic polymers (e.g., polyacrylamide and partially hydrolyzed polyacrylamide) and polysaccharides (e.g., xanthan gum, guar gum, diutan gum, gellan gum, welan gum, and schizophyllan) have been studied for polymer flooding processes. Most of the synthetic polymers are mechanically and thermally stable. However, these polymers are non-degradable and sensitive to salinity. Polysaccharides, on the other hand, are biocompatible, biodegradable, and stable at the high temperatures.

Surfactant plays a major role in EOR. It helps to achieve ultralow interfacial tension, which significantly increases the mobility of the trapped oil and also helps to improve wettability between oil and rock. Anionic surfactants such as the alkyl aryl sulfonates, sodium dodecyl sulfate, sodium octyl sulfate, alpha-olefin sulfonate, and N-ethoxy sulfonate are extensively being used in EOR due to their less adsorption on sandstones and clays. However, most of these surfactants are toxic, non-biodegradable, and can adsorb on the surface of the porous rocks.

This work is focused on the development of an alternative cost-effective and sustainable natural surfactant derived from the weed *Eichhornia crassipes*, and study its beneficial effects on EOR. The surfactant has been characterized by the FTIR, GC–MS, ^{1}H NMR, FESEM, and FETEM analyses. The surface and interfacial tension have been measured. The influence of the synthesized surfactant on the rheological properties of xanthan gum (a polysaccharide) has been studied and compared with that of a commercially used surfactant (i.e., sodium dodecyl sulfate). The experimental data acquired from the rheological analysis of the surfactant–polymer solutions under varying shear rate were fitted by several non-Newtonian fluid models. An effective reduction in the interfacial properties, improvement in the rheological properties, and stability against heat and salinity suggest its potential application in EOR.

Loss of surfactant by adsorption on porous media is one of the most critical concerns of the surfactant flooding method of EOR. Hence, the present study is also dedicated to analyze the adsorption of the synthesized surfactant on sandstone and sand surfaces under reservoir-like conditions. The mechanism, equilibrium, and kinetics of adsorption of the synthesized natural surfactant on sandstone and sand surfaces have been investigated through batch experiments at different concentrations (i.e., 1000–5000 mg dm^{-3}), temperatures (i.e., 298–333 K), and a fixed salinity. The mineralogy and morphology of the adsorbent samples were examined by the XRD and FESEM analyses. The mechanism of surfactant adsorption and maximum adsorption were determined by various isotherms and kinetic models. The standard Gibbs free energy changes (i.e., ΔG°) for adsorption on sandstone and sand were found to be –21.48 and –20.80 kJ mol^{-1}, respectively.

The interfacial phenomena are associated with the adsorption of the surfactant at the oil–rock and oil–water interfaces. Therefore, it is essential to understand the mechanism of adsorption of surfactant at the oil–water interface for better implementation of surfactant flooding. The adsorption of the synthesized surfactant on the oil–water interface was

investigated using small-angle X-ray scattering, interfacial rheology, zeta potential, and phase behavior analyses. A noteworthy improvement in the stability of the oil-in-water emulsion was observed in the presence of the surfactant. An effective 27% increase in the zeta potential and ~26.9 times increase in the film elasticity signify the substantial adsorption of the surfactant at the oil–water interface.

Moreover, the feasibility of the use of the synthesized surfactant for EOR was studied based on the wettability alteration and IFT measurements under reservoir-like conditions (i.e., high temperature and pressure). Further, core flooding experiments were carried out by injecting the surfactant–polymer slugs of different concentration into the sandstone core sample under reservoir-like conditions. An effective reduction of ~37–41% in the IFT and ~43% in wettability was observed with increasing surfactant concentration. Based on the core flooding experiments, 13.3–22.4% additional oil recovery was achieved. Based on the aforesaid studies, the performance of the synthesized surfactant is promising for EOR applications.

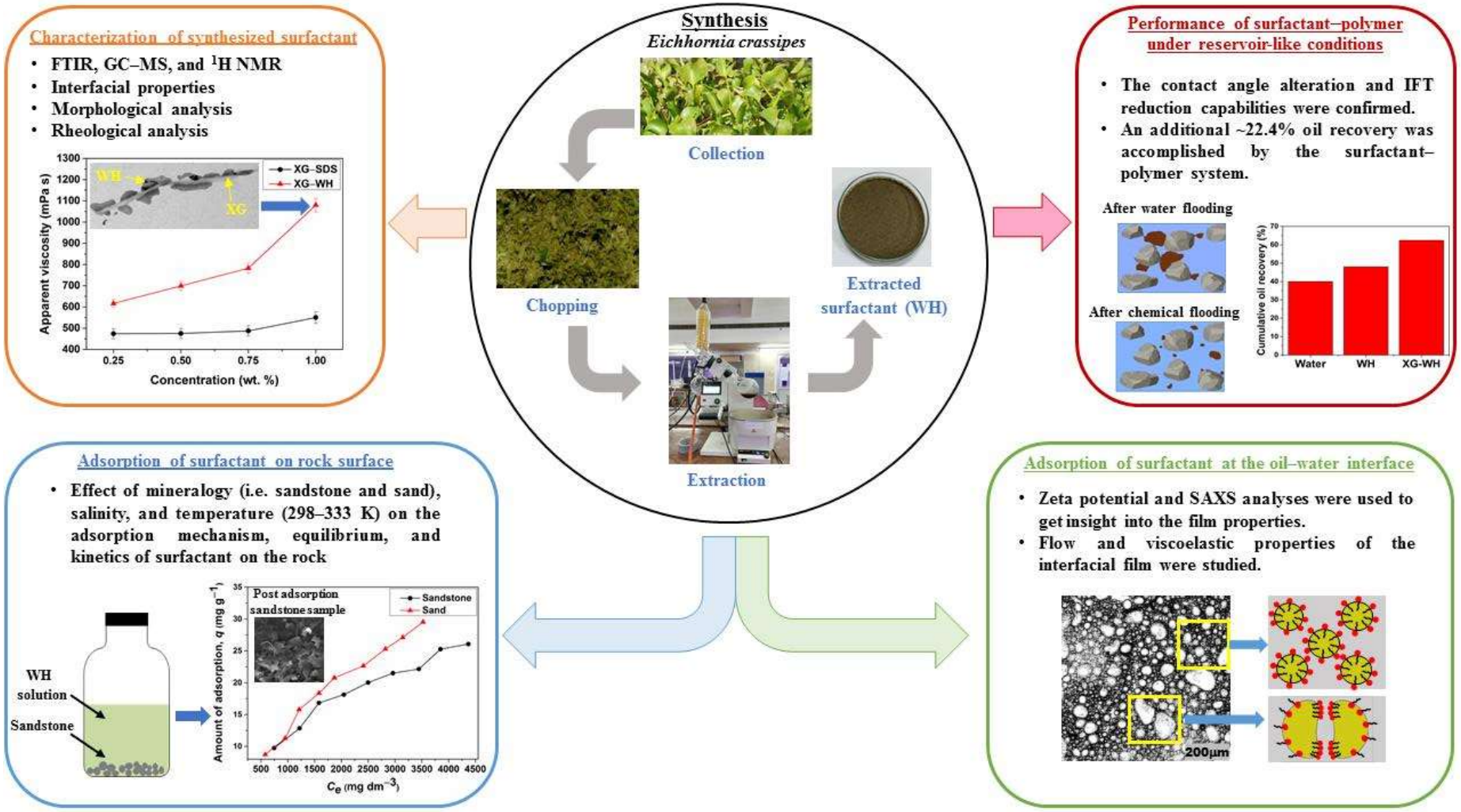

Figure. Graphical abstract of the Ph.D. work.

Contents

List of tables

List of figures

Chapter 1

Introduction

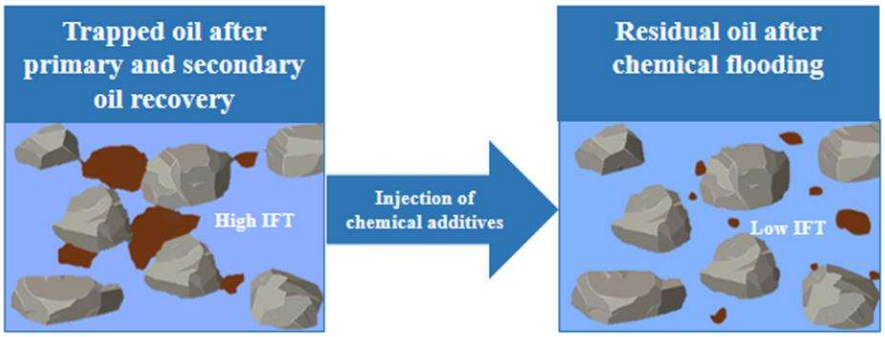

Introduction

This chapter presents the general overview of the oil recovery techniques, emphasizing the mechanism of the chemical method of oil recovery. The research problem has been identified and the aims of this thesis have been given along with its scope and organization of thesis.

1.1 General overview

Many major oil-producing reservoirs around the world have already reached or are close to maturity. In the past decades, the rate of discovery rate of new oil reserves has also been on the decline. On the other hand, the world is expected to remain heavily dependent on fossil fuels for the next several decades to meet its growing energy demand, since the renewable energy sector would be incapable of generating energy to the necessary levels. The currently-practiced conventional primary and secondary oil recovery methods are capable of delivering only around 20–40% of the *in situ* oil to the surface [1]. The rest of the oil remains trapped in the reservoir. Enhanced oil recovery (EOR) is a tertiary oil recovery technique, which can mobilize the trapped crude oil in the porous rocks [2,3]. EOR can be classified into three major groups, i.e., thermal, gas injection, and chemical methods.

At the end of water-flooding (i.e., a secondary oil recovery method), oil is trapped in between the rocks due to the electrostatic charge around them, high capillary forces, and high interfacial tension (IFT) between water and oil [4]. Oil production can be increased by increasing the overall displacement efficiency, which is a function of time, liquid viscosity, permeability, IFT, wettability, and capillary pressure. It is directly related to the mobility ratio of oil in the trapped zone of a reservoir. The principle of the chemical method of EOR involves injecting external chemical additives (mainly alkalis, surfactants, and polymers). This decreases the IFT between oil and water, and increases the viscosity of the displacing fluid (i.e., water), which results in the reduction of the water/oil mobility ratio [5–7]. The study of the

chemical method of EOR is an emerging area of research involving a consistent development of chemical additives for efficient oil recovery. Over the last decade, researchers have published more than 3000 articles in journals, books, and conference proceedings. Figure 1.1 demonstrates the year-wise publication on the chemical method of EOR.

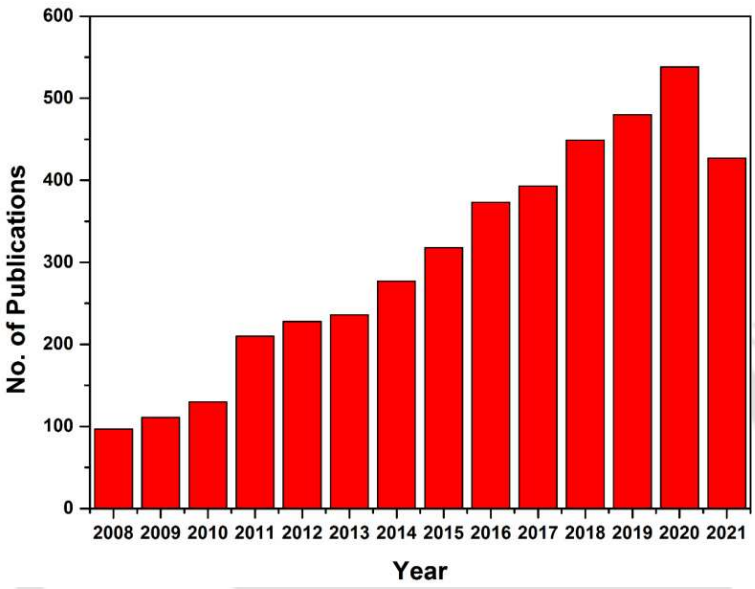

Figure 1.1. Year-wise publications on the chemical method of EOR. Source: Scopus, keyword: chemical EOR.

The success of this method depends on the effective synergy between the chemical additives. Alkali reacts with the naturally-available acids in crude oil, resulting in the formation of soap *in situ*, which lowers the IFT between oil and water to the desirable extent [6]. Surfactant and polymer are injected into the reservoir, which substantially reduce the IFT and match the mobility between the oil and water for a better oil recovery [6–8]. The mechanism of the alkali–surfactants–polymer (ASP) method is shown in Figure 1.2. The surfactant helps to achieve an ultralow IFT, which increases the mobility of the residual oil and also prevents the mobilized oil from being trapped by the capillary forces. The application of commercially-used surfactants offers stability at high temperature, the capability to customize as per the reservoir conditions, and has favorable interactions with the polymers [9]. However, most of these surfactants are costly, dangerous to the environment, and can adsorb on the surface of the

porous rocks. Thus, many researchers have been looking for the natural surfactants and exploring their potency in EOR [10–15]. The importance of natural surfactant is increasing as they are less toxic, biodegradable, have higher foaming capability, and stable at high temperatures, pH, and salinity.

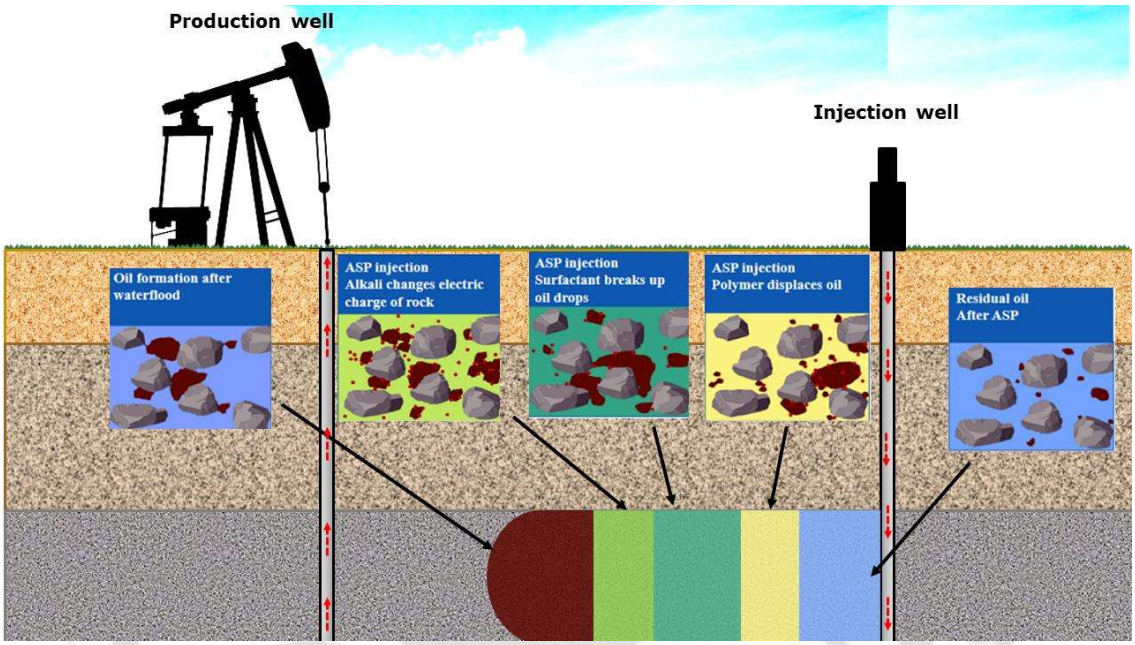

Figure 1.2. Mechanism of the ASP method of EOR.

Water-soluble polymers, on the other hand, increase the viscosity of the aqueous phase as well as improve the mobility ratio [6], i.e., the ratio of the mobility of the displacing fluid (i.e., water) to the mobility of the displaced fluid (i.e., crude oil). For the favorable mobility of trapped oil, this ratio should be less than or equal to unity. The injected polymer helps to achieve a favorable mobility ratio, which eventually does not bypass the displaced fluid in the reservoir [16]. The polymer also helps to reduce the relative permeability of water in the reservoir and hence to displace the trapped oil from the same. However, these polymers have serious mechanical degradation issues. Therefore, it is necessary to have a very good understanding of the rheological behavior of the polymer at the reservoir conditions for

material selection and the effective design of the flooding experiments. It also provides insight on the stability of the polymer and its retention in the porous medium.

This work aims to synthesize a cost-effective and sustainable novel natural surfactant from *Eichhornia crassipes* and study its beneficial effects on EOR. It is one of the very fast-growing ubiquitous aqueous plants across the globe, which creates numerous critical problems such as damage to the eco-system, troubles in irrigation, increase in the mosquito population, inconvenience in water transport, and health hazards. *Eichhornia crassipes* is a rich source of various organic compounds, which contain nearly 20% cellulose, 48% hemicellulose, and 3.5% lignin. Considering such high cellulose and hemicellulose contents, the *Eichhornia crassipes* could be used as a primary raw material for the production of numerous value-added products [17]. Based on the several screening criteria for the selection of chemical additives [8], we have analyzed the performance of the synthesized surfactant by several interfacial, thermal, adsorption, and rheological analyses.

1.2 Evaluation of chemical additives for EOR

1.2.1 Interfacial tension

The performance of a surfactant used in EOR is directly dependent on its ability to reduce IFT between crude oil and water. This interfacial phenomenon is associated with the adsorption of the surfactant at the oil–water interface. Therefore, it is essential to understand the mechanism of adsorption of surfactant at the oil–water interface for better implementation of surfactant flooding. Surfactant adsorption at the oil–water interface is primarily governed by the concentration of surfactant in the aqueous phase [18]. The IFT reduces with increasing surfactant concentration and reaches a minimum at the critical micelle concentration (CMC). Generally, below the CMC, the IFT reduces rapidly with the surfactant concentration due to the presence of vacant sites at the interface (see Figure 1.3). At the CMC, a monolayer of the surfactant molecules is formed on the interface, and hence the IFT becomes constant. When

the concentration of surfactant is increased further (i.e., above CMC) (see Figure 1.3), the change in IFT is rather small [19]. The decrease in the IFT facilitates the movement of entrapped oil through the reservoir [20].

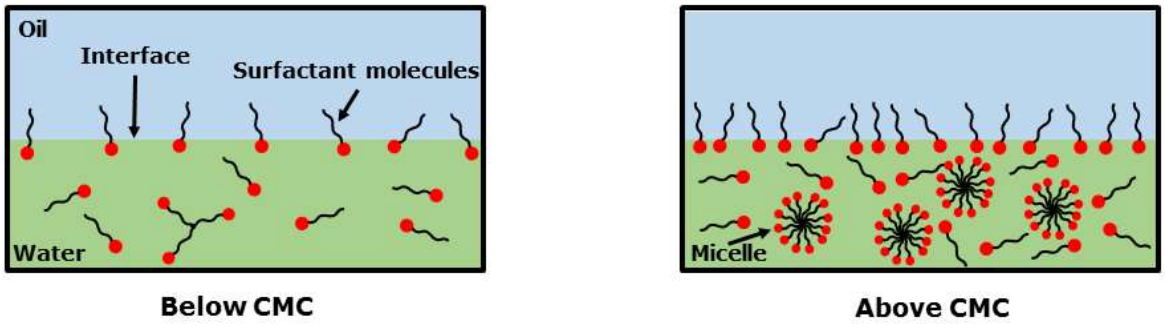

Figure 1.3. Mechanism of the adsorption of the surfactant molecules at the oil–water interface.

1.2.2 Wettability alteration

The wetting nature of a reservoir is often intermediate to oil-wet, and it depends on the crude oil composition, rock mineralogy, and reservoir conditions. The adherence of polar components of crude oil that had migrated into the reservoir can be related to the mechanism of wettability alteration of originally water-wet to oil-wet reservoir. Following crude oil migration into the reservoir pores, a layer of brine forms between the crude oil and the rock surface, preventing the crude oil from coming into contact with the rock. The existence of van der Waals forces, charge transfer, and hydrogen bonding between the rock surface and crude oil causes the brine layer to rupture. As a result, crude oil components adsorb on the rock surface, causing the reservoir rock to become "oil-wet" [21]. The amount of oil adsorbed on the rock surface varies depending on the reservoir type (i.e., sandstone and carbonate). The basic and acidic compounds of crude oil have a strong tendency to adsorb onto the sandstone (negatively-charged rock) and carbonate (positively-charged rock) surfaces, respectively [22].

As the surfactant is introduced into the reservoir, it has either hydrophobic or hydrophilic interactions with the crude oil's adsorbed components. In this manner, the crude oil

components associate with the surfactant and facilitate the movement of the crude oil through the reservoir. Furthermore, as flooding progresses, surfactant molecules cover the rock surface, which inhibit the interaction between the rock surface and crude oil. This leads to the change in the wettability of rock from oil-wet to water-wet [21]. The mechanism of wettability alteration is shown in Figure 1.4. However, it is important to note that the excess adsorption of the surfactant on the rock surface can lead to the loss of surfactant, which is a prime shortcoming of surfactant flooding.

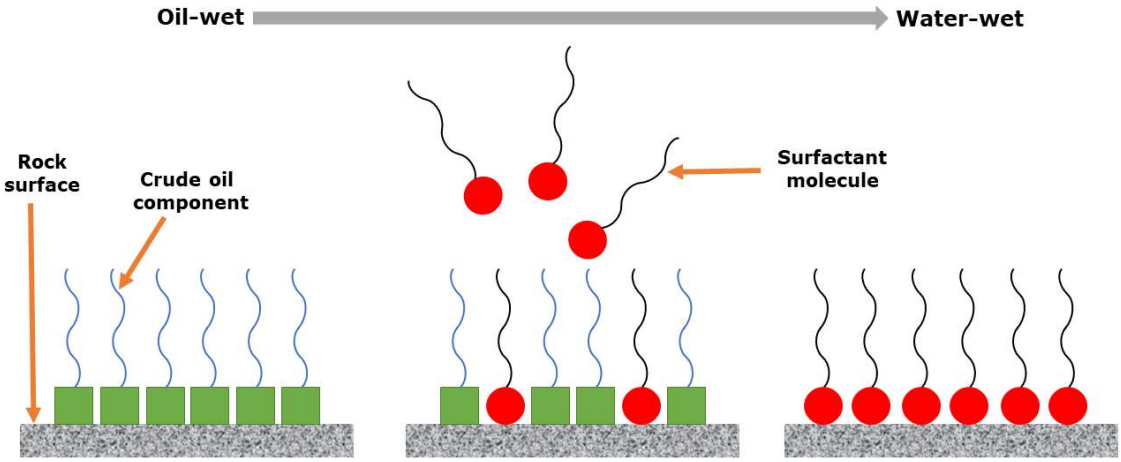

Figure 1.4. Mechanism of the wettability alteration.

1.2.3 Emulsion stability

The stability of emulsion plays a vital role in EOR. It can be correlated with the coalescence and aggregation rates of the droplets. Emulsion stability has primarily been studied at three scales, *viz*. macroscopic, mesoscopic, and microscopic [23] (see Figure 1.5). A knowledge of the macroscopic scale is required to understand the efficacy of chemical additives and their interaction with the crude oil [24]. Mainly, it includes the phase behavior studies, which determine the phase volume of the water/oil mixture in the presence of chemical additives. Coalescence, flocculation, and sedimentation of a dispersed phase can be reflected better by the mesoscopic scale. Further, the microscopic scale is utilized to investigate the development of a film at the oil–water interface [25].

The strength of the interfacial film is the most critical factor influencing the emulsion stability. In case the strength of the interfacial film is less, droplets would be prone to rapid coalescence, and hence the emulsion stability would decrease. On the contrary, emulsion stability increases as the strength of the interfacial film increases [26]. This is directly proportional to the selection of the emulsifiers (mainly surfactant, nanoparticles, and polymers), their concentration and interaction, emulsion droplet size, and crude oil composition [27–30]. At low emulsifier concentration, the strength of the interfacial film is weak due to the less adsorption of the emulsifier at the oil–water interface, which eventually forms an unstable emulsion. However, as the emulsifier concentration increases, the extent of adsorption of the emulsifier at the oil–water interface increases, and therefore a stable emulsion is formed.

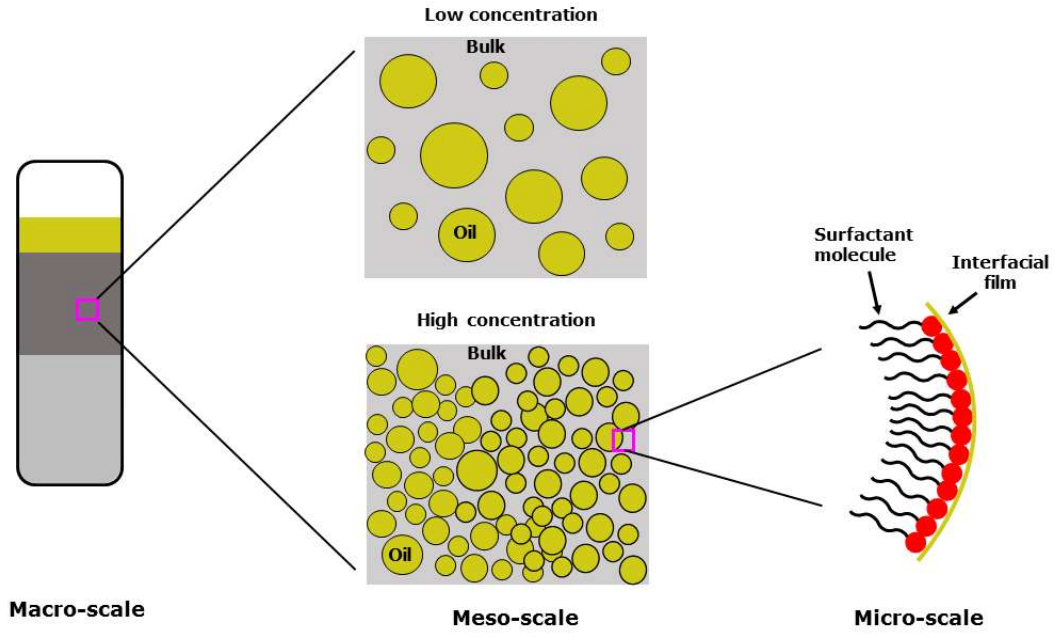

Figure 1.5. Schematic on the multiscale study approach for emulsion stability.

1.2.4 Surfactant adsorption

The loss of surfactant by adsorption on the pore surfaces of the porous media is a significant shortcoming of surfactant flooding. Due to this loss, the surfactant requirement increases, resulting in a higher operating cost and reduction in the surfactant's effectiveness. Thus, it is essential to analyze the mechanism of adsorption of a surfactant on a porous rock under

reservoir-like conditions [3,9]. Numerous mechanisms such as adsorption by the polarization of dispersion forces and π-electrons, hydrophobic bonding, and ion exchange are related to the adsorption of surfactant molecules on the surface of porous rocks [31,32]. The adsorption depends on the mineralogy, type of surfactant, and its concentration, temperature, and salinity [33]. Mostly anionic surfactants are used for the EOR applications in sandstone reservoirs due to their less adsorption on the quartz and clays, which are the common constituents of the sandstone formations [9]. Cationic surfactants, on the other hand, due to their high adsorption on the negatively-charged surfaces of clays and sand, are not useful for oil recovery in sandstones [34]. However, cationic surfactants can improve the impulsive imbibition rate of water into the preferentially oil-wet carbonate rocks. Nonionic surfactants have no charge on their head groups in aqueous solution and they are mostly utilized as a cosurfactant to reduce the adsorption of the anionic/cationic surfactant [3].

Given the *in situ* reservoir conditions, evaluation of the influence of salinity and temperature on the adsorption is very important for the EOR applications. Salts containing divalent ions (e.g., $CaCl_2$ and $MgCl_2$) have an enormous impact on adsorption in comparison with the salts containing monovalent ions (e.g., NaCl and KCl) [11,21]. Some salts can precipitate the surfactant, which is highly undesirable. Therefore, it is challenging to design effective surfactant flooding, which can withstand the saline environment in the reservoir [35]. A high salt concentration increases the adsorption of the surfactant by reducing the electrostatic repulsive force between the head-groups. Temperature, on the other hand, affects the adsorption capacity of the surfactant, based on the nature of the process (i.e., exothermic or endothermic). In most cases, adsorption is an exothermic process [33]. As a result, the increase in temperature decreases the adsorption of surfactant due to the increase in the kinetic energy of the species [36].

1.2.5 Rheological properties

Knowledge of the rheology of a polymer in association with other additives used in EOR at reservoir conditions is essential for the selection of chemicals as well as for the efficient design of chemical flooding. It affects the mobility ratio of oil in the reservoir [37], and therefore it is significant to have knowledge of flow behavior at different reservoir conditions. The flow behavior (primarily the viscosity) of polymer solution can be determined by rheometer at steady shear. Further, it also gives insight into the stability of polymer, as well as the retention of polymer in the porous medium. The influences of the rheological behavior of various chemical additives at different reservoir conditions (salinity, temperature, concentration, etc.) on the oil mobility ratio, stability, and interactive forces at the solid–liquid interface are also critically important to be considered for successful EOR application.

Furthermore, the viscoelastic nature (i.e., material with both viscous and elastic behavior) of polymer solutions can be well-demonstrated by oscillatory shear tests. Generally, the storage modulus (G') and loss modulus (G'') demonstrate the viscoelastic solid-like and liquid-like behavior, respectively. The G' and G'' are used to measure the amount of energy accumulated and released in polymeric solutions under oscillatory stress [38,39]. Materials attributed to the combination of G' and G'' can be placed into the Maxwellian behavior category. A typical spring-dashpot representation of the Maxwell model is shown in Figure 1.6. Amplitude sweep (also termed as "*strain sweep*") is applied to determine the linear viscoelastic (LVE) region of the polymer solution. The LVE region indicates the range in which the test can be carried out without destroying the structure of the sample. Once the LVE region is determined, a frequency sweep can be employed to determine the viscoelasticity of the polymer solution.

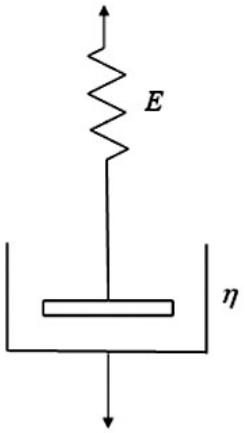

Figure 1.6. Typical spring-dashpot representation of the Maxwell model.

The elasticity of polymer solution plays an essential role in enhancing the oil recovery. The superiority of normal stress over the shear stress between the oil and polymer promotes to pull the trapped oil as well as to push the fluid ahead [3]. This phenomenon is called the "*pushing and pulling*" mechanism (see Figure 1.7). Generally, the entanglement of injected long-chain polymers may get fragmented, which agglomerates with the oil [40]. It takes-off the stuck oil from the reservoir. Additionally, the higher elasticity of the polymer improves the displacement efficiency of the trapped oil.

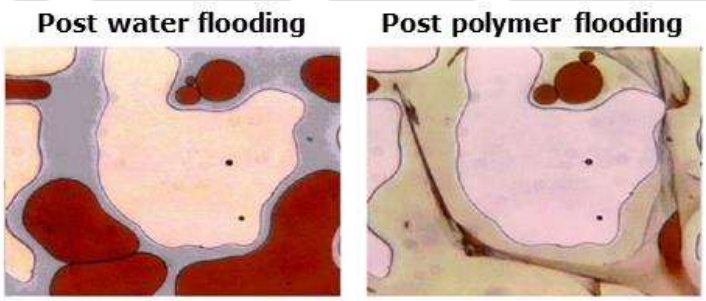

Figure 1.7. Visualization of the "pushing and pulling" mechanism [41]. Reproduced by permission from Society of Petroleum Engineers Inc., © 2000.

Generally, the surfactant adsorbs spontaneously from the bulk phase at the oil–water interface, where the resultant free energy is lesser than that in the solution. The adsorbed surfactant not only changes the IFT but also develops an interfacial film with viscoelastic properties [42]. An interfacial rheology is a potential tool that can be used to study the structural properties of the interfacial film and its stability [43,44]. It illustrates the functional association

between the stress applied at the interface and its deformation. An interface (i.e., air–water or oil–water) can be deformed in two ways, *viz.* dilational and shear, in order to analyze its rheological behavior [45]. The dilational type includes constant expansion and contraction of the droplet [46]. Interfacial shear, on the other hand, involves shearing the interface to deform its shape [47]. The interfacial shear rheology is based on the same rheological principles as that of the bulk rheology [42]. However, there are a few limiting factors while shearing the interface at higher shear rates. In such circumstances, the influence of bulk flow has a substantial impact on interfacial deformation. The Boussinesq number (Bo) provides valuable information on the rate of deformation of the interfacial film. It is the ratio of the surface to bulk viscous effects (see equation 1.1).

$$\text{Bo} = \frac{\text{Surface shear viscosity}}{\text{Bulk viscosity} \times \text{ radius of the measuring cell}} \tag{1.1}$$

If Bo > 1, the bulk flow has no effect on the interfacial deformation. Otherwise (< 1), the bulk flow has a significant influence on the interfacial deformation [47].

Generally, the interface is sheared using a rotating solid geometry, such as a bicone, a du Noüy ring, or a needle, to measure study the shear rheology [48–50]. The interfacial stress response $\left(\sigma_s\right)$ can be determined by

$$\sigma_s = G_s\varepsilon_s + \eta_s \frac{d\varepsilon_s}{dt} \tag{1.2}$$

In case of an oscillational shear, the stress response can be determined by a complex interfacial shear modulus $\left(G_s^*\right)$ (see equation 1.3).

$$G_s^*\left(\omega\right) = G_s'\left(\omega\right) + iG_s''\left(\omega\right) \tag{1.3}$$

1.3 Objectives

The objective of this study was to synthesize an economical yet effective surfactant from the abundantly-available weed, *Eichhornia crassipes*, with the intention of using it in the EOR. The specific aims and objectives are as follows:

- Extract a natural surfactant from the locally collected *Eichhornia crassipes* plant, and determine its structure, and interfacial and rheological properties.
- Study the natural surfactant–polymer (i.e., xanthan gum) system for its mechanical and thermal stability, and tolerance to the salinity and hardness of water.
- Examine the rheological properties of the natural surfactant–polymer system and compare it with the conventional polymer and surfactant–polymer systems.
- Study the adsorption of the synthesized surfactant at the oil–water interface.
- Study the adsorption of the synthesized surfactant on sand and rock, and determine its adsorption kinetics, mechanism, and equilibrium adsorption characteristics.
- Investigate the wettability-alteration potential of the synthesized natural surfactant with the help of contact angle measurements under reservoir-like conditions.
- Evaluate the performance of core flooding experiments with the synthesized surfactant–polymer assembly.

1.4 Scope of the study

The chemical method of EOR has immense scope in the oil field. Every oil field has different conditions, due to which new challenges arise. Recently, researchers are paying attention to the potential of the natural surfactants for the application in EOR due to their eco-friendly nature and competitive performance with a traditional synthetic surfactant. The main target of this research work is to synthesize a natural surfactant for EOR from the noxious *Eichhornia crassipes* weed. In view of the screening criteria proposed by Taber et al. [8, 51], numerous

analyses such as the measurement of IFT, wettability, adsorption, rheological characteristics, phase behavior, and core flooding are carried out to study the performance of the developed natural surfactant.

1.5 Thesis overview

For addressing the above-mentioned objectives, this PhD thesis has been organized in the following eight chapters:

Chapter 1 (Introduction): This chapter presents the general overview of the oil recovery techniques, emphasizing the mechanism of the chemical method of oil recovery. The research problem has been identified and the aims of this thesis have been given along with its scope and organization of thesis.

Chapter 2 (Literature review): In this chapter, the state of art of performance of the water-soluble chemical additives such as alkalis, surfactants, and polymers used for chemical EOR are presented and critically analyzed. This chapter also discusses the concepts and techniques related to the chemical methods of EOR and highlights the rheological properties of the chemicals involved in the efficient EOR methods.

Chapter 3 (Materials and methods): In this chapter, the materials used in the experimental studies and their sources are listed. Detailed information on the procedure of synthesis of the natural surfactant, sample preparation methods, equipment used, and the experimental procedures are provided.

Chapter 4 (Characterization of natural surfactant from *Eichhornia crassipes* for its possible application in EOR): This chapter focuses on the characterization of the synthesized natural surfactant from *Eichhornia crassipes* and study its beneficial effects on EOR. The synthesized surfactant was characterized by several spectroscopical, morphological, and interfacial analyses. Furthermore, the influence of the synthesized surfactant on the rheological

properties of the conventionally-used polysaccharide (i.e., xanthan gum) was studied and compared with that of a commercially-used surfactant (i.e., sodium dodecyl sulfate).

Chapter 5 (Impact of mineralogy, salinity, and temperature on the adsorption characteristics of the synthesized natural surfactant): This chapter mainly focuses on evaluating the adsorption of the synthesized natural surfactant on the porous media. This study features the kinetics, mechanism, and equilibrium of adsorption of the surfactant on sand and sandstone rock. This study also highlights the influence of brine and temperature on the adsorption of the surfactant.

Chapter 6 (The Role of Adsorption of a Natural Surfactant at Oil–Water Interface in Enhanced Oil Recovery: Interfacial Structural Analysis and Rheology): This chapter highlights the impact of the synthesized natural surfactant on the properties of the oil–water interface, and further correlates with its possible application in the EOR. It involves studies on interfacial shear rheology of the oil–water interface, which helps to characterize the flow behavior and the viscoelastic properties of the interfacial film. Furthermore, the adsorption of the surfactant molecules at the oil–water interface is studied using small-angle X-ray scattering, zeta potential, and morphological analyses.

Chapter 7 (Performance assessment of the natural surfactant–polymer additive under reservoir-like conditions): This chapter highlights the evaluation of the synthesized natural surfactant for its potential application in the EOR under reservoir-like conditions (i.e., under high temperature and pressure). It includes the analysis of wettability alteration and IFT reduction capabilities of the synthesized surfactant. The ability of the surfactant to stabilize the oil–water emulsion was studied by the phase behavior analysis. Based on the aforesaid studies, an optimized amount of the chemical additives was selected and used in the core flooding experiments. An effective reduction of IFT and wettability, and enhancement in the oil recovery suggest that the synthesized surfactant is promising for EOR applications.

Chapter 8 (Summary and future perspectives): This chapter provides a summary of the work and provides new ideas for future research.

Figure 1.8 illustrates the thesis organization flow chart.

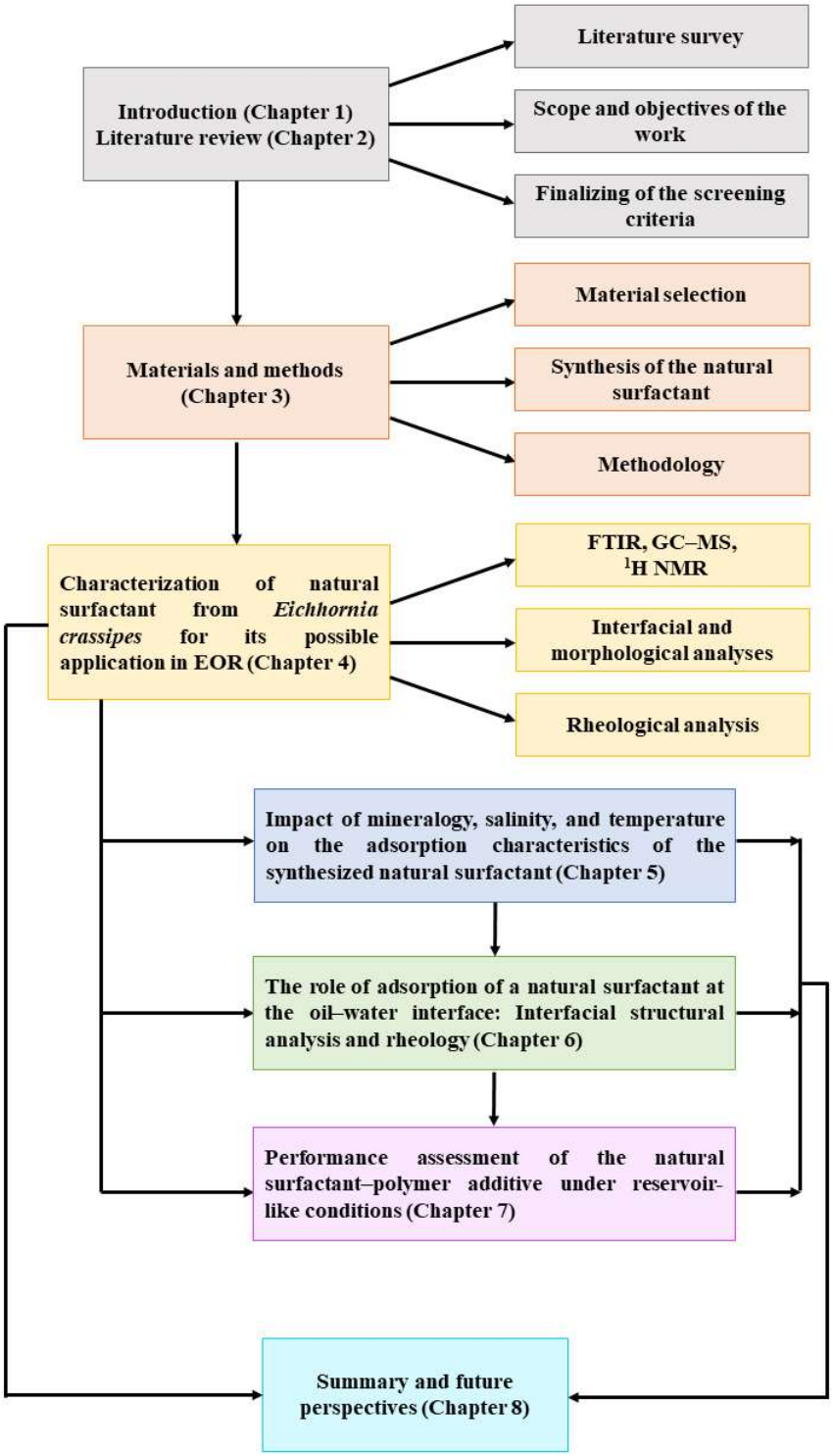

Figure 1.8. An overview of the thesis.

Nomenclature

G'	storage modulus, Pa
G''	loss modulus, Pa
G_s	interfacial shear modulus, Pa m
G_s'	interfacial storage modulus, Pa m
G_s''	interfacial loss modulus, Pa m
G_s^*	interfacial complex shear modulus, Pa m
t	time, s

Greek letters

ε_s	interfacial shear strain
η_s	interfacial viscosity, mPa s m
σ_s	interfacial shear stress, Pa m

Abbreviations

ASP	alkali–surfactant–polymer
Bo	Boussinesq number
CMC	critical micelle concentration
EOR	enhanced oil recovery
IFT	interfacial tension
LVE	linear viscoelastic region

References

[1] Nelson R, Lawson J, Thigpen D, Stegemeier G. Cosurfactant-enhanced alkaline flooding. SPE Enhanced Oil Recovery Symposium. 15–18 April 1984; Tulsa, Oklahoma, USA.

[2] Lake LW, Venuto PB. A niche for enhanced oil recovery in the 1990s. Oilfield Rev J 1992;4:55–61.

[3] Sheng J. Modern chemical enhanced oil recovery: Theory and practice. Gulf Professional Publishing: Massachusetts, USA, 2010.

[4] Seethepalli A, Adibhatla B, Mohanty K. Wettability alteration during surfactant flooding of carbonate reservoirs. SPE/DOE Symposium on Improved Oil Recovery. 17–21 April 2004; Tulsa, Oklahoma, USA.

[5] Machale J, Majumder SK, Ghosh P, Sen TK. Role of chemical additives and their rheological properties in enhanced oil recovery. Rev Chem Eng 2020;36:789–830.

[6] Olajire AA. Review of ASP EOR (alkaline surfactant polymer enhanced oil recovery) technology in the petroleum industry: Prospects and challenges. Energy 2014;77:963–82.

[7] Sheng JJ. A comprehensive review of alkaline–surfactant–polymer (ASP) flooding. Asia-Pac J Chem Eng 2014;9:471–89.

[8] Taber JJ, Martin F, Seright R. EOR screening criteria revisited–Part 1: Introduction to screening criteria and enhanced recovery field projects. SPE Reservoir Eng 1997;12:189–98.

[9] Green DW, Willhite GP. Enhanced oil recovery. Society of Petroleum Engineers: Richardson, Texas, USA, 1998.

[10] Ahmadi MA, Arabsahebi Y, Shadizadeh SR, Behbahani SS. Preliminary evaluation of mulberry leaf-derived surfactant on interfacial tension in an oil–aqueous system: EOR application. Fuel 2014;117:749–55.

[11] Ahmadi MA, Shadizadeh SR. Spotlight on the new natural surfactant flooding in carbonate rock samples in low salinity condition. Sci Rep 2018;8:1–15.

[12] Chhetri A, Watts K, Rahman M, Islam M. Soapnut extract as a natural surfactant for enhanced oil recovery. Energy Sources, A 2009;31:1893–903.

[13] Emadi S, Shadizadeh SR, Manshad AK, Rahimi AM, Nowrouzi I, Mohammadi AH. Effect of using *Zyziphus Spina Christi* or Cedr Extract (CE) as a natural surfactant on oil mobility control by foam flooding. J Mol Liq 2019;293:111573.

[14] Pal N, Saxena N, Laxmi KD, Mandal A. Interfacial behaviour, wettability alteration, and emulsification characteristics of a novel surfactant: Implications for enhanced oil recovery. Chem Eng Sci 2018;187:200–12.

[15] Saxena N, Goswami A, Dhodapkar P, Nihalani M, Mandal A. Bio-based surfactant for enhanced oil recovery: Interfacial properties, emulsification and rock-fluid interactions. J Pet Sci Eng 2019;176:299–311.

[16] Sastry N, Dave P, Valand M. Dilute solution behaviour of polyacrylamides in aqueous media. European Polym J 1999;35:517–25.

[17] Sindhu R, Binod P, Pandey A, Madhavan A, Alphonsa JA, Vivek N, Gnansounou E, Castro E, Faraco V. Water hyacinth a potential source for value addition: An overview. Bioresour Technol 2017;230:152–62.

[18] Ghosh P. Colloid and interface science. PHI Learning: New Delhi, India, 2009.

[19] Möbius D, Miller R, Fainerman VB. Surfactants: Chemistry, interfacial properties, applications. Elsevier: Amsterdam, Netherlands, 2001.

[20] Kamal MS, Hussein IA, Sultan AS. Review on surfactant flooding: Phase behavior, retention, IFT, and field applications. Energy Fuels 2017;31:7701–20.

[21] Saxena N, Kumar A, Mandal A. Adsorption analysis of natural anionic surfactant for enhanced oil recovery: The role of mineralogy, salinity, alkalinity and nanoparticles. J Pet Sci Eng 2019;173:1264–83.

[22] RezaeiDoust A, Puntervold T, Austad T. Chemical verification of the EOR mechanism by using low saline/smart water in sandstone. Energy Fuels 2011;25:2151–62.

[23] Zhou Y, Yin D, Chen W, Liu B, Zhang X. A comprehensive review of emulsion and its field application for enhanced oil recovery. Energy Sci Eng 2019;7:1046–58.

[24] Park SJ, Won JH, Lim J-C, Kim JH, Park S. Phase behavior and characterization of W/O microemulsion systems containing sodium dodecyl sulfate/butyl lactate/isopropyl myristate/water. J Ind Eng Chem 2005;11:20–6.

[25] Abdulredha MM, Aslina HS, Luqman CA. Overview on petroleum emulsions, formation, influence and demulsification treatment techniques. Arabian J Chem 2020;13:3403–28.

[26] Manev ED, Nguyen AV. Critical thickness of microscopic thin liquid films. Adv Colloid Interface Sci 2005;114:133–46.

[27] Castro Dantas T, Soares A P, Wanderley Neto A, Dantas Neto A, Barros Neto E. Implementing new microemulsion systems in wettability inversion and oil recovery from carbonate reservoirs. Energy Fuels 2014;28:6749–59.

[28] Dai C, Li H, Zhao M, Wu Y, You Q, Sun Y, Zhao G, Xu K. Emulsion behavior control and stability study through decorating silica nano-particle with dimethyldodecylamine oxide at n-heptane/water interface. Chem Eng Sci 2018;179:73–82.

[29] Durand A, Marie E. Macromolecular surfactants for miniemulsion polymerization. Adv Colloid Interface Sci 2009;150:90–105.

[30] Kumar N, Mandal A. Oil-in-water nanoemulsion stabilized by polymeric surfactant: Characterization and properties evaluation for enhanced oil recovery. Eur Polym J 2018;109:265–76.

[31] Dang CTQ, Chen ZJ, Nguyen NTB, Bae W, Phung TH. Development of isotherm polymer/surfactant adsorption models in chemical flooding. SPE Asia Pacific Oil and Gas Conference and Exhibition. 20–22 September 2011; Jakarta, Indonesia.

[32] Zhang R, Somasundaran P. Advances in adsorption of surfactants and their mixtures at solid/solution interfaces. Adv Colloid Interface Sci 2006;123:213–29.

[33] Belhaj AF, Elraies KA, Mahmood SM, Zulkifli NN, Akbari S, Hussien OS. The effect of surfactant concentration, salinity, temperature, and pH on surfactant adsorption for chemical enhanced oil recovery: A review. J Pet Explor Prod Technol 2020;10:125–37.

[34] Liu S. Alkaline surfactant polymer enhanced oil recovery process. Ph.D. Thesis. Department of Chemical Engineering, Rice University, Houston, Texas, USA: 2008.

[35] Tabary R, Bazin B, Douarche F, Moreau P, Oukhemanou-Destremaut F. Surfactant flooding in challenging conditions: Towards hard brines and high temperatures. SPE Middle East Oil and Gas Show and Conference. 10–13 March 2013; Manama, Bahrain.

[36] Somasundaran P, Huang L. Adsorption/aggregation of surfactants and their mixtures at solid–liquid interfaces. Adv Colloid Interface Sci 2000;88:179–208.

[37] Kamal MS, Sultan AS, Al-Mubaiyedh UA, Hussein IA. Review on polymer flooding: Rheology, adsorption, stability, and field applications of various polymer systems. Polym Rev 2015;55:491–530.

[38] Larson RG. The structure and rheology of complex fluids. Oxford University Press New York, USA, 1999.

[39] Macosko CW. Rheology: Principles, measurements, and applications. Wiley: New Jersey, USA, 1996.

[40] Mohammadi S, Maghzi A, Ghazanfari M, Masihi M, Mohebbi A, Kharrat R. On the control of glass micro-model characteristics developed by laser technology. Energy Sources, A 2013;35:193–201.

[41] Wang D, Xia H, Liu Z, Yang Q. Study of the mechanism of polymer solution with visco-elastic behavior increasing microscopic oil displacement efficiency and the forming of steady oil thread flow channels. SPE Asia Pacific Oil and Gas Conference and Exhibition. 17–19 April 2001; Jakarta, Indonesia.

[42] Krägel J, Derkatch SR. Interfacial shear rheology. Curr Opin Colloid Interface Sci 2010;15:246–55.

[43] Lyu Y, Gu C, Fan X, Tao J, Yao X, Dai C, Zhao G. Interfacial rheology of a novel dispersed particle gel soft heterogeneous combination flooding system at the oil–water interface. Colloids Surf, A 2018;559:23–34.

[44] Roth S, Murray BS, Dickinson E. Interfacial shear rheology of aged and heat-treated *β*-lactoglobulin films: Displacement by nonionic surfactant. J Agric Food Chem 2000;48:1491–7.

[45] Sun H-Q, Zhang L, Li Z-Q, Zhang L, Luo L, Zhao S. Interfacial dilational rheology related to enhance oil recovery. Soft Matter 2011;7:7601–11.

[46] Erk KA, Martin JD, Schwalbe JT, Phelan Jr FR, Hudson SD. Shear and dilational interfacial rheology of surfactant-stabilized droplets. J Colloid Interface Sci 2012;377:442–9.

[47] Vishal B. Foaming and rheological properties of aqueous solutions: An interfacial study. Rev Chem Eng 2021.

[48] Brooks CF, Fuller GG, Frank CW, Robertson CR. An interfacial stress rheometer to study rheological transitions in monolayers at the air–water interface. Langmuir 1999;15:2450–9.

[49] Erni P, Fischer P, Windhab EJ, Kusnezov V, Stettin H, Läuger J. Stress-and strain-controlled measurements of interfacial shear viscosity and viscoelasticity at liquid/liquid and gas/liquid interfaces. Rev Sci Instrum 2003;74:4916–24.

[50] Vandebril S, Franck A, Fuller GG, Moldenaers P, Vermant J. A double wall-ring geometry for interfacial shear rheometry. Rheol Acta 2010;49:131–44.

[51] Taber J, Martin F, Seright R. EOR screening criteria revisited–Part 2: Applications and impact of oil prices. SPE Reservoir Eng 1997;12:199–206.

Chapter 2

Literature review

Published article: Machale J, Majumder SK, Ghosh P, Sen TK. Role of chemical additives and their rheological properties in enhanced oil recovery. Reviews in Chemical Engineering 2020;36:789–830.

Literature review

In this chapter, the state of art of performance of the water-soluble chemical additives such as alkalis, surfactants, and polymers used for chemical EOR are presented and critically analyzed. This chapter also discusses the concepts and techniques related to the chemical methods of EOR and highlights the rheological properties of the chemicals involved in the efficient EOR methods.

2.1 Background

In order to increase the oil production, the overall displacement efficiency, which is a function of time, liquid viscosity, permeability, interfacial tension (IFT), wettability, and capillary pressure should be increased [1]. The displacement efficiency (E_{do}) depends on the microscopic and macroscopic displacement efficiencies. It is the ratio of the amount of oil recovered to the oil initially present in the swept volume, which is mathematically expressed as [2]

$$E_{do} = \frac{S_{oi} - S_{or}}{S_{oi}} \tag{2.1}$$

The capillary force plays a vital role in EOR. It acts at the oil–water and oil–rock interfaces to decrease their surface energy, which eventually helps in increasing the displacement of trapped oil. Even after the primary and secondary oil recoveries, some amount of oil remains trapped in the reservoir. Oil is usually trapped by the capillary force, which is directly related to permeability, IFT, and the mobility ratio [1]. The mobility ratio is defined as

$$\text{Mobility ratio} = \left[\frac{\text{Mobility of the displacing fluid (i.e., water)}}{\text{Mobility of the displaced fluid (i.e., oil)}} \right] \tag{2.2}$$

The mobility ratio should be less than or equal to unity for a good recovery. In such cases, it is called a favorable number. Otherwise (i.e., >1), it is called an unfavorable number, as water becomes more mobile than oil.

2.2 Polymer flooding

2.2.1 Currently-used polymers in EOR

For the better recovery of oil, it is important to control its mobility. The purpose of mobility control is to change the mobility ratio to a favorable number so that the injected fluid does not bypass the displaced fluid (i.e., crude oil) in the reservoir [3]. Since it is not possible to change the properties of the crude oil or the permeability of the reservoir, most of the mobility-control methods change the properties of the injected fluid. The commonly-used mobility control agent is the polymer. Mobility is inversely proportional to the viscosity, and therefore the polymer should act as an effective viscosifier for the aqueous phase [4]. Fundamentally, the addition of polymer to the reservoir increases the viscosity of water and hence reduces its relative permeability in the reservoir [5]. It improves the sweep efficiency significantly, which helps to displace the oil from the reservoir, and hence the efficiency of oil recovery increases. Polymer flooding has been efficiently used for more than 40 years to recover the remaining oil from the reservoir. Due to the decreased water production and enhanced oil production, the total cost of the polymer flooding technique is less than that of water flooding.

Commonly, synthetic and polysaccharides are the most-used polymers in the flooding process [6]. Polyacrylamide (PAM), a water-soluble polymer, was the first thickening agent used in polymer flooding [7]. Many researchers have reported various attempts to alter PAM's chemical structure or synthesize new acrylamide-based copolymers with improved properties such as shear resistance, brine compatibility, and temperature stability [8,9]. Partially hydrolyzed polyacrylamide (HPAM) is a copolymer of PAM and poly-acrylic acid (PAA) [7,10]. It can be synthesized by the partial hydrolysis of PAM or by the copolymerization of

sodium acrylate with acrylamide. The rate of hydrolysis of the amide functional group increases with temperature [11]. The performance of such a polymer depends upon the degree of hydrolysis [12]. The major part of these molecules consists of a hydrophilic backbone. Xanthan gum (XG), a polysaccharide and a water-soluble polymer, is extensively used in the EOR for its effective and stable thickening properties. It is produced by the fermentation of glucose or fructose by the bacterium *Xanthomonas Campestris* [13,14]. The structures of XG, PAM, and HPAM are shown in Figure 2.1.

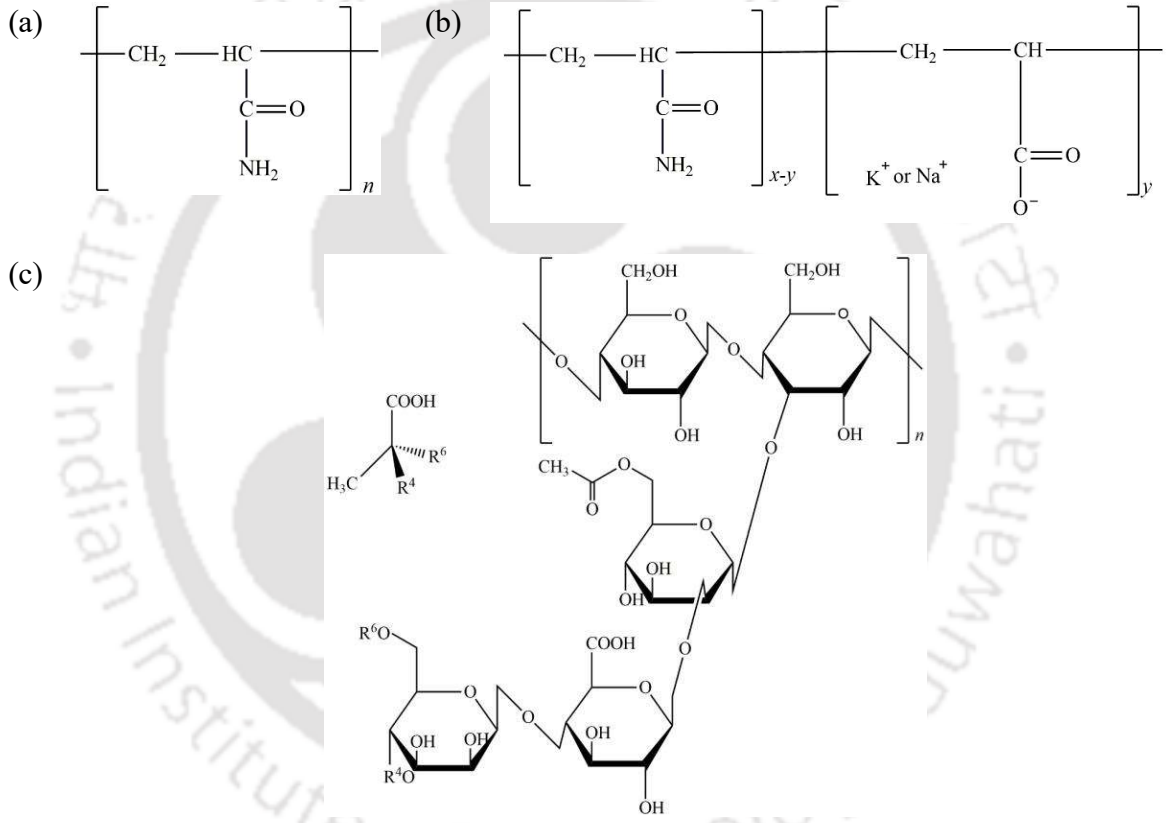

Figure 2.1. Structures of (a) PAM, (b) HPAM, and (c) XG.

XG is biocompatible, biodegradable, and stable at high temperatures [14,15]. PAM has a greater resistance to the enzymes and possesses good properties as a flocculant. HPAM, on the other hand, is tolerant to strong mechanical and bacterial attacks [1]. Every polymer has its own merits and demerits for a specific reservoir. A high salinity macroscopically flocculates the acrylic acid backbone of PAM and HPAM, which causes a noticeable reduction in viscosity

[16,17]. XG, on the other hand, is very sensitive to bacterial degradation [18]. Since mobility ratio depends on the viscosity of the solution, the studies on viscosity variations under different reservoir conditions (such as temperature, salinity etc.) are important in EOR. Ghoumrassi-Barr and Aliouche [19] observed that the XG is substantially more stable than HPAM, which means that XG-flooding has a greater EOR efficiency even in difficult reservoir conditions.

2.2.2 Influence of salinity, temperature, and concentration on the rheological properties of polymeric solutions used in EOR

Ghannam and Esmail [20] have carried out a thorough study on the rheological properties of aqueous PAM solutions, including the measurement of steady shear flow parameters, transient shear stress response, yield stress, thixotropic behavior, creep recovery, dynamic responses, and temperature effects in the temperature range of 283–323 K. PAM has a strong shear-thinning behavior. The viscosity of PAM solution decreases with increasing temperature. The yield stress and the thixotropic behavior of PAM are found to be more significant at the higher concentrations. Like PAM, HPAM also has a strong shear-thinning nature. It can tolerate high mechanical forces, and it is resistant to bacterial attacks. HPAM exhibits a rheopectic behavior (i.e., its viscosity increases with the time of application of shear, at a constant shear rate). The viscosity of HPAM increases with the increasing degree of hydrolysis [21]. It has been observed that the HPAM solution remains stable up to 413 K, and it is not a good option to inject HPAM into reservoirs above 433 K because of the faster decomposition of the polymer at high temperatures [19]. Figure 2.2 shows the variation of viscosity of the PAM and HPAM solutions with shear rate [21].

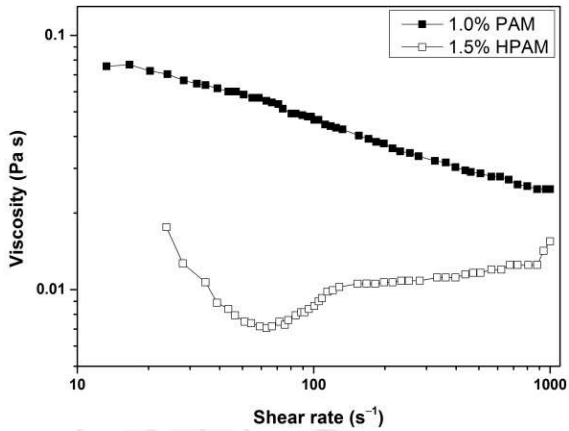

Figure 2.2. Variation of viscosity of PAM and HPAM solutions with the shear rate. [21] [adapted by permission from Elsevier Ltd., © 2007].

Similar to the synthetic polymers, XG also shows a shear-thinning behavior [14,22]. Under the impact of high shear rates, the steady shear viscosity of the XG solutions decreases attributable to the disentanglement of the polymer network and the partial alignment of the individual macromolecules in the direction of shear flow [22]. XG shows a significant effect of temperature because of its microstructure. It is well-known that the average speed of the molecules in liquid increases as the temperature increases. Therefore, the time they spend in interaction with their adjacent neighbors decreases. Thus, the average intermolecular forces decrease. The linear viscoelastic behavior of the concentrated XG solutions is dominated by an elastic nature rather than a viscous nature, and a gel-like structure is present in these systems. As the polymer concentration is increased, XG solutions become more elastic, and they can be characterized by a slower relaxation mechanism [15]. The shear modulus increases with increasing temperature, but it is almost independent of the XG and the salt concentrations [23].

It has been observed that the viscosity of polymer solutions decreases with increasing salinity. The addition of Na^+ effectively neutralizes the negative charge [24], resulting in the shrinkage of the molecular chains and a decrease in the hydrodynamic radius. The addition of aqueous NaCl solution increases the ionic strength of the medium. Generally, the polymer chains are stretched in an aqueous medium because of the repulsive forces between the negative

charges on the chains. Thus, the hydrodynamic radius of the polymer chain is large in the aqueous solution, and therefore, the viscosity of the polymer solution is high. It is observed that the repulsive forces within the polymer chain decrease as the concentration of Na^+ is increased. Hence the polymer chain coils up, and the hydrodynamic radius of the polymer chain reduces. Both these factors are responsible for the reduction in the viscosity of the polymer solution. Overall viscosity of the polymeric solution increases with increasing concentrations but decreases with increasing salinity. Therefore, the viscosity should be optimized to get favorable mobility ratio [25]. The optimal range of viscosity also depends on the nature and the characteristics of the reservoir.

Researchers have recognized that oil recovery can be improved by the elasticity of the polymer. Due to the more elastic properties of the polymer, normal stress between the polymer solution and oil becomes more dominating than the shear stress. Normal stress not only helps to pull the oil from the trapped zone but it also pushes the fluid ahead [26]. This is called the "*pushing and pulling*" mechanism. Usually, the injected polymers are long-chained, and due to the capillary forces, the entanglement of these chains may be broken, and the polymer agglomerates with the oil [27]. This helps to strip off the trapped oil from the reservoir. E_{do} can be improved with the higher elasticity of the polymer [28].

The storage modulus (G') of PAM is more than its loss modulus (G''), which indicates that PAM has an elastic behavior that is more dominating at the lower range of frequency [20]. Similarly, HPAM and XG show dominating elastic behavior over viscous behavior [14,15,29]. The domination of G' over G'' across the entire strain range depicts the gel-like structure of the polymer solutions [30]. Sometimes, a slight decrease in G' has been observed up to a certain strain amplitude, beyond which a sharp decrease in G'' has been observed with increasing strain amplitude. This indicates a strain-thinning feature of the aqueous polymer solution. This strain-

thinning feature may be attributed to the destruction and formation of their internal structure responding to an externally imposed stimulus [31]. Depending on the interactions between the microstructures, it has been found that there are at least four types of strain behavior [32], as shown in Table 2.1. From the strain sweep results, it was found that the XG solution showed weak strain overshoot, whereas PAM and HPAM showed strain-thinning behavior [14,15,33].

Table 2.1. Types of strain behavior

Strain behavior	Result
Strain-thinning	Both G' and G'' decrease
Strain-hardening	Both G' and G'' increase
Weak strain overshoot	G' decreases; G'' initially increases and then decreases
Strong strain overshoot	Both G' and G'' increase and then decrease

2.2.3 Recently-used polysaccharides in EOR and their rheological properties

Recently, many researchers have paid attention to the polysaccharides such as gellan gum, guar gum, welan gum, diutan gum, cashew gum, and schizophyllan for the application EOR [34-37]. Due to their special physicochemical properties, these polymers are widely employed for thickening, emulsification, stabilization, and gelation [35]. They are biocompatible, biodegradable, and environment-friendly. Therefore, microbial polysaccharides are commonly used in foods, pharmaceutics, cosmetics, cement, and oil recovery [38-41]. The structures of these polysaccharides are shown in Figure 2.3.

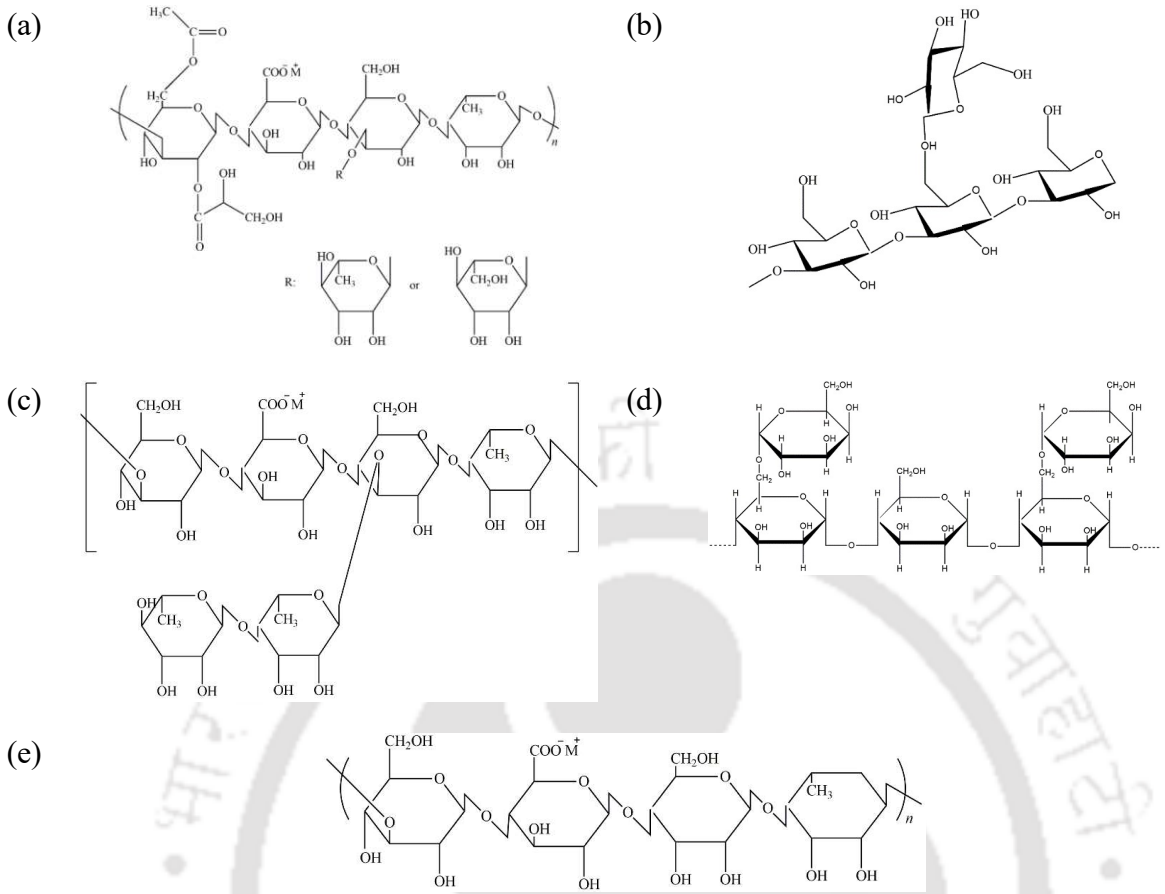

Figure 2.3. The structures of (a) welan gum, (b) schizophyllan, (c) diutan gum, (d) guar gum, and (e) gellan gum.

The water-soluble polysaccharides mentioned above demonstrate a strong shear-thinning behavior [34–37,42–46]. The stretching macromolecules of the polysaccharide intertwine to form aggregates at a low shear rate. The flow resistance of many aggregates results in high viscosity. Nevertheless, the aggregates are broken down as the shear rate increases, dispersing the macromolecules along the flow direction, causing a reduction in the viscosity. The shear-thinning behavior of gellan gum is observed due to the breakdown of an intermolecular association, where microgel particles may exist partially [46]. The addition of an inorganic salt facilitates the association of charged helical structures in different ways. The salt-induced gelation of xanthan is attributed to the prominent viscosity retention rate, and the same for gellan is caused by the competitive hydration [35]. Based on the valence of the cation, changes in viscosity and retention rate of the polysaccharide are observed. This leads to the

formation of cross-links between the molecules and multivalent cations, due to which reduction in rheological properties of the polysaccharide are noticed.

Schizophyllan is generally synthesized by the fungus *Schizophyllum commune Fries.* Schizophyllan has been extensively used in cancer treatment and personal care. Due to its excellent stability against heat, salinity, and shear, researchers have taken a keen interest in studying its potential for use in EOR. In 2012, schizophyllan solution was injected in an oil field at Ludwigshafen (Germany), and preliminary results confirmed that this polymer has potential for the application of EOR [47]. In comparison with the currently-used polymers, schizophyllan demonstrated a superior viscosity at high salinity, thermal stability (up to 408 K), and minimum viscosity loss under very harsh reservoir conditions [48]. Such excellent performance was possible due to its complex triple helical structure. It has been observed from the core flooding experiments that ~28% of additional oil could be recovered by injecting the schizophyllan solution [47].

Guar gum is generally unable to hydrate completely, and hence it shows very strong scaling behavior with molecular weight, polymer concentration, and temperature [34,49]. The scaling behavior confirms the dynamic properties of the guar gum solution. Due to intense molecular interactions at low concentrations, aqueous diutan gum forms aggregates in the solution. The viscosity and viscoelasticity retention rates of diutan gum solutions are much greater than those of XG solutions at the same temperature and salinity [35]. Diutan gum is most stable at high salinity due to its double helix structure. Salts and temperature significantly impact the characteristics of welan gum solution because of the anionic charges on its backbone [50]. Xu et al. [37] have presented a comparative study of the rheological properties of aqueous welan gum and XG solutions. It has been observed that although the molecular weight of welan gum is less than that of XG, the aqueous solution of welan gum showed higher viscoelasticity than XG. A comparison has been shown in Figure 2.4 to illustrate the effect of shear rate on

diutan gum, XG, and welan gum. Similar to XG, welan gum also shows good resistance to salt, temperature, and the dominating behavior of G' over G''.

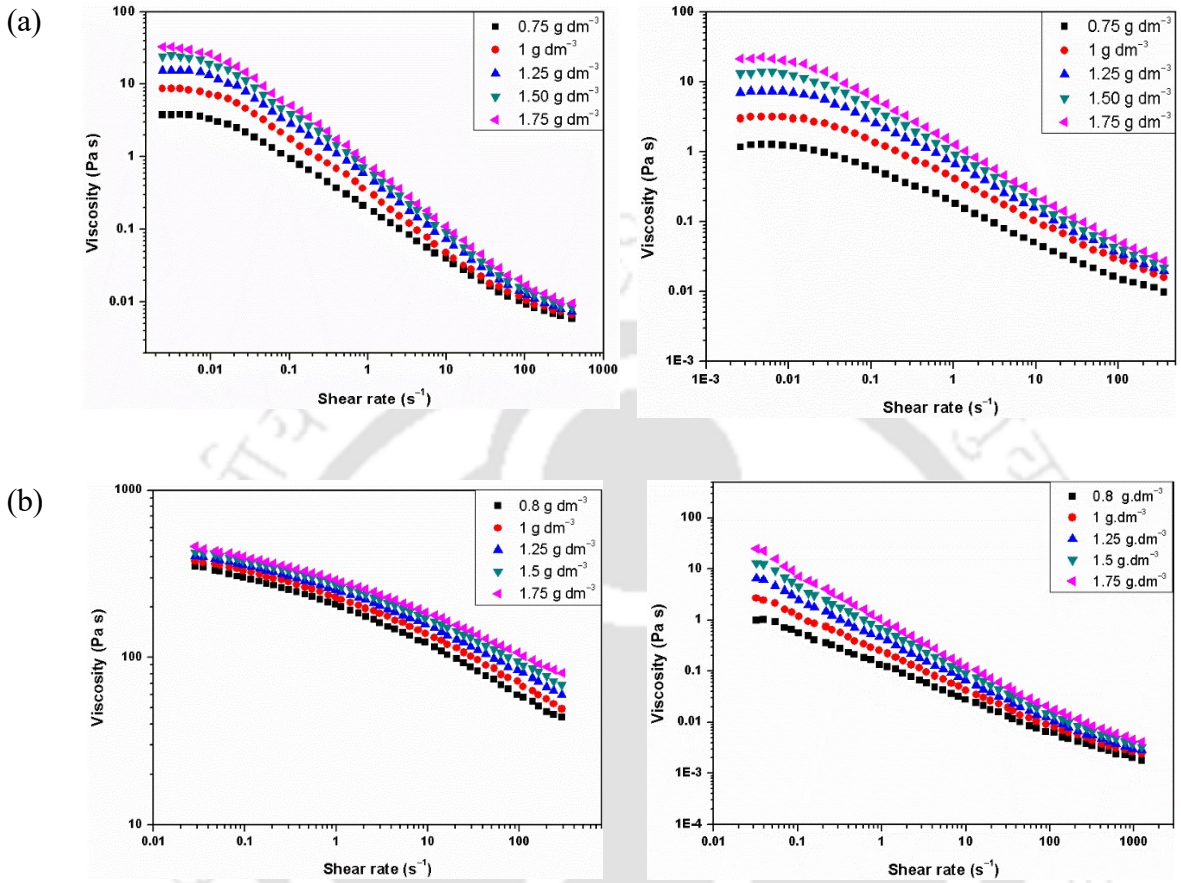

Figure 2.4. Viscosity as a function of shear rate at different concentrations of (a) diutan gum (left) and XG (right) [36] [adapted by permission from Elsevier Ltd., © 2015], and (b) welan gum (left) and XG (right) [37] [adapted by permission from Elsevier Ltd., © 2013].

2.2.4 Flow of polymer solutions through porous media

Understanding the flow behavior of polymer solutions in the porous media is very important for the EOR processes [51,52]. This can be done by inspecting the rheological properties of the polymer solution [10,12,52]. A porous medium comprises a matrix containing void spaces or pores. Typically, many of the pores are interconnected, allowing the fluid to flow through them. Soils, rocks, and sand are examples of porous media. Any model for the flow of polymer solutions through porous media should satisfy two conditions [51]. Primarily, the model should

have expansion and contraction regions, which are responsible for pressure drop in the porous medium. Secondly, the rheological model should contain the distinguishing transition from the Newtonian behavior at the low shear rates to the shear-thinning behavior at the high shear rates, as shown in Figure 2.5.

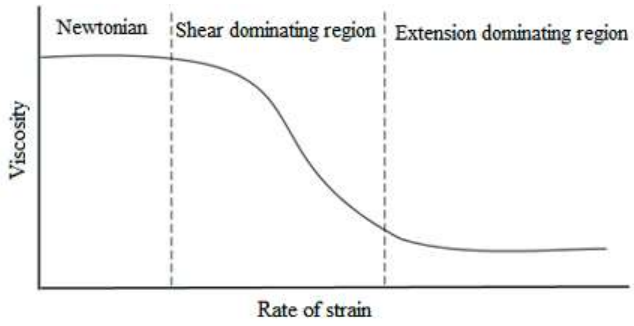

Figure 2.5. The transition from Newtonian to non-Newtonian flow behavior.

Darcy's law describes the flow of Newtonian liquids through the porous media [53]. Almost all synthetic as well as natural polymer solutions used in EOR, are non-Newtonian in nature. Unfortunately, Darcy's law does not fully satisfy the flow of non-Newtonian fluids through porous media, and hence many attempts have been made to modify the Darcy's law to describe the flow of non-Newtonian fluids in porous media. A few examples of the non-Newtonian models are presented in Table 2.2 [54]. It is interesting to observe the shear-thickening behavior of polymer solutions in porous media. This is likely due to the long chains of the polymers, which generally intertwine to the porous media at higher flow rates [12].

Durst et al. [55] studied the flow of HPAM in porous media under various solvent conditions. According to them, the maximum increase in pressure drop was mainly due to the high molecular weight of the polymers. A correlation between the experimental data and the Durst–Hass model was made. It was found that the strain rate at which the onset of increased pressure drop was observed decreased with the increasing viscosity of the solution. It was found that the specific resistance coefficient for the HPAM solution for flow through porous media

depended on the concentration of polymer and its molecular weight, but it was independent of the viscosity of the solvent.

Table 2.2. Non-Newtonian rheological models

Model	Equation	References
Power law	$\eta = K\dot{\gamma}^{n-1}$	[56]
Ellis	$\eta = \dfrac{\eta_0}{1+\left(\dfrac{\tau}{\tau_{1/2}}\right)^{\alpha-1}}$	[56]
Carreau	$\eta = \eta_\infty + \dfrac{\eta_0 - \eta_\infty}{\left[1+\left(\dot{\gamma}t_c\right)^2\right]^{\frac{1-n}{2}}}$	[57]
Herschel–Bulkley	$\tau = \tau_0 + K\dot{\gamma}^n,\ \tau > \tau_0$	[58]
Maxwell	$\tau + \lambda_1 \dfrac{\partial \tau}{\partial t} = \eta_0 \dot{\gamma}$	[59]
Jeffreys	$\tau + \lambda_1 \dfrac{\partial \tau}{\partial t} = \eta_0 \left(\dot{\gamma} + \lambda_2 \dfrac{\partial \dot{\gamma}}{\partial t}\right)$	[59]
Upper Convection Maxwell	$\tau + \lambda_1 \overset{\nabla}{\tau} = \eta_0 \dot{\gamma}$	[56]
Oldroyd-B	$\tau + \lambda_1 \overset{\nabla}{\tau} = \eta_0 \left(\dot{\gamma} + \lambda_2 \overset{\nabla}{\dot{\gamma}}\right)$	[60]
Godfrey	$\eta(t) = \eta_i - \Delta\eta'\left[1-\exp\left(-t/\lambda'\right)\right] - \Delta\eta''\left[1-\exp\left(-t/\lambda''\right)\right]$	[61]
Stretched Exponential Model	$\eta(t) = \eta_i + \left(\eta_{\inf} - \mu_i\right)\left[1-\exp\left\{-\left(t/\lambda_s\right)^c\right\}\right]$	[56]

A study was made by Kulicke and Haas [52] to study the flow behavior of PAM through a porous medium. They studied the influence of chain length, concentration, and

thermodynamic quality of the solvent. Similar to HPAM, PAM showed an increase in the resistance coefficient with increasing concentration of the polymer, although it did not affect the onset behavior. The polymer chain length was found to be the controlling factor for the onset, which saturated the effect of non-Newtonian flow phenomena.

2.3 Surfactant–polymer flooding

2.3.1 Mechanism of surfactant flooding for EOR

The term "surfactant" originated from "surface active agent". These are organic compounds having at least one hydrophilic (water-soluble) and one hydrophobic (oil-soluble) group in their molecule. Due to this physical characteristic, surfactants can significantly lower the IFT and alter the wettability between oil and water in the oil field. Although most surfactants lower the IFT between water and oil, there are some exceptions. Circa 1970, surfactants were considered as good EOR agents [62]. For high oil recovery, surfactants play two significant roles by helping achieve ultralow IFT [63]. Firstly, the ultralow IFT increases the mobility of the residual oil and creates an oil bank where both oil and water flow as continuous phases. Secondly, the ultralow IFT at the moving displacement front prevents the mobilized oil from being trapped by the capillary forces. The surfactant selection depends upon its ability to reduce the IFT, its stability against temperature and salinity, pressure, type of rock, phase behavior parameters, adsorption, and core flooding requirements under reservoir conditions [64-66]. Recently, co-surfactants have been blended with the main surfactant to improve the properties of the surfactant solution. The co-surfactant helps either as a promoter or as an active agent in the blended surfactant solution to produce a synergistic effect and deliver optimum conditions with regard to temperature, pressure, and salinity.

A surfactant is usually represented by an amphiphilic structure, as shown in Figure 2.6. The hydrophilic portion is termed as *head,* while the hydrophobic portion is called the *tail*. Consistent with the charge of the head group, surfactants can be characterized into four groups,

i.e., anionic, cationic, nonionic, and zwitterionic. The anionic surfactants have negatively charged head groups and the counterions are usually Na^{+}, K^{+}, and Al^{+3} [67]. Temperature can significantly affect the IFT and critical micelle concentration (CMC) of the anionic surfactant systems. Table 2.3 summarizes the use of anionic surfactants for EOR.

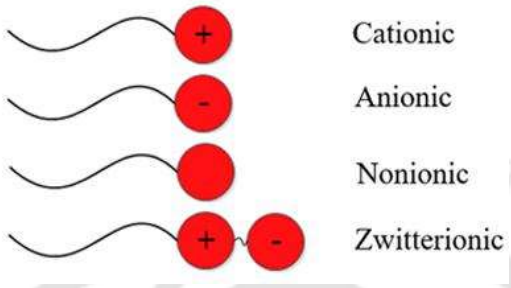

Figure 2.6. Classification of surfactants.

Cationic surfactants, on the other hand, have a positively charged head group. In general, cationic surfactants are more expensive than anionic surfactants. Table 2.4 gives a summary of the cationic surfactants used in EOR. The head group of the nonionic surfactant molecule does not carry any charge. However, it is polar for most of the surfactants. These compounds are mainly used as co-surfactants to enhance the physical properties of the surfactant solution and promote the EOR process [68]. Alcohols, phenols, ethers, esters, and amides are some examples of nonionic surfactants. Table 2.5 gives a summary of the nonionic surfactants used in EOR. Recently, numerous researchers have been considering zwitterionic surfactants for EOR due to their dual charged head groups (i.e., positive and negative). Zwitterionic surfactants such as hydroxyl sulfonate betaine, alkyl dimethylpropane, didodecylmethylcarboxyl betaine, and carboxyl betaine types have shown good interfacial properties and they can withstand harsh reservoir conditions (including high temperature and salinity) [69–71].

Table 2.3. Anionic surfactants used in the EOR process

Surfactant	Remarks	Structure	References
Alkyl aryl sulfonates	1. Non-biodegradable 2. Can be customized as per reservoir conditions 3. Stable at high temperatures 4. Unstable at high salinity and in the presence of divalent ions	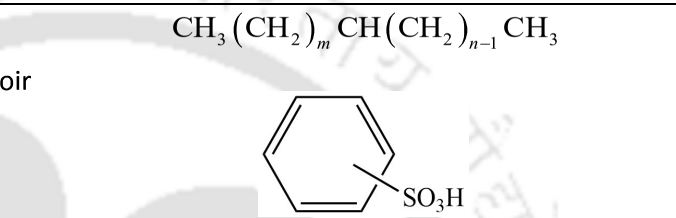	[63,72,73]
Alkyl benzene sulfonate (linear)	1. A sub-category of alkyl aryl sulfonates 2. Negatively-charged hydrophilic group 3. Harmful to the environment due to their toxic nature 4. Less influence of salinity	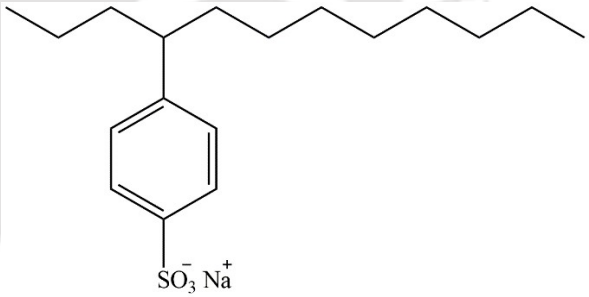	[74–76]
Alkyl sulfate	1. Sodium dodecyl sulfate and sodium octyl sulfate are common examples of alkyl sulfate 2. Biodegradable 3. Sensitive to temperature 4. Economical	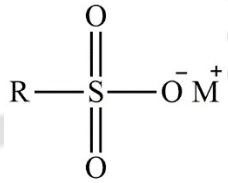 R = any hydrophobic hydrocarbon chain	[77,78]

	5. Strong interaction with nonionic polymers		
N-ethoxy sulfonate	1. Cloud point is over 373 K 2. Stable at higher reservoir temperatures 3. Stable and soluble with the injection of high salinity brine 4. Does not precipitate in the presence of divalent ions such as Ca^{2+} and Mg^{2+}	$H(OCH_2CH_2)_n - O - SO_2 - R$ R = alkyl radical, branched or linear, or an alkyl group n = integer	[79–81]
Alcohol propoxy sulfate	1. Stable up to 6 kg/m^3 salinity 2. Sensitive to temperature 3. Additional 30% oil recovery can be achieved along with internal olefin sulfonate 4. The branched surfactant can create an IFT of 0.01 mN/m	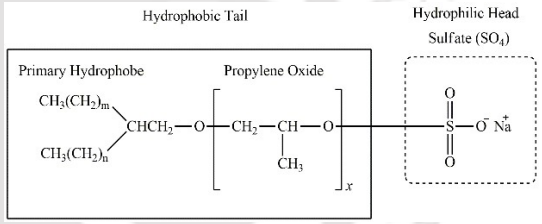	[82,83]
Alpha-olefin sulfonate	1. Stable over a wide range of pH 2. Exhibit good foaming and detergency even in the hard water 3. Good foaming agent 4. Good strength of the foam	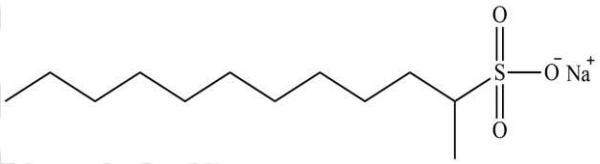	[84–87]

	5. High temperature stability above 523–573 K	
Docusate sodium	1. Double-tailed anionic surfactant 2. Well-suited for ASP flooding, especially for conventional reservoirs 3. Combining with polymer, it forms complex structures 4. Good for fractured or low permeability reservoirs	[88,89]
Alkyl ether sulfates	1. Very sensitive to high temperature 2. Not suitable for high salinity 3. The addition of ethoxy group to their structure increases the stability of the surfactant	[90,91]

Table 2.4. Cationic surfactants used in EOR

Surfactant	Remarks	Structure	References
Cetyltrimethyl-ammonium bromide (CTAB)	1. Stable up to 373 K and 60 kg/m^3 salinity 2. IFT reduces with temperature	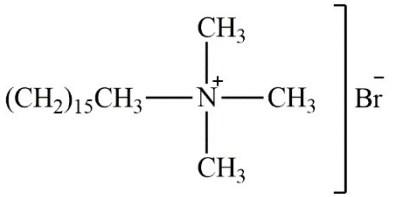	[92–94]
Cocoalkyl-trimethyl-ammonium chloride	1. More successful in sandstone reservoirs 2. More effectively alters wettability in the sandstone reservoirs	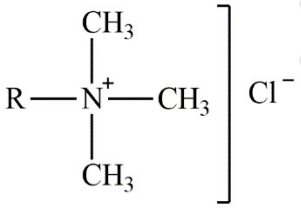	[81]
Dodecyl-trimethyl-ammonium bromide (DTAB)	1. Similar to CTAB 2. It may not reduce the IFT to ultra-low values 3. Mixture with nonionic surfactant can recover 80% original oil in place (OOIP)	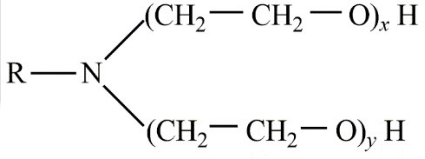	[95–97]

Table 2.5. Nonionic surfactants used in EOR

Surfactant	Remarks	Structure	References
Alkyl ethoxy carboxylates	1. Performs as a nonionic surfactant at neutral pH and as an anionic surfactant at alkaline pH 2. The combination of ethoxy and carboxylate groups increases this surfactant's resistivity to high temperature and high salinity (both monovalent and divalent salts)	$RO(CH_2CH_2O)_x CH_2COO^-M^+$	[98,99]
Polyethoxylated alkyl phenols	1. Can sustain only a narrow temperature range, i.e., 310–324 K 2. Performs well in high salinity	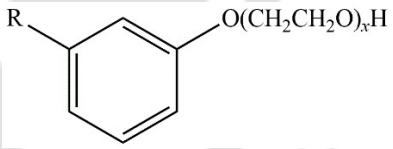	[100–102]
Poly (ethylene/ propylene) glycol ether	1. Increases the capillary displacement efficiency of an aqueous flooding medium 2. Stable at high temperature and salinity Biodegradable	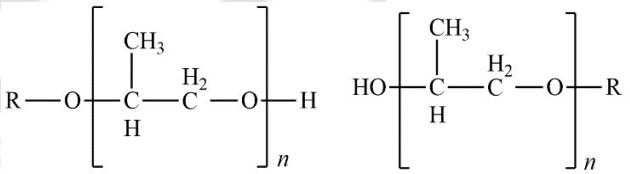	[99,103]

Tridecyl alcohol 30 ethoxylate (TDA 30 EO)	1. Similar to the alkylphenol ethoxylate family 2. Good recovery occurs in carbonate reservoirs at high temperatures up to 373 K and high salinity up to 200 kg/m^3 3. 80% OOIP was reported	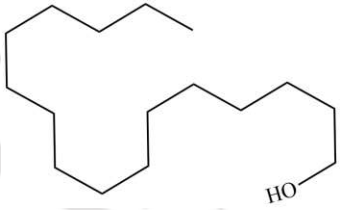	[81]
Triphenyl methane (TPM)	1. Good stability in harsh conditions such as high salinity (up to 18.6% TDS) in the presence of divalent ions and at high temperatures (> 343 K) 2. It shows viscoelastic behavior, particularly at low concentration 3. Most suitable for sandstone reservoir	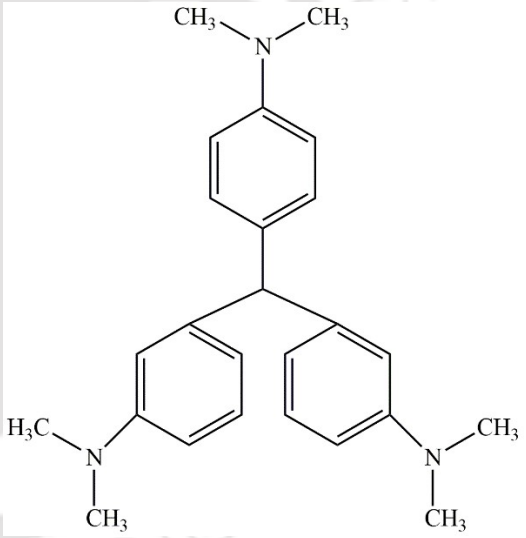	[104]

2.3.2 Utilization of surfactant mixtures for EOR

Mixed surfactants demonstrate significant synergism in improving interfacial properties, which is better than the individual surfactants [105]. Numerous researchers have claimed noteworthy enhancement in IFT reduction and emulsion stability using mixed surfactant, even under harsh reservoir conditions [106,107]. Kesarwani et al. [108] studied a mixture of SDS (anionic) and Tween 20 (nonionic) for EOR. They have evaluated the performance of the surfactant mixture based on the adsorption, rheological, and interfacial analyses. An effective 63% reduction in the surfactant adsorption on the rock surface was observed for the binary mixture in comparison with the individual surfactants. Furthermore, this anionic–nonionic surfactant mixture achieved an ultra-low IFT (i.e., 9.7 $\mu N\ m^{-1}$) and an additional oil recovery of 76.3% OOIP. In another study, Pal et al. [109] investigated a mixture of CTAB (cationic) and Tween 60 (nonionic) for EOR. The synergism between these surfactants diminished electrostatic and steric self-repulsions among the cationic and nonionic hydrophilic portions of the surfactants. Therefore, an effective reduction in the loss of the surfactant due to its adsorption on the rock surface has been observed. Li et al. [105] employed a combination of anionic and cationic surfactant mixtures and observed that the surfactant mixtures have a strong electrostatic interaction. This leads to the formation of a microstructure and a noteworthy reduction in the IFT and wettability [110,111].

2.3.3 Recent developments in natural surfactants for EOR

Recently, many researchers have been looking for natural surfactants and exploring their potency in EOR. Numerous researchers have synthesized several natural surfactants derived from soapnut, *Madhuca longifolia*, and various oils (e.g., palm, sunflower, coconut, castor, and jatropha) [112-117]. These low-cost natural surfactants can accomplish ultra-low IFT with minimum loss of surfactant, better stability under reservoir-like conditions, and alter the wettability of rock (i.e., from oil-wet to water-wet). Hence, these surfactants are promising in

the EOR application. A novel, ecofriendly, and cost-efficient surfactant derived from the leaves of *Ziziphus spina-christi* has received the attention of many researchers for its application in EOR [118–120]. As a result of its wettability-alteration and IFT-reduction capabilities, as well as its ability to improve the relative oil permeability, a significant additional oil (i.e., 15–25%) can be recovered to the surface (see Figure 2.7) [119,121].

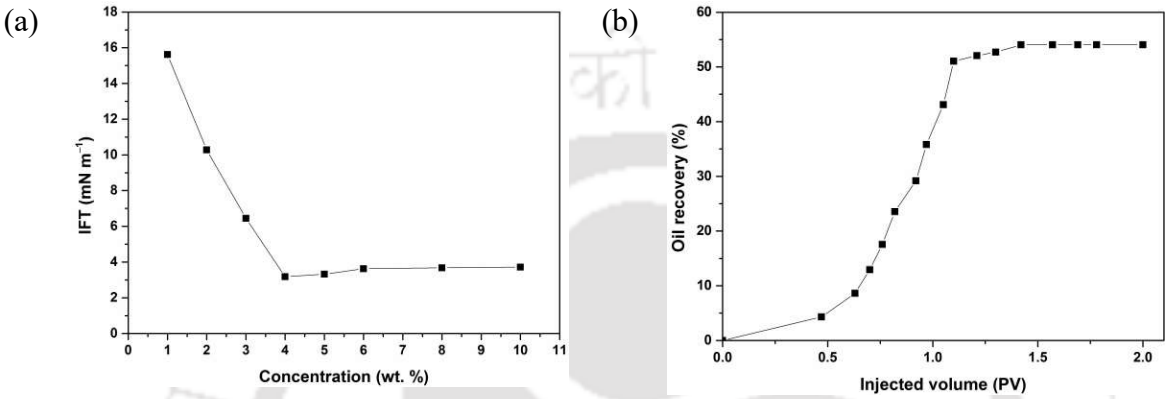

Figure 2.7. Variation of (a) IFT with the surfactant concentration and (b) oil recovery with the injected volume of surfactant [119]. [adapted by permission from Elsevier Ltd., © 2019]

Reetha, which is a conventionally used natural surfactant in the Indian community, has the potential for utilization in EOR [122]. Its use leads to good emulsion stability, foaming capability, and a drop in the energy of the oil–water interface. A natural surfactant derived from the *Anabasis Setifera* plant with good thermal stability, wettability-alteration, and IFT-reduction characteristics, has achieved an effective 15.4% additional oil recovery [123]. Dashtaki et al. [124] derived a natural surfactant from the *Vitagnus* plant and investigated its possible utilization in EOR. An additional 10% oil was recovered by injecting 3 g dm^{-3} synthesized surfactant. This was possibly achieved due to a significant reduction in the IFT (i.e., ~65.4%) and wettability-alteration (i.e., oil-wet to water-wet).

A natural surfactant derived from the *Myrtus communis* plant has the ability to achieve an ultra-low IFT, which aids in enhancing the oil recovery by 14.3 % [125]. Similar abilities have been reported for the natural surfactants derived from mulberry, *Glycyrrhiza glabra*,

Matricaria chamomilla, and *Zephyranthes carinata*. Table 2.6 summarizes the use of various natural surfactants for EOR. Natural surfactants could be a safe substitute for EOR, considering their significant benefits. However, the synthesis of natural surfactants on a large scale is still a challenging task.

Numerous studies have been reported on the adsorption of various natural surfactants on rock surfaces. Saxena et al. [116] analyzed the role of the rock type, alkali, salinity, and nanoparticles on the mechanism of adsorption of an anionic surfactant derived from soapnut fruits. An increase in the adsorption was observed with the increasing concentration of the surfactant. The adsorption was lower on the sandstone in comparison with carbonate and bentonite. The degree of adsorption was described well by the Langmuir and Redlich–Peterson isotherms. The pseudo-second-order model explained the adsorption kinetics of the surfactant on the rock surface. The same researchers have conducted a study with a natural surfactant developed from the Jatropha oil [117].

Adsorption of *Zizyphus spina-christi* on various rock samples (i.e., sandstone, carbonate, and clay) has been studied by numerous researchers [121,126–130]. The adsorption isotherms were well-fitted by the Freundlich isotherm and pseudo-second-order kinetic model. Multilayer adsorption of this surfactant on the rock surfaces has also been reported [130]. Based on the kinetic studies, it has been observed that interparticle diffusion is not the rate-controlling process, and

Table 2.6. Plant-based natural surfactants used in the EOR process

Surfactant derived from	Surfactant type	Chemical additives	Oil type	IFT (mN m^{-1})	Rock	Wettability (°)	Core flooding (% OOIP)	Reference
Ziziphus spina-christi (cedar)	Nonionic	–	Kerosene	48 to 9	–	–	–	[120]
		–	Crude oil	31.6 to 5.5	Sandstone	160 to 83 (at 8%)	–	[122,131]
		–	Crude oil	3.2 (at 5 wt. %)	–	–	15	[119]
		–	Crude oil	33 to 11	Carbonate	–	19–45	[132]
		Nano-silica	Kerosene	9.7 (at 8 wt. %)	Carbonate		26–28	[133]
Mulberry	Nonionic	–	Kerosene	43.9 to 17.9	Carbonate	–	19.6	[118]
	Nonionic	–	Crude oil	17.5	Glass micromodel	–	11.7	[134]
Matricaria chamomilla	–	–	Kerosene	30.6 to 12.67		–	–	[135]
Jatropha oil	Anionic	–	Heptane, decane, and dodecane	0.002, 0.004, and 0.005 for heptane–, decane–, and dodecane–water interface, respectively	Sandpack	117.6 to 24.9	30	[112]

Soapnut	Anionic	Guar gum	–	–	Sandpack	–	15–24	[136]
		–	Crude oil	18 to 3.5	–	–	–	[137]
		Partially hydrolyzed polyacrylamide (HPAM)	Crude oil	13–0.002	Sandstone	83.5 to 20.8 (at CMC, i.e., 8000 mg dm^{-3})	30	[116]
		–	Heptane, decane, and dodecane	0.13, 0.1, and 0.07 for heptane–, decane–, and dodecane–water interface, respectively (at 9.2 mol m^{-3})	–	–	–	[117]
Palm oil	Anionic	–	Crude oil	0.001 (at CMC, i.e., 8000 mg dm^{-3})	Carbonate and quartz	1. Carbonate 82.5 to 20.7 2. Quartz 80.3 to 17.3 (at CMC, i.e., 8000 mg dm^{-3})	25–27	[138]
Tribulus terrestris	Nonionic	–	Crude oil	45.3 to 13.5	Carbonate	145.9 to 54.4	26	[139]
Madhuca longifolia	Anionic	HPAM	Crude oil	0.03 (at CMC i.e., 9000 mg dm^{-3} and 353 K)	Sandstone	–	20	[140]
Sunflower oil	Gemini	–	Crude oil	0.32 (at 303 K) 0.12 (at 323 K) 0.09 (at 343 K)	–	–	–	[113,141]

boundary layer diffusion is also responsible for the adsorption to some extent [130]. The adsorption of a natural surfactant synthesized from *Glycyrrhiza glabra* on sandstone and carbonate rocks has also been investigated [142,143]. This robust and inexpensive natural surfactant was capable of improving the rock wettability, and it led to an additional 45.92% OOIP [124]. Barati et al. [144] studied the adsorption of a nonionic surfactant derived from *Trigoonella foenum-graecum* on a carbonate rock. The adsorption mechanism and kinetics were well-described by the Langmuir and pseudo-second-order models, respectively.

2.3.4 Mechanistic interaction between surfactant and polymer solution in EOR

As discussed earlier in Section 2.2, the mobility of oil can be controlled by using a polymer. The addition of small amounts of surfactants can modify the viscosity of the aqueous polymer solution (see Figure 2.8). When a polymer is associated with surfactant flooding, it can control the mobility at the lower IFT. Unlike the surfactant, the existence of polymer generally does not decrease residual oil saturation, except for some special instances. However, it greatly increases the sweep efficiency. Whenever the mobility ratio is high, and the reservoir heterogeneity is harsh, polymer flooding may be more helpful [1]. It has been reported that the interactions between the polymer and surfactant lead to the formation of association structures [16,26]. Such association structures alter the solution and interfacial properties. The interaction between surfactant and polymer depends on the molecular structures of the two compounds and the electric charge on one or both of them [145,146]. In general, the coexistence of the polymer and surfactant molecules modify the adsorption characteristics at the solid–liquid interfaces, liquid–liquid IFT, rheological properties of the solutions, stability of colloidal dispersions, and solubilization capacity in water for the sparingly soluble molecules [147–149]. The molecular features controlling the surfactant–polymer interaction are the steric interactions between the surfactant head groups and the polymer segments, the shielding of the micelle–water contact by the polymer, and the hydrophobicity of the polymer [150]. The

presence of the polymer reduces the CMC of surfactant due to the decrease in size of the spherical micelles and allows the formation of rod-like micelles.

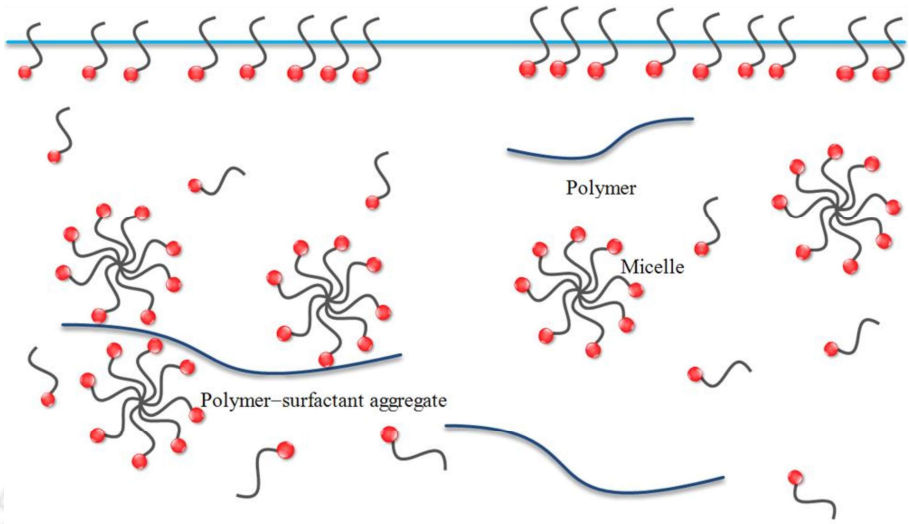

Figure 2.8. Schematic diagram of the formation of a polymer–surfactant aggregate.

The morphologies of the association complexes depend on the molecular properties of the polymer and the surfactant. To understand the morphologies of the association complexes and to estimate the size of the polymer-bound micelles, nuclear magnetic resonance (NMR) [151], neutron scattering [152], and fluorescence spectroscopy [153] have been used. Various classical techniques such as dialysis [154], measurement of surface tension [155,156], viscosity [52], electrical conductivity [155], dye solubilization [157,158], and specific ion activity [159,160] have been employed to study the extent of surfactant association with the polymer molecules.

For developing a systematic understanding of the polymer–surfactant interactions, it is necessary to consider the structural models of polymer–surfactant aggregates that may form in aqueous solutions. Khan et al. [98] studied the interaction between polymer and surfactant and its influence on the physicochemical properties of the aqueous solution. It was found that the behavior of surfactant–polymer interaction depended on both the surfactant and polymer concentrations. The interaction between the anionic surfactant and the nonionic polymer was

much more than any other polymer–surfactant combination [147]. Usually, the surface tension of surfactant solutions increased in the presence of polymers, and it increased with increasing polymer concentration. The interaction between the polymer and surfactant began after the critical aggregation concentration (CAC) and above the polymer saturation point, after which there was no additional change of surface tension and conductivity of the solution.

It has been observed that the presence of salt decreases the CMC of ionic surfactants [161,162]. For a surfactant–polymer system, CAC also decreased radically in the presence of salt, indicating that the association started at a much lower concentration of the surfactant [148], which eventually resulted in a significant reduction of the surface tension of the solution. Such a decrease in surface tension was possibly due to the increased binding ability between the surfactant and polymer in the presence of salt. Suksamranchit and Sirivat [100] reported that the development of micelles and surfactant–polymer complexes were promoted in salt solutions of higher ionic strength. This is due to the reduction in the electrostatic repulsion between the ionic surfactant head groups, which stabilize the surfactant micelle structure. Mya et al. [8] have reported a strong interaction between the polymers and anionic surfactants. Cationic surfactants, on the other hand, were less interactive with polymers than the anionic surfactants. The interaction between an uncharged polymer and a nonionic surfactant was found to be very weak.

To achieve electroneutrality, a charged surface is surrounded by the counterions. According to Kronberg et al. [163], the formation of micelles and adsorption of surfactant on the surface of a polymer is due to the effect of entropy, or a combination of the electrostatic forces and entropy. A low entropy corresponds to the case when these counterions do not move freely in the solution. Conversely, the highest entropy may be achieved when the counterions are consistently dispersed in the solution. Kronberg et al. [163] further debated that the electrostatic forces are not solely responsible for the formation of the polymer–surfactant

complex inasmuch as electrostatic interaction already exists between the polymer and surfactant. However, the release of counterions from both the polymer surface and surfactant promotes the formation of the surfactant–polymer complex. The addition of salt to such systems reduces the driving force for complex formation, and hence, rheological properties get affected dramatically.

2.3.5 Rheological behavior of surfactant–polymer (SP) combinations for EOR

The presence of surfactant has a significant effect on the viscosity of the polymer solution. Zhang et al. [102] have investigated the interfacial rheology of the PAM–surfactant systems. Their results indicate the dependence of interfacial viscosity on shear rate. Interestingly, the interfacial viscosity decreased with the increasing concentration of the ionic surfactant. Generally, as the surfactant concentration is increased, more surfactant molecules are concentrated at the oil–water interface, as predicted by the Gibbs adsorption equation. This increase in the surfactant concentration at the interface increased the interfacial viscosity. However, the interfacial viscosity was found to be unchanged with the concentration of nonionic surfactant. The interfacial viscosity decreased with shear rate, implying the formation of a structure at the oil–water interface. The structure was destroyed at a higher shear rate. In a similar work, Lyu et al. [164] have investigated the rheology of a dispersed particle gel in association with tetradecyl hydroxyl sulfo betaine (a surfactant) at the oil–water interface.

Cairns et al. [165] studied the rheological properties of the film at the crude oil–water interface using a biconical bob rheometer. They observed that the interfacial shear viscosity increased with the aging of the film. Zhou et al. [166] studied the rheology of the film formed at the oil–water interface where silica nanoparticles were adsorbed, and they correlated the rheological properties with the emulsion stability. Anseth et al. [167] studied the rheology of a film formed by a polymeric surfactant at the silicon oil–water interface. Interestingly, the chemical additives accumulated at the interface in such a way that the solid particles in the

Pickering emulsion developed a solid-like network. Eventually, it enhanced the stability of the emulsion by resisting coalescence. Rane et al. [168] examined the rheological properties of the asphaltenes adsorbed at the oil–water interface. They explained the adsorption by using the Langmuir equation of state.

Supee and Idris [103] investigated the effects of surfactant–polymer formulation and variation of salinity on oil recovery. They found that the viscosity of the surfactant–polymer formulation increased with increasing HPAM concentration, and the IFT decreased with increasing concentration of the surfactant. The increase in salinity decreased the viscosity and increased the IFT of the surfactant–polymer formulation. Samanta et al. [24] found that the apparent viscosity of HPAM reduced with increasing concentration of the anionic surfactant, sodium dodecyl sulfate (SDS). This might be due to the physical as well as the chemical interaction between SDS and HPAM, which affected the viscosity of HPAM through the charge-shielding mechanism. In another study, Chen et al. [169] compared the performance of HPAM in association with numerous types of surfactants (i.e., anionic, cationic, and nonionic) for EOR. The η_0 of 2 g dm^{-3} HPAM was found to be increasing with the addition of SDS (an anionic surfactant) and dodecyl glucopyranoside (a nonionic surfactant). This is mainly due to the interaction of the surfactant molecules with the hydrophobic part of HPAM. This leads to the formation of an association structure between the surfactant and polymer, which further enhanced the viscosity of the polymer solution [170]. However, further increment in the surfactant concentration can disrupt the association structure. Therefore, as the concentration of these surfactants reached 0.5 mol m^{-3}, a noteworthy reduction in η_0 was observed (see Figure 2.9). DTAB (a cationic surfactant), on the other hand, had a minor impact on the HPAM. The η_0 for the HPAM–DTAB solution was constant at low surfactant concentration. However,

as the concentration increased, η_0 was observed to be decreasing, which was possibly because of the electrostatic attraction between HPAM and DTAB.

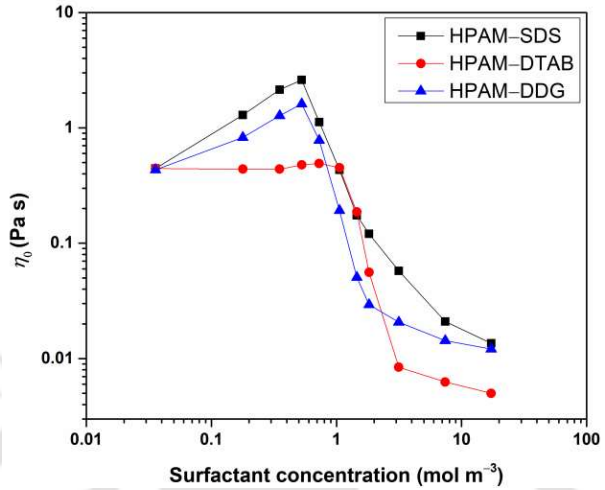

Figure 2.9. Variation of the η_0 of aqueous HPAM solutions with surfactant concentration (at 298 K) [169]. [adapted by American Chemical Society, © 2021].

Nedjhioui et al. [104] investigated the combined effects of XG, SDS, and salt on the XG–SDS system. They observed an increase in the viscosity of the aqueous solution of XG in the presence of SDS. This might be due to the strong interaction of the surfactant with a hydrophobic group of the polymer that led to the formation of an association structure between the polymer chains, which increased the viscosity. However, this interaction may vary with the type of surfactant. These authors also that the surface tension decreased with the increasing concentrations of XG and SDS. The effect of salt is very important inasmuch as it is responsible for the reduction of surface tension of the mixture. It is a consequence of the reduction in the electrostatic repulsion between the charged head groups adsorbed at the interface [171]. Sveistrup et al. [172] have studied the influence of nonionic surfactant (i.e., Tween 80) on the XG–SDS system. They observed that the reduction in the rheological properties of XG–SDS–Tween 80 system was due to the complex interactions, which directly affected the helical structure of XG. Unlike the SDS, SDS–Tween 80 weakens the backbone of XG, which eventually reduces the performance of the polymer in EOR. Hosseini-Nasab et al. [173]

investigated a novel polymer-free surfactant–glycerol system for EOR. In their study, AOS and a polymeric fluorocarbon ester were used as the surfactants. It was observed that glycerol acted as a viscosifier effectively, and the surfactant reduced the IFT. The glycerol–surfactant system has the potential to be utilized in EOR. Nevertheless, further studies need to be carried out under certain reservoir conditions such as high temperature, high salinity, and low permeability.

2.4 Alkali–surfactant–polymer (ASP) flooding

One significant mechanism of ASP flooding is the formation of soap *in situ* by the reaction of alkali with naturally available organic acids present in the crude oil. It further acts synergistically with the surfactant, which produces ultralow IFT, increases the capillary number, and enhances the microscopic displacing efficiency [1,16,67]. Crude oils present in different reservoir rocks can lead to varied behaviors when they contact alkali under dissimilar environmental conditions (such as different temperatures, salinity, hardness, and pH). However, the researchers have converged to the point that the acidic components in the crude oil are the most important factors for alkali flooding. Some alkalis used by various workers for EOR are summarized in Table 2.7.

Chen et al. [174] made a comparative study between inorganic and organic alkali–polymer flooding in which they reported that the addition of inorganic alkali reduced the viscosity of polymer while the organic alkali increased the same. Li et al. [175] have found that the IFT reached its minimum for the surfactant–polymer–organic alkali systems at an optimum electrolyte concentration. The chemicals involved in ASP flooding are expensive and have a great impact on the environment. This could be overcome by proper detection and re-injection of the product chemical slug. Wang and Gu [176] have developed numerous methodologies for the detection of chemical concentration in the product slug. It has been observed from the core flood experiments that re-injected chemicals could deliver 8–20% of oil effectively.

Table 2.7. Alkalis used for the application of EOR

Alkali	Nature	Advantages and Disadvantages	Reference
Sodium hydroxide	Inorganic	• Low cost, easily available, good IFT reduction, good recovery, fair water wetness, and fair sweep improvement • Poor minimization of surfactant adsorption, high consumption, scaling as well as corrosion problems	[177,178]
Sodium carbonate	Inorganic	• Economic, low consumption, fair minimization of surfactant adsorption, fair sweep improvement, fair recovery, and fair IFT reduction • Scaling and corrosion problems	[179,180]
Ethylene-diamine	Organic	• Along with polymer, oil recovery increases • No scaling or corrosion problem	[174,181,182]
Sodium orthosilicate	Inorganic	• Best IFT reduction, moderate consumption • Best minimization of surfactant adsorption, water wetness, sweep improvement, and recovery • Costly	[183]
Ammonia	Inorganic	• Low requirement, low surfactant adsorption, and high recovery • Health, safety, and environmental issues need to be studied in detail	[184]

2.4.1 Interaction between alkali, surfactant, and polymer solutions

The interactions between acidic crude oil and alkali have been investigated by determining their physicochemical properties [185]. The presence of the carboxylic acid group in the crude oil was confirmed by FTIR. This group is responsible for the formation of surfactant *in situ* after interaction with an alkali. The presence of an alkali increases the pH, which helps to improve wettability during the flooding processes [186]. Ramakrishnan and Wasan [187] found that the IFT between oil and water was sensitive to both sodium hydroxide concentration and salinity. Depending on the rock mineralogy, alkali can interact with the reservoir rock in several ways, which includes surface exchange and hydrolysis, congruent and incongruent dissolution, and formation of insoluble salt by reaction with the ions, which cause hardness in the fluid and those exchanged from the rock surface [188].

2.4.2 Influence of alkali on the rheological properties of surfactant–polymer solution

An alkali can modify the viscosity of polymer solutions in two ways. Firstly, alkali releases cations in the polymer solution, and these cations can reduce the polymer viscosity due to the charge-shielding mechanism. Secondly, an alkali can hydrolyze the amide groups on the polymer chain (base hydrolysis) [24]. The viscosity of alkali–polymer solutions depends on the alkali type, concentration, and time after initial mixing [168]. It has been reported that the viscosity of alkali–polymer solutions is decreased by the addition of sodium chloride and anionic surfactants [8,9,102,189,190].

Ma and Xia [191] carried out a detailed study to determine the effect of the rheological properties of the ASP system on the rate of residual oil recovery after water flooding. Although the viscosity of ASP system was found to decrease, yet the total recovery rate was uplifted to 94%. Bataweel and Nasr-El-Din [192] studied the rheological properties of various combinations of synthetic ASP solutions. They found an increase in the viscosity of the ASP

system in the presence of a betaine-based zwitterionic surfactant. In contrast, alpha-olefin sulfonate, which is an anionic surfactant, caused a decline in the same. The oscillation shear test confirmed the dominating behavior of G' over G''. This confirmed the elastic behavior of the respective ASP systems. Lei et al. [193] studied the rheological behavior of an ASP/oil emulsion in porous media. The rheological behavior of the emulsion exhibited macroscopic flow adjustment for regions of varying permeability with reference to the two-dimensional positive rhythm geological model. This geological model is categorized into three layers in the vertical direction. Generally, each layer has a thickness of 5 m with a permeability variation coefficient of 0.75. Usually, water is first injected till its saturation attains 90%, which results in the formation of a high permeability zone in the production zone. Considering high oil saturation after water flooding, the next step is chemical flooding by keeping continued water injection in the production zone.

Cao et al. [194] developed a model for the rheological behavior of crude oil and ASP emulsion. Their study highlighted the rheological behavior, IFT, and stability mechanism of the ASP and oil emulsion. The stability and viscosity of the oil emulsion with the ASP solution were found to be high at the higher concentrations of the surfactant. Polymer, on the other hand, was responsible for the stability of the oil–water emulsion inasmuch as it reduced collision of the droplets in the emulsion. Hou et al. [178] studied the role of viscoelasticity of ASP solutions in EOR. They have reported that viscoelasticity plays a beneficial role in improving the sweeping of the residual oil from the trapped zone. The G', G'' and relaxation time decreased with increasing alkali concentration, whereas an increase in the IFT was observed at the lower concentration of alkali.

2.4.3 Alkali-free surfactant–polymer system for EOR

The use of alkali in EOR is debatable because of various demerits of alkalis, as discussed in Table 2.7. They are of corrosive nature and have various hazardous effects on the environment.

Hongyan et al. [195] carried out a study on the development and application of dilute surfactant–polymer (SP) flooding setup for the Shengli oil field (in the People's Republic of China). In order to overcome the drawbacks associated with ASP flooding, an alkali-free SP flooding technology was developed, and its application in the Shengli oil field was extensively investigated. Alkali-free system was favorable for the polymer to increase viscosity, thereby reducing the amount of polymer needed for the system. Zhang et al. [196] developed a novel betaine surfactant from fatty acid for alkali-free SP combination flooding. This surfactant had long-term stability at high salinity, temperature, and low permeability, in which it managed to maintain ultra-low IFT. Alkali-free surfactant-polymer flooding can avoid scaling, strong emulsification, and corrosion caused by the alkali, thus reducing the investment and operating costs [197].

2.5 Chemical additive injection in pilot plant and/or actual oil field

As a result of the unfavorable mobility ratio in primary and secondary methods, several oil fields have adopted the ASP method of EOR. Injection of surfactant, alkali, polymer, and combination of these chemical additives can expand oil recovery in a cost-efficient way. Beneficial performance of the mobility control agent, IFT reduction capability, wettability modification, and flow through porous media are some of the important factors, which need to be considered for effective EOR. Countries like China, the USA, Russia, and India have already adopted the ASP method. Numerous factors such as selection of chemical additives, phase behavior analysis, rheological studies, and core flooding analysis guide the operations in the EOR method. The Daqing field (in the People's Republic of China) is the major oil field where the ASP method was successfully implemented in 1984. In the initial stage, the oil production rate was increased by three times after injecting the polymer.

India has adopted the chemical method in the Sanand (Gujarat) oilfield. Here, field-scale polymer flooding has been practiced for the last twelve years. Considering the high mobility contrast and poor recovery of ~15% OOIP under depletion drive, polymer flooding was adopted as an EOR in this field [198]. The first major oil discovery in the Barmer Basin of India was made in the Mangala field (Rajasthan). In this field, the initial water injection phase has been completed, and the injection of polymer slug is in progress. The polymer flood will be followed by ASP injection for further evaluation of chemical EOR potential [199]. The importance of EOR in the Mangala oilfield was realized soon after its discovery. As the recovery was low using the primary method of oil recovery, the ASP chemical method was taken into consideration. Extensive screening and laboratory and simulation studies have been carried out, all of which have established that chemical EOR using polymer or ASP processes has significant potential to increase the recovery in this oilfield [200]. As the recovery was less using the primary method of oil recovery, adaptation of the ASP chemical method was taken into consideration. Using this method, an ultimate recovery of 59.1% was obtained at the North Gujarat oilfield [201]. Recently, a study examined the effect of micellar–polymer flooding through the porous media of two depleted oilfields in the Bhogpara and Nahorkatiya basins (Assam, India). Black liquor, which is used as the micelle or surfactant along with the polymer, released much of the oil trapped in the rock, and hence the recovery was enhanced [202]. Table 2.8 discusses some of the major successful pilot/field implementations of the chemical method of EOR worldwide.

Table 2.8. Successful pilot/field implementation of the chemical method of EOR

Oil field	Country	Alkali	Surfactant	Polymer	Oil recovery (OOIP)	References
Cambridge	USA	Na_2CO_3	Petrostep B-100[1]	PAM	28.1%	[203–205]
Daqing	China	NaOH and Na_2CO_3	Petroleum sulfonate, linear heavy alkylbenzene sulfonate, and HABS	HPAM	18–25%	[203,205]
Gudong	China	Na_2CO_3	CY1, OP10	HPAM	13.4%	[206,207]
Jhalora	India	Na_2CO_3	Petroleum sulfonate	PAM	23%	[208]
Kalol	India	Na_2CO_3	Petroleum sulfonate	HPAM	7.4%	[209]
Karamay	China	Na_2CO_3	Petroleum sulfonate	HPAM	12%	[210,211]
Mangala	India	NaOH and Na_2CO_3	ORS	Flopaam[2] and Alcoflood[3]	15%	[199,212,213]
Mannville B	Canada	NaOH	ORS-97HF	Flopaam[2]	11.1%	[214]
Southwest Saskatchewan	Canada	NaOH and Na_2CO_3	Petroleum sulfonic acids	PAM	39.1%	[215]
Tanner	USA	NaOH	ORS-41HF	Alcoflood	17%	[216]
Viraj	India	Na_2CO_3	Petroleum sulfonate	HPAM	18%	[217,218]
West Kiehl	USA	Na_2CO_3	Petrostep B-100[1]	Pusher 7000[4]	51.1%	[219,220]
West Salym	Russia	Na_2CO_3	IOS	Flopaam[2]	15–20%	[221,222]

[1]Petrostep B-100 is a petroleum sulfonate supplied by Stepan Chemical (USA); [2] Flopaam is an HPAM manufactured by SNF Floerger (France); [3] Alcoflood is a PAM copolymer manufactured and supplied by BASF (Germany); [4] Pusher 7000 is a PAM supplied by Dow Chemical (USA).

2.6 Economics

The cost of chemical additives and crude oil plays a vital role in the effective cost of EOR. Around 4622 million tons of oil were consumed across the world as a primary fuel in the year 2017 [223]. It is remarkable to note that the chemical method of EOR is more economical than the traditional methods. Numerous noteworthy progress has been achieved, and more desirable chemical additives have been developed to achieve such a massive oil requirement [224]. Proper selection of chemical additives (based on the screening criteria) and the optimum quantity to be injected in the reservoir (based on the pilot plant and/or core flooding experiments) can control the cost of production of oil [225]. However, the cost of chemical additives and the time of production can be uncertain [226].

An effective EOR process can be classified into two models, i.e., based on performance and economics. The performance model collects inputs such as the reservoir topography and the oil properties, depending on the strategies, selection of chemical additives, and injectivity. On the other hand, the economics model comprises several costs such as drilling, surface equipment, operating expenses, surface maintenance, monitoring, and verification. It also considers the technical cost [227]. From these two models together, the profitability of flooding can be calculated by the net present value and return on investment [228]. It is interesting to observe that SP flooding is more effective than ASP flooding in terms of the net present value [229].

The economic analysis gives a thorough understanding to regulate any fundamental restriction, which can eventually direct future developments [230]. In any case, the availability, aptness, and economic feasibility of chemical additives must be carefully considered in the early stage of the EOR project. The commencement of the EOR project depends on funding, risk, management, tax, and government policies [231].

Nomenclature

c	dimensionless constant
E_{do}	displacement efficiency
G'	storage modulus, Pa
G''	loss modulus, Pa
K	consistency factor, mPa s
n	flow behavior index
S_{oi}	initial oil saturation
S_{or}	residual oil saturation
t	time, s
t_c	characteristic time of flow system, s

Greek letters

α	rheological parameter
$\dot{\gamma}$	rate of strain, s^{-1}
λ_1, λ_2	relaxation time, s
λ', λ'', λ_s	time constants, s
η	viscosity, mPa s
η_0	zero-shear viscosity, mPa s
η_i	initial-time viscosity, mPa s
$\eta_{\inf}$	infinite-time viscosity, mPa s
η_∞	infinite-shear viscosity, mPa s
$\Delta\eta', \Delta\eta''$	viscosity deficits, mPa s

τ	stress, Pa
τ_0	yield stress, Pa
$\tau_{1/2}$	stress when $\eta = \eta_0/2$, Pa

Abbreviation

ASP	alkali–surfactant–polymer
CAC	critical aggregation concentration
CMC	critical micelle concentration
CTAB	cetyltrimethylammonium bromide
DTAB	dodecyltrimethylammonium bromide
EOR	enhanced oil recovery
HPAM	partially hydrolyzed polyacrylamide
IFT	interfacial tension
OOIP	original oil in place
PAM	polyacrylamide
SDS	sodium dodecyl sulfate
SP	surfactant polymer

References

[1] Lake LW, Venuto PB. A niche for enhanced oil recovery in the 1990s. Oilfield Rev J 1992;4:55–61.

[2] Green DW, Willhite GP. Enhanced oil recovery. Society of Petroleum Engineers: Richardson, Texas, USA, 1998.

[3] Sastry N, Dave P, Valand M. Dilute solution behaviour of polyacrylamides in aqueous media. European Polym J 1999;35:517–25.

[4] Raffa P, Broekhuis AA, Picchioni F. Polymeric surfactants for enhanced oil recovery: A review. J Pet Sci Eng 2016;145:723–33.

[5] Yandita R, Hartanti A, Abidin A, Noezar I. Reaction Condition Optimalization To Improve Superabsorbent Polymer Composite Absorbancy. International Conference on Innovation in Polymer Science and Technology. 1 December 2011; Bali, Indonesia.

[6] Sorbie KS. Polymer-Improved oil recovery. CRC Press: Boca Raton, Florida, USA, 1991.

[7] Wever DAZ, Picchioni F, Broekhuis AA. Polymers for enhanced oil recovery: A paradigm for structure–property relationship in aqueous solution. Prog Polym Sci 2011;36:1558–628.

[8] Mya KY, Jamieson AM, Sirivat A. Interactions between the nonionic surfactant and polyacrylamide studied by light scattering and viscometry. Polymer 1999;40:5741–9.

[9] Wang L, Tiu C, Liu T. Effects of nonionic surfactant and associative thickener on the rheology of polyacrylamide in aqueous glycerol solutions. Colloid Polym Sci 1996;274:138–44.

[10] Sorbie K, Clifford P, Jones E. The rheology of pseudoplastic fluids in porous media using network modeling. J Colloid Interface Sci 1989;130:508–34.

[11] Abbas S, Sanders AW, Donovan JC. Applicability of hydroxyethylcellulose polymers for chemical EOR. SPE Enhanced Oil Recovery Conference. 2–4 July 2013; Kuala Lumpur, Malaysia.

[12] Cao R, Cheng L, Lian P. Flow behavior of viscoelastic polymer solution in porous media. J Dispersion Sci Technol 2015;36:41–50.

[13] Davidson RL. Handbook of water-soluble gums and resins. McGraw-Hill: New York, USA, 1980.

[14] Rochefort WE, Middleman S. Rheology of xanthan gum: Salt, temperature, and strain effects in oscillatory and steady shear experiments. J Rheol 1987;31:337–69.

[15] Song KW, Kuk HY, Chang GS. Rheology of concentrated xanthan gum solutions: Oscillatory shear flow behavior. Korea-Australia Rheol J 2006;18:67–81.

[16] Olajire AA. Review of ASP EOR (alkaline surfactant polymer enhanced oil recovery) technology in the petroleum industry: Prospects and challenges. Energy 2014;77:963–82.

[17] Pu W, Shen C, Wei B, Yang Y, Li Y. A comprehensive review of polysaccharide biopolymers for enhanced oil recovery (EOR) from flask to field. J Ind Eng Chem 2018;61:1–11.

[18] Abidin A, Puspasari T, Nugroho W. Polymers for enhanced oil recovery technology. Procedia Chem 2012;4:11–6.

[19] Ghoumrassi-Barr S, Aliouche D. A rheological study of xanthan polymer for enhanced oil recovery. J Macromol Sci, B 2016;55:793–809.

[20] Ghannam MT, Esmail MN. Rheological properties of aqueous polyacrylamide solutions. J Appl Poly Sci 1998;69:1587–97.

[21] Lewandowska K. Comparative studies of rheological properties of polyacrylamide and partially hydrolyzed polyacrylamide solutions. J Appl Poly Sci 2007;103:2235–41.

[22] Song KW, Kim YS, Chang GS. Rheology of concentrated xanthan gum solutions: Steady shear flow behavior. Fibers Polym 2006;7:129–38.

[23] Choppe E, Puaud F, Nicolai T, Benyahia L. Rheology of xanthan solutions as a function of temperature, concentration and ionic strength. Carbohydr Polym 2010;82:1228–35.

[24] Samanta A, Bera A, Ojha K, Mandal A. Effects of alkali, salts, and surfactant on rheological behavior of partially hydrolyzed polyacrylamide solutions. J Chem Eng Data 2010;55:4315–22.

[25] Kamal MS, Sultan AS, Al-Mubaiyedh UA, Hussein IA. Review on polymer flooding: Rheology, adsorption, stability, and field applications of various polymer systems. Polym Rev 2015;55:491–530.

[26] Sheng J. Modern chemical enhanced oil recovery: Theory and practice. Gulf Professional Publishing: Massachusetts, USA, 2010.

[27] Mohammadi S, Maghzi A, Ghazanfari M, Masihi M, Mohebbi A, Kharrat R. On the control of glass micro-model characteristics developed by laser technology. Energy Sources, A 2013;35:193–201.

[28] Luo J, Liu Y, Zhu P. Polymer solution properties and displacement mechanisms. Enhanced oil recovery–polymer flooding. Beijing, China: Petroleum Industry Press; 2006, p. 1-72.

[29] Ait-Kadi A, Carreau P, Chauveteau G. Rheological properties of partially hydrolyzed polyacrylamide solutions. J Rheol 1987;31:537–61.

[30] Song K, Chang G, Kim C, Lee J, Paik J. Rheological characterization of aqueous poly (ethylene oxide) solutions (I): Limits of linear viscoelastic response and nonlinear behavior with large amplitude oscillatory shear deformation. J Korean Fiber Soc 1996;33:1083–93.

[31] Isono Y, Ferry JD. Stress relaxation and differential dynamic modulus of polyisobutylene in large shearing deformations. J Rheol 1985;29:273–80.

[32] Hyun K, Kim SH, Ahn KH, Lee SJ. Large amplitude oscillatory shear as a way to classify the complex fluids. J Non-Newtonian Fluid Mech 2002;107:51–65.

[33] Kreiba A. The rheological properties of aqueous polyacrylamide solutions. Masters' Thesis. Department of Mechanical Engineering, Concordia University, Quebec, Canada: 2000.

[34] Wientjes RH, Duits MH, Jongschaap RJ, Mellema J. Linear rheology of guar gum solutions. Macromolecules 2000;33:9594–605.

[35] Xu L, Dong M, Gong H, Sun M, Li Y. Effects of inorganic cations on the rheology of aqueous welan, xanthan, gellan solutions and their mixtures. Carbohydr Polym 2015;121:147–54.

[36] Xu L, Gong H, Dong M, Li Y. Rheological properties and thickening mechanism of aqueous diutan gum solution: Effects of temperature and salts. Carbohydr Polym 2015;132:620–9.

[37] Xu L, Xu G, Liu T, Chen Y, Gong H. The comparison of rheological properties of aqueous welan gum and xanthan gum solutions. Carbohydr Polym 2013;92:516–22.

[38] Hamcerencu M, Desbrieres J, Popa M, Riess G. Stimuli-sensitive xanthan derivatives/N-isopropylacrylamide hydrogels: Influence of cross-linking agent on interpenetrating polymer network properties. Biomacromol 2009;10:1911–22.

[39] Maruyama Y, Mikami B, Hashimoto W, Murata K. A structural factor responsible for substrate recognition by bacillus sp. GL1 xanthan lyase that acts specifically on pyruvated side chains of xanthan. Biochem 2007;46:781–91.

[40] Moreira AS, Coimbra MA, Nunes FM, Simoes J, Domingues MRM. Evaluation of the effect of roasting on the structure of coffee galactomannans using model oligosaccharides. J Agric Food Chem 2011;59:10078–87.

[41] Paul F, Morin A, Monsan P. Microbial polysaccharides with actual potential industrial applications. Biotechnol Adv 1986;4:245–59.

[42] Behari K, Pandey P, Kumar R, Taunk K. Graft copolymerization of acrylamide onto xanthan gum. Carbohydr Polym 2001;46:185–9.

[43] Chagas BS, Machado DL, Haag RB, De Souza CR, Lucas EF. Evaluation of hydrophobically associated polyacrylamide-containing aqueous fluids and their potential use in petroleum recovery. J Appl Poly Sci 2004;91:3686–92.

[44] da Silva DA, de Paula RC, Feitosa JP. Graft copolymerisation of acrylamide onto cashew gum. Eur Polym J 2007;43:2620–9.

[45] Maia AM, Silva HV, Curti PS, Balaban RC. Study of the reaction of grafting acrylamide onto xanthan gum. Carbohydr Polym 2012;90:778–83.

[46] Tako M, Sakae A, Nakamura S. Rheological properties of gellan gum in aqueous media. Agric Biol Chem 1989;53:771–6.

[47] Gao C. Application of a novel biopolymer to enhance oil recovery. J Pet Explor Prod Technol 2016;6:749–53.

[48] Leonhardt B, Ernst B, Reimann S, Steigerwald A, Lehr F. Field testing the polysaccharide schizophyllan: results of the first year. SPE Improved Oil Recovery Symposium. 12–16 April 2014; Tulsa, Oklahoma, USA.

[49] Gastone F, Tosco T, Sethi R. Guar gum solutions for improved delivery of iron particles in porous media (Part 1): Porous medium rheology and guar gum-induced clogging. J Contam Hydrol 2014;166:23–33.

[50] Kaur V, Bera MB, Panesar PS, Kumar H, Kennedy J. Welan gum: Microbial production, characterization, and applications. Int J Biol Macromol 2014;65:454–61.

[51] Duda JL, Hong SA, Klaus EE. Flow of polymer solutions in porous media: inadequacy of the capillary model. Ind Eng Chem Fundam 1983;22:299–305.

[52] Kulicke WM, Haas R. Flow behavior of dilute polyacrylamide solutions through porous media. 1. Influence of chain length, concentration, and thermodynamic quality of the solvent. Ind Eng Chem Fundam 1984;23:308–15.

[53] Darcy H. Les fontaines publiques de la ville de Dijon. Dalmont: Paris, France, 1856.

[54] Sochi T. Non-Newtonian flow in porous media. Polymer 2010;51:5007–23.

[55] Durst F, Haas R, Kaczmar B. Flows of dilute hydrolyzed polyacrylamide solutions in porous media under various solvent conditions. J Appl Polym Sci 1981;26:3125–49.

[56] Macosko CW. Rheology: Principles, measurements, and applications. Wiley: New Jersey, USA, 1996.

[57] Carreau PJ. Rheological equations from molecular network theories. Trans Soc Rheol 1972;16:99–127.

[58] Herschel WH, Bulkley R. Consistency measurements of gum benzene solutions. Colloid J 1926;39:291–300.

[59] Larson RG. The structure and rheology of complex fluids. Oxford University Press New York, USA, 1999.

[60] Oldroyd JG. On the formulation of rheological equations of state. Proc Roy Soc, A 1950;200:523–41.

[61] Godfrey J. Steady shear measurement of thixotropic fluid properties. Rheol Acta 1973;12:540–5.

[62] Healy RN, Reed RL, Stenmark D. Multiphase microemulsion systems. SPE J 1976;16:147–60.

[63] Hirasaki GJ, Miller CA, Puerto M. Recent advances in surfactant EOR. SPE J 2011;16:889–907.

[64] Iglauer S, Wu Y, Shuler P, Blanco M, Tang Y, Goddard III W. Alkyl polyglycoside surfactants for improved oil recovery. SPE/DOE Symposium on Improved Oil Recovery. 17–21 April 2004; Tulsa, Oklahoma, USA.

[65] Iglauer S, Wu Y, Shuler P, Tang Y, Goddard WA. New surfactant classes for enhanced oil recovery and their tertiary oil recovery potential. J Pet Sci Eng 2010;71:23–9.

[66] Wu J, Xu Y, Dabros T, Hamza H. Effect of EO and PO positions in nonionic surfactants on surfactant properties and demulsification performance. Colloids Surf, A 2005;252:79–85.

[67] Liu S. Alkaline surfactant polymer enhanced oil recovery process. Ph.D. Thesis. Department of Chemical Engineering, Rice University, Houston, Texas, USA: 2008.

[68] Gupta R, Mohanty K. Temperature effects on surfactant-aided imbibition into fractured carbonates. SPE J 2010;15:588–97.

[69] Bashir A, Haddad AS, Rafati R. A review of fluid displacement mechanisms in surfactant-based chemical enhanced oil recovery processes: Analyses of key influencing factors. Pet Sci 2021. doi: 10.1016/j.petsci.2021.11.021.

[70] Kamal MS, Hussein IA, Sultan AS. Review on surfactant flooding: Phase behavior, retention, IFT, and field applications. Energy Fuels 2017;31:7701–20.

[71] Massarweh O, Abushaikha AS. The use of surfactants in enhanced oil recovery: A review of recent advances. Energy Rep 2020;6:3150–78.

[72] Aguilar F, López I, Prieto C, Montes J, Lázaro J, Barrio I, Álvarez E, Rodriguez B. Alkyl aryl sulfonate surfactants for EOR: Scale up from lab to pilot. SPE Improved Oil Recovery Conference. 11–13 April 2016; Tulsa, Oklahoma, USA

[73] Showell M. Powdered detergents. Marcel Dekker: New York, USA, 1997.

[74] Hirasaki GJ, Miller CA, Pope GA. Surfactant based enhanced oil recovery and foam mobility control. Semi Annual Technical Report. Report No.: DE-FC26-03NT15406. Rice University, Houston, Texas, USA: 2005.

[75] Oya M, Takemoto Y, Ishikawa Y. Large decrease in acute aquatic toxicity of linear alkylbenzene sulfonate in hard water and seawater by adding adsorbent. J Oleo Sci 2008;57:15–21.

[76] Tichelkamp T, Hosseinzade Khanamiri H, Nourani M, Åge Stensen J, Torsæter O, Øye G. EOR potential of mixed alkylbenzenesulfonate surfactant at low salinity and the effect of calcium on "optimal ionic strength". Energy Fuels 2016;30:2919–24.

[77] Hai M, Han B. Study of interaction between sodium dodecyl sulfate and polyacrylamide by rheological and conductivity measurements. J Chem Eng Data 2006;51:1498–501.

[78] Mahdavi S, Aalaie J, Miri T, Razavi S, Rahmani M. Study of polyacrylamide–surfactant system on the water–oil interface properties and rheological properties for EOR. Arabian J Chem 2016;10:1136–46.

[79] Aoudia M, Al-Maamari RS, Nabipour M, Al-Bemani AS, Ayatollahi S. Laboratory study of alkyl ether sulfonates for improved oil recovery in high-salinity carbonate reservoirs: A case study. Energy Fuels 2010;24:3655–60.

[80] Carmona I, Schecter R, Wade W, Weerasooriya U. Ethoxylated oleyl sulfonates as model compounds for enhanced oil recovery. SPE J 1985;25:351–7.

[81] Sharma G, Mohanty K. Wettability alteration in high-temperature and high-salinity carbonate reservoirs. SPE J 2013;18:646–55.

[82] Johannessen AM, Spildo K. Enhanced oil recovery (EOR) by combining surfactant with low salinity injection. Energy Fuels 2013;27:5738–49.

[83] Wu Y, Iglauer S, Shuler P, Tang Y, Blanco M, Goddard W. Synergistic effect of alkyl polyglycoside and sorbitan mixtures on lowering interfacial tension and enhancing oil recovery. Am Chem Soc, Div Polym Chem, Prepr 2004;49:208–10.

[84] Fu L, Zhang G, Ge J, Liao K, Pei H, Jiang P, Li X. Study on organic alkali–surfactant–polymer flooding for enhanced ordinary heavy oil recovery. Colloids Surf, A 2016;508:230–9.

[85] Sakthivel S, Velusamy S, Nair VC, Sharma T, Sangwai JS. Interfacial tension of crude oil–water system with imidazolium and lactam-based ionic liquids and their evaluation for enhanced oil recovery under high saline environment. Fuel 2017;191:239–50.

[86] Vikingstad AK, Aarra MG. Comparing the static and dynamic foam properties of a fluorinated and an alpha olefin sulfonate surfactant. J Pet Sci Eng 2009;65:105–11.

[87] Vikingstad AK, Aarra MG, Skauge A. Effect of surfactant structure on foam–oil interactions: Comparing fluorinated surfactant and alpha olefin sulfonate in static foam tests. Colloids Surf, A 2006;279:105–12.

[88] Dang CTQ, Nguyen NTB, Chen Z, Nguyen HX, Bae W, Phung TH. A comprehensive evaluation of the performances of alkaline/surfactant/polymer flooding in conventional and unconventional reservoirs. SPE Asia-Pacific Oil and Gas Conference and Exhibition. 22–24 October 2012; Perth, Australia.

[89] Nguyen NTB, Bae W, Dang CTQ, Ryoo W, Lu V. Effect of alkalis on phase behavior of mixtures between single and double tail anionic surfactants. SPE Asia Pacific Oil and Gas Conference and Exhibition. 20–22 September 2011; Jakarta, Indonesia

[90] Hofman Y, Angstadt H. Analysis of enhanced oil recovery formulations. Chromatographia 1987;24:666–70.

[91] Kathel P, Mohanty KK. EOR in tight oil reservoirs through wettability alteration. SPE Annual Technical Conference and Exhibition. 30 September–2 October 2013; New Orleans, Louisiana, USA.

[92] Brackman JC, Engberts JB. Influence of polymers on the micellization of cetyltrimethylammonium salts. Langmuir 1991;7:2097–102.

[93] Mukherjee I, Sarkar D, Moulik SP. Interaction of gums (guar, carboxymethylhydroxypropyl guar, diutan, and xanthan) with surfactants (DTAB, CTAB, and TX-100) in aqueous medium. Langmuir 2010;26:17906–12.

[94] Saeed R, Usman M, Rasool N, Ahmad M, Khan ZA, Farooqi ZH, Siddiq M, Zahoor AF. Partitioning of thiophene derivatives between solvent and micellar media of cationic surfactant, cetyl trimethyl ammonium bromide. J Mol Liq 2017;240:389–94.

[95] Junquera E, Aicart E. Mixed micellization of dodecylethyldimethylammonium bromide and dodecyltrimethylammonium bromide in aqueous solution. Langmuir 2002;18:9250–8.

[96] Sheng JJ. Surfactant enhanced oil recovery in carbonate reservoirs. Enhanced oil recovery field case studies. Oxford, UK: Gulf Professional Publishing; 2013, p. 281–99.

[97] Torres LL, Chauveau M, Hayes PL. Macromolecular structure of dodecyltrimethylammonium chloride at the silica/water interface studied by sum frequency generation spectroscopy. J Phys Chem C 2015;119:23917–27.

[98] Khan MY, Samanta A, Ojha K, Mandal A. Interaction between aqueous solutions of polymer and surfactant and its effect on physicochemical properties. Asia-Pac J Chem Eng 2008;3:579–85.

[99] Witte FM, Engberts JB. Micelle–polymer complexes: Aggregation numbers, micellar rate effects and factors determining the complexation process. Colloids Surf 1989;36:417–26.

[100] Suksamranchit S, Sirivat A. Influence of ionic strength on complex formation between poly (ethylene oxide) and cationic surfactant and turbulent wall shear stress in aqueous solution. Chem Eng J 2007;128:11–20.

[101] Zhai L, Tan X, Li T, Chen Y, Huang X. Influence of salt and polymer on the critical vesicle concentration in aqueous mixture of zwitterionic/anionic surfactants. Colloids Surf, A 2006;276:28–33.

[102] Zhang J, Wang X, Liu H, Tang J, Jiang L. Interfacial rheology investigation of polyacrylamide–surfactant interactions. Colloids Surf, A 1998;132:9–16.

[103] Supee A, Idris A. Effects of surfactant–polymer formulation and salinities variation towards oil recovery. Arab J Sci Eng 2014;39:4251–60.

[104] Nedjhioui M, Moulai-Mostefa N, Canselier JP, Bensmaili A. Investigation of combined effects of xanthan gum, sodium dodecyl sulphate, and salt on some physicochemical properties of their mixtures using a response surface method. J Dispersion Sci Technol 2009;30:1333–41.

[105] Li Y, Puerto M, Bao X, Zhang W, Jin J, Su Z, Shen S, Hirasaki G, Miller C. Synergism and performance for systems containing binary mixtures of anionic/cationic surfactants for enhanced oil recovery. J Surfact Deterg 2017;20:21–34.

[106] Jia H, Lian P, Leng X, Han Y, Wang Q, Jia K, Niu X, Guo M, Yan H, Lv K. Mechanism studies on the application of the mixed cationic/anionic surfactant systems to enhance oil recovery. Fuel 2019;258:116156.

[107] Li Y, Zhang W, Kong B, Puerto M, Bao X, Sha O, Shen Z, Yang Y, Liu Y, Gu S. Mixtures of anionic/cationic surfactants: A new approach for enhanced oil recovery in low-salinity, high-temperature sandstone reservoir. SPE J 2016;21:1164–77.

[108] Kesarwani H, Saxena A, Mandal A, Sharma S. Anionic/nonionic surfactant mixture for enhanced oil recovery through the investigation of adsorption, interfacial, rheological, and rock wetting characteristics. Energy Fuels 2021;35:3065–78.

[109] Pal N, Vajpayee M, Mandal A. Cationic/nonionic mixed surfactants as enhanced oil recovery fluids: Influence of mixed micellization and polymer association on interfacial, rheological, and rock-wetting characteristics. Energy Fuels 2019;33:6048–59.

[110] Agneta M, Zhaomin L, Chao Z, Gerald G. Investigating synergism and antagonism of binary mixed surfactants for foam efficiency optimization in high salinity. J Pet Sci Eng 2019;175:489–94.

[111] Geng T, Zhang C, Jiang Y, Ju H, Wang Y. Synergistic effect of binary mixtures contained newly cationic surfactant: Interaction, aggregation behaviors and application properties. J Mol Liq 2017;232:36–44.

[112] Pal N, Kumar S, Bera A, Mandal A. Phase behaviour and characterization of microemulsion stabilized by a novel synthesized surfactant: Implications for enhanced oil recovery. Fuel 2019;235:995–1009.

[113] Pal N, Samanta K, Mandal A. A novel family of non-ionic gemini surfactants derived from sunflower oil: Synthesis, characterization, and physicochemical evaluation. J Mol Liq 2019;275:638–53.

[114] Pal N, Saxena N, Laxmi KD, Mandal A. Interfacial behaviour, wettability alteration, and emulsification characteristics of a novel surfactant: Implications for enhanced oil recovery. Chem Eng Sci 2018;187:200–12.

[115] Pal N, Saxena N, Mandal A. Phase behavior, solubilization, and phase transition of a microemulsion system stabilized by a novel surfactant synthesized from castor oil. J Chem Eng Data 2017;62:1278–91.

[116] Saxena N, Kumar A, Mandal A. Adsorption analysis of natural anionic surfactant for enhanced oil recovery: The role of mineralogy, salinity, alkalinity and nanoparticles. J Pet Sci Eng 2019;173:1264–83.

[117] Saxena N, Kumar S, Mandal A. Adsorption characteristics and kinetics of synthesized anionic surfactant and polymeric surfactant on sand surface for application in enhanced oil recovery. Asia-Pac J Chem Eng 2018;13:e2211.

[118] Bachari Z, Isari AA, Mahmoudi H, Moradi S, Mahvelati EH. Application of natural surfactants for enhanced oil recovery–Critical review. World Multidisciplinary Earth Sciences Symposium 2018; Prague, Czech Republic.

[119] Emadi S, Shadizadeh SR, Manshad AK, Rahimi AM, Nowrouzi I, Mohammadi AH. Effect of using *Zyziphus Spina Christi* or Cedr Extract (CE) as a natural surfactant on oil mobility control by foam flooding. J Mol Liq 2019;293:111573.

[120] Pordel Shahri M, Shadizadeh S, Jamialahmadi M. A new type of surfactant for enhanced oil recovery. Pet Sci Technol 2012;30:585–93.

[121] Ahmadi MA, Shadizadeh SR. Adsorption of novel nonionic surfactant and particles mixture in carbonates: Enhanced oil recovery implication. Energy Fuels 2012;26:4655–63.

[122] Saha R, Uppaluri RV, Tiwari P. Impact of natural surfactant (Reetha), polymer (xanthan gum), and silica nanoparticles to enhance heavy crude oil recovery. Energy Fuels 2019;33:4225–36.

[123] Nowrouzi I, Mohammadi AH, Manshad AK. Water–oil interfacial tension (IFT) reduction and wettability alteration in surfactant flooding process using extracted saponin from *Anabasis Setifera* plant. J Pet Sci Eng 2020;189:106901.

[124] Dashtaki SRM, Ali JA, Manshad AK, Nowrouzi I, Mohammadi AH, Keshavarz A. Experimental investigation of the effect of *Vitagnus* plant extract on enhanced oil recovery process using interfacial tension (IFT) reduction and wettability alteration mechanisms. J Pet Explor Prod Technol 2020;10:2895–905.

[125] Nowrouzi I, Mohammadi AH, Manshad AK. Preliminary evaluation of a natural surfactant extracted from *Myrtus communis* plant for enhancing oil recovery from carbonate oil reservoirs. J Pet Explor Prod Technol 2021. doi: 10.1007/s13202-021-01336-6

[126] Ahmadi MA, Galedarzadeh M, Shadizadeh SR. Wettability alteration in carbonate rocks by implementing new derived natural surfactant: Enhanced oil recovery applications. Transp Porous Med 2015;106:645–67.

[127] Ahmadi MA, Shadizadeh SR. Experimental investigation of adsorption of a new nonionic surfactant on carbonate minerals. Fuel 2013;104:462–7.

[128] Ahmadi MA, Shadizadeh SR. Induced effect of adding nano silica on adsorption of a natural surfactant onto sandstone rock: Experimental and theoretical study. J Pet Sci Eng 2013;112:239–47.

[129] Ahmadi MA, Shadizadeh SR. Spotlight on the new natural surfactant flooding in carbonate rock samples in low salinity condition. Sci Rep 2018;8:1–15.

[130] Arabloo M, Ghazanfari MH, Rashtchian D. Wettability modification, interfacial tension and adsorption characteristics of a new surfactant: Implications for enhanced oil recovery. Fuel 2016;185:199–210.

[131] Sofla SJD, Sharifi M, Sarapardeh AH. Toward mechanistic understanding of natural surfactant flooding in enhanced oil recovery processes: The role of salinity, surfactant concentration and rock type. J Mol Liq 2016;222:632–9.

[132] Ahmadi MA, Shadizadeh SR. Implementation of a high-performance surfactant for enhanced oil recovery from carbonate reservoirs. J Pet Sci Eng 2013;110:66–73.

[133] Ahmadi MA, Shadizadeh SR. Nano-surfactant flooding in carbonate reservoirs: A mechanistic study. Eur Phys J Plus 2017;132:246.

[134] Moslemizadeh A, Dehkordi AF, Barnaji MJ, Naseri M, Ravi SG, Jahromi EK. Novel bio-based surfactant for chemical enhanced oil recovery in montmorillonite rich reservoirs: Adsorption behavior, interaction impact, and oil recovery studies. Chem Eng Res Des 2016;109:18–31.

[135] Shadizadeh S, Kharrat R. Experimental investigation of matricaria chamomilla extract effect on oil-water interfacial tension: Usable for chemical enhanced oil recovery. Pet Sci Technol 2015;33:901–7.

[136] Samanta A, Ojha K, Mandal A. The characterization of natural surfactant and polymer and their use in enhanced recovery of oil. Pet Sci Technol 2011;29:765–77.

[137] Chhetri A, Watts K, Rahman M, Islam M. Soapnut extract as a natural surfactant for enhanced oil recovery. Energy Sources, A 2009;31:1893–903.

[138] Saxena N, Pal N, Dey S, Mandal A. Characterizations of surfactant synthesized from palm oil and its application in enhanced oil recovery. J Taiwan Inst Chem Eng 2017;81:343–55.

[139] Moradi S, Isari AA, Bachari Z, Mahmoodi H. Combination of a new natural surfactant and smart water injection for enhanced oil recovery in carbonate rock: Synergic impacts of active ions and natural surfactant concentration. J Pet Sci Eng 2019;176:1–10.

[140] Saxena N, Saxena A, Mandal A. Synthesis, characterization and enhanced oil recovery potential analysis through simulation of a natural anionic surfactant. J Mol Liq 2019;282:545–56.

[141] Pal N, Kumar N, Verma A, Ojha K, Mandal A. Performance evaluation of novel sunflower oil-based gemini surfactant(s) with different spacer lengths: application in enhanced oil recovery. Energy Fuels 2018;32:11344–61.

[142] Ahmadi MA, Galedarzadeh M, Shadizadeh SR. Spotlight on the use of new natural surfactants in colloidal gas aphron (CGA) fluids: A mechanistic study. Eur Phys J Plus 2017;132:519.

[143] Arabloo M, Ghazanfari MH, Rashtchian D. Spotlight on kinetic and equilibrium adsorption of a new surfactant onto sandstone minerals: a comparative study. J Taiwan Inst Chem Eng 2015;50:12–23.

[144] Barati A, Najafi A, Daryasafar A, Nadali P, Moslehi H. Adsorption of a new nonionic surfactant on carbonate minerals in enhanced oil recovery: Experimental and modeling study. Chem Eng Res Des 2016;105:55–63.

[145] Ortona O, D'Errico G, Paduano L, Sartorio R. Ionic surfactant–polymer interaction in aqueous solution. PCCP 2002;4:2604–11.

[146] Wang C, Tam K. New insights on the interaction mechanism within oppositely charged polymer/surfactant systems. Langmuir 2002;18:6484–90.

[147] Goddard ED. Polymer–surfactant interaction Part I. Uncharged water-soluble polymers and charged surfactants. Colloids Surf 1986;19:255–300.

[148] Goddard ED, Ananthapadmanabhan KP. Interactions of surfactants with polymers and proteins. CRC press: Boca Raton, Florida, USA, 1993.

[149] Lucassen-Reynders EH. Anionic surfactants: Physical chemistry of surfactant action. Marcel Dekker: New York, USA, 1981.

[150] Nagarajan R. Polymer–surfactant interactions. New Horizons: Detergents for the New Millennium Conference Invited Paper. 2001; Fort Myers, Florida, USA.

[151] Cabane B. Structure of some polymer–detergent aggregates in water. J Phys Chem 1977;81:1639–45.

[152] Mittal KL, Fendler EJ. Solution behavior of surfactants: Theoretical and applied aspects. Plenum Press: New York, USA, 1982.

[153] Turro NJ, Baretz BH, Kuo PL. Photoluminescence probes for the investigation of interactions between sodium dodecylsulfate and water-soluble polymers. Macromolecules 1984;17:1321–4.

[154] Fishman M, Eirich F. Interactions of aqueous poly (N-vinylpyrrolidone) with sodium dodecyl sulfate. I. Equilibrium dialysis measurements. J Phys Chem 1971;75:3135–40.

[155] Arai H, Murata M, Shinoda K. The interaction between polymer and surfactant: The composition of the complex between polyvinylpyrrolidone and sodium alkyl sulfate as revealed by surface tension, dialysis, and solubilization. J Colloid Interface Sci 1971;37:223–7.

[156] Murata M, Arai H. The interaction between polymer and surfactant: The effect of temperature and added salt on the interaction between polyvinylpyrrolidone and sodium dodecyl sulfate. J Colloid Interface Sci 1973;44:475–80.

[157] Lange H. Interaction between sodium alkylsulfates and polyvinylpyrrolidone in aqueous solutions. Kolloid Z Z Polym 1971;243:101–9.

[158] Saito S. Binding of surfactants by polymers. J Colloid Sci 1960;15:283–6.

[159] Birch B, Clarke D, Lee R, Oakes J. Surfactant-selective electrodes: Part III. Evaluation of a dodecyl sulphate electrode in surfactant solutions containing polymers and a protein. Anal Chim Acta 1974;70:417–23.

[160] Gilanyi T, Wolfram E. Interaction of ionic surfactants with polymers in acqueous solution. Colloids Surf 1981;3:181–98.

[161] Behera MR, Varade SR, Ghosh P, Paul P, Negi AS. Foaming in micellar solutions: Effects of surfactant, salt, and oil concentrations. Ind Eng Chem Res 2014;53:18497–507.

[162] Varade SR, Ghosh P. Foaming in aqueous solutions of zwitterionic surfactant: Effects of oil and salts. J Dispersion Sci Technol 2017;38:1770–84.

[163] Kronberg B, Holmberg K, Lindman B. Surface chemistry of surfactants and polymers. John Wiley and Sons: Chichester, United Kingdom, 2014.

[164] Lyu Y, Gu C, Fan X, Tao J, Yao X, Dai C, Zhao G. Interfacial rheology of a novel dispersed particle gel soft heterogeneous combination flooding system at the oil-water interface. Colloids Surf, A 2018;559:23–34.

[165] Cairns R, Grist D, Neustadter E. The effect of crude oil–water interfacial properties on water–crude oil emulsion stability. London, UK: Academic Press; 1974.

[166] Zhou H, Dai C, Zhang Q, Li Y, Lv W, Cheng R, Wu Y, Zhao M. Interfacial rheology of novel functional silica nanoparticles adsorbed layers at oil–water interface and correlation with Pickering emulsion stability. J Mol Liq 2019;293:111500.

[167] Anseth JW, Bialek A, Hill RM, Fuller GG. Interfacial rheology of graft-type polymeric siloxane surfactants. Langmuir 2003;19:6349–56.

[168] Rane JP, Pauchard V, Couzis A, Banerjee S. Interfacial rheology of asphaltenes at oil–water interfaces and interpretation of the equation of state. Langmuir 2013;29:4750–9.

[169] Chen S, Han M, AlSofi AM. Synergistic effects between different types of surfactants and an associating polymer on surfactant–polymer flooding under high-temperature and high-salinity conditions. Energy Fuels 2021;35:14484–98.

[170] Chen S, Siu H, Duhamel J. Interactions between hydrophobically modified alkali-swellable emulsion polymers and sodium dodecyl sulfate probed by fluorescence and rheology. J Phys Chem B 2014;118:351–61.

[171] Nedjhioui M, Moulai-Mostefa N, Morsli A, Bensmaili A. Combined effects of polymer/surfactant/oil/alkali on physical chemical properties. Desalination 2005;185:543–50.

[172] Sveistrup M, van Mastrigt F, Norrman J, Picchioni F, Paso K. Viability of biopolymers for enhanced oil recovery. J Dispersion Sci Technol 2016;37:1160–9.

[173] Hosseini-Nasab S, Zitha P, Mirhaj S, Simjoo M. A new chemical-enhanced oil recovery method? Colloids Surf, A 2016;507:89–95.

[174] Chen Z, Zhao X, Wang Z, Fu M. A comparative study of inorganic alkaline/polymer flooding and organic alkaline/polymer flooding for enhanced heavy oil recovery. Colloids Surf, A 2015;469:150–7.

[175] Li HR, Li ZQ, Song XW, Li CB, Guo LL, Zhang L, Zhang L, Zhao S. Effect of organic alkalis on interfacial tensions of surfactant/polymer solutions against hydrocarbons. Energy Fuels 2015;29:459–66.

[176] Wang W, Gu Y. Detection and reuse of the produced chemicals in chemical enhanced oil recovery operations. Pet Sci Technol 2005;23:1033–57.

[177] Baruah A, Pathak AK, Ojha K. Phase behaviour and thermodynamic properties of lamellar liquid crystal developed for viscoelastic surfactant based fracturing fluid. Chem Eng Sci 2015;131:146–54.

[178] Hou J, Liu Z, Zhang S, Yang J. The role of viscoelasticity of alkali/surfactant/polymer solutions in enhanced oil recovery. J Pet Sci Eng 2005;47:219–35.

[179] Bryan J, Kantzas A. Potential for alkali-surfactant flooding in heavy oil reservoirs through oil-in-water emulsification. J Can Pet Technol 2009;48:37–46.

[180] Stoll M, Al-Harthy S, Van Wunnik J, Faber M. Alkaline–surfactant–polymer flood: From the laboratory to the field. SPE EOR Conference at Oil & Gas West Asia. 2010; Muscat, Oman

[181] Lima MCFS, do Amparo SZ, Ribeiro H, Soares Jr AL, Viana MM, Seara LM, Paniago RM, Silva GG, Caliman V. Aqueous suspensions of carbon black with ethylenediamine and polyacrylamide-modified surfaces: Applications for chemically enhanced oil recovery. Carbon 2016;109:290–9.

[182] Pu WF, Liu R, Wang KY, Li KX, Yan ZP, Li B, Zhao L. Water-soluble core–shell hyperbranched polymers for enhanced oil recovery. Ind Eng Chem Fundam 2015;54:798–807.

[183] Burk J. Comparison of sodium carbonate, sodium hydroxide, and sodium orthosilicate for EOR. SPE Reservoir Eng 1987;2:9–16.

[184] Southwick JG, van den Pol E, van Rijn CH, van Batenburg DW, Boersma DM, Svec Y, Mastan AA, Raney K. Ammonia as alkali for ASP floods - Comparison to sodium carbonate. SPE Improved Oil Recovery Symposium. 2014; Tulsa, Oklahoma, USA.

[185] Samanta A, Ojha K, Mandal A. Interactions between acidic crude oil and alkali and their effects on enhanced oil recovery. Energy Fuels 2011;25:1642–9.

[186] Samanta A, Bera A, Ojha K, Mandal A. Comparative studies on enhanced oil recovery by alkali–surfactant and polymer flooding. J Petrol Explor Prod Technol 2012;2:67–74.

[187] Ramakrishnan T, Wasan D. A model for interfacial activity of acidic crude oil/caustic systems for alkaline flooding. SPE J 1983;23:602–12.

[188] Sabhapondit A, Borthakur A, Haque I. Water soluble acrylamidomethyl propane sulfonate (AMPS) copolymer as an enhanced oil recovery chemical. Energy Fuels 2003;17:683–8.

[189] Dautzenberg H, Karibyants N. Polyelectrolyte complex formation in highly aggregating systems. Effect of salt: Response to subsequent addition of NaCl. Macromol Chem Phys 1999;200:118–25.

[190] Yuan H, Shen L, Du Y, Zhao S, Yu J. Micellization of sodium dodecyl sulfonate and Triton X-100 in polyacrylamide water solution studied by ^{1}H NMR relaxation and two-

dimensional nuclear overhauser enhancement spectroscopy. Colloid Polym Sci 1999;277:1026–32.

[191] Ma WG, Xia H. The effect of rheological properties of alkali–surfactant–polymer system on residual oil recovery rate after water flooding. SPE Asia Pacific Oil and Gas Conference and Exhibition. 18–20 October 2010; Brisbane, Queensland, Australia.

[192] Bataweel MA, Nasr-El-Din HA. Rheological study for surfactant–polymer and novel alkali–surfactant–polymer solutions. North Africa Technical Conference and Exhibition. 20–22 February 2012; Cairo, Egypt.

[193] Lei ZD, Yuan SY, Song J. Rheological behavior of alkali–surfactant–polymer/oil emulsion in porous media. J Central South University Technol 2008;15:462–6.

[194] Cao R, Cheng L, Ma YZ. Model for rheological behavior of crude oil and alkali–surfactant–polymer emulsion. Open Fuels Energy Sci J 2014;7:55–61.

[195] Hongyan W, Xulong C, Jichao Z, Aimei Z. Development and application of dilute surfactant–polymer flooding system for Shengli oilfield. J Pet Sci Eng 2009;65:45–50.

[196] Zhang F, Zhang Q, Zhou Z, Cai H. Development of novel surfactant for alkali-free surfactant/polymer combination flooding green technology. SPE Asia Pacific Enhanced Oil Recovery Conference. 11–13 August 2015; Kuala Lumpur, Malaysia.

[197] Youyi Z, Zhang Y, Jialing N, Weidong L, Qingfeng H. The research progress in the alkali-free surfactant–polymer combination flooding technique. Pet Explor Dev 2012;39:371–6.

[198] Dass C, Jain MA, Dhawan AK, Misra TR. Monitoring of polymer flooding project at Sanand field of India. SPE Indian Oil and Gas Technical Conference and Exhibition. 4–6 March 2008; Mumbai, India.

[199] Pandey A, Suresh Kumar M, Jha MK, Tandon R, Punnapully B, Kalugin MA, Khare A, Beliveau D. Chemical EOR pilot in Mangala field: Results of initial polymer flood phase. SPE Improved Oil Recovery Symposium. 14–18 April 2012; Tulsa, Oklahoma, USA.

[200] Jha MK, Pandey A, Tandon R, Beliveau D. Pulse testing for enhanced reservoir characterization of the EOR pilot area in Mangala field. SPE Enhanced Oil Recovery Conference. 19–21 July 2011; Kuala Lumpur, Malaysia.

[201] Goyal K, Arora P, Chilingar GV. Recovery of medium-viscosity crude oil of north Gujarat oil field, India, using polymer and caustic flooding. Energy Sources 1980;5:45–52.

[202] Das B, Gogoi S, Mech D. Micellar-polymer for enhanced oil recovery for Upper Assam Basin. Resour Efficient Technol 2017;3:82–7.

[203] Jun S, Yang C-z, Yang Z-y, Guang-zhi L, Hong Y, Dai Z-j, Li Y-q, Zhong-qui Y. Surfactant-alkaline-polymer flooding pilot project in non-acidic paraffin oil field in Daqing. SPE Asia Pacific oil and gas conference and exhibition. 16–18 October 2000; Brisbane, Australia.

[204] Vargo J, Turner J, Vergnani B, Pitts MJ, Wyatt K, Surkalo H, Patterson D. Alkaline-surfactant-polymer flooding of the Cambridge Minnelusa field. SPE Reservoir Eval Eng 2000;3.

[205] Zhu Y, Hou Q, Liu W, Ma D, Liao G-Z. Recent progress and effects analysis of ASP flooding field tests. SPE Improved Oil Recovery Symposium. 14–18 April 2012; Tulsa, Oklahoma, USA.

[206] Wang C, Wang B, Cao X, Li H. Application and design of alkaline-surfactant-polymer system to close well spacing pilot Gudong oilfield. SPE Western Regional Meeting. 25–27 June 1997; Long Beach, California, USA.

[207] Zhijian Q, Yigen Z, Xiansong Z, Jialin D. A successful ASP flooding pilot in Gudong oil field. SPE/DOE improved oil recovery symposium. 19–22 April 1998; Tulsa, Oklahoma, USA.

[208] Jain AK, Dhawan AK, Misra TR. ASP flood pilot in Jhalora (K-IV), India-A case study. SPE oil and gas India conference and exhibition. 28–30 March 2012; Mumbai, India.

[209] Hanotia A, Singh B, Samanta S. ASP flood pilot test at tertiary stage in Kalol field–A case history. SPE Oil & Gas India Conference and Exhibition. 24–26 November 2015; Mumbai, India.

[210] Delshad M, Han W, Pope G, Sepehrnoori K, Wu W, Yang R, Zhao L. Alkaline/surfactant/polymer flood predictions for the Karamay Oil Field. SPE/DOE Improved Oil Recovery Symposium. 19–22 April 1998; Tulsa, Oklahoma, USA.

[211] Gu H, Yang R, Guo S, Guan W, Yue X, Pan Q. Study on reservoir engineering: ASP flooding pilot test in Karamay Oilfield. SPE International Oil and Gas Conference and Exhibition in China. 2–6 November 1998; Beijing, China.

[212] Pandey A, Beliveau D, Suresh Kumar M, Pitts MJ, Qi J. Evaluation of chemical flood potential for Mangala Field, Rajasthan, India-Laboratory experiment design and results. International Petroleum Technology Conference. 3–5 December 2008; Kuala Lumpur, Malaysia.

[213] Pandey A, Koduru N, Stanley M, Pope GA, Weerasooriya UP. Results of ASP pilot in Mangala field: A success story. SPE Improved Oil Recovery Conference. 11–13 April 2016; Tulsa, Oklahoma, USA.

[214] McInnis LE, Hunter KD, Ellis-Toddington TT, Grawbarger DJ. Case Study of the Taber Mannville B ASP Flood. SPE Enhanced Oil Recovery Conference. 2–4 July 2013; Kuala Lumpur, Malaysia.

[215] Huang S, Dong M. Alkaline/surfactant/polymer (ASP) flood potential in southwest Saskatchewan oil reservoirs. J Can Pet Technol 2002;43:56–61.

[216] Pitts MJ, Dowling P, Wyatt K, Surkalo H, Adams KC. Alkaline-surfactant-polymer flood of the Tanner Field. SPE/DOE symposium on improved oil recovery. 22–26 April 2006; ulsa, Oklahoma, USA.

[217] Pratap M, Gauma M. Field implementation of alkaline–surfactant–polymer (ASP) flooding: A maiden effort in India. SPE Asia Pacific Oil and Gas Conference and Exhibition. 18–20 October 2004; Perth, Australia.

[218] Singh B, Parulkar S, Kumar A. Successful pilot implementation of ASP flooding through CEOR/IOR application–A case study. SPE Oil and Gas India Conference and Exhibition. 4–6 April 2017; Mumbai, India.

[219] Clark S, Pitts MJ, Smith S. Design and application of an alkaline–surfactant–polymer recovery system to the West Kiehl Field. SPE Adv Technol Ser 1993;1:172–9.

[220] Meyers J, Pitts MJ, Wyatt K. Alkaline–surfactant–polymer flood of the West Kiehl, Minnelusa Unit. SPE/DOE enhanced oil recovery symposium. 22–24 April 1992; Tulsa, Oklahoma,USA.

[221] Karpan V, Volokitin Y, Shuster M, Tigchelaar W, Chmuzh I, Koltsov I, Tkachev I, Van Batenburg D, Faber M, Skripkin A. West Salym ASP pilot: Project front-end engineering. SPE Improved Oil Recovery Symposium. 12–16 April 2014; Tulsa, Oklahoma, USA.

[222] Volokitin Y, Sakhibgareev R, Shaymardanov M, Nurieva O. Chemical and analytical work in support of west Salym field enhanced oil recovery project (ASP). SPE Russian Oil and Gas Exploration and Production Technical Conference and Exhibition. 16–18 October 2012; Moscow, Russia.

[223] Finley M. BP statistical review of world energy June 2017. Annual reportUnited Kingdom: 2017.

[224] Zhang Y, Mills D, Dong M. Determining the most profitable ASP flood strategy for enhanced oil recovery. Canadian International Petroleum Conference. 10–12 June 2003; Calgary, Alberta.

[225] Taber JJ, Martin F, Seright R. EOR screening criteria revisited–Part 1: Introduction to screening criteria and enhanced recovery field projects. SPE Reservoir Eng 1997;12:189–98.

[226] Brashear J, Kuuskraa V. The potential and economics of enhanced oil recovery. J Pet Technol 1978;30:1231–9.

[227] Zekri A, Jerbi K. Economic evaluation of enhanced oil recovery. Oil Gas Sci Technol 2002;57:259–67.

[228] McCoy ST, Rubin ES. The effect of high oil prices on EOR project economics. Energy Proc 2009;1:4143–50.

[229] Abadli F. Simulation study of enhanced oil recovery by ASP (Alkaline, surfactant and polymer) flooding for Norne field C-segment. Masters' Thesis. Department of Petroleum Engineering and Applied Geophysics, Norwegian University of Science and Technology, Trondheim, Norway: 2012.

[230] Bondor P. Applications of economic analysis in EOR research. J Pet Technol 1993;45:310–2.

[231] Alvarado V, Manrique E. Enhanced oil recovery: An update review. Energies 2010;3:1529–75.

Chapter 3

Materials and methods

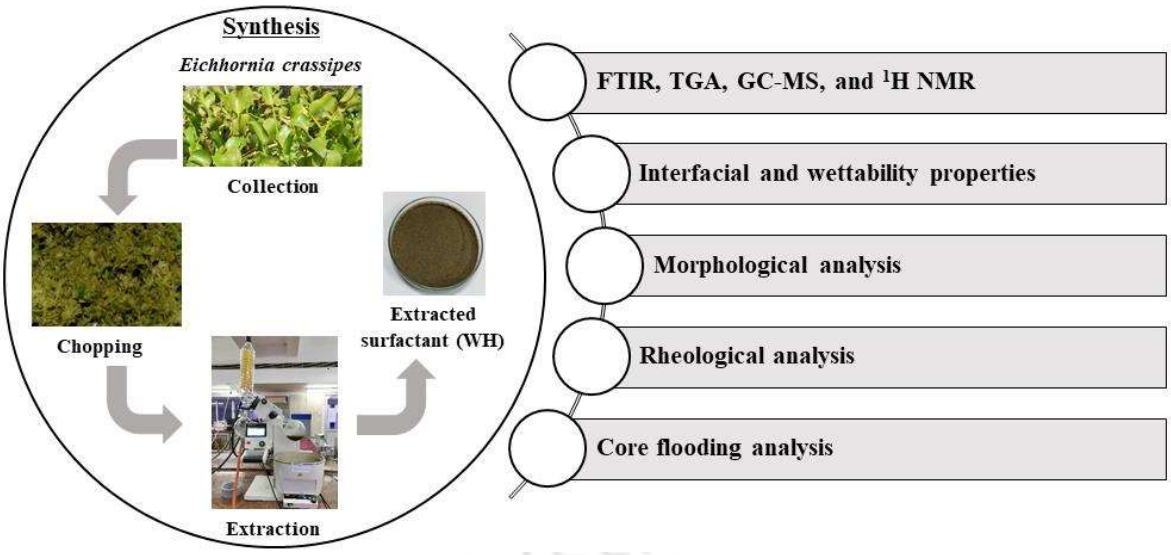

Materials and methods

In this chapter, the materials used in the experimental studies and their sources are listed. Detailed information on the procedure of synthesis of the natural surfactant, sample preparation methods, equipment used, and the experimental procedures are provided.

3.1 General overview

The proposed study is comprised of four stages. The first two stages of this work are dedicated to the synthesis of the natural surfactant from the weed, *Eichhornia crassipes*, its characterization, and measurement of interfacial properties. In addition, the effect of the natural surfactant on the rheological behavior of xanthan gum (which is a conventionally-used polymer in enhanced oil recovery) has been analyzed over a wide range of shear rate, frequency, and temperature. The details of the major equipment used in these two stages, i.e., Fourier-transform infrared spectrophotometer (FTIR), field-emission scanning electron microscope (FESEM), field-emission transmission electron microscope (FETEM), nuclear magnetic resonance (NMR) spectrophotometer, thermogravimetric analyzer (TGA), rheometer, tensiometer, rotavapor, gas chromatograph–mass spectrophotometer (GC–MS), optical microscope, and zeta potentiometer (available at the Department of Chemical Engineering and Central Instruments Facility at Indian Institute of Technology Guwahati), and the experimental procedures are presented in this chapter.

The next two stages (i.e., stages three and four) of this work are dedicated to the study of the adsorption of the synthesized surfactant on the porous media, analysis of wettability alteration and interfacial tension (IFT) reduction under reservoir-like conditions (i.e., at high temperature and pressure, and under anaerobic condition), small-angle X-ray scattering (SAXS) analysis, and performance evaluation of the synthesized surfactant by core flooding experiments. Equipment such as FESEM, X-ray diffractometer (XRD), UV-Vis

spectrophotometer, interfacial tensiometer (based on sessile and pendent drop methods), optical microscope, and core flooding setup (available at the Western Australia School of Mines: Minerals, Energy and Chemical Engineering Curtin University, Australia) were used for these experimental studies. The details of these experimental procedures are given in this chapter.

3.2 Materials

An eco-friendly natural surfactant developed from an aquatic plant (i.e., *Eichhornia crassipes*) was used in the present study. Deuterated chloroform (99.8%), potassium bromide (99.9%), and paraffin oil were purchased from Merck Specialties (India). Helium gas (99.99%) was procured from Assam Air Products (India). Xanthan gum (XG) and sodium dodecyl sulfate (SDS) (≥ 99.0%) were purchased from Sigma-Aldrich (India). Inorganic salts such as sodium chloride (99.5%), magnesium chloride (≥ 98.0%), calcium chloride (≥ 98.0%), and sodium sulfate (99.0%) were purchased from Sigma Aldrich (India). A synthetic brine was prepared by dissolving the desired amount of salts in double-distilled water. The composition of the brine is given in Table 3.1.

Table 3.1. Components of the synthetic brine

Ion	Na^+	Ca^+	Mg^+	Cl^-	SO_4^{2-}	**Total**
Concentration (mg dm^{-3})	3601.8	1344.0	36.4	7121.3	1258.4	13361.9

The sand sample was collected from the Curtin University campus (Perth, Australia). It was rigorously washed to remove the dirt. The sample was dried at 373 K for 24 h and sieved to 60–80 mesh. A set of sandstone rock samples was procured from the Kocurek Industries (Caldwell, USA). Further, the rock samples were crushed and sieved to 60–80 mesh.

The crude oil used in this study was procured from Tesoro Refining and Marketing (USA). The density, acid number, and base number were found to be 890 kg m^{-3} (at 293 K),

1.7 KOH g^{-1}, and 1.2 KOH g^{-1}, respectively. The major composition of the oil was measured by gas chromatography, and the details are shown in Table 3.2. The details of the compounds recognized in the crude oil are provided Figure A1 and Table A1 (Appendix A1).

Table 3.2. Composition of the crude oil

Properties	Asphaltenes	Naphthenes	Wax	Sulfur
Content (wt. %)	31.7	26.3	3.8	3.9

A set of Berea sandstone core samples was purchased from Kocurek Industries (USA). The permeability and porosity of the core samples were measured by using an automated gas poro-permeameter. The results are given in Table 3.3.

Table 3.3. Details of the core samples and the chemical additives used for the core flooding experiments

Sample No.	Core Sample	Weight (g)	Porosity (%)	Brine Permeability (m^2)
1	Berea sandstone	180.3	20.45	1.23×10^{-13}
2		181.6	20.57	1.24×10^{-13}
3		179	20.34	1.21×10^{-13}

3.3 Methods

3.3.1 Synthesis of natural surfactant

Eichhornia crassipes was collected from the lakes of Indian Institute of Technology Guwahati (India). Roots of the plants were removed, and the remaining portions were thoroughly cleaned and air-dried. Approximately 100 g of the chopped leaves and stems were soaked overnight in 0.5 dm^3 of 50% (v/v) aqueous ethanol solution at 323 K. Thereafter, the samples were filtered and the surfactant was extracted in a rotary evaporator [manufacturer: Buchi (Switzerland); model: R300] *in vacuo* at 323–328 K. The solid residues left after filtration were ground and soaked again in 0.5 dm^3 of 50% (v/v) aqueous ethanol solution for 24 h. Once the extraction

was complete, the green semi-liquid material was allowed to dry in a hot air oven at 313 K. Around 5 g of the synthesized surfactant (which we would abbreviate as WH, based on its common name, i.e., Water Hyacinth) was obtained from a single batch and the same was stored in a desiccator for further use. The cost of 1 g of the synthesized natural surfactant was about ₹53.56 (Appendix A2).

3.3.2 Characterization of surfactant by FTIR, GC–MS, NMR, and TGA analyses

An FTIR spectrophotometer [manufacturer: Shimadzu (Japan); model: IRAffinity-1] was employed to characterize the functional groups of the synthesized surfactant. A thin pellet was prepared by mixing the samples with KBr. The spectrum was obtained in the transmission mode in the wavenumber range of 4000–400 cm^{-1}.

The GC–MS analysis of the synthesized surfactant was conducted in a gas chromatograph and mass spectrometer [manufacturer: Perkin Elmer (USA); model: Claurus 680 GC/Claurus 600C MS] with an Elite-5MS capillary column (length: 60 m, internal diameter: 0.25 mm) [manufacturer: Perkin Elmer (USA)]. The oven temperature of the GC was primarily maintained at 333 K for 3 min, then ramped with a heating rate of 278 K min^{-1} to 473 K for 3 min, followed by another ramp with a heating rate of 279 K min^{-1} to 673 K for 10 min. Helium gas was used as the carrier, and its flow rate was 8 cm^3 min^{-1}. 2×10^{-3} cm^3 of the sample containing 0.01 wt. % WH in ethanol was injected.

The ^1H NMR spectrum of the synthesized surfactant was analyzed using an NMR spectrometer [manufacturer: Bruker (USA); model: 600 MHz]. The samples were dissolved in $CDCl_3$, filtered with a 0.2 µm syringe filter, and then filled into the NMR tubes. The chemical shift at 7.26 ppm corresponds to $CDCl_3$, and it was considered as the internal reference.

The thermal degradability of the synthesized surfactant was analyzed by a thermogravimetric analyzer [manufacturer: Netzsch (Germany); model: TG 209 F1 Libra].

Around 8 mg of the sample was placed in a crucible and heated from 293 to 1373 K at the rate of 10 K min^{-1}.

3.3.3 Measurement of interfacial properties

The surface tension of the aqueous WH solutions and the tension at the interface between the aqueous surfactant solution and paraffin oil were measured by a tensiometer [manufacturer: Kyowa (Japan); model: DY300] by the du Noüy ring method at 298 K. The procedure given in the ASTM Standard D1331-14 (2014) was followed. First, the platinum ring was burnt to remove any contamination until it became red hot. Then the sample vessel was cleaned thoroughly. Next, the surfactant solution was transferred to the sample vessel and carefully placed in the measuring section of the tensiometer. The movement of the ring was controlled by the Dynalyzer software (provided with the tensiometer). The ring was immersed inside the surfactant solution to the appropriate depth and slowly pulled out until it detached from the surface (i.e., the air–water interface). A decrease in surface tension was measured upon increasing the surfactant concentration. The lowest surface tension was considered as a critical micelle concentration (CMC).

The tension at the interface between the aqueous surfactant solution and paraffin oil was measured by the du Noüy ring method. The procedure described in the ASTM Standard D1331-14 (2014) was adopted. Further, the measurement mode of the tensiometer was changed to “IFT Analysis” by using the Dynalyzer software. The sample vessel was very carefully placed in the measuring section of the tensiometer. Next, the surfactant solution was placed in the sample vessel, and the ring was dipped inside the aqueous phase such that it was close to the surface of the aqueous phase. Then the paraffin oil was gradually poured over the surfactant solution. The oil was carefully poured near the wall of the vessel using a clean glass slide. The interface between the aqueous phase and the paraffin oil was allowed to stand for 30 min to reach equilibrium. The IFT was measured by gently pulling the ring out through the interface.

The conductivity of the surfactant solutions was measured by a conductivity meter [manufacturer: Rakiro (India); model: Aquasol AM-AL-01]. The CMC obtained from the surface tension and conductivity measurements corroborated well. All the measurements were repeated at least three times for each sample, and the average values are reported in Chapter 4.

3.3.4 Zeta potential measurements

The zeta potential measurements of the synthesized surfactant and paraffin oil–surfactant solution interface were measured by using a zeta potentiometer [manufacturer: Beckman Coulter (Switzerland); model: Delsa Nano C]. The aqueous samples were injected into the flow cell of the zeta potentiometer with the help of a syringe. The zeta potential of the paraffin oil–surfactant solution interface was measured with the help of the Smoluchowski equation [1]

$$\zeta = \left(\frac{\mu}{\varepsilon \varepsilon_0} \right) U \tag{3.1}$$

3.3.5 Morphological and mineralogy analyses

A FESEM [manufacturer: Zeiss (USA); model: GeminiSEM 300)] was used for the morphological analysis conducted on the dried samples of WH and XG–WH. The surface of the samples was double-coated with gold by sputtering. After this, the samples were mounted on the stubs by using the carbon tap. A few drops of the aqueous solution were mounted on the copper grid and dried at 313 K to analyze the detailed morphological structure using FETEM [manufacturer: Jeol (Japan); model: 2100F].

Furthermore, a morphological analysis of the oven-dry rock samples before and after adsorption was done with FESEM [manufacturer: Tescan (Czech Republic); model: Mira3 XMU)]. The surface of the samples was double-coated with gold by sputtering. The mineralogy of the sandstone rock and sand was studied with XRD [manufacturer: Bruker (USA); model: D8A].

3.3.6 Wettability measurements at reservoir-like conditions

Wettability alteration is a commonly-used mechanism for the improvement of oil recovery. The contact angle of the crude oil on the rock soaked with the surfactant–brine solution was measured with an IFT measurement instrument [manufacturer: Vinci Technologies (France); model: IFT 700]. Figure 3.1 shows the schematics of the experimental setup. A slice of the sandstone rock was cleaned with a plasma cleaning device [manufacturer: Diener (Germany); model: Zepto]. A rock slice was pasted on the surface with the help of an industrial super glue. The measurements were carried out at two experimental conditions (i.e., at 298 K and 1.38 MPa, and at 333 K and 13.8 MPa).

First, the system was put *in vacuo*, and then immersed into a surfactant–brine solution for 24 h under the experimental conditions. Once the equilibrium was achieved, a drop of the crude oil was injected by a stainless-steel needle (inner diameter = 0.6 mm) on the rock sample. A sessile drop was formed on the rock, which was used to investigate the wettability alteration potential of the natural surfactant. The tests for each sample were repeated at least three times to check the repeatability of the results.

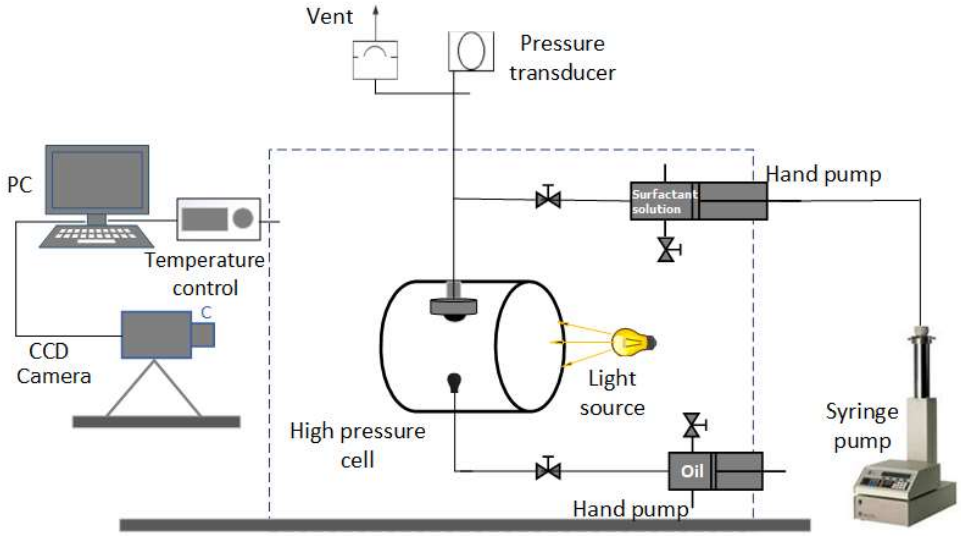

Figure 3.1. Experimental system for contact angle measurement at high temperature and pressure.

3.3.7 Interfacial tension measurement at reservoir-like conditions

The IFT between the crude oil and the aqueous surfactant solution was measured with the same equipment that was used for the contact angle measurements. The pendant drop method was used for the IFT measurements. An operational procedure similar to that adopted for the contact angle measurements was followed, i.e., initially, the system was kept *in vacuo* and then submerged into a surfactant–brine solution for 24 h under several experimental conditions. After the equilibrium was established, a drop of the crude oil was produced at the needle tip, and then the IFT at the oil–water interface was determined by the drop shape analysis using the built-in software of the tensiometer. A schematic of the experimental setup is shown in Figure 3.2. The tests for each sample were repeated at least three times to check the repeatability of the results.

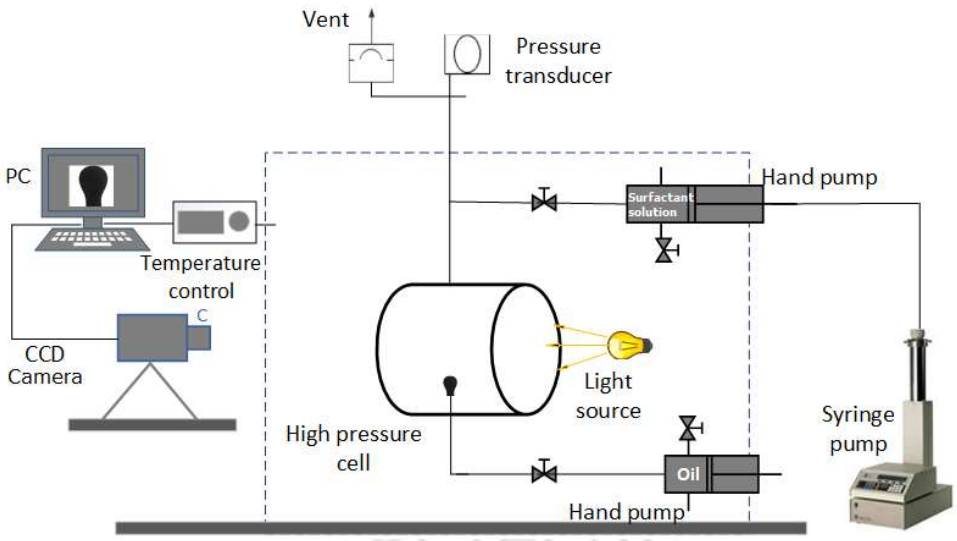

Figure 3.2. Experimental system for the measurement of interfacial tension at high temperature and pressure.

3.3.8 Emulsion stability and size distribution of the oil droplets

The oil–water emulsion was prepared by mixing the surfactant solution (i.e., 0.1–1 wt. %) in paraffin oil (at 5:1 ratio) using a homogenizer [manufacturer: IKA (Germany); model: T10 Basic Ultra-Turrax] at 15000 rpm. Further, the emulsion samples were transferred into flat

bottom tubes and observed over 20 d. The emulsion systems thus prepared were analyzed by using a microscope [manufacturer: Carl Zeiss (Germany); model: Axiostar plus]. The microscopic images were used to determine the size of the oil droplets in the emulsion using the ImageJ® software (bundled with Java 1.8.0_172) [2].

3.3.9 Small-angle X-ray scattering

The small-angle X-ray scattering (SAXS) experiments were carried out by using a SAXS instrument [model: NANOSTAR, manufacturer: Bruker (USA)]. An Excillum Gallium Metaljet was used as a radiation source (wavelength 1.340 Å), which was focused with crossed Göbel mirrors and collimated with two 150 µm pinholes. The emulsion sample was held in a 2-mm quartz-glass capillary and inserted into the sample holder. The structural analysis of the emulsion was carried out by fitting the scattering data by unified Guinier exponential/power-law equation [3].

$$I(q) = G\exp\left(-q^2 R_g^2/3\right) + B\left(1/q^*\right)^P \tag{3.2}$$

$$q^* = q\Big/\left[\operatorname{erf}\left(qR_g/6^{0.5}\right)\right]^3 \tag{3.3}$$

3.3.10 Rheological behavior

A known amount of the XG powder was added to the required amount of Millipore water and stirred intensely (at 300 rpm) by a magnetic stirrer for 3–5 h at 298 K. The intense stirring helped to avoid the formation of lumps [4]. It also enabled us to prepare a homogeneous solution. The desired solution of the surfactant was prepared, and then XG was added. These samples were used for analyzing the effect of surfactant on the rheological properties of XG. During sample preparation, the top of the beaker was sealed with an airtight film to avoid the evaporation of water.

The rheological behavior of the aqueous XG solutions was investigated by using a modular compact rheometer [manufacturer: Anton Paar (Austria); model: MCR 301]. The cone

and plate geometry (cone angle: 1°, cone diameter: 50 mm) was used, and the gap was set at 0.1 mm. The steady shear test was carried out to study the flow behavior of the solutions over the shear rate range of 0.01–1000 s^{-1}. The influence of concentration, surfactant, and salinity on the flow behavior of aqueous polymer solution was investigated at 298 K. Experiments were also carried out to analyze the effect of temperature ranging from 293–353 K. To study the dynamic oscillatory behavior, amplitude and frequency sweeps were carried out. The amplitude sweep tests were carried out over the strain range of 0.1–1000% at 1 Hz to determine the linear viscoelastic (LVE) region. Once the LVE region was determined, the frequency sweep test was carried out by varying the frequency over the range of 0.01–100 Hz and keeping the strain constant.

3.3.11 Interfacial shear rheology

The shear rheology of the water–paraffin oil interface (at which WH was adsorbed) was investigated by using an interfacial rheometer [manufacturer: Anton Paar (Austria); model: MCR 301]. The biconical-bob sensor (cone angle: 5°, cone diameter: 68 mm) and a measuring cell (height: 90 mm, diameter: 80 mm) were used. Initially, the measuring cell was filled up to its marked limit (i.e., 110 dm^3) with the aqueous WH solution. Further, the contact of the bob with the air–water interface was confirmed by determining the normal force (see Figure 3.3). Then, the measuring point was calculated with the help of the in-built software (i.e., RheoPlus, version 3.62). Once the sensor reached the air–water interface, the paraffin oil was gently poured over the aqueous phase till the measurement mark. The steady shear test was performed to measure the interfacial shear viscosity over the shear rate range of 1–100 s^{-1}. The dynamic oscillatory test, on the other hand, was performed to study the viscoelastic properties of the interfacial film of WH over a wide range of frequency (i.e., 0.001–0.1 Hz) and a constant strain of 0.01%.

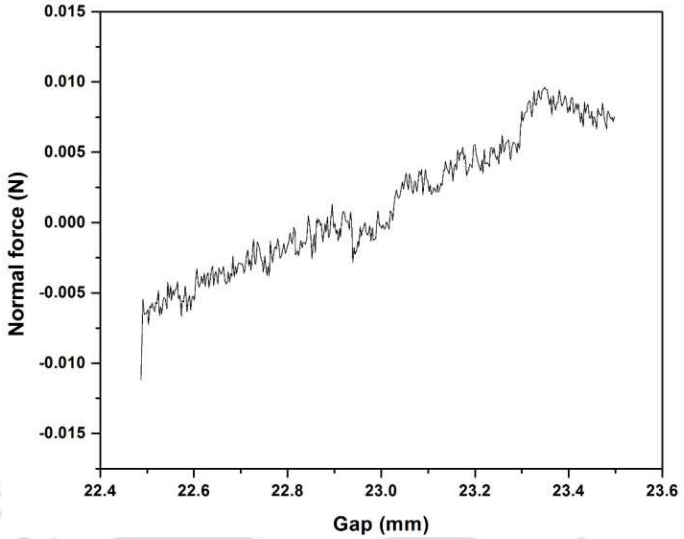

Figure 3.3. Gap setting in the interfacial rheometer.

3.3.12 Adsorption studies

The adsorption studies were performed in the batch mode. The sandstone and sand samples were immersed in the surfactant solution having a concentration in the range of 1000 to 5000 mg dm^{-3}. The samples were thoroughly mixed at the desired temperature (i.e., 298–333 K) in an orbital shaker at 100 rpm. Samples were collected at different times (i.e., 1–24 h) from the aqueous phase and centrifuged to find the equilibrium concentration using a UV-spectrophotometer [manufacturer: Shimadzu (Japan); model: UV-1800]. A flowchart of the adsorption experiments is shown in Figure 3.4. The amount of surfactant adsorbed at time t was calculated from the following equation:

$$q = \frac{(C_0 - C_t)V}{m} \tag{3.4}$$

The effects of the concentration of surfactant, salinity, and temperature on the adsorption characteristics of the surfactant were investigated.

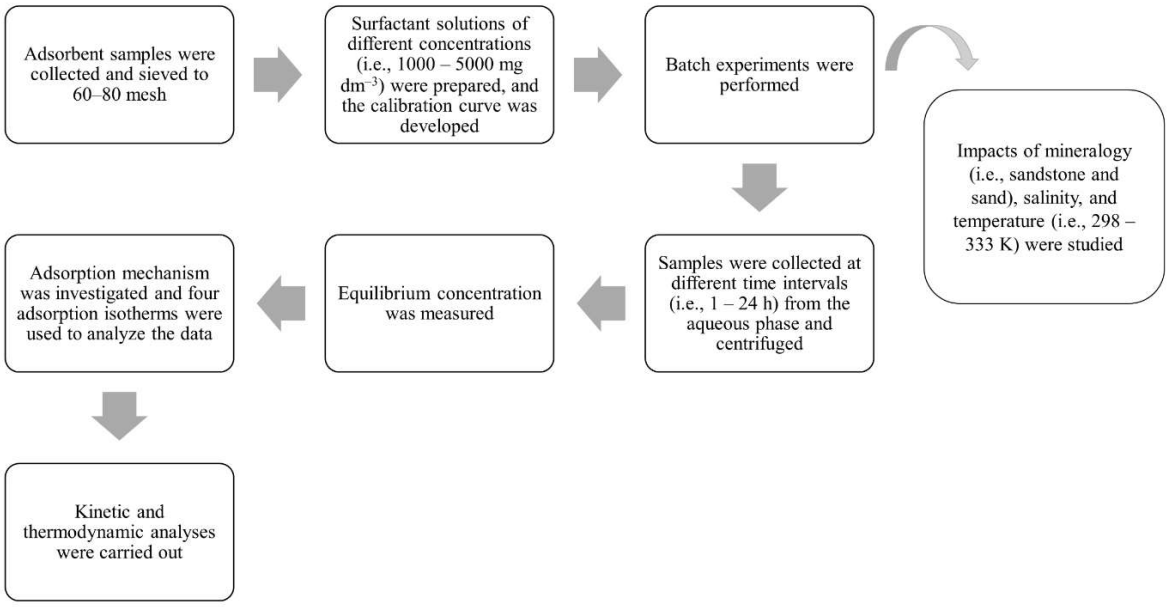

Figure 3.4. Flowchart of the adsorption experiments.

3.3.13 Core flooding measurements

The experimental setup for core flooding is shown in Figure 3.5. First, the core sample was loaded into the core holder. The system was put *in vacuo* for 24 h. Thereafter, it was pressure-saturated with the synthetic brine and then left for another 24 h to age. The crude oil was injected into the system until the water-cut reached < 1%. The system was aged again for 24 h. Water flooding was carried out by injecting the brine again to arrive at the residual oil saturation. Next, the surfactant solution was injected (approximately 1.5–2.5 PV), which was followed by the polymer flooding (approximately 2.5–5 PV). The system pressure and temperature were maintained at 13.8 MPa and 333 K, respectively. The confining pressure was maintained at 20.7 MPa all along the flooding process.

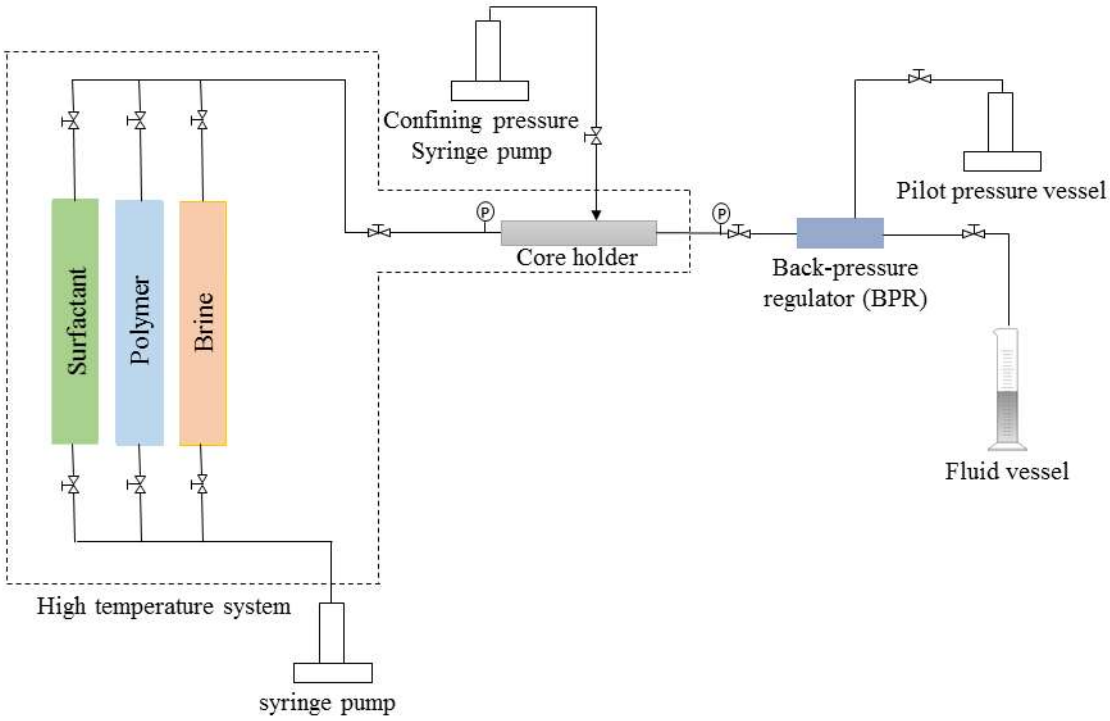

Figure 3.5. Schematic of the experimental setup for core flooding.

Nomenclature

B	pre-factor specific to the type of power-law scattering
C_0	initial concentration of the surfactant, mg dm^{-3}
C_t	concentration of surfactant at time t, mg dm^{-3}
G	Guinier exponential pre-factor
m	mass of the rock sample, g
P	Porod exponent
q	amount of adsorbate adsorbed, mg g^{-1}
q_s	scattering angle, $Å^{-1}$
R_g	radius of gyration, Å
S	surface area, m^2
ΔT_s	film thickness, Å
U	electrophoretic mobility, $m^2\ V^{-1}\ s^{-1}$
V	volume of the solution, dm^3

Greek letters

ε	dielectric constant of the aqueous phase
ε_0	permittivity of free space, $C^2\ J^{-1}\ m^{-1}$
ζ	zeta potential, V
μ	viscosity, Pa s

Abbreviations

FESEM	field-emission scanning electron microscopy
FETEM	field-emission transmission electron microscopy

FTIR	Fourier-transform infrared spectroscopy
GC–MS	gas chromatography–mass spectrometry
IFT	interfacial tension
LVE	linear viscoelastic region
NMR	nuclear magnetic resonance
SAXS	small-angle X-ray scattering
SDS	sodium dodecyl sulfate
TGA	thermogravimetric analysis
WH	surfactant synthesized from *Eichhornia crassipes* (common name: Water Hyacinth)
XRD	X-ray diffractometer
XG	xanthan gum

References

[1] Stachurski J, MichaŁek M. The effect of the ζ potential on the stability of a non-polar oil-in-water emulsion. J Colloid Interface Sci 1996;184:433–6.

[2] Saha R, Uppaluri RV, Tiwari P. Silica nanoparticle assisted polymer flooding of heavy crude oil: Emulsification, rheology, and wettability alteration characteristics. Ind Eng Chem Res 2018;57:6364–76.

[3] Beaucage G. Small-angle scattering from polymeric mass fractals of arbitrary mass-fractal dimension. J Appl Cryst 1996;29:134–46.

[4] Song KW, Kim YS, Chang GS. Rheology of concentrated xanthan gum solutions: Steady shear flow behavior. Fibers Polym 2006;7:129–38.

Chapter 4

Characterization of natural surfactant from *Eichhornia crassipes* for its possible application in EOR

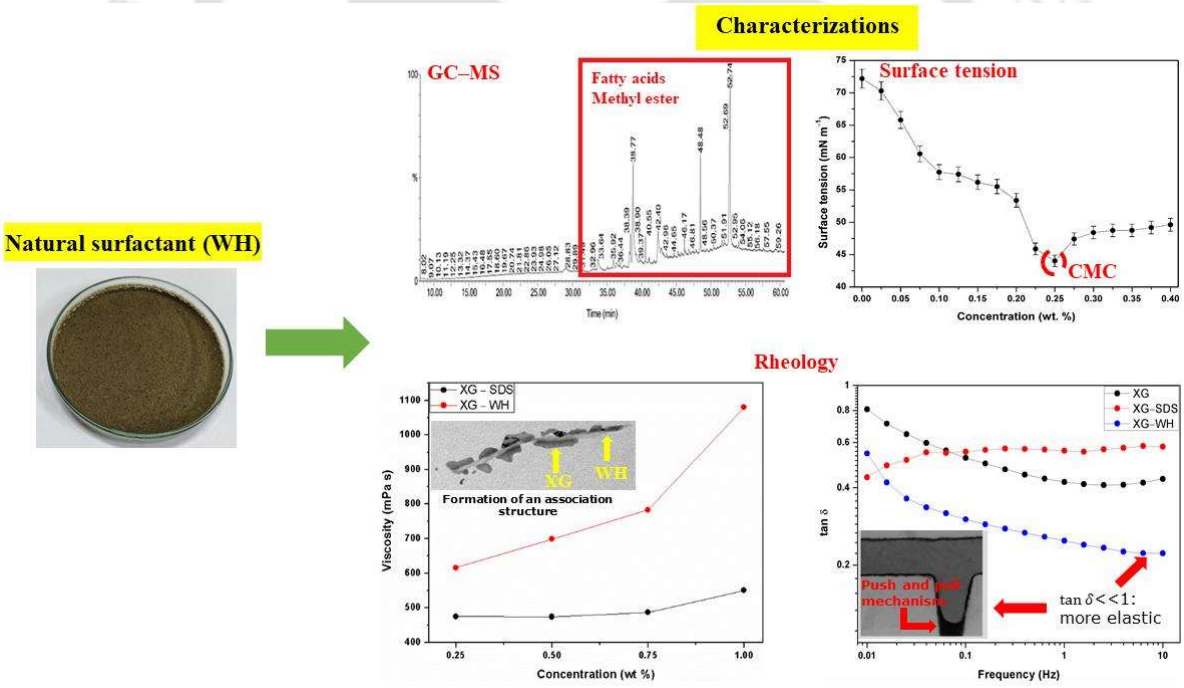

Published article: Machale J, Majumder SK, Ghosh P, Sen TK. Development of a novel biosurfactant for enhanced oil recovery and its influence on the rheological properties of polymer. Fuel 2019;257:116067.

Characterization of natural surfactant from *Eichhornia crassipes* for its possible application in EOR

This chapter focuses on the characterization of the synthesized natural surfactant from Eichhornia crassipes and study its beneficial effects on EOR. The synthesized surfactant was characterized by several spectroscopical, morphological, and interfacial analyses. Furthermore, the influence of the synthesized surfactant on the rheological properties of the conventionally-used polysaccharide (i.e., xanthan gum) was studied and compared with that of a commercially-used surfactant (i.e., sodium dodecyl sulfate).

4.1 General overview

This work is mainly focused on the characterization of a natural surfactant derived from the weed *Eichhornia crassipes*. The synthesized surfactant (WH) has been characterized by the Fourier-transform infrared spectroscopy (FTIR), gas chromatography–mass spectrometry (GC–MS), thermogravimetric analysis (TGA), nuclear magnetic resonance (NMR) spectroscopy, field-emission scanning electron microscopy (FESEM), and field-emission transmission electron microscopy (FETEM) to confirm the chemical and morphological structures.

The critical micelle concentration (CMC) of the surfactant was determined from the surface tension and conductivity measurements. Studies on rheological properties are important characterization techniques for the selection of chemicals used in the oil recovery process. In this work, linear as well as nonlinear rheological properties have been quantified to evaluate the potential of the natural surfactant for enhanced oil recovery (EOR). The influence of the synthesized surfactant on the rheological properties of xanthan gum (XG) has been studied and compared with that of sodium dodecyl sulfate (SDS).

4.2 Results and discussion

4.2.1 FTIR spectrum of the surfactant

The FTIR spectrum of the synthesized surfactant is shown in Figure 4.1. The spectrum showed an absorption band at 3230 cm^{-1}, which appeared due to the O–H stretches in the phenolic compounds. The presence of a peak at 2927 cm^{-1} signifies the C–H stretch, which is a characteristic of the alkane, alkene, and aromatic compounds. The peaks at 2361 and 1606 cm^{-1} are attributed to the stretching of C–N and C=O, respectively. The absorption at 1434 cm^{-1} corresponds to $–CH_3$ and $–CH_2–$ asymmetric stretches. The bands at 1370 and 1319 cm^{-1} indicate the C–O stretch, whereas the peak at 1011 cm^{-1} corresponds to the –O–C–C bond of the ester. The sharp peak at 600 cm^{-1} shows the C–H bond in alkyne.

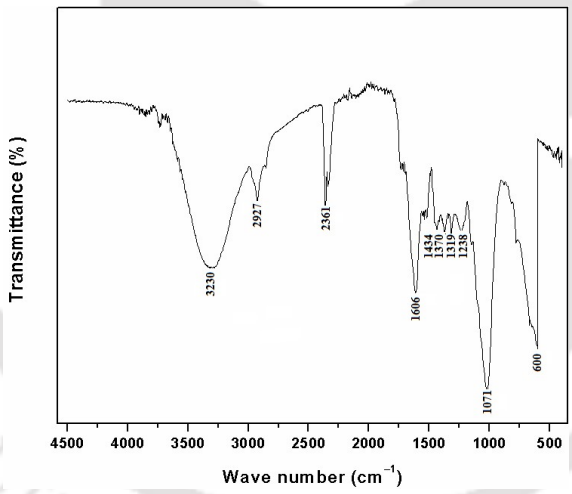

Figure 4.1. FTIR spectrum of WH.

4.2.2 GC–MS analysis of the surfactant

The GC–MS analysis was conducted to get information on the chemical composition of the synthesized surfactant. The mass spectrum of the synthesized surfactant is shown in Figure 4.2. Palmitic acid, cyclohexanecarboxylic acid, 4-methoxy-2-methyloct-5-yn-4-yl ester, petroselenic acid, phthalic acid, hexamethylcyclotrisiloxane, and 6-ethyloct-3-yl 2-ethylhexyl

ester, were the most prominent compounds present in the surfactant (Table 4.1). The surfactant contained mainly fatty acids, esters, and aromatic compounds.

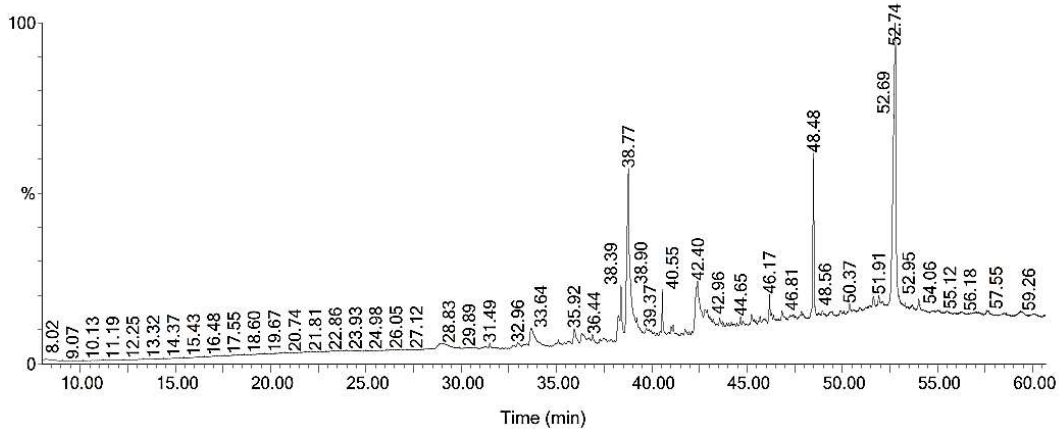

Figure 4.2. GC–MS spectrum of WH.

Table 4.1. Compounds recognized in the synthesized surfactant

Sl. No.	Retention time (min)	Area (%)	Compound	Molecular formula
1	33.70	2.54	Methyl palmitate	$C_{17}H_{34}O_2$
2	35.92	0.85	Stearyl methacrylate	$C_{22}H_{42}O_2$
3	38.40	1.83	Methacrylic acid, nonadecyl ester	$C_{23}H_{44}O_2$
4	38.77	12.92	Palmitic acid	$C_{16}H_{32}O_2$
5	40.55	0.89	Methacrylic acid, nonadecyl ester	$C_{23}H_{44}O_2$
6	41.12	0.27	Oleic acid	$C_{18}H_{34}O_2$
7	42.40	5.48	Petroselenic acid	$C_{18}H_{34}O_2$
8	45.23	0.42	Hentriacontane	$C_{31}H_{64}$
9	46.17	0.65	Bis (2-ethylhexyl) adipate	$C_{22}H_{42}O_4$
10	48.48	4.28	Phthalic acid, 6-ethyloct-3-yl 2-ethylhexyl ester	$C_{26}H_{42}O_4$
11	51.63	1.04	Terephthalic acid, 2-ethylhexyl propyl ester	$C_{19}H_{28}O_4$
12	51.91	1.42	Hexamethylcyclotrisiloxane	$C_6H_{18}O_3Si_3$
13	52.77	22.28	Cyclohexanecarboxylic acid, 4-methoxy-, 2-methyloct-5-yn-4-yl ester	$C_{17}H_{28}O_3$
14	54.00	0.80	Hexamethylcyclotrisiloxane	$C_6H_{18}O_3Si_3$

Palmitic acid is a saturated fatty acid with a 16-carbon backbone and a terminal carboxyl group. It can be produced by the hydrolysis of the fat present in the plant. It is the main intermediate product, which is used for the production of cosmetic creams, soaps, and emulsifiers. The emulsion formed with water and hexane in the presence of palmitic acid (i.e., 20 mol m^{-3}) was found to be stable for a long time. Also, the interfacial tension at the water–hexane interface decreased by 2.5 times after the addition of 50 mol m^{-3} palmitic acid [1]. In addition to palmitic acid, the existence of several fatty acids, such as oleic and petroselenic acids, was also found from the GC–MS analysis. These fatty acids are less toxic, biodegradable, and possess surface-active properties. Besides the fatty acids, the occurrence of esters such as methacrylic acid nonadecyl ester, stearyl methacrylate, bis (2-ethylhexyl) adipate, phthalic acid 6-ethyloct-3-yl 2-ethylhexyl ester, terephthalic acid 2-ethylhexyl propyl ester, and cyclohexanecarboxylic acid, 4-methoxy-, 2-methyloct-5-yn-4-yl ester signifies the surface-active properties of the synthesized surfactant.

4.2.3 ^{1}H NMR analysis of the surfactant

The ^{1}H NMR analysis was carried out to affirm the structure of the surfactant (see Figure 4.3). The chemical shift for the methyl group appeared at 0.87–0.89 mg dm^{-3}. The sharp peak at 1.24–1.35 mg dm^{-3} confirms the series of methylene functional group. The presence of allylic carbon and carbonyl proton is confirmed at 1.78 and 2.34 mg dm^{-3}, respectively. Extensive multiple peaks over 2.06–2.08 and 3.71–3.75 mg dm^{-3} show the presence of the ester group. The chemical shift at 4.69 mg dm^{-3} is due to the hydroxylic compound, and that at 5.38 mg dm^{-3} corresponds to the phenolic compound. The chemical shifts discussed above clearly demonstrate the existence of palmitic acid and the methyl ester group in the synthesized surfactant.

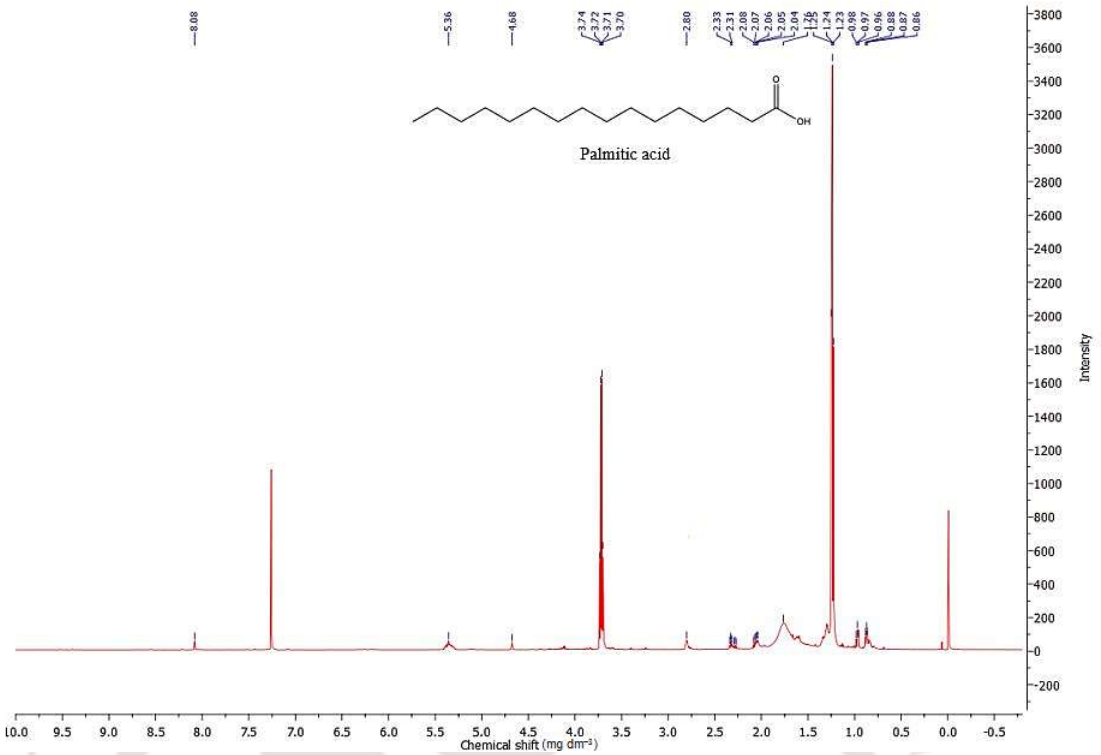

Figure 4.3. ^{1}H NMR spectrum of WH.

4.2.4 Measurement of zeta potential

The electrophoretic mobility of the surfactant molecules was measured, and the zeta potential was determined from their mobility. The zeta potential of the synthesized surfactant was found to be –26.4 mV, which signifies its anionic nature. It is the result of the carboxylic acid groups present in its structure. As mentioned in Section 2.3, the anionic surfactants are extensively used in the EOR applications due to their relatively low adsorption on the sandstone and clays. Also, they have low cost and good stability [2].

4.2.5 TGA of the surfactant

The results of thermogravimetric (TG) and derivative thermogravimetric (DTG) analyses of the synthesized surfactant under nitrogen atmosphere are shown in Figure 4.4. The heating rate was 10 K/min. It was observed that the decomposition of cellulose and hemicellulose began in the range of 470–590 K. About 14.1% residue of the sample was left even at 1400 K. Over the past few decades, the chemical method of EOR has been practiced successfully over a wide

range of reservoir temperature up to 385 K. It is remarkable that at 385 K, the surfactant retained 96% of its mass, which demonstrates its thermal stability and usability in EOR.

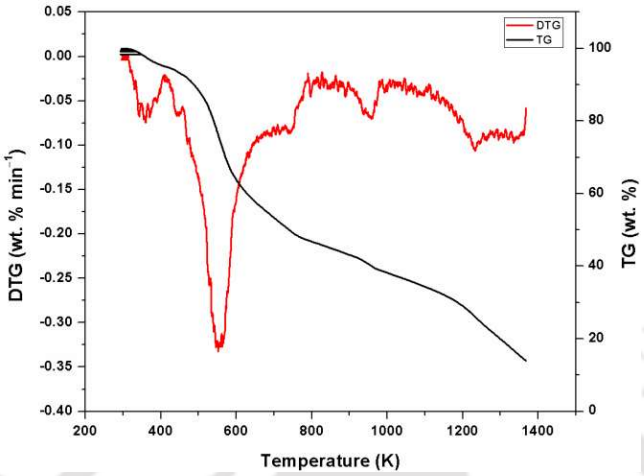

Figure 4.4. TG and DTG profiles of WH.

4.2.6 Surface tension and conductivity measurements

The surface tensions of the aqueous WH solutions are shown in Figure 4.5a. A reduction in surface tension was noticed upon increasing the WH concentration. The lowest surface tension was observed at ~0.25 wt. %, which indicates the saturation of the air–water interface by the surfactant molecules. Therefore, the CMC of WH is ~0.25 wt. %. The formation of micelles leads to abrupt modifications in the physical properties of the surfactant solution after the CMC, which may be the reason for the slight increase in the surface tension beyond the CMC [3]. In comparison with other natural surfactants [4–6], the surface tension of the present system is promising inasmuch as WH can effectively reduce it by ~60%. In comparison, the CMC of SDS is 0.23 wt. % [7].

The conductivity of the aqueous surfactant solution increased with the surfactant concentration (see Figure 4.5b). There was a sharp increase in conductivity between 0.2 and 0.25 wt. %, and the subsequent increase was rather small and almost linear. When the ionic surfactant is dissolved in water, it dissociates into ions. Initially, due to the small number of ions, the conductivity is low. However, with increasing surfactant concentration, the

conductivity increases until a point is reached where the micelles are formed. The mobility of the micelles is lower than the surfactant molecules, and the counterions neutralize the charge on the micelles. Hence, below the CMC, the surfactant monomers behave as strong electrolytes, and above the CMC, the micelles are partially-ionized clusters with lower mobility. The sharp increase in conductivity near the CMC is a characteristic of certain surfactants [8], whereas the breakpoint in the conductivity–concentration curve is not very sharp for some surfactants [9]. Therefore, from the surface tension and the conductivity measurements, we can conclude that the CMC of the WH was ~0.25 wt. %.

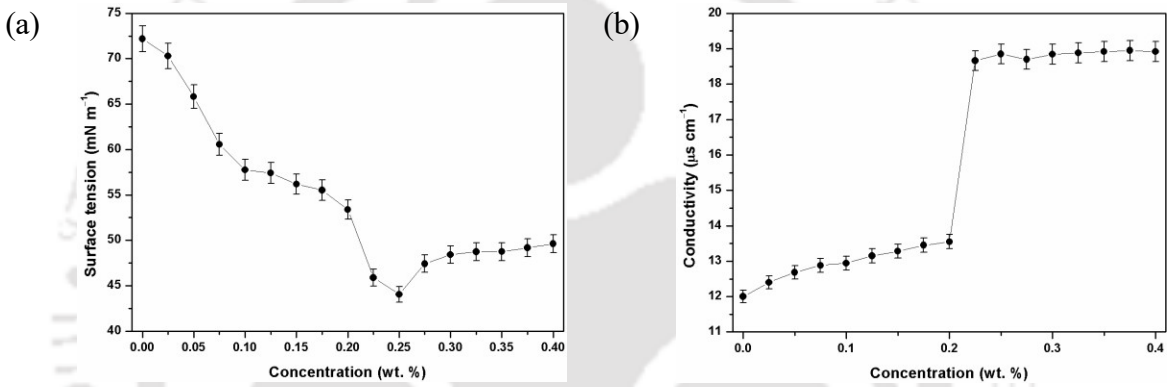

Figure 4.5. Variation of (a) surface tension and (b) conductivity with the concentration of the synthesized surfactant.

4.2.7 Morphological analysis

Figure 4.6 shows the morphology of WH and WH–XG systems. The surfactant extracted from *Eichhornia crassipes* clearly shows the existence of fibers with a morphological diameter of 290–370 nm. On the other hand, the surfactant–polymer system indicates fibers with an enhanced morphological diameter of 750–900 nm. Figure 4.6c shows the surface morphology of the fibers present in the synthesized surfactant. It can be observed that XG adsorbed on the surface of the fibers, which led to the formation of an associated structure (see Figure 4.6d). The rheological properties of the polymer solution improved noticeably after the addition of WH due to this reason, which is discussed in detail in Section 4.2.8.

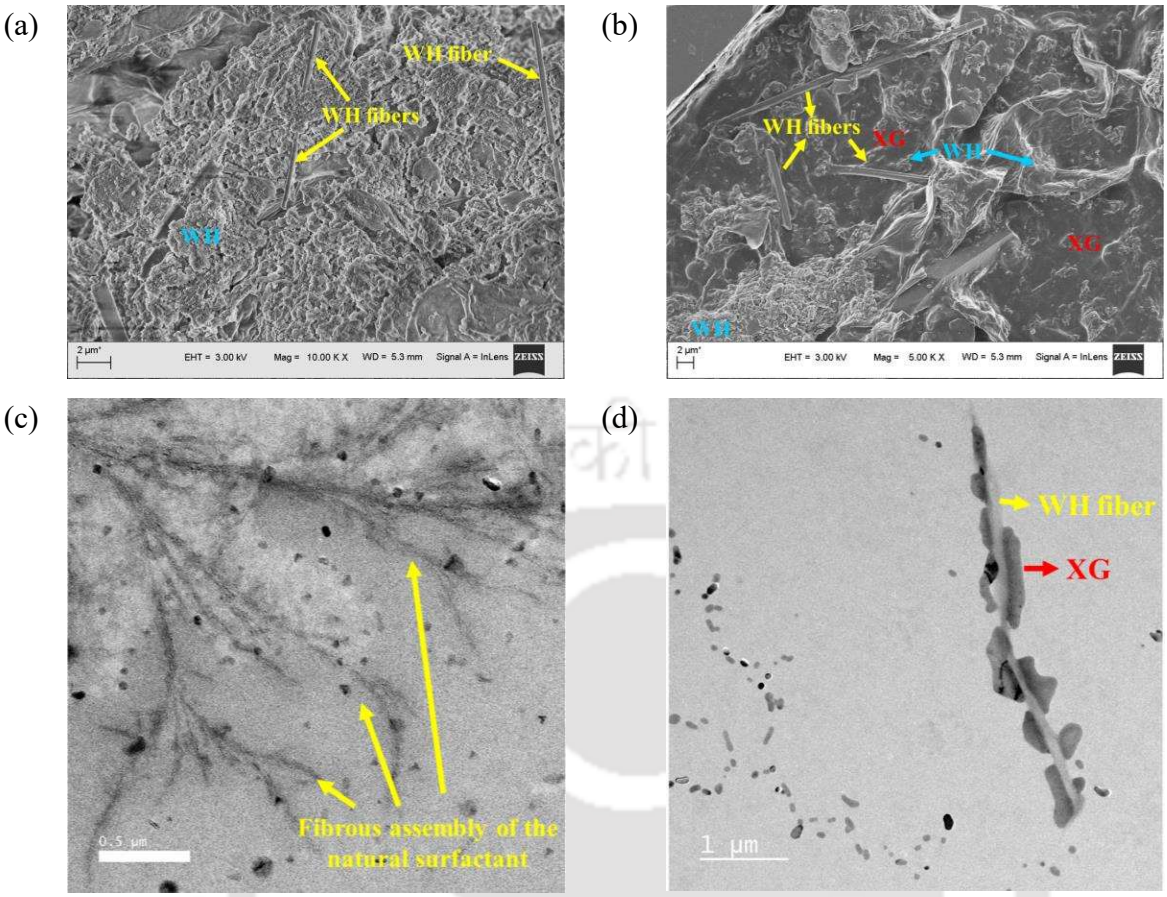

Figure 4.6. FESEM micrographs of (a) WH and (b) XG–WH, and FETEM micrographs of (c) WH and (d) XG–WH.

4.2.8 Rheological analysis

4.2.8.1 Steady shear flow

The addition of polymer to the reservoir increases the viscosity of the displacing fluid (i.e., water), which reduces its relative permeability in the reservoir. It is well known that the viscosity of the polymer solution increases with the concentration of polymer [10]. This is due to the increase in the formation of cross-linking bonds. For the application in EOR, it has been reported that 0.5 wt. % XG is very suitable [11]. Therefore, we have used this concentration of XG throughout this study. The increase in the apparent viscosity of the XG solution with the concentration of XG is shown in Figure 4.7.

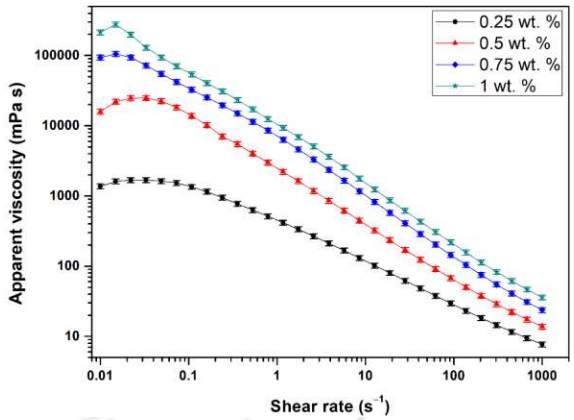

Figure 4.7. Apparent viscosities of the XG solutions of different concentrations as a function of shear rate at 298 K.

Figure 4.8a shows the effect of surfactant concentration on the apparent viscosity of the aqueous XG solution at 10 s^{-1} shear rate. Most of the flow through the porous media in the oil reservoir occurs at this shear rate [11]. The suitability of the water-soluble polymers used in EOR is measured by the increase in the apparent viscosity of the aqueous phase. The apparent viscosity of 0.5 wt. % XG solution was found to be 446 mPa s at 10 s^{-1} shear rate.

There was hardly any increase in the apparent viscosity of the XG solution after the addition of SDS. However, WH significantly increased its apparent viscosity. This is probably due to the strong interaction of the surfactant with the hydrophobic groups of the polymer, leading to the formation of an association structure between the polymer chains. The dramatic increase in the viscosity of the aqueous XG–WH solution may as well due to the presence of the fibers in the surfactant. The XG coiled up on the surface of the fibers of WH, leading to the formation of a complex association structure (see Figure 4.6). Considering the swelling of the fiber and formation of the association structure, WH may be used with the polymer as an effective viscosifier in EOR.

Figure 4.8b illustrates the flow behavior of the polymer solutions at different shear rates. It was observed that the apparent viscosity of the polymer solutions decreased with increasing shear rate, which indicates shear-thinning or pseudoplastic behavior. The reduction

of apparent viscosity with increasing shear rate is due to the alignment of the polymer chains in the flow direction and reduction in intermolecular interaction with the neighboring polymer chains [12,13]. Beyond the shear rate of 1 s^{-1}, the apparent viscosity of the XG–SDS solution was almost similar to that of the XG solution, which may be due to the sudden breakup of the association structure in the XG–SDS complex.

Nedjhioui et al. [12] have reported an increase in the apparent viscosity of the XG solution in the presence of SDS. On the contrary, the apparent viscosity of synthetic polymers decreases in the presence of SDS [14,15]. The aqueous XG–WH solution had a higher apparent viscosity than the XG and XG–SDS solutions. The fibers firmly held the association in the XG–WH system, and evidently, it was superior to the XG–SDS system.

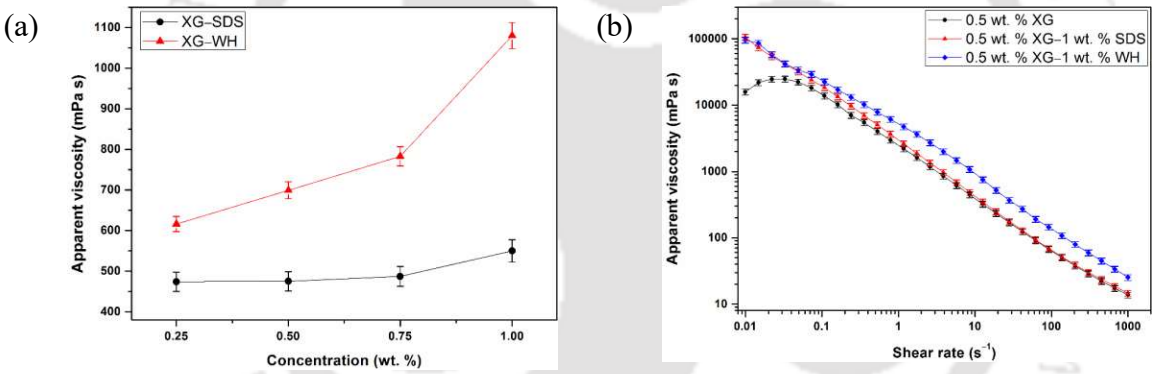

Figure 4.8. (a) Variation of the apparent viscosity of the aqueous XG solutions with surfactant concentration at 10 s^{-1} shear rate and (b) variation of the apparent viscosity of aqueous polymer solutions with shear rate (at 298 K).

The experimental data obtained from the steady shear flow tests were fitted by the power-law model,

$$\eta = K\dot{\gamma}^{n-1} \tag{4.1}$$

The values of *n* for all the polymer solutions were found to be less than unity, which indicates the shear-thinning behavior. It was also observed that *n* decreased with increasing polymer concentration, which indicates the formation of a gel-like structure. The power-law model

parameters for the polymer and the polymer–surfactant systems are given in Table 4.2. There was a very little variation in the values of n and K with the increasing concentration of SDS for the XG–SDS systems, and the variation in the flow behavior was insignificant as well. A decrease in n and an increase in K was observed in the XG–WH system. There was a reduction in the values of n (i.e., 0.30 to 0.23) with the increasing concentration of WH (i.e., 0.25–0.75 wt. %) for the XG–WH systems. However, with further increment in the WH concentration (i.e., 1 wt. %), n slightly increased to 0.27. As $n < 1$, the polymer–surfactant system signifies a shear thinning behavior.

Table 4.2. Power-law model parameters for polymer and polymer–surfactant systems

Sample	***n***	***K***	R^2
0.25 wt. % XG	0.48	337.3	0.97
0.5 wt. % XG	0.28	1986.1	0.98
0.75 wt. % XG	0.25	5470.2	0.99
1 wt. % XG	0.20	9078.2	0.99
0.5 wt. % XG–0.25 wt. % SDS	0.26	2290.8	0.99
0.5 wt. % XG–0.5 wt. % SDS	0.28	2118.4	0.98
0.5 wt. % XG–0.75 wt. % SDS	0.26	2558.6	0.98
0.5 wt. % XG–1 wt. % SDS	0.25	2837.9	0.99
0.5 wt. % XG–0.25 wt. % WH	0.30	2529.3	0.98
0.5 wt. % XG–0.5 wt. % WH	0.27	3280.9	0.99
0.5 wt. % XG–0.75 wt. % WH	0.23	3944.5	0.99
0.5 wt. % XG–1 wt. % WH	0.27	4345.1	0.99

The Carreau–Yasuda equation for the non-Newtonian fluids under steady shear flow is given by [16]

$$\eta = \eta_\infty + (\eta_0 + \eta_\infty)\left[1 + (\lambda\dot{\gamma})^a\right]^{\frac{n-1}{a}} \tag{4.2}$$

This model has five parameters $(\text{i.e., } \eta_0,\ \eta_\infty,\ \lambda,\ n, \text{ and } a)$ to describe the fluid rheology, where a is a constant, η_0 is the zero-shear viscosity, η_∞ is the infinite-shear viscosity, and λ is a constant ($1/\lambda$ is the critical shear rate at which the viscosity begins to decrease). The power-law slope is $(n-1)$, and the parameter a represents the width of the transition region between η_0 and the power-law region. Similar to the power-law model, the solution demonstrates shear-thinning behavior if n is less than unity. The Carreau–Yasuda model parameters for the polymer and the polymer–surfactant systems are given in Table 4.3.

It is clear from Table 4.3 that n was less than unity, which confirms the shear-thinning behavior of the polymer as well as the polymer–surfactant solutions. It was observed that n decreased with increasing concentration of the additives. Among all the systems, the 0.5 wt. % XG–1 wt.% WH solution showed the strongest shear thinning behavior with $n = 1\times10^{-4}$. η_0 was maximum for this system. In fact, it was almost 3.5 times that of the 1 wt. % XG solution. Thus, we can conclude that the 0.5 wt. % XG–1 wt.% WH system can decrease the water mobility, which ultimately would reduce the relative permeability of water in the reservoir [17]. With an increase in the viscosity, the sweep efficiency can be improved, which would augment the oil recovery. A comparison between the rheological behaviors of the 0.5 wt. % XG, 0.5 wt. % XG–1 wt. % SDS, and 0.5 wt. % XG–1 wt. % WH systems have been discussed in Sections 4.2.8.2–4.2.8.5.

4.2.8.2 Effect of temperature and salinity

Figure 4.9(a) shows the effect of temperature (i.e., 298–373 K) on the apparent viscosity of the polymer solutions at 10 s^{-1} shear rate. A substantial reduction in the apparent viscosity of all the polymer solutions was observed with increasing temperature. Generally, the speed of the molecules in liquid increases as the temperature increases. Therefore, the time they spend interacting with their adjacent neighbors decreases. Thus, the average intermolecular forces

Table 4.3. Carreau–Yasuda equation parameters for polymer solutions

Sample	$\eta_0 \left(\times 10^3\right)$	η_∞	λ	a	n	R^2
0.25 wt. % XG	1.60	0.10	8.15	1.99	0.40	0.99
0.5 wt. % XG	20.63	3.80	14.78	8.11	0.26	0.97
0.75 wt. % XG	252.03	8.10	36.47	0.51	0.08	0.98
1 wt. % XG	272.80	5.70	47.45	1.12	0.15	0.93
0.5 wt. % XG–0.25 wt. % SDS	36.95	4.00	26.30	1.96	0.20	0.99
0.5 wt. % XG–0.5 wt. % SDS	24.14	3.20	18.18	7.03	0.25	0.97
0.5 wt. % XG–0.75 wt. % SDS	31.47	4.60	17.94	4.43	0.18	0.98
0.5 wt. % XG–1 wt. % SDS	77.81	6.60	47.45	1.90	0.15	0.92
0.5 wt. % XG–0.25 wt. % WH	29.50	1.70	13.92	1.18	0.20	0.96
0.5 wt. % XG–0.5 wt. % WH	97.70	3.90	35.13	0.60	0.15	0.99
0.5 wt. % XG–0.75 wt. % WH	116.20	26.00	47.45	0.92	0.18	0.98
0.5 wt. % XG–1 wt. % WH	958.40	11.30	47.45	0.25	0.0001	0.96

decrease. The complex helical structures of XG promote strong rheological properties. However, as temperature increases beyond 333 K, these helical structures break and disorient into random coils. Therefore, a reduction in the apparent viscosity of XG above 333 K was observed. A similar observation has been reported elsewhere [18].

An increase in the apparent viscosity of an aqueous solution of XG in the presence of SDS was observed. This might be due to the strong interaction of the SDS molecules with a hydrophobic group of the XG that led to the formation of a loose-association structure between the polymer chains, which increased the viscosity [12]. The SDS micelles have a thermal stability up to 328 K [19]. Therefore, a sharp decrease in the apparent viscosity of the XG–SDS system was observed post 333 K.

The WH has a good thermal stability (discussed in Section 4.2.5). The XG coiled up on the surface of the fibers of WH, leading to the formation of a complex association structure (see Figure 4.6(d)). The apparent viscosity of the XG–WH was found to decrease with temperature. However, at 373 K, it was still higher than the XG and XG–SDS. The apparent viscosity of the solutions followed the sequence: XG–WH > XG–SDS > XG. This trend remained the same when the temperature was increased to 373 K. However, the addition of SDS and WH effectively increased the viscosity of the XG solution by 46.6 and 68.8%, respectively, even at 373 K.

The influence of brine on the apparent viscosity of the polymer solutions was studied at 298 K, and the results are shown in Figure 4.9b. A strong electroviscous effect was observed. The addition of Na^+ efficiently neutralized the negative charge on the polymer chains [14], resulting in their contraction and reduction in their hydrodynamic radius. On the other hand, Ca^{2+} disrupted the structure of XG by binding themselves to the negatively charged carboxyl groups, which eventually reduced the viscosity of the polymer solution [20]. The performance of the aqueous XG–WH solution was superior to the XG and XG–SDS solutions. However,

the apparent viscosity of the brine-free XG–WH solution was slightly higher than that in the presence of brine.

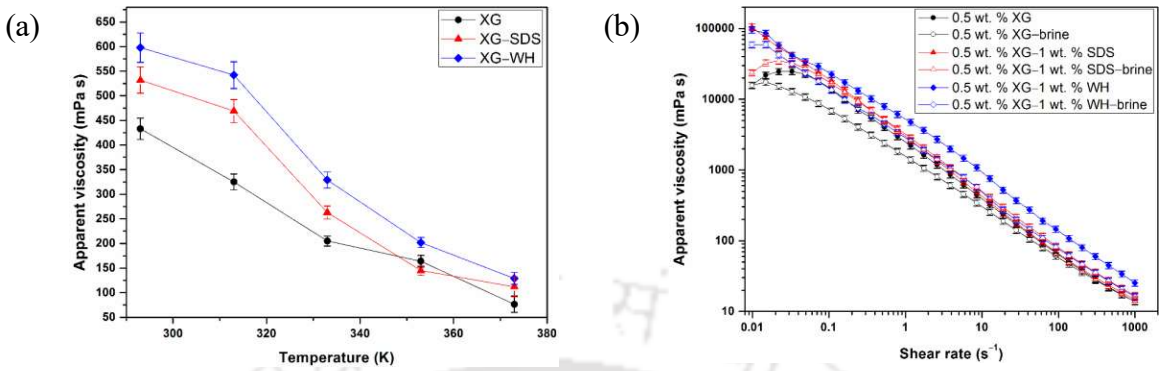

Figure 4.9. Effect of (a) temperature and (b) salinity on the flow behavior of the polymer solutions.

4.2.8.3 Mechanical degradation

The mechanical degradation of the aqueous XG, XG–SDS, and XG–WH solutions at various shear rates is shown in Figure 4.10. Initially, the sample was sheared from 10 to 1000 s^{-1} for 30 min. This was followed by a relaxation period of 10 min. Finally, it was again sheared for 30 min. The mechanical degradation of the polymer sample was quantified in terms of the viscosity loss by using the equation (4.3) [21],

$$\text{Viscosity loss } (\%) = \left(\frac{\mu_0 - \mu}{\mu_0}\right) \times 100 \tag{4.3}$$

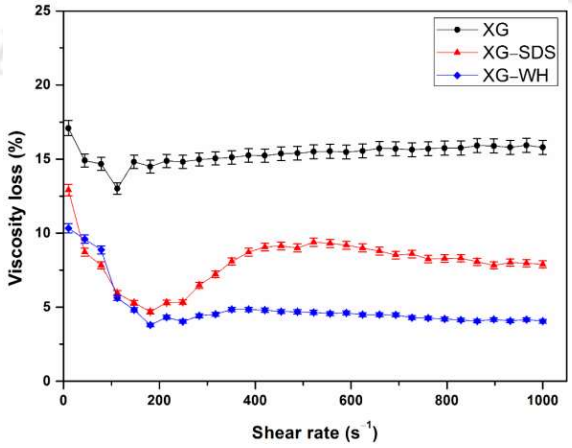

Figure 4.10. Mechanical degradation of the polymer solutions at different shear rates after a fixed shearing time (i.e., 30 min).

It is observed that the XG and the XG–SDS systems experienced more viscosity loss. This could be due to the structure disruption, which eventually reduced the viscosity. On the other hand, the XG–WH system showed extraordinary resistance to mechanical shear. The presence of fibers helped XG to be more stable, rigid, and provide strength to the polymer network [22].

4.2.8.4 Oscillatory shear flow

The viscoelastic nature of the polymer solutions was studied by the oscillatory shear test. First, the amplitude sweep test was carried out over the strain range of 0.1−1000% to determine the linear viscoelastic (LVE) region, within which the test would be carried out without destroying the structure of the sample. When the applied strain maintains a constant value of G', it signifies that the structure of the sample is maintained. However, when the applied strain is too high, the sample may break down, and the value of G' is decreased. Figure 4.11a shows the strain dependence of the storage and loss moduli for the aqueous polymer solutions at 298 K at a fixed frequency (i.e., 1 Hz).

It can be observed that G' dominated over G'' across the entire strain range. Thus, under these experimental conditions, the material behaved like a viscoelastic solid. Figure 4.11a indicates a strain-thinning feature of the aqueous polymer solutions inasmuch as G' reduced with increasing strain amplitude. This strain-thinning feature may be due to the destruction of the material's internal structure while responding to an externally-imposed stimulus [23]. The XG–WH solution was found to be more elastic, and it was characterized by a slower relaxation mechanism [24].

From Figure 4.11a, it is observed that G'' showed overshoot after 4% strain for the XG−WH solution. Due to the complex helical structure of XG and the fibers of WH, the molecules aligned and united to form a loosely-associated structure [25]. With increasing strain, this structure resisted the deformation up to a certain limit where G'' increased.

Thereafter, the structure was demolished by a large deformation over the critical strain, after which the polymer chains aligned with the flow field and G'' decreased. As the strain was increased further, the polymer chains disentangled and then aligned with the flow field. This effect became more significant in the anisotropic systems, which flowed more readily, and the moduli decreased further.

After determining the LVE region, the frequency sweep tests were conducted in small amplitude oscillatory shear flow fields to determine the viscoelasticity of the polymer solution. Figure 4.11b shows that the linear viscoelastic behavior of these polymer solutions was dominated by an elastic nature inasmuch as $G' > G''$, which showed the gel-like structure of the polymer solutions [24]. It is also observed from Figure 4.11b that G' of the aqueous XG–WH solution was higher than that of the other polymer solutions. This may be attributed to the attractive interaction between the fibers and the helical macromolecules of XG. This eventually formed weak polymer networks by means of hydrogen bonds and physical entanglement [22]. In comparison with the results reported [11,14,24,26,27], the elastic nature of the XG–WH solutions were found to be superior to the other polymer–surfactant solutions.

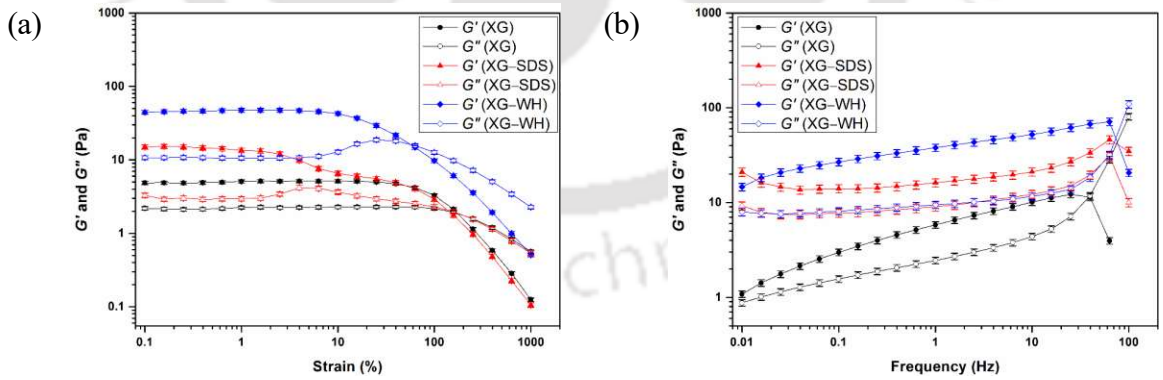

Figure 4.11. (a) Amplitude sweep and (b) frequency sweep of the polymer solutions.

From Figures 4.11, it is clear that the polymer solutions may be described by a slower relaxation mechanism. This can also be demonstrated by plotting the loss tangent, i.e., $\left[\tan\delta = G''(\omega)/G'(\omega)\right]$ as a function of frequency. When $\tan\delta >> 1$, the material is usually

liquid-like. On the other hand, for $\tan\delta << 1$, a solid-like behavior is observed [28,29]. It is clear from Figure 4.12 that $\tan\delta$ was less than unity for all polymer solutions. Its value was lowest for the aqueous XG–WH solution, which indicates a solid-like viscoelastic behavior.

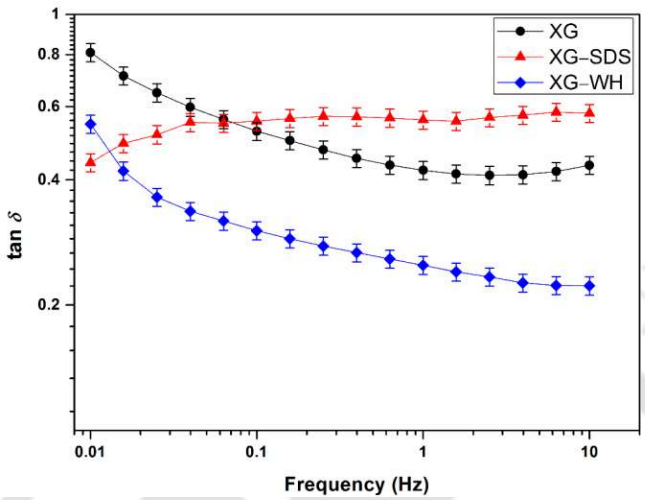

Figure 4.12. Loss tangent as a function of frequency for the polymer solutions.

4.2.8.5 Temperature sweep

The performance of the polymer solutions during heating was investigated by a temperature sweep in which the temperature was increased from 282 to 343 K. A steady frequency (1 Hz) and strain (5%) was maintained (see Figure 4.13). The XG solution was degraded with increasing temperature, which made it the least suitable choice for EOR. In the case of the aqueous XG–SDS and XG–WH solutions, the G' and G'' initially decreased but increased rapidly after 325 K, which indicates the formation of a strong and ordered network. It is clear that the G' and G'' for the XG–WH solution were nearly 2 to 20 times greater than those of the XG–SDS solution. This indicates a more stable, organized, and strong structure of the XG–WH system.

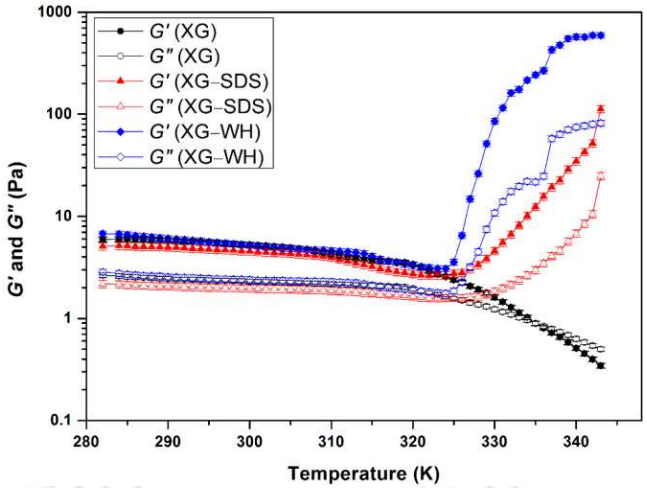

Figure 4.13. Effect of temperature on the G' and G'' of the polymer solutions.

4.3 Conclusions

The presence of fatty acids and various esters was confirmed from FTIR, GC–MS, and ^{1}H NMR analyses. The composition of the synthesized surfactant justifies its surface-active properties. Its TGA analysis showed good thermal stability. The CMC of the surfactant was ~0.25 wt. %. The presence of fibers in the surfactant helped it enhance the rheological properties of XG. The apparent viscosity of the XG–surfactant solution decreased with increasing shear rate, which indicated a shear thinning behavior. The flow behavior index was less than unity for the power law and the Carreau–Yasuda models, which further confirmed the shear thinning behavior. The XG–WH system was found to be the most effective due to its stronger shear thinning behavior in comparison with the conventional XG and XG–SDS systems. In addition to shear, the XG–WH system was found to be more stable at high temperatures, in saline media, and against mechanical degradation. Oscillatory shear tests confirmed the viscoelastic behavior of the polymer solutions. The XG–WH system was found to be better than the conventional systems over a wide range of strain and frequency. The dominating elastic properties of the XG–WH system would be helpful in pulling the oil out from the trapped zone as well as pushing the fluid ahead. This “push and pull” mechanism may effectively enhance oil recovery.

Nomenclature

a	constant in equation (4.2)
G'	storage modulus, Pa
G''	loss modulus, Pa
n	flow behavior index
K	consistency index, mPa s

Greek letters

$\dot{\gamma}$	shear rate, s^{-1}
η	viscosity, mPa s
η_0	zero-shear viscosity, mPa s
η_∞	infinite-shear viscosity, mPa s
λ	constant in equation (4.2), s
μ	viscosity determined after 10 min relaxation time, mPa s
μ_0	viscosity determined before 10 min relaxation time, mPa s

Abbreviations

CMC	critical micelle concentration
DTG	derivative of thermogravimetric analysis
EOR	enhanced oil recovery
FESEM	field-emission scanning electron microscopy
FETEM	field-emission transmission electron microscopy
FTIR	Fourier-transform infrared spectroscopy
GC–MS	gas chromatography–mass spectrometry
LVE	linear viscoelastic region

NMR	nuclear magnetic resonance
SDS	sodium dodecyl sulfate
TGA	thermogravimetric analysis
WH	surfactant synthesized from *Eichhornia crassipes* (commonly known as Water Hyacinth)
XG	xanthan gum

References

[1] Santini E, Guzmán E, Ferrari M, Liggieri L. Emulsions stabilized by the interaction of silica nanoparticles and palmitic acid at the water–hexane interface. Colloids Surf, A 2014;460:333–41.

[2] Green DW, Willhite GP. Enhanced oil recovery. Society of Petroleum Engineers: Richardson, Texas, USA, 1998.

[3] Lv M, Luo C, Yang J, Zhou Y, Liu C, Xu B. Effect of number of oxypropylene on dynamic interfacial tensions of extended surfactants. Colloids Surf, A 2019;570:429–37.

[4] Saxena N, Pal N, Dey S, Mandal A. Characterizations of surfactant synthesized from palm oil and its application in enhanced oil recovery. J Taiwan Inst Chem Eng 2017;81:343–55.

[5] Torres L, Moctezuma A, Avendaño JR, Muñoz A, Gracida J. Comparison of bio-and synthetic surfactants for EOR. J Pet Sci Eng 2011;76:6–11.

[6] Pradhan A, Bhattacharyya A. Quest for an eco-friendly alternative surfactant: Surface and foam characteristics of natural surfactants. J Clean Prod 2017;150:127–34.

[7] Bera A, Kumar T, Ojha K, Mandal A. Adsorption of surfactants on sand surface in enhanced oil recovery: Isotherms, kinetics and thermodynamic studies. Appl Surf Sci 2013;284:87–99.

[8] Chidi O, Adebayo IV. Determination of critical micelle concentration and thermodynamic evaluations of micellization of GMS. Mod Chem Appl 2018;6:251.

[9] Carpena P, Aguiar J, Bernaola-Galván P, Carnero Ruiz C. Problems associated with the treatment of conductivity− concentration data in surfactant solutions: simulations and experiments. Langmuir 2002;18:6054–8.

[10] Song KW, Kim YS, Chang GS. Rheology of concentrated xanthan gum solutions: Steady shear flow behavior. Fibers Polym 2006;7:129–38.

[11] Saha R, Uppaluri RV, Tiwari P. Silica nanoparticle assisted polymer flooding of heavy crude oil: Emulsification, rheology, and wettability alteration characteristics. Ind Eng Chem Res 2018;57:6364–76.

[12] Nedjhioui M, Moulai-Mostefa N, Canselier JP, Bensmaili A. Investigation of combined effects of xanthan gum, sodium dodecyl sulphate, and salt on some physicochemical properties of their mixtures using a response surface method. J Dispersion Sci Technol 2009;30:1333–41.

[13] Nedjhioui M, Moulai-Mostefa N, Morsli A, Bensmaili A. Combined effects of polymer/surfactant/oil/alkali on physical chemical properties. Desalination 2005;185:543–50.

[14] Samanta A, Bera A, Ojha K, Mandal A. Effects of alkali, salts, and surfactant on rheological behavior of partially hydrolyzed polyacrylamide solutions. J Chem Eng Data 2010;55:4315–22.

[15] Zhang J, Wang X, Liu H, Tang J, Jiang L. Interfacial rheology investigation of polyacrylamide–surfactant interactions. Colloids Surf, A 1998;132:9–16.

[16] Morozov A, Spagnolie SE. Introduction to complex fluids. Complex Fluids in Biological Systems. New York, USA: Springer; 2015, p. 3–52.

[17] Sorbie KS. Polymer-improved oil recovery. CRC Press: Boca Raton, Florida 1991.

[18] Reinoso D, Martin-Alfonso M, Luckham P, Martinez-Boza F. Rheological characterisation of xanthan gum in brine solutions at high temperature. Carbohydr Polym 2019;203:103–9.

[19] Makowska J, Wyrzykowski D, Pilarski B, Chmurzyński L. Thermodynamics of sodium dodecyl sulphate (SDS) micellization in the presence of some biologically relevant pH buffers. J Therm Anal Calorim 2015;121:257–61.

[20] Dário AF, Hortêncio LM, Sierakowski MR, Neto JCQ, Petri DF. The effect of calcium salts on the viscosity and adsorption behavior of xanthan. Carbohydr Polym 2011;84:669–76.

[21] Wei B, Romero-Zerón L, Rodrigue D. Formulation of a self-assembling polymeric network system for enhanced oil recovery applications. Adv Polym Tech 2014;33:21413.

[22] Xin X, Xu G, Gong H, Bai Y, Tan Y. Interaction between sodium oleate and partially hydrolyzed polyacrylamide: A rheological study. Colloids Surf, A 2008;326:1–9.

[23] Song K, Chang G, Kim C, Lee J, Paik J. Rheological characterization of aqueous poly (ethylene oxide) solutions (I): Limits of linear viscoelastic response and nonlinear behavior with large amplitude oscillatory shear deformation. J Kor Fiber Soc 1996;33:1083–93.

[24] Song KW, Kuk HY, Chang GS. Rheology of concentrated xanthan gum solutions: Oscillatory shear flow behavior. Korea-Australia Rheol J 2006;18:67–81.

[25] Rochefort WE, Middleman S. Rheology of xanthan gum: Salt, temperature, and strain effects in oscillatory and steady shear experiments. J Rheol 1987;31:337–69.

[26] Mahdavi S, Aalaie J, Miri T, Razavi S, Rahmani M. Study of polyacrylamide–surfactant system on the water–oil interface properties and rheological properties for EOR. Arabian J Chem 2016;10:1136–46.

[27] Saha R, Uppaluri RVS, Tiwari P. Impact of natural surfactant (Reetha), polymer (xanthan Gum) and silica nanoparticles to enhance heavy crude oil recovery. Energy Fuels 2019;33:4225–36.

[28] Harrison G, Franks G, Tirtaatmadja V, Boger D. Suspensions and polymers–common links in rheology. Korea-Australia Rheol J 1999;11:197–218.

[29] Ross-Murphy S, Shatwell K. Polysaccharide strong and weak gels. Biorheology 1993;30:217–27.

Chapter 5

Impact of mineralogy, salinity, and temperature on the adsorption characteristics of the synthesized natural surfactant

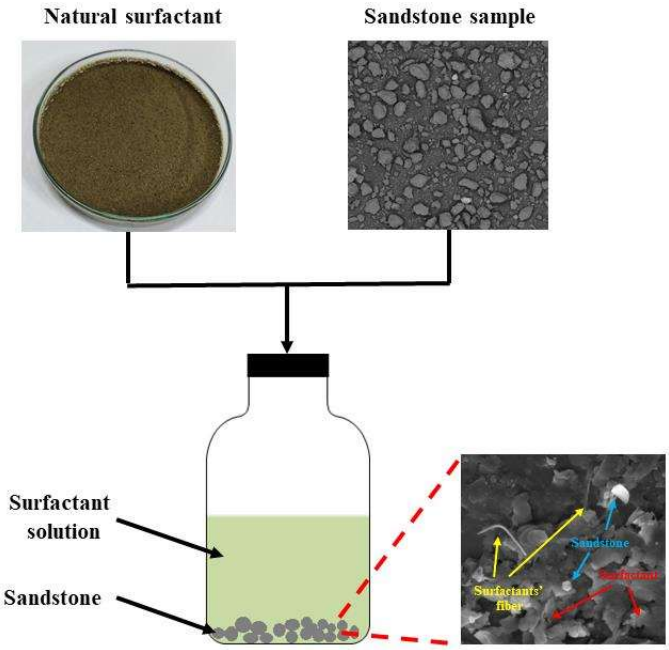

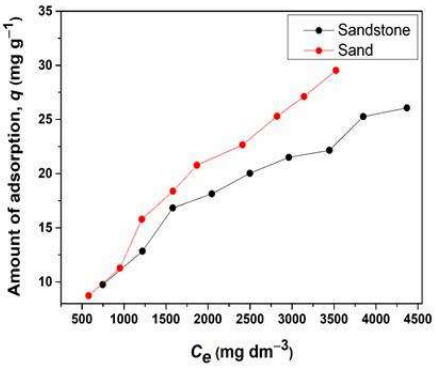

Published article: Machale J, Majumder SK, Ghosh P, Sen TK, Saeedi A. Impact of mineralogy, salinity, and temperature on the adsorption characteristics of a novel natural surfactant for enhanced oil recovery. Chemical Engineering Communications 2022;209:143–57.

Impact of mineralogy, salinity, and temperature on the adsorption characteristics of the synthesized natural surfactant

This chapter mainly focuses on evaluating the adsorption of the synthesized natural surfactant on the porous media. This study features the kinetics, mechanism, and equilibrium of adsorption of the surfactant on sand and sandstone rock. This study also highlights the influence of brine and temperature on the adsorption of the surfactant.

5.1 General overview

Loss of surfactants by adsorption on the porous rock surface is one of the significant drawbacks of surfactant flooding. Thus, it is essential to analyze the mechanism of adsorption of the surfactant on a porous rock under reservoir-like conditions [1–3]. Adsorption of the natural surfactant on the sandstone and sand surfaces was investigated with the help of Langmuir, Freundlich, Temkin, and Linear isotherms [4–7]. Details of these adsorption isotherms are summarized in Table 5.1.

Table 5.1. Details of the adsorption isotherms

Adsorption isotherm	Equation	Remarks
Langmuir	$q_e = \frac{q_0 K_L C_e}{K_L C_e + 1}$	It is commonly used to describe the adsorption in a monolayer system.
Freundlich	$q_e = K_f C_e^{1/n}$	It deals with adsorption on the heterogeneous surface with several adsorption sites.
Temkin	$q_e = B \ln K_t + B \ln C_e$	It considers the influence of the interaction between the adsorbate molecules on adsorption.
Linear	$q_e = K_H C_e$	It is established on the basis of the Henry equation. Acceding to this isotherm, the amount adsorbed increases linearly with the equilibrium concentration.

The kinetics of adsorption of the surfactant on the rock surface was illustrated with the help of the pseudo-first-order, pseudo-second-order, and intraparticle diffusion models. Furthermore,

thermodynamics of adsorption of the natural surfactant on the rock surfaces was studied. The fit of the models and the respective model parameters are discussed in the chapter. The details of the experiments are given in Section 3.3.12.

5.2 Results and discussion

5.2.1 Adsorbent characterization

The mineralogical constituents of the sandstone and sand samples were characterized by the X-ray diffractometer (XRD). It is clear from Figure 5.1 that the samples had a single-phase structure as indicated by the single-headed peak. The major peaks at 26.82° and 26.65° in the sandstone and sand, respectively, confirm the presence of quartz. The XRD analysis also confirmed the presence of a few impurities such as feldspar (21.11°, in the sand), albite (23.88°, in the sandstone), iron (36.69°, in the sand), and kaolin (42.54° and 45.93°, in the sandstone and sand, respectively).

The surface morphology, roughness, and texture of the adsorbent (both before and after adsorption) were analyzed using a field-emission scanning electron microscope (FESEM) (see Figure 5.2). The surfaces of sandstone and sand were found to be porous. These characteristics influenced the adsorption capacity and film thickness of the adsorbate molecules on the adsorbent surface.

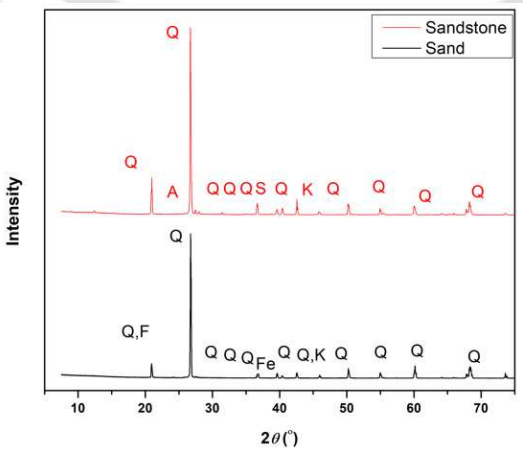

Figure 5.1. XRD images of sandstone and sand (Q: Quartz, F: Feldspar, A: Albite, Fe: Iron, and K: Kaolin).

(a) (b)

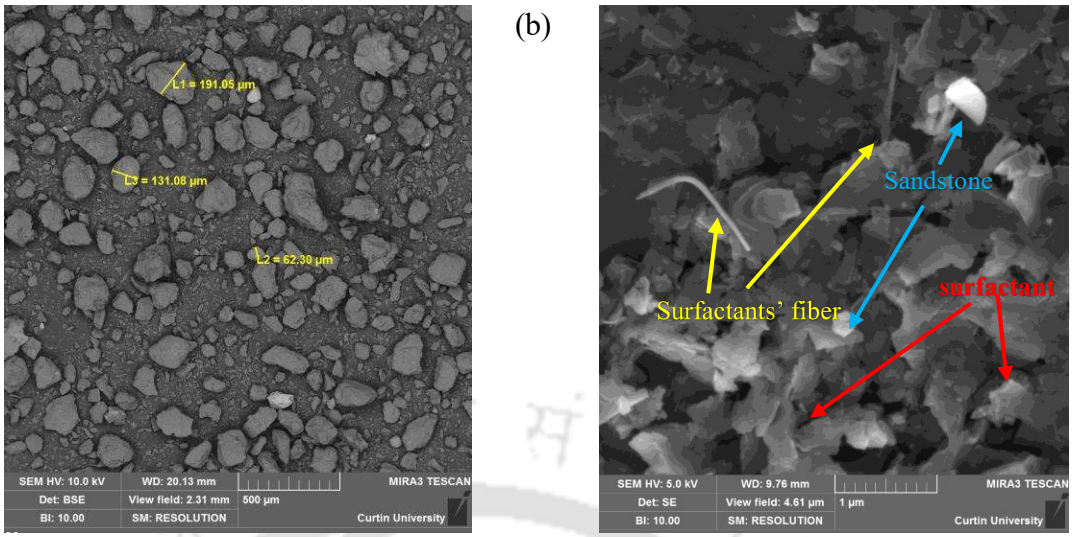

Figure 5.2. The FESEM micrographs of the sandstone sample (a) before and (b) after surfactant adsorption.

5.2.2 Adsorption of surfactant

The absorbance of the surfactant solutions from its solutions at different concentrations was measured by the UV–visible spectrophotometer. Figure 5.3 shows that a significant absorbance was observed in the wavelength range of 194–218 nm at all surfactant concentrations. The average wavelength (i.e., 206 nm) was set to obtain the calibration curve (see Figure 5.3b).

(a) (b)

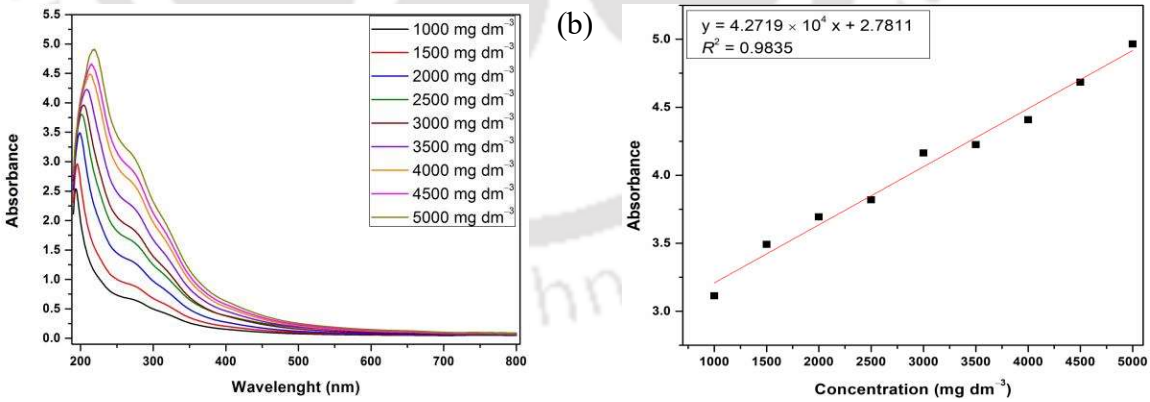

Figure 5.3. (a) Absorbance spectra and (b) calibration curve for the natural surfactant (x is the concentration and y is the absorbance).

Adsorption of the surfactant on the sandstone and sand surfaces at varying surfactant concentrations was measured, and the results are shown in Figure 5.4. It is evident that the amount of surfactant adsorbed increased with increasing surfactant concentration. The

electrostatic force between the hydrophilic portion of the surfactant and the negatively-charged adsorbent, chemical interaction between the fatty acids and the rock surface, and the hydrophobic effect govern the adsorption of the surfactant molecules. A similar result has been reported by numerous researchers [8,9]. Generally, a monolayer of the surfactant molecules is developed over the rock surface at the lower concentrations of the surfactant. As the surfactant concentration increased beyond the critical micellar concentration (CMC), the molecules self-assembled to form micelles. The adsorption of the surfactant increased after the CMC due to the presence of micelles in the bulk phase [10].

5.2.3 Analysis of adsorption data by isotherms

5.2.3.1 Langmuir isotherm

Figure 5.5 shows the fit of the Langmuir isotherm to the experimental data for both types of rock surfaces. The parameters of this isotherm, obtained by curve fitting, are given in Table 5.2. The separation factor (R_L) for the Langmuir isotherm is given by

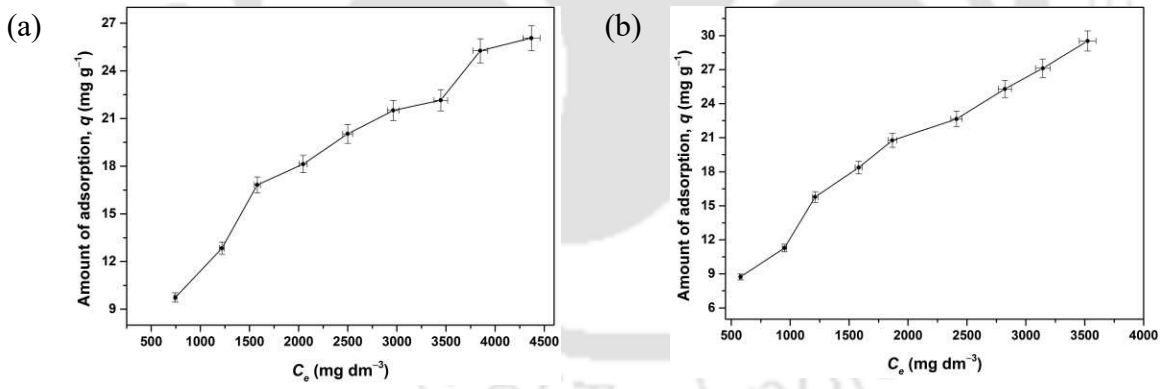

Figure 5.4. Variation of equilibrium adsorption with the initial surfactant concentration on (a) sandstone and (b) sand.

$$R_L = \frac{1}{1 + K_L C_e} \tag{5.1}$$

The adsorption of surfactant on rock is considered favorable for $0 < R_L < 1$. However, the values of R_L at the CMC of the surfactant (i.e., 2500 mg dm^{-3}) for sandstone and sand were

found to be around 0.52 and 0.68, respectively, which indicate favorable adsorption of the surfactant on these rocks.

5.2.3.2 Freundlich isotherm

Analysis of the experimental data with the Freundlich isotherm, and its parameters are shown in Figure 5.5 and Table 5.2, respectively. A good agreement was observed between the experimental data and the fitted isotherm for both samples. The higher values of the adsorption capacity indicate a significant adsorption of the surfactant on both sandstone and sand.

5.2.3.3 Temkin isotherm

The experimental data were fitted by the Temkin isotherm, as shown in Figure 5.5. It is apparent from the isotherm parameters (see Table 5.2) that the Temkin model is inappropriate to explain the adsorption of the surfactant on the rock samples.

5.2.3.4 Linear isotherm

The linear isotherm also failed to fit the experimental data. The fit of the model is shown in Figure 5.5, and the values of K_H are given in Table 5.2.

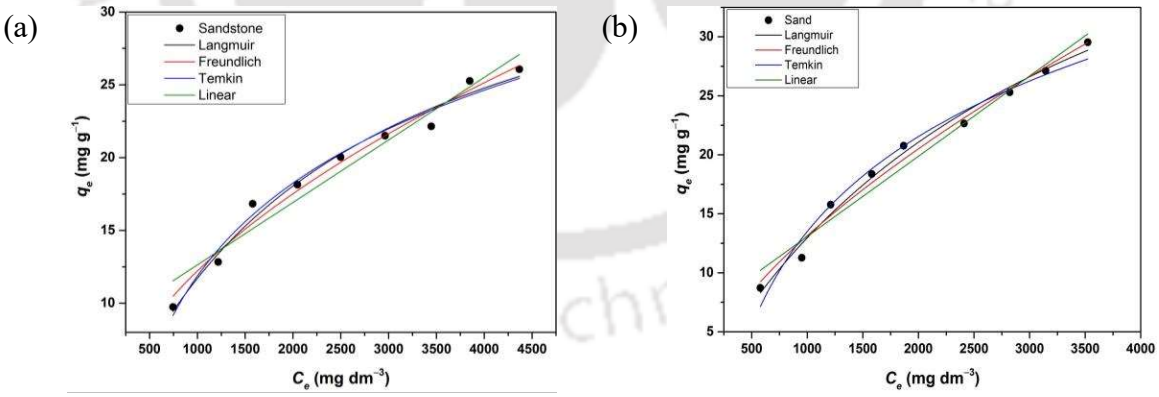

Figure 5.5. Effect of concentration of surfactant on the adsorption, and the fit of the adsorption isotherms for (a) sandstone and (b) sand.

Table 5.2. Parameters of the adsorption isotherms

Isotherm	Sandstone			Sand		
Langmuir	K_L (dm^3 mg^{-1})	q_0 (mg g^{-1})	R^2	K_L (dm^3 mg^{-1})	q_0 (mg g^{-1})	R^2
	4.22×10^{-4}	39.46	0.98	3.00×10^{-4}	56.11	0.99
Freundlich	K_f (dm^3 mg^{-1})	n	R^2	K_f (dm^3 mg^{-1})	n	R^2
	0.33	1.92	0.98	0.15	1.56	0.98
Temkin	K_t (dm^3 mg^{-1})	B	R^2	K_t (dm^3 mg^{-1})	B	R^2
	3.63×10^{-3}	9.20	0.98	3.20×10^{-3}	11.60	0.96
Linear	K_H (dm^3 m^{-2})		R^2	K_H (dm^3 m^{-2})		R^2
	4.30×10^{-3}		0.95	6.90×10^{-3}		0.97

5.2.4 Effect of salinity on the adsorption of surfactant

Salinity is among the most critical factors, which affect the adsorption of surfactant [11]. Adsorption of the surfactant increased in the saline medium (see Figure 5.6). It was mainly due to the physicochemical interactions between the surfactant molecules, rock particles, and salt ions [12]. The reduction of the electrostatic repulsion between the surfactant molecules led to the enhancement in the surfactant adsorption on the rock surface [13]. In addition, salt counterions may adsorb on the surface of the surfactant, which eventually reduces the charge of the surface [14]. The values of the parameters of the isotherm are reported in Table 5.3.

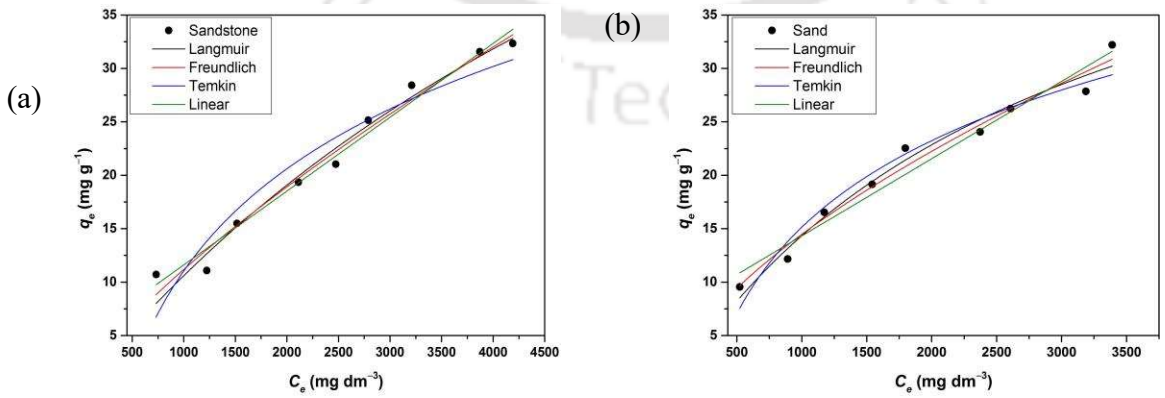

Figure 5.6. Effect of salinity on the adsorption of the surfactant on the (a) sandstone and (b) sand samples, and the fit of the adsorption isotherms.

Table 5.3. Effect of salinity on the adsorption of surfactant on the rock surfaces, and the parameters of the adsorption models

Isotherm	Sandstone			Sand		
Langmuir	K_L (dm^3 mg^{-1})	q_0 (mg g^{-1})	R^2	K_L (dm^3 mg^{-1})	q_0 (mg g^{-1})	R^2
	1.24×10^{-4}	95.71	0.97	3.14×10^{-4}	56.28	0.97
Freundlich	K_f (dm^3 mg^{-1})	n	R^2	K_f (dm^3 mg^{-1})	n	R^2
	0.06	1.32	0.97	0.20	1.61	0.97
Temkin	K_t (dm^3 mg^{-1})	B	R^2	K_t (dm^3 mg^{-1})	B	R^2
	2.23×10^{-3}	13.80	0.91	3.65×10^{-3}	11.68	0.95
Linear	K_H (dm^3 m^{-2})		R^2	K_H (dm^3 m^{-2})		R^2
	7×10^{-3}		0.98	7×10^{-3}		0.96

5.2.5 Impact of temperature on the adsorption of surfactant

The influence of temperature on the adsorption of the surfactant is one of the necessary aspects for screening the surfactant. In this study, a substantial reduction in the adsorption was observed with increasing temperature. This suggests that the adsorption was exothermic [8]. The impact of temperature on surfactant adsorption is subject to the adsorption density. Reduction in the adsorption occurred due to the increase in the kinetic energy of the surfactant molecules [15,16]. The fits of the models to the experimental data at different temperatures are shown in Figures 5.7 and 5.8, and the values of the parameters of the isotherms are reported in Tables 5.4 and 5.5.

(a)

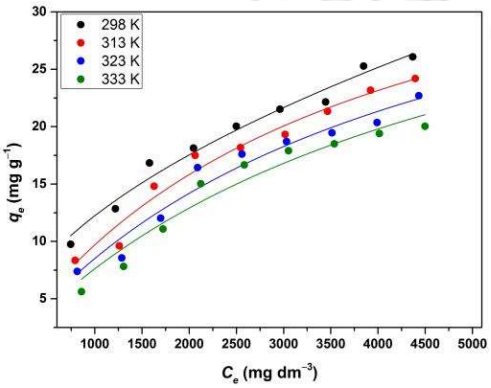

(b)

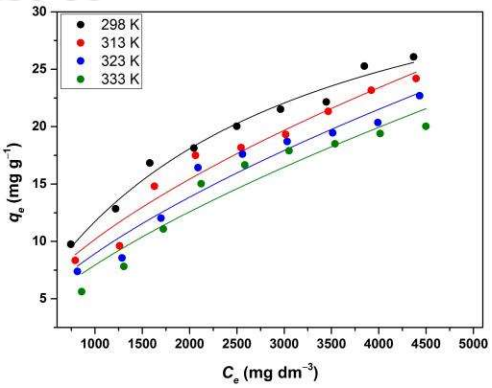

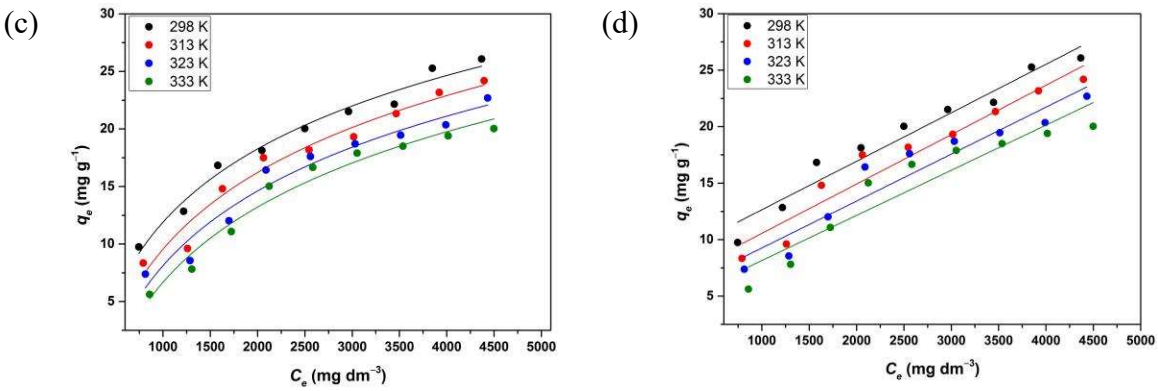

Figure 5.7. Effect of temperature on the adsorption of surfactant on sandstone, and the fit of (a) Langmuir, (b) Freundlich, (c) Temkin, and (d) Linear adsorption isotherms.

Table 5.4. Parameters of the isotherms for the adsorption of the surfactant on the sandstone surface at 313–333 K

Isotherm	**Temperature (K)**	**Isotherm Parameters**		
Langmuir		K_L (dm^3 mg^{-1})	q_0 (mg g^{-1})	R^2
	313	2.90×10^{-4}	43.12	0.97
	323	2.46×10^{-4}	42.98	0.95
	333	2.17×10^{-4}	42.51	0.95
Freundlich		K_f (dm^3 mg^{-1})	n	R^2
	313	0.16	1.66	0.96
	323	0.11	1.57	0.94
	333	0.08	1.50	0.92
Temkin		K_t (dm^3 mg^{-1})	B	R^2
	313	2.66×10^{-3}	9.64	0.96
	323	2.37×10^{-3}	9.38	0.95
	333	2.02×10^{-3}	9.44	0.97
Linear		K_H (dm^3 m^{-2})		R^2
	313	4.4×10^{-3}		0.94
	323	4.2×10^{-3}		0.92
	333	4.0×10^{-3}		0.89

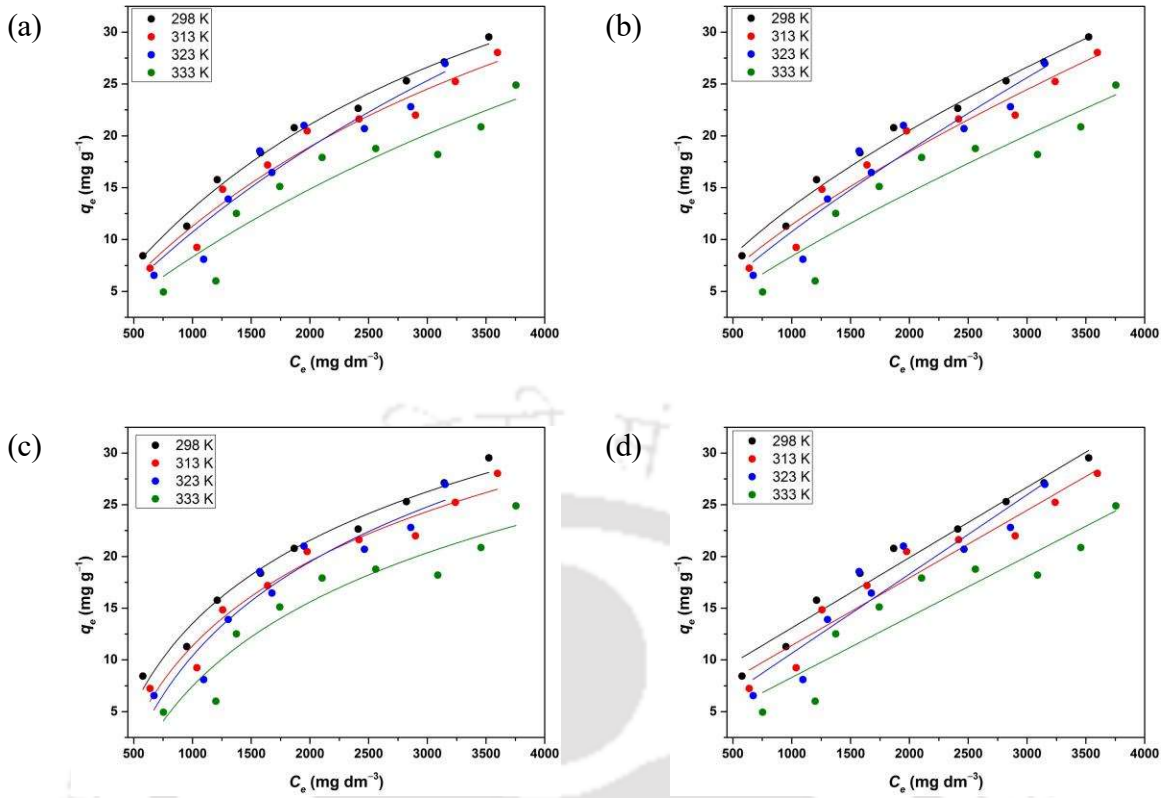

Figure 5.8. Effect of temperature on the adsorption of surfactant on sand, and the fit of (a) Langmuir, (b) Freundlich, (c) Temkin, and (d) Linear adsorption isotherms.

Table 5.5. Parameters of the isotherms for the adsorption of the surfactant on the sand surface at 313–333 K

Isotherm	**Temperature (K)**	**Isotherm Parameters**		
Langmuir		K_L (dm^3 mg^{-1})	q_0 (mg g^{-1})	R^2
	313	2.33×10^{-4}	59.51	0.95
	323	1.54×10^{-4}	79.84	0.90
	333	1.33×10^{-4}	70.35	0.88
Freundlich		K_f (dm^3 mg^{-1})	n	R^2
	313	0.094	1.66	0.94
	323	0.045	1.26	0.88
	333	0.035	1.25	0.87
Temkin		K_t (dm^3 mg^{-1})	B	R^2
	313	2.60×10^{-3}	11.84	0.95

	323	2.20×10^{-3}	13.12	0.91
	333	1.88×10^{-3}	11.75	0.90
Linear		K_H (dm^3 m^{-2})		R^2
	313	6.5×10^{-3}		0.93
	323	7.7×10^{-3}		0.88
	333	6.0×10^{-3}		0.87

5.2.6 Kinetics of adsorption

Adsorption involves solid–liquid interaction and transfer of mass from the liquid phase to the solid surface. The rate and mechanism of adsorption can be well-described by studying the adsorption kinetics. There are mainly three types of adsorption kinetics, which are discussed in the following sections. The studies on adsorption kinetics were carried out by measuring the amount of surfactant adsorbed at different times (see Figure 5.9).

(a)

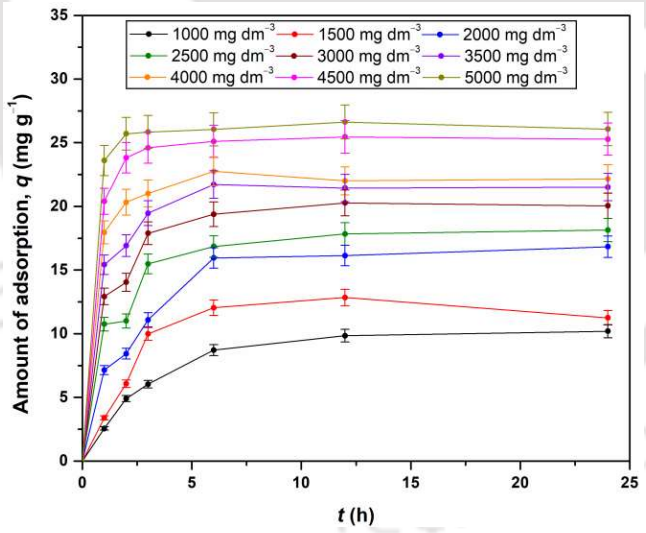

(b)

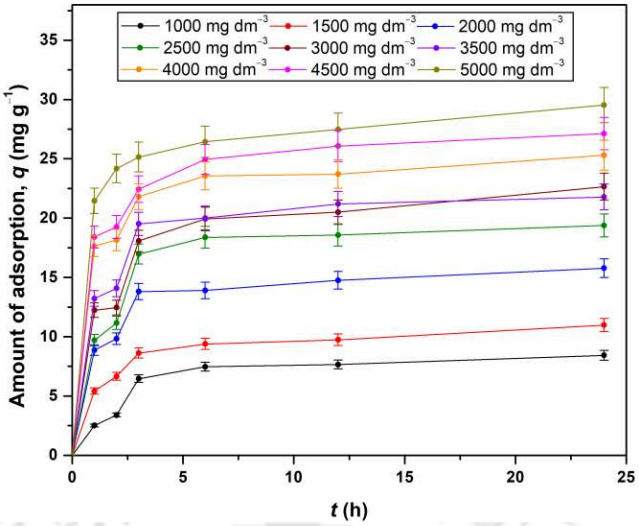

Figure 5.9. Amount of the surfactant adsorbed at different times on (a) sandstone and (b) sand.

5.2.6.1 Pseudo-first-order kinetic model

The pseudo-first-order kinetic model is given by the following equation:

$$\ln\left(q_e - q_t\right) = \ln\left(K_1 q_e\right) - K_1 t \tag{5.2}$$

This model was fitted to the experimental data, and the model parameters (i.e., K_1 and q_e) for both sandstone and sand are given in Table 5.6. Based on the R^2 values (i.e., $R^2 < 0.9$), it is apparent that this model was unable to explain the adsorption kinetics for most of the systems, especially at the high surfactant concentrations. However, this model was able to describe the adsorption kinetics at the lower surfactant concentrations.

Table 5.6. Parameters of the pseudo-first-order model for adsorption of the surfactant on the rock surfaces

Concentration (mg dm^{-3})	Sandstone			Sand		
	K_1 (h^{-1})	q_e (mg g^{-1})	R^2	K_1 (h^{-1})	q_e (mg g^{-1})	R^2
1000	0.311	10.16	0.99	0.374	8.20	0.92
1500	0.387	12.60	0.95	0.628	10.10	0.88
2000	0.410	16.64	0.94	0.725	14.86	0.82

2500	0.681	17.57	0.79	0.593	18.99	0.89
3000	0.837	19.70	0.82	0.611	21.12	0.79
3500	1.081	21.10	0.77	0.773	20.95	0.79
4000	1.617	21.91	0.84	1.069	23.61	0.61
4500	1.637	25.10	0.97	0.974	25.38	0.63
5000	2.322	26.11	0.92	1.413	27.11	0.63

5.2.6.2 Pseudo-second-order kinetic model

The pseudo-second-order model is given by the following equation:

$$\frac{t}{q_t} = \frac{1}{K_2 q_e^2} + \frac{t}{q_e} \tag{5.3}$$

The values of K_2 and q_e were calculated from the slope and intercept of the fitted line (Figure 5.10), and they are given in Table 5.7. An increment in the calculated values of q_e was observed with increasing surfactant concentration. Both the calculated and experimental values of q_e were close to each other. This finding, together with the fact that the coefficient of determination $\left(R^2\right)$ was greater than 0.99, show that the pseudo-second-order model gave the best fit. This supports the pseudo-second-order model's assumption that the adsorption was chemisorption, with more than one-step possibly involved in it [17].

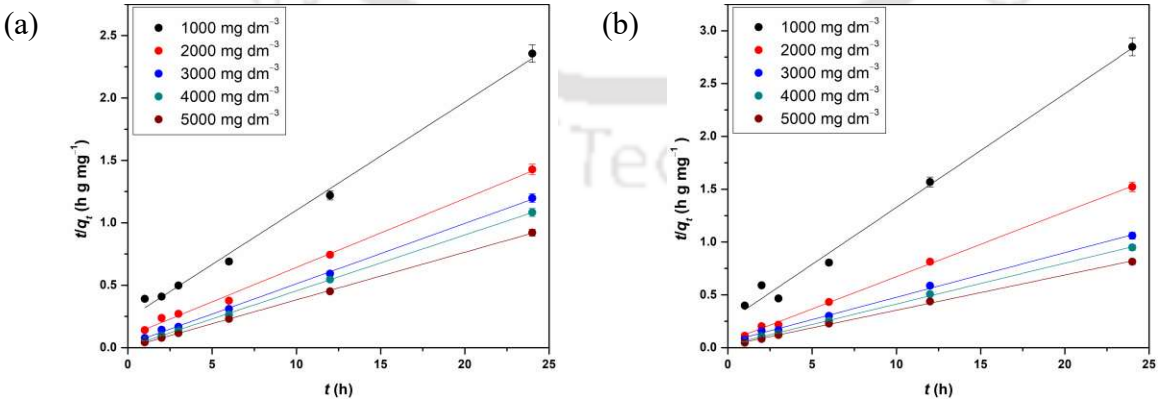

Figure 5.10. The fit of the pseudo-second-order model to the exponential data for the adsorption of surfactant on (a) sandstone and (b) sand.

Table 5.7. Parameters of the pseudo-second-order model for adsorption of surfactant on the rock surface

Concentration (mg dm^{-3})	Sandstone			Sand		
	K_2 (g mg^{-1} h^{-1})	q_e (mg g^{-1})	R^2	K_2 (g mg^{-1} h^{-1})	q_e (mg g^{-1})	R^2
1000	0.03	11.52	0.99	0.05	9.28	0.99
1500	0.07	12.31	0.98	0.06	11.43	0.99
2000	0.03	18.11	0.99	0.06	16.34	0.99
2500	0.06	18.87	0.99	0.05	20.24	0.99
3000	0.08	20.67	0.99	0.03	23.64	0.99
3500	0.12	21.93	0.99	0.06	22.52	0.99
4000	0.30	22.32	0.99	0.06	25.84	0.99
4500	0.29	25.51	0.99	0.05	27.85	0.99
5000	0.32	26.17	0.99	0.05	29.94	0.99

5.2.6.3 Intra-particle diffusion model

The pseudo-first-order and pseudo-second-order kinetic models are helpful to comprehend the reaction type and rate constants during adsorption of surfactant on the rock surface. However, these models are not effective to understand internal and external diffusion processes. Hence, the intra-particle diffusion model (i.e., equation 5.4) can be used to explain the diffusion process [10].

$$q_t = K_i t^{0.5} + C \tag{5.4}$$

This model was fitted to the experimental data, and the parameters were determined (Table 5.8). Figure 5.11 shows the amount of surfactant adsorbed as a function of $(t)^{0.5}$. It is evident from Table 5.8 that the values of R^2 are much less than unity. This is possibly because of the variation in the rate of mass transfer in the initial and final stages of adsorption [8]. Hence, intra-particle diffusion was not the rate-limiting step in adsorption.

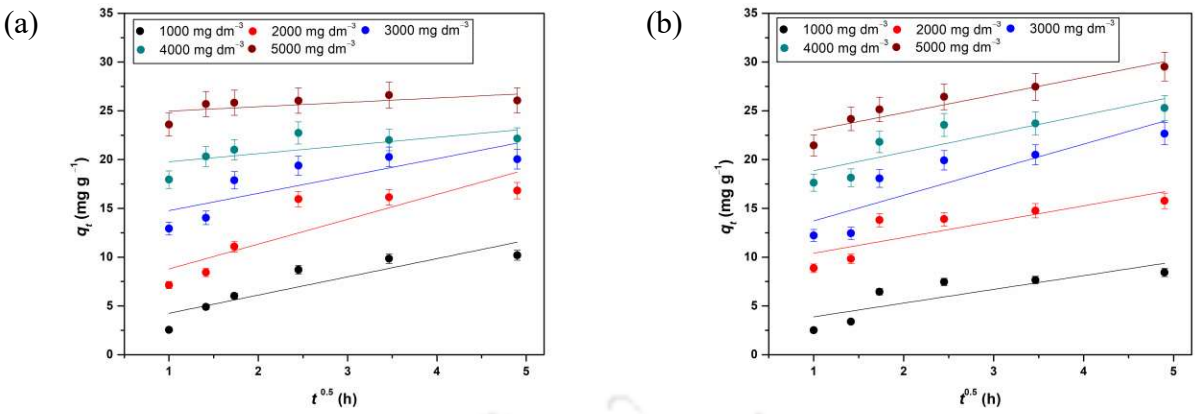

Figure 5.11. Fit of the intra-particle diffusion model to the experimental data for the adsorption of surfactant on (a) sandstone and (b) sand.

Table 5.8. Parameters of the intra-particle diffusion model for adsorption of surfactant on rock surface

Concentration (mg dm^{-3})	Sandstone			Sand		
	K_i (mg g^{-1} h^{-1})	C	R^2	K_i (mg g^{-1} h^{-1})	C	R^2
1000	1.87	2.38	0.81	1.41	2.47	0.71
1500	1.85	4.65	0.52	1.27	5.28	0.81
2000	2.55	6.24	0.76	1.62	8.78	0.71
2500	1.91	10.22	0.71	2.28	10.01	0.64
3000	1.77	12.99	0.66	2.62	11.09	0.77
3500	1.45	15.78	0.63	2.08	13.10	0.68
4000	0.84	18.94	0.49	1.90	16.96	0.78
4500	0.90	21.88	0.46	2.25	17.41	0.83
5000	0.45	24.52	0.39	1.80	21.20	0.89

5.2.7 Thermodynamics of adsorption

Thermodynamic parameters [i.e., the changes in standard Gibbs free energy $(\Delta G°)$, enthalpy $(\Delta H°)$, and entropy $(\Delta S°)$] were calculated for the adsorption of the natural surfactant on the rock surfaces. $\Delta G°$ was calculated from the following equations:

$$\Delta G° = -RT \ln K° \tag{5.5}$$

$$\ln K^\circ = \frac{\Delta S^\circ}{R} - \frac{\left(\Delta H^\circ / R\right)}{T} \tag{5.6}$$

The method suggested in the literature [10,18,19] was used to calculate the standard equilibrium constant $\left(K^\circ\right)$. As per its definition given by the IUPAC [20], K° must be dimensionless for calculating the true value of ΔG°. Therefore, K° was calculated (from equation 5.7) [18].

$$K^\circ = 5.55 \times 10^4 \, M \, K_L \tag{5.7}$$

As discussed in Sections 4.2.2 and 4.2.3, palmitic acid was confirmed as the dominant constituent in the synthesized natural surfactant by ^{1}H NMR and GC–MS analyses. Therefore, the molecular weight of adsorbate $\left(M\right)$ was taken as 256.43 g mol^{-1}. A plot of $\ln K^\circ$ vs. $1/T$ was prepared to determine the thermodynamic parameters (see Figure 5.12). The values of ΔG° and ΔH° were found to be negative, which signifies the spontaneous, feasible, and exothermic nature of the adsorption [21]. Besides, small positive values of ΔS° signify a minor randomness of at the solid–liquid interface [22]. The thermodynamic parameters for the adsorption of the surfactant on the sandstone and sand surfaces at different temperatures are shown in Table 5.9.

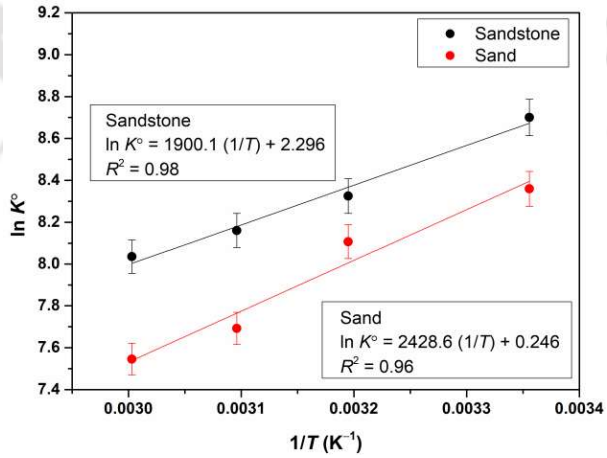

Figure 5.12. Plot of $\ln K^\circ$ vs. $1/T$ to determine the ΔH° and ΔS°.

Table 5.9. Thermodynamic parameters for adsorption of the surfactant on the rock surfaces

Temperature	Sandstone			Sand		
(K)	$\Delta G°$ (kJ mol^{-1})	$\Delta H°$ (kJ mol^{-1})	$\Delta S°$ (kJ mol^{-1} K^{-1})	$\Delta G°$ (kJ mol^{-1})	$\Delta H°$ (kJ mol^{-1})	$\Delta S°$ (kJ mol^{-1} K^{-1})
298	–21.48	–15.80	0.02	–20.80	–20.19	0.002
313	–21.77			–20.83		
323	–21.96			–20.85		
333	–22.15			–20.87		

5.3 Conclusions

Equilibrium and kinetics of adsorption of the synthesized surfactant on sandstone and sand were studied. The experimental data were analyzed with four adsorption isotherms and three kinetic models. Thermodynamic parameters for adsorption were also determined. Based on the experimental data and model-fitting, the following conclusions have been made:

1. The amount of surfactant adsorbed increased with increasing surfactant concentration. This was due to the concentration gradient between the bulk solution and the solid surface.
2. The adsorption of the surfactant on both types of rock surfaces was well-represented by the Langmuir adsorption isotherm. The pseudo-second-order model explained the adsorption kinetics well.
3. Salinity had an active role in the adsorption process, inasmuch as it increased the adsorption of the surfactant on the rock surfaces due to electrostatic screening.
4. Reduction in the adsorption occurred with increasing temperature, which demonstrated that the adsorption was an exothermic process.
5. Negative values of $\Delta G°$ and $\Delta H°$ specify the spontaneous and exothermic nature of the adsorption process.

Nomenclature

B	Temkin isotherm constant
C	intercept in equation (5.4)
C_e	equilibrium concentration of the surfactant, mg dm^{-3}
$K°$	standard equilibrium constant
K_1	pseudo-first-order rate constant, h^{-1}
K_2	pseudo-second-order rate constant, g mg^{-1} h^{-1}
K_f	Freundlich isotherm constant, dm^3 mg^{-1}
K_H	linear isotherm constant, dm^3 m^{-2}
K_i	intra-particle diffusion rate constant, mg g^{-1} h^{-1}
K_L	Langmuir isotherm constant, dm^3 mg^{-1}
K_t	equilibrium binding constant, dm^3 mg^{-1}
m	mass of rock sample, g
M	molecular weight of adsorbate, g mol^{-1}
q_0	maximum amount of adsorbate that can be adsorbed, mg g^{-1}
q_e	amount of surfactant adsorbed, mg g^{-1}
q_t	amount of surfactant adsorbed on the surface of the rock at time t, mg g^{-1}
R	correlation coefficient
R_L	separation factor
V	volume of the solution, dm^3

Greek letters

$\Delta G°$	standard Gibbs free energy change, kJ mol^{-1}
$\Delta H°$	standard enthalpy change, kJ mol^{-1}

$\Delta S°$	standard entropy change, kJ mol^{-1} K^{-1}

Abbreviations

CMC	critical micellar concentration
EOR	enhanced oil recovery
FESEM	field-emission scanning electron microscopy

References

[1] Belhaj AF, Elraies KA, Mahmood SM, Zulkifli NN, Akbari S, Hussien OS. The effect of surfactant concentration, salinity, temperature, and pH on surfactant adsorption for chemical enhanced oil recovery: A review. J Pet Explor Prod Technol 2020;10:125–37.

[2] Green DW, Willhite GP. Enhanced oil recovery. Society of Petroleum Engineers: Richardson, Texas, USA, 1998.

[3] Sheng J. Modern chemical enhanced oil recovery: Theory and practice. Gulf Professional Publishing: Massachusetts, USA, 2010.

[4] Freundlich H. Over the adsorption in solution. J Phys Chem 1906;57:1100–7.

[5] Langmuir I. The constitution and fundamental properties of solids and liquids. Part I. Solids. J Am Chem Soc 1916;38:2221–95.

[6] Ruthven DM. Principles of adsorption and adsorption processes. John Wiley: New York, 1984.

[7] Temkin M, Pyzhev V. Recent modifications to Langmuir isotherms. Acta Physiochim URSS 1940;12:217–25.

[8] Barati A, Najafi A, Daryasafar A, Nadali P, Moslehi H. Adsorption of a new nonionic surfactant on carbonate minerals in enhanced oil recovery: Experimental and modeling study. Chem Eng Res Des 2016;105:55–63.

[9] Ma K, Cui L, Dong Y, Wang T, Da C, Hirasaki GJ, Biswal SL. Adsorption of cationic and anionic surfactants on natural and synthetic carbonate materials. J Colloid Interface Sci 2013;408:164–72.

[10] Saxena N, Kumar A, Mandal A. Adsorption analysis of natural anionic surfactant for enhanced oil recovery: The role of mineralogy, salinity, alkalinity and nanoparticles. J Pet Sci Eng 2019;173:1264–83.

[11] Bera A, Ojha K, Mandal A, Kumar T. Interfacial tension and phase behavior of surfactant–brine–oil system. Colloids Surf, A 2011;383:114–9.

[12] Chang Z, Chen X, Peng Y. The adsorption behavior of surfactants on mineral surfaces in the presence of electrolytes-A critical review. Miner Eng 2018;121:66–76.

[13] Pethkar A, Paknikar K. Recovery of gold from solutions using Cladosporium cladosporioides biomass beads. J Biotechnol 1998;63:121–36.

[14] Kolev V, Danov K, Kralchevsky P, Broze G, Mehreteab A. Comparison of the van der Waals and Frumkin adsorption isotherms for sodium dodecyl sulfate at various salt concentrations. Langmuir 2002;18:9106–9.

[15] Fava A, Eyring H. Equilibrium and kinetics of detergent adsorption-a generalized equilibration theory. J Phys Chem 1956;60:890–8.

[16] Ziegler VM, Handy LL. Effect of temperature on surfactant adsorption in porous media. Soc Pet Eng J 1981;21:218–28.

[17] Arias F, Sen TK. Removal of zinc metal ion (Zn^{2+}) from its aqueous solution by kaolin clay mineral: A kinetic and equilibrium study. Colloids Surf, A 2009;348:100–8.

[18] Ghosal PS, Gupta AK. Determination of thermodynamic parameters from Langmuir isotherm constant-revisited. J Mol Liq 2017;225:137–46.

[19] Zhou X, Zhou X. The unit problem in the thermodynamic calculation of adsorption using the Langmuir equation. Chem Eng Commun 2014;201:1459–67.

[20] Mills I. Quantities, units and symbols in physical chemistry. Blackwell Scientific Publications: Oxford, UK, 1993.

[21] Bera A, Kumar T, Ojha K, Mandal A. Adsorption of surfactants on sand surface in enhanced oil recovery: Isotherms, kinetics and thermodynamic studies. Appl Surf Sci 2013;284:87–99.

[22] Ahmadi MA, Shadizadeh SR, Chen Z. Thermodynamic analysis of adsorption of a naturally derived surfactant onto shale sandstone reservoirs. Eur Phys J Plus 2018;133:420.

Chapter 6

The Role of Adsorption of a Natural Surfactant at Oil–Water Interface in Enhanced Oil Recovery: Interfacial Structural Analysis and Rheology

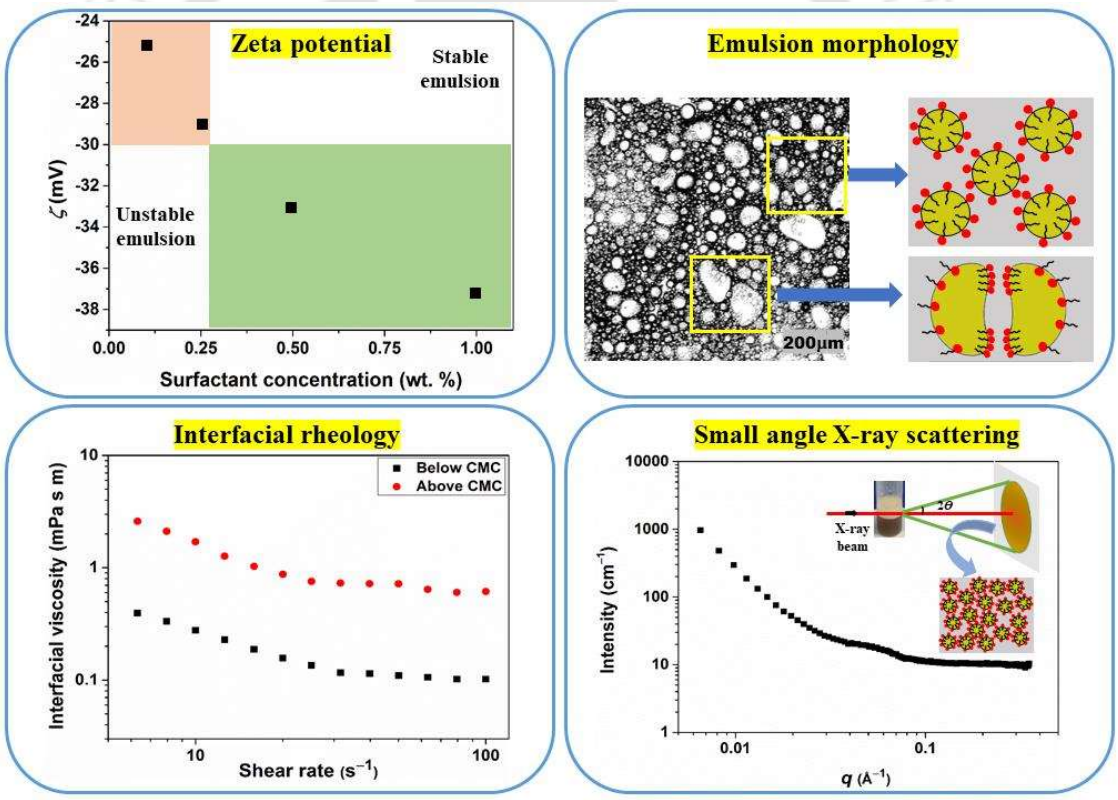

Submitted article: Machale J, Majumder SK, Ghosh P, Sen TK, Saeedi A. The role of adsorption of a natural surfactant at oil–water interface: Interfacial structural analysis and rheology. Colloids and Surfaces A. (under review)

The Role of Adsorption of a Natural Surfactant at Oil–Water Interface in Enhanced Oil Recovery: Interfacial Structural Analysis and Rheology

This chapter highlights the impact of the synthesized natural surfactant on the properties of the oil–water interface, and further correlates with its possible application in the EOR. It involves studies on interfacial shear rheology of the oil–water interface, which helps to characterize the flow behavior and the viscoelastic properties of the interfacial film. Furthermore, the adsorption of the surfactant molecules at the oil–water interface is studied using small-angle X-ray scattering, zeta potential, and morphological analyses.

6.1 General overview

Numerous analyses such as the measurement of surface tension and interfacial tension (IFT), wettability, adsorption, rheological characteristics, phase behavior, and core flooding are widely carried out to study the performance of the chemical additives for enhanced oil recovery (EOR) [1–5]. However, the chemical additives injected into the oil reservoir interact with the crude oil and adsorb on the oil–water interface, forming a complex interfacial film. Therefore, explicit knowledge of the film characteristics is essential for interpreting the displacement of the entrapped oil from the reservoir [6]. This depends on the interfacial properties of the oil–water system, which are controlled by the physicochemical properties of the crude oil and water chemistry [7–10].

Generally, the surfactant adsorbs spontaneously from the bulk phase at the oil–water interface, where the resultant free energy is lesser than that in the bulk of the solution. The adsorbed surfactant not only changes the IFT but also develops an interfacial film with viscoelastic properties [11]. An interfacial rheology is a potential tool that can be used to study

the structural properties of the interfacial film and its stability [12,13]. It illustrates the functional association between the stress applied at the interface and its deformation.

The analysis of phase behavior and the electrical properties of the interface are some of the most important aspects of understanding the formation of the film at the oil–water interface by the self-assembly of the surface-active agents [14,15]. However, it has been observed that a significant aspect of the development and stabilization of the interfacial film is not comprehended through these analyses. Therefore, along with the aforesaid analyses, small-angle X-ray scattering (SAXS) can provide more insight into the characteristics of this film [16].

6.2 Results and discussion

6.2.1 Interfacial tension

The tension at the interface between the aqueous surfactant solution and paraffin oil was measured. A significant reduction in the IFT was observed in the presence of the surfactant (see Figure 6.1). The IFT decreased with increasing surfactant concentration and reached a minimum value at 0.2 wt. %, which indicates the saturation of the oil–water interface by the surfactant molecules. The presence of micelles leads to an abrupt modification in the physical properties of the surfactant solution after the critical micelle concentration (CMC), which may be the reason for the slight increase in the IFT beyond the CMC [17,18]. In comparison with other natural surfactants [19–21], the IFT of the present system are promising inasmuch as WH can effectively reduce it by ~50%. Alpandi et al. [22] have measured the IFT between paraffin oil and water in the presence of a natural surfactant derived from the *Vernonia amygdalina* plant. They observed that the minimum IFT was attained in the presence of 6 wt. % surfactant.

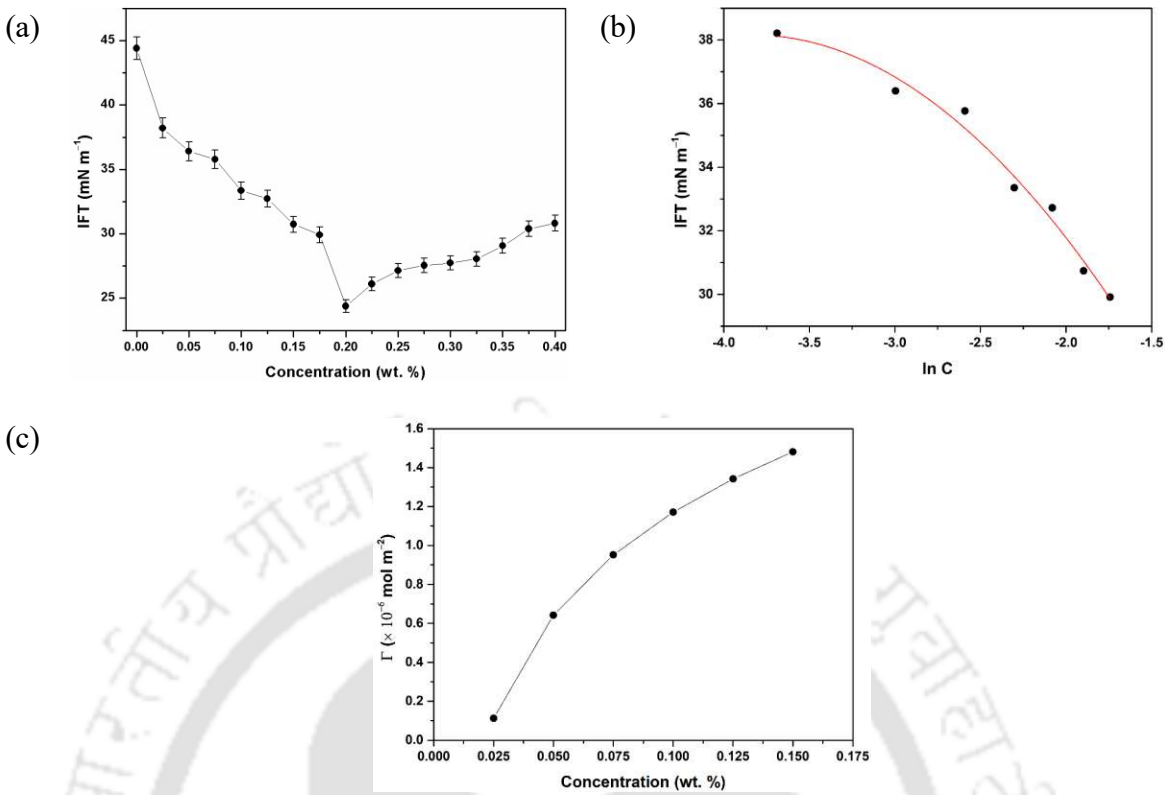

Figure 6.1. Variation of (a) IFT with WH concentration, (b) IFT with logarithm WH concentration, and (c) Γ with WH concentration.

The surface excess concentration (Γ) has been determined using the Gibbs adsorption equation:

$$\Gamma = -\frac{1}{2RT}\frac{d\gamma}{d\ln c} \tag{6.1}$$

The IFT data were plotted in Figure 6.1(b) as IFT (γ) vs. ln(c). The data were fitted by a second-order polynomial equation:

$$\gamma = -1.8916(\ln c)^2 - 14.5156(\ln c) + 10.3133 \tag{6.2}$$

Further,

$$\frac{d\gamma}{d\ln c} = -3.7832(\ln c) - 14.5156 \tag{6.3}$$

From, Figure 6.1(c), it is clear that the concentration of WH molecules at the oil–water interface increases with increasing WH concentration.

6.2.2 Zeta potential analysis

The electrostatic charge at the interface generated by the surface-active chemical additives is an essential aspect of the EOR [23]. The effect of electric charge on the oil droplets on the emulsion stability was studied by measuring the zeta potential. The zeta potential gives a measure of the electrostatic repulsive force between the oil droplets in the emulsion system [24]. The effect of surfactant concentration on the zeta potential is shown in Figure 6.2. The emulsion droplets were negatively charged because the fatty acids and esters present in the surfactant (discussed in Section 4.2.1) adsorbed on their surfaces [25]. An increase in the zeta potential from –25.2 to –37.2 mV was observed with the increase in the surfactant concentration (i.e., 0.1 – 1 wt. %). An increase in the density of the surfactant molecules at the oil–water interface (and consequent increment in the interfacial charge density) can be inferred from the increase in the zeta potential [26]. As the surfactant concentration increased above the CMC (i.e., 0.25 wt. %), probably a multilayer of the surfactant molecules on the oil–water interface was formed. The density of the surfactant molecules at the interface increased, resulting in a higher zeta potential. The values of the zeta potential reflect the good stability of the emulsion [27].

6.2.3 Phase behavior

The effect of surfactant concentration (i.e., 0.1 – 1 wt. %) on the paraffin oil–water emulsion characteristics was observed for 20 d (see Figure 6.3). It is evident from Figure 6.3 that the emulsion became creamier and thicker with increasing surfactant concentration. Below the CMC (i.e., 0.25 wt. %) (discussed in Chapter 4), the emulsion became clear (after 20 d), which

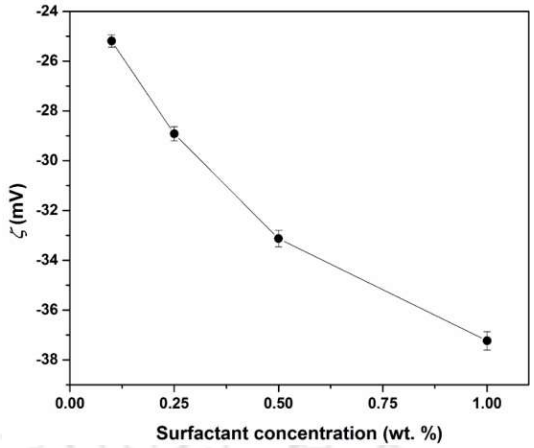

Figure 6.2. Variation of zeta potential at the paraffin oil–surfactant solution interface at different concentrations of the surfactant.

can be a result of its poor stability. Further, the emulsion's stability improved with increasing surfactant concentration. This is due to the enhanced adsorption of the surfactant molecules on the oil droplets [28].

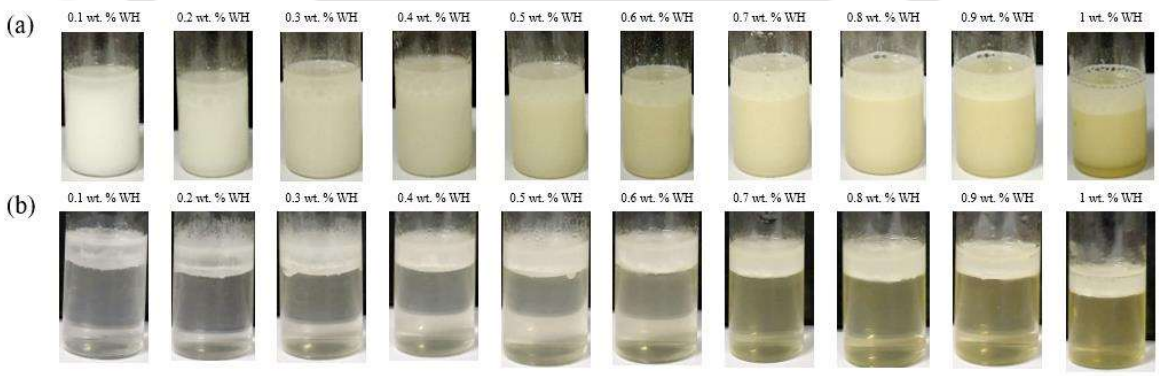

Figure 6.3. Stability of emulsions at different surfactant concentrations for (a) $t = 0$ and (b) $t = 20$ d.

Furthermore, we have studied the influence of surfactant concentration on the emulsion characteristics using microscopic analysis (see Figure 6.4). The amount of oil in the emulsion was found to increase with increasing surfactant concentration. The number of oil droplets was rather small for the 0.1 wt. % WH system [see Figure 6.4a]. This was due to a small amount of surfactant adsorbed on the surface of the oil droplets [29]. The presence of bigger oil droplets (i.e., 20–140 μm) is also evident from Figure 6.4a. These droplets were prone to quick coalescence, and hence the emulsion stability decreased. However, it is obvious from Figures

6.4b and 6.4c that the extent of emulsification increased at 0.25 and 1 wt. % WH, which was due to the more adsorption of the surfactant molecules on the oil droplets. Furthermore, the number of small oil droplets was found to be increasing with surfactant concentration (see Figure 6.4b and 6.4c). An increase in the number of dispersed oil droplets and more stability of the emulsion promoted a higher removal of the trapped oil, which improved the oil recovery [30].

Low molecular weight fatty acids (which are the main components of the synthesized natural surfactant) have a high tendency to adsorb at the oil–water interface [13]. Generally, the adsorption of surfactant on the oil droplets is a two-step process. At the low surfactant concentrations (i.e., below the CMC), the adsorption occurs rapidly due to the presence of vacant sites at the interface. At the CMC, a monolayer of the surfactant molecules is formed on the interface. The negatively-charged groups of the surfactant molecules lead to the development of an electrostatic double layer at the oil–water interface, and hence around the oil droplets [31]. When the oil droplets approach each other, the ions of the diffuse double layer are confined to a narrow space, which is entropically unfavorable. This leads to the repulsive disjoining pressure between the oil droplets, and the coalescence of the droplets is minimized. In addition, the force of repulsion between the droplets is proportional to their size [32].

When the surfactant concentration is higher than the CMC, the micelles present in the film tend to be ousted when two oil droplets are brought close to each other [33,34]. It is clear from Figure 6.4b that the stability of the emulsion at the higher surfactant concentration (i.e., above 0.7 wt. % WH) was unchanged even after 20 d. At the CMC, the surfactant molecules form a monolayer on the oil droplets and cover the entire surface. As the concentration of surfactant is increased, further adsorption may lead to the development of multilayers at the interface [35,36]

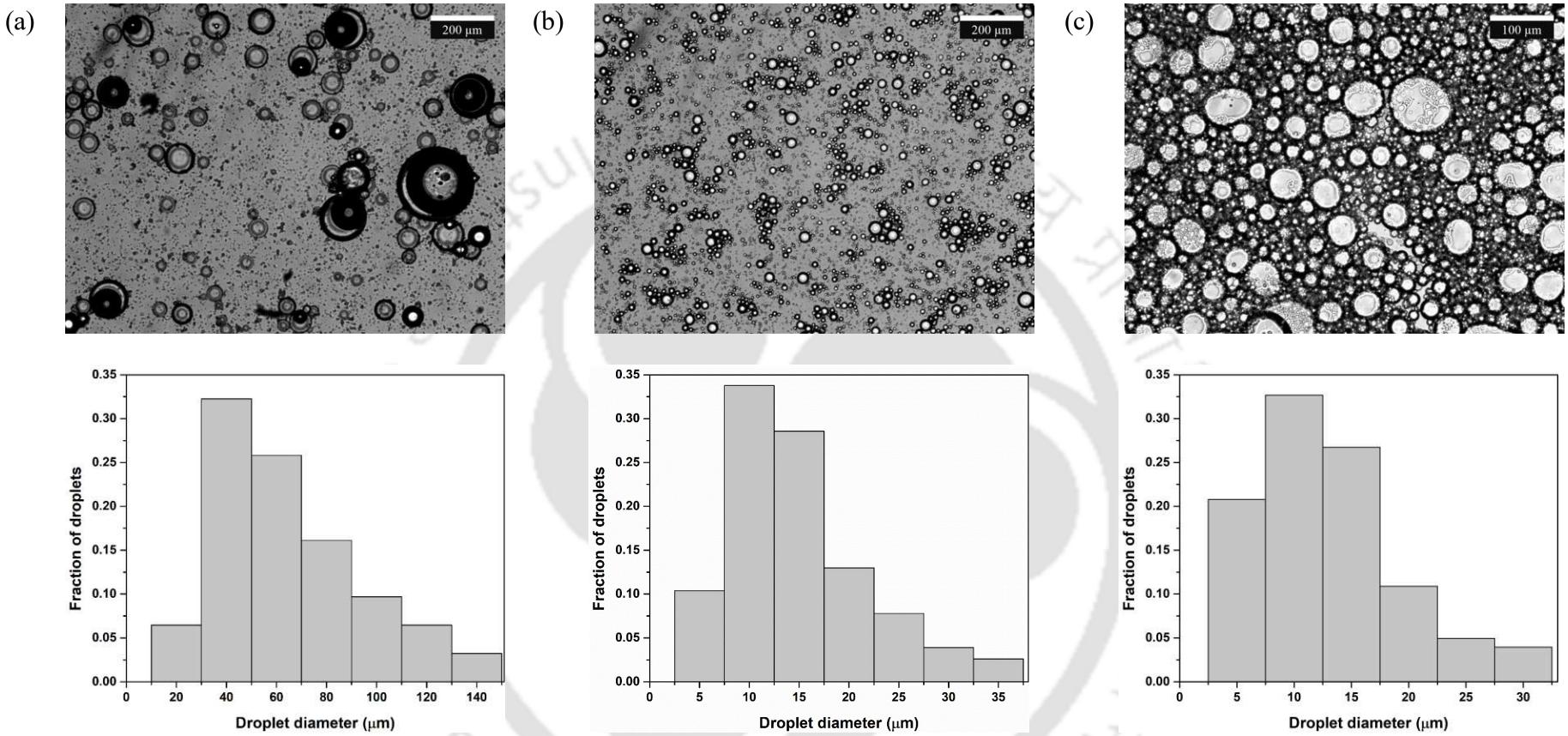

Figure 6.4. Emulsion morphology and the size distribution of the oil droplets in the presence of (a) 0.1, (b) 0.25, and (c) 1 wt. % WH.

with the micelles present in the film. This phenomenon is termed as the stratification, which promotes structural repulsion [37]. The strong structural repulsion inhibits the coalescence of the droplets, even at small distances [see Figure 6.4c].

Figure 6.5 demonstrate the interaction between the dispersed oil droplet for 1 wt. % WH emulsion system. The presence of stable emulsion stabilized by the surfactant is well-comprehensible from Figure 6.5. Furthermore, it is evident that two adjacent oil-in-water bulk phases approached close to each other driven by the capillary pressure arising due to the difference in curvature of the interfaces, as described by the Young–Laplace equation [38]. The pressure difference across the curved surfaces eventually led to the merger of the two adjacent surfaces. However, the structural repulsion between the oil droplets hindered coalescence, which led to the encapsulation of the oil droplets [see Figure 6.5a–c]. Several studies have suggested that such encapsulation improved oil recovery by 17–43.3 % [39,40].

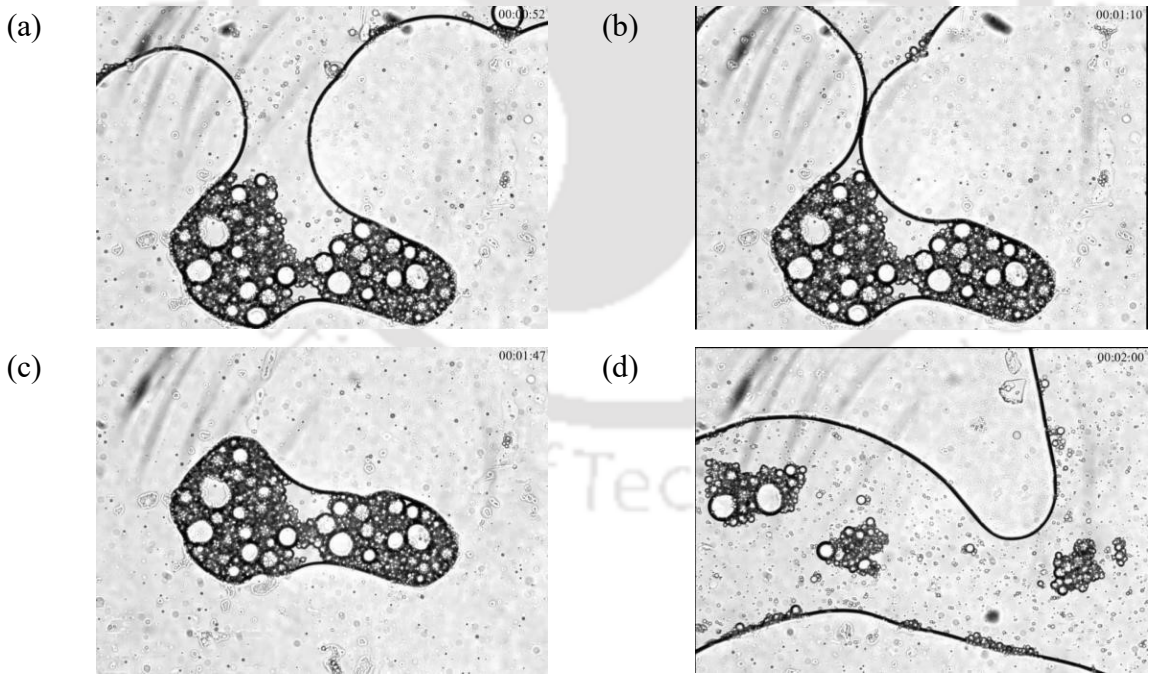

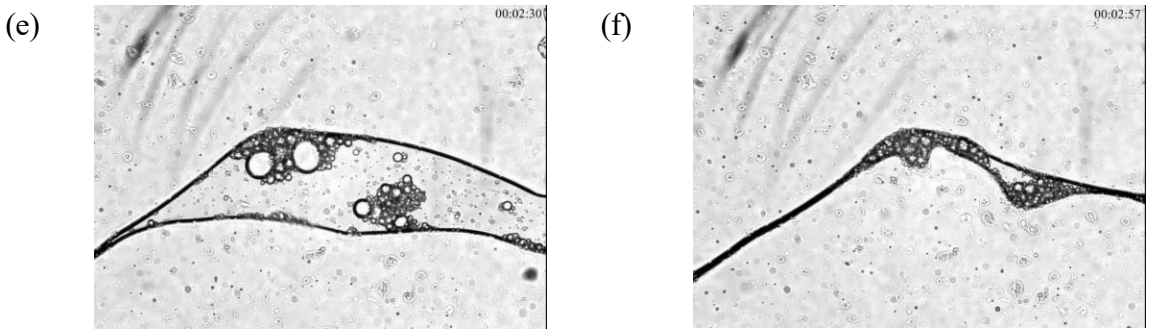

Figure 6.5. Demonstration of (a–c) oil encapsulation and (d–f) film formation.

6.2.4 Shear rheology of the surfactant layer at the oil–water interface

Interfacial viscosity is one of the crucial parameters for understanding the capillary phenomena [41]. These phenomena in oil recovery correlate with the displacement efficiency of crude oil in the reservoir. Figure 6.6a demonstrates the influence of surfactant concentration on the interfacial viscosity of the oil–water interface at 10 s^{-1} shear rate. A significant increment in the interfacial shear viscosity was observed with increasing surfactant concentration. This demonstrates the formation of a viscous layer by the adsorption of the surfactant molecules at the oil–water interface [42]. The interfacial shear viscosity of 1 wt. % WH–oil system was found to be 1.7 mPa s m at 10 s^{-1}.

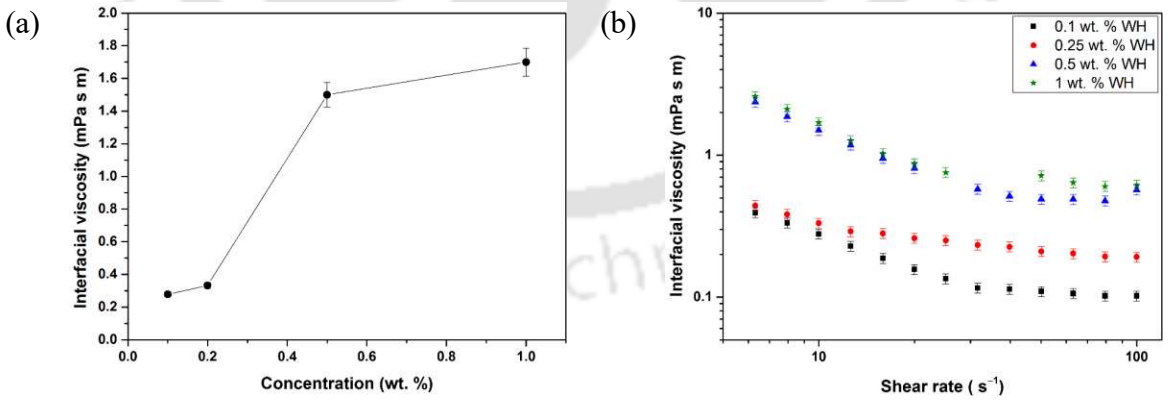

Figure 6.6. Variation of interfacial shear viscosity at different surfactant concentrations (a) at the constant shear rate of 10 s^{-1} and (b) at varying shear rates (i.e., 1 – 100 s^{-1}).

Figure 6.6b demonstrates the influence of shear rate on the surfactant layer at the oil–water interface. It was observed that the interfacial viscosity reduced with increasing shear rate,

which depicts a shear-thinning behavior. It happened mainly because of the slow weakening of the microstructure of the surfactant layer at the interface. After the CMC (i.e., 0.25 wt. %) was reached, a very nominal increment in the interfacial shear viscosity was observed, which justifies the saturation of the oil–water interface. The interfacial film stability is mainly governed by the extent of adsorption of the surfactant molecules at the oil–water interface [43,44] and the interaction between them. At low concentration, the number of surfactant molecules adsorbed at the oil–water interface is rather small, and therefore, a weak interfacial film is formed. As the surfactant concentration increased, the interfacial viscosity of the film increased [45].

Lin et al. [46] studied the adsorption of asphaltenes (a natural surfactant present in the crude oil) at both air–water and oil–water interfaces using a combination of interfacial shear rheology and visualization approaches. The interfacial viscosity of air–water and decane oil–water interfaces (in presence of 0.4 μg cm^{-2} asphaltene) was reported to be 10^{-5} and 10^{-2} Pa s m, respectively, at 1 s^{-1}. In another study, Badri and Ghosh [47] studied the interfacial shear rheological properties of hexadecyltrimethylammonium bromide (HTAB) (a cationic surfactant used for the EOR applications) and silica (SiO_2) nanoparticles at the air–water interface. The adsorption of HTAB–SiO_2 composites at the air–water interface has been verified by bulk rheology, interfacial rheology, and zeta potential analyses. The interfacial viscosity of the 0.1 mol m^{-3} HTAB–0.5 wt. % SiO_2 composite was observed to be decreasing with increasing shear rate, which implies a pseudoplastic or shear-thinning behavior. Besides, the interfacial viscosity was reported to be 2×10^{-4} Pa s m at 1 s^{-1}.

The Boussinesq number provides a valuable information on the rate of deformation of the interfacial film. It is the ratio of the surface to bulk viscous effects (see equation 1.1). It is clear from Figure 6.7 that the Bo was greater than the unity, which indicates that the surfactant molecules mostly covered the oil–water interface [23]. As the concentration of surfactant

increased, the oil–water interface became saturated, and hence, only small changes in Bo were observed in the 0.5 and 1 wt. % WH systems.

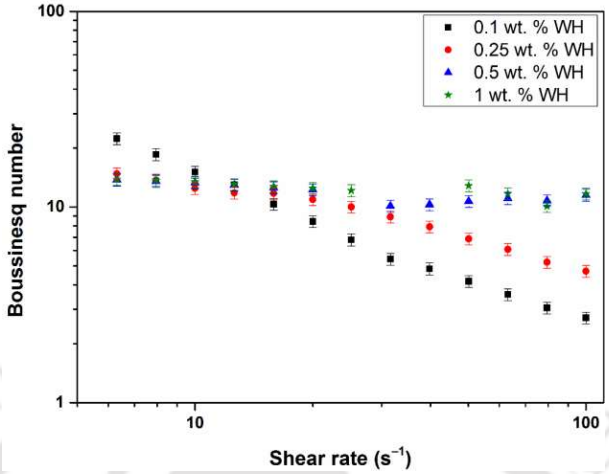

Figure 6.7. Boussinesq number as a function of shear rate for different concentrations of the surfactant.

The impact of surfactant concentration on the viscoelasticity of the oil–water interface was investigated through the frequency sweep tests (see Figure 6.8). A similar approach was adopted by Santini et al. [48]. It is clear from Figure 6.8 that the interface between the paraffin oil and the surfactant solution depicted viscoelastic behavior. The tendency to form the viscoelastic interfacial film can also be correlated with the density of the surfactant molecules at the interface. In the event of less packing density, the surfactant molecules are capable of orienting in such a manner that the interaction with the neighbor molecules would reduce. Thus, when the oscillatory shear was applied, the interface acted like a fluid (i.e., $G_s'' > G_s'$). On the other hand, when the density of the surfactant molecules was high, the resultant interaction increased, and the interface acted more like an elastic solid (i.e., $G_s' > G_s''$) [49].

Unlike the interfacial shear viscosity, a minor modification in the viscoelastic properties was noticed for the 0.1 – 0.5 wt. % WH systems. This is possibly due to the viscoelastic deformation and sensitivity of the oil–water interface. However, a substantial improvement in the viscoelasticity of the interface was observed for the 1 wt. % WH system. The increase in

the interfacial film stability with increasing surfactant concentration can be correlated with the dominating elasticity (i.e., $G_s' > G_s''$) at the high frequency. Generally, the elastic stress developed as a result of the viscoelastic deformation of the oil–water interface. This elastic stress helped in pulling the residual oil out from the trapped region [42].

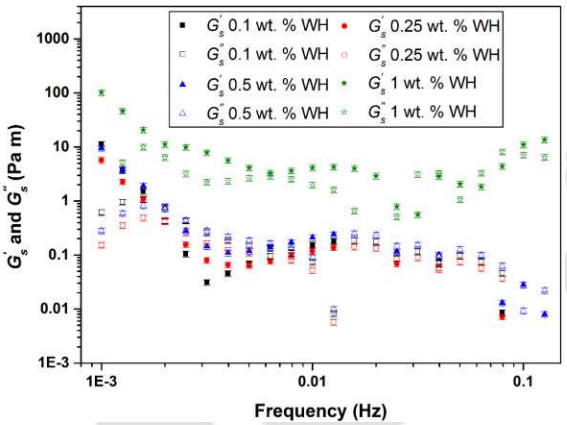

Figure 6.8. Interfacial storage (G_s') and loss (G_s'') moduli for the surfactant layer at the oil–water interface at different surfactant concentrations.

The viscoelasticity of the film was further demonstrated from the interfacial complex modulus data (see Figure 6.9). At low frequency, the surfactant molecules could adsorb or desorb for establishing an equilibrium between the bulk and adsorbed layers. Furthermore, a dynamic equilibrium was established at a higher frequency range because of the exchange of the surfactant molecules and change in the interface area.

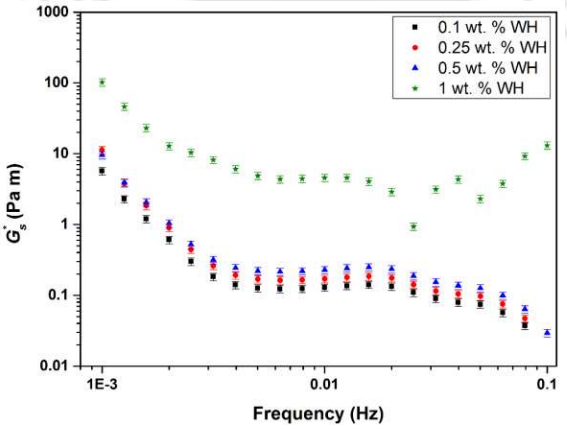

Figure 6.9. Variation of the interfacial complex modulus $\left(G_s^*\right)$ with frequency.

6.2.5 Small-angle X-ray scattering (SAXS)

The SAXS analysis was used to investigate the characteristics of the film at the interface at the molecular level. Figure 6.10 shows the SAXS profile for emulsion scattering. The zeta potential for the paraffin oil–1 wt. % WH emulsion system was –37.2 mV. The scattering profile indicates the protonation state of the fatty acids, aromatic compounds, and esters within the surfactant that influence the properties of the interfacial film. It is possible that the strong electrostatic interactions and structural forces promoted the formation of a stable emulsion system [24,50]. Based on the scattering results, we have determined the droplet size and the respective unified Guinier-exponential power-law parameters (using equations 3.2 and 3.3), which are shown in Table 6.1.

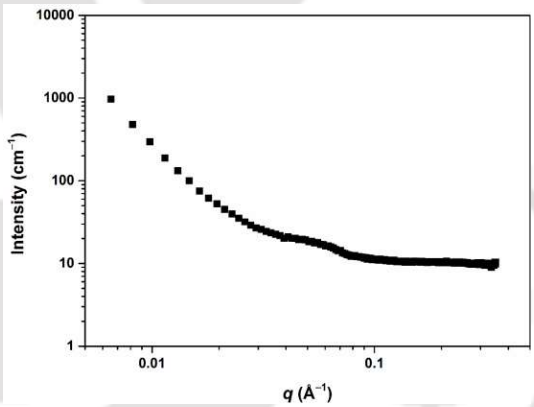

Figure 6.10. SAXS data (i.e., intensity versus scattering angle) for the paraffin oil–1 wt. % WH emulsion system.

The emulsion had surface fractals since $4 > P > 3$, which confirms the formation of spherical droplets [51]. The surface fractal scattering may possibly be restrained by the agglomeration of the surfactant molecules on the oil droplets [52]. The radius of gyration of the small droplets was found to be 28.56 Å. The film thickness (ΔT_S) was found to be 18.52 Å (calculated using equation 6.4).

$$\Delta T_s = \sqrt{12 R_g} \tag{6.4}$$

Furthermore, the surface area to volume ratio in the paraffin oil–surfactant emulsion system was 1396.3 $m^2\ cm^{-3}$.

Table 6.1. Parameters of the unified Guinier-exponential power law for the paraffin oil–1 wt. % WH emulsion system

	Parameters			
	G	R_g (Å)	***B***	***P***
Large droplets	0.00	10.00^{10}	1.44×10^{-6}	3.12
Small droplets	12.01	28.56	8.85×10^{-5}	4.00

6.3 Conclusion

Adsorption of a natural surfactant synthesized from *Eichhornia Crassipes* at the oil–water interface was investigated. The phase behavior, zeta potential, interfacial rheology, and SAXS were studied to understand the emulsion stability and interfacial film properties. Based on the experimental outcomes, the conclusions are as follows:

1. The number of oil droplets, and eventually, the stability of emulsion, increased with increasing surfactant concentration.
2. An increase in zeta potential confirms the adsorption of surfactant molecules at the oil–water interface.
3. The spherical shape of the emulsion and the surface fractal scattering were confirmed by the SAXS analysis.
4. The adsorption of the surfactant molecules at the oil–water interface led to an enhancement in the interfacial shear viscosity and the complex moduli.
5. Viscoelastic films acted as a mechanical barrier to coalescence, which aided emulsion stability.

Nomenclature

B	pre-factor specific to the type of power-law scattering
G	exponential Guinier pre-factor
G_s'	interfacial storage modulus, Pa m
G_s''	interfacial loss modulus, Pa m
G_s^*	interfacial complex modulus, Pa m
P	Porod exponent
q	scattering angle, $Å^{-1}$
R_g	radius of gyration, Å
S	surface area, m^2
V	volume, cm^{-3}

Greek letters

ΔT_s	film thickness, Å

Abbreviation

CMC	critical micelle concentration
EOR	enhanced oil recovery
IFT	interfacial tension
SAXS	small-angle X-ray scattering
WH	surfactant synthesized from *Eichhornia crassipes* (commonly known as Water Hyacinth)

References

[1] Anghel D. Phase behavior and interfacial phenomena in microemulsions used for enhanced oil recovery. Interfaces in Condensed Systems. Berlin, Germany: Springer; 1990, p. 188–95.

[2] Belhaj AF, Elraies KA, Mahmood SM, Zulkifli NN, Akbari S, Hussien OS. The effect of surfactant concentration, salinity, temperature, and pH on surfactant adsorption for chemical enhanced oil recovery: A review. J Pet Explor Prod Technol 2020;10:125–37.

[3] Elakneswaran Y, Ubaidah A, Takeya M, Shimokawara M, Okano H. Effect of electrokinetics and thermodynamic equilibrium on low-salinity water flooding for enhanced oil recovery in sandstone reservoirs. ACS omega 2021;6:3727–35.

[4] Mohammed M, Babadagli T. Wettability alteration: A comprehensive review of materials/methods and testing the selected ones on heavy-oil containing oil-wet systems. Adv Colloid Interface Sci 2015;220:54–77.

[5] Sheng J. Modern chemical enhanced oil recovery: Theory and practice. Gulf Professional Publishing: Massachusetts, USA, 2010.

[6] Sun H-Q, Zhang L, Li Z-Q, Zhang L, Luo L, Zhao S. Interfacial dilational rheology related to enhance oil recovery. Soft Matter 2011;7:7601–11.

[7] Alvarado V, Manrique E. Enhanced oil recovery: An update review. Energies 2010;3:1529–75.

[8] Borwankar R, Wasan D. Dynamic interfacial tensions in acidic crude oil/caustic systems. Part II: Role of dynamic effects in alkaline flooding for enhanced oil recovery. AIChE J 1986;32:467–76.

[9] Dong M, Ma S, Liu Q. Enhanced heavy oil recovery through interfacial instability: A study of chemical flooding for Brintnell heavy oil. Fuel 2009;88:1049–56.

[10] Massarweh O, Abushaikha AS. The use of surfactants in enhanced oil recovery: A review of recent advances. Energy Rep 2020;6:3150–78.

[11] Krägel J, Derkatch SR. Interfacial shear rheology. Curr Opin Colloid Interface Sci 2010;15:246–55.

[12] Lyu Y, Gu C, Fan X, Tao J, Yao X, Dai C, Zhao G. Interfacial rheology of a novel dispersed particle gel soft heterogeneous combination flooding system at the oil–water interface. Colloids Surf, A 2018;559:23–34.

[13] Roth S, Murray BS, Dickinson E. Interfacial shear rheology of aged and heat-treated *β*-lactoglobulin films: Displacement by nonionic surfactant. J Agric Food Chem 2000;48:1491–7.

[14] Pal N, Kumar S, Bera A, Mandal A. Phase behaviour and characterization of microemulsion stabilized by a novel synthesized surfactant: Implications for enhanced oil recovery. Fuel 2019;235:995–1009.

[15] Pal N, Saxena N, Mandal A. Phase behavior, solubilization, and phase transition of a microemulsion system stabilized by a novel surfactant synthesized from castor oil. J Chem Eng Data 2017;62:1278–91.

[16] Lutz R, Aserin A, Wachtel EJ, Ben-Shoshan E, Danino D, Garti N. A study of the emulsified microemulsion by SAXS, cryo-TEM, SD-NMR, and electrical conductivity. J Dispersion Sci Technol 2007;28:1149–57.

[17] Lv M, Luo C, Yang J, Zhou Y, Liu C, Xu B. Effect of number of oxypropylene on dynamic interfacial tensions of extended surfactants. Colloids Surf, A 2019;570:429–37.

[18] Zhao C, Jiang Y, Li M, Cheng T, Yang W, Zhou G. The effect of NaOH on lowering interfacial tension of oil/alkylbenzene sulfonates solution. RSC Adv 2018;8:6169–77.

[19] Saxena N, Pal N, Dey S, Mandal A. Characterizations of surfactant synthesized from palm oil and its application in enhanced oil recovery. J Taiwan Inst Chem Eng 2017;81:343–55.

[20] Sofla SJD, Sharifi M, Sarapardeh AH. Toward mechanistic understanding of natural surfactant flooding in enhanced oil recovery processes: The role of salinity, surfactant concentration and rock type. J Mol Liq 2016;222:632–9.

[21] Shadizadeh S, Kharrat R. Experimental investigation of matricaria chamomilla extract effect on oil-water interfacial tension: Usable for chemical enhanced oil recovery. Pet Sci Technol 2015;33:901–7.

[22] Alpandi A, Inasyah F, Sidek A, Husin H, Junin R, Jaafar M. Critical micelle concentration, interfacial tension and wettability alteration study on the surface of paraffin oil-wet sandstone using saponin. IOP Conference series: Materials science and engineering. 23–25 January 2021; Johor, Malaysia.

[23] Bera A, Ojha K, Mandal A, Kumar T. Interfacial tension and phase behavior of surfactant–brine–oil system. Colloids Surf, A 2011;383:114–9.

[24] Rezk MY, Allam NK. Impact of nanotechnology on enhanced oil recovery: A mini-review. Ind Eng Chem Res 2019;58:16287–95.

[25] Sang Y, Yang F, Chen S, Xu H, Zhang S, Yuan Q, Gan W. Molecular interactions at the hexadecane/water interface in the presence of surfactants studied with second harmonic generation. J Chem Phys 2015;142:224704.

[26] Varade SR, Ghosh P. Foaming in aqueous solutions of zwitterionic surfactant: Effects of oil and salts. J Dispersion Sci Technol 2017;38:1770–84.

[27] Pate K, Safier P. Chemical metrology methods for CMP quality. Advances in chemical mechanical planarization (CMP). Amsterdam, Netherlands: Elsevier; 2016, p. 299–325.

[28] Machale J, Al-Bayati D, Almobarak M, Ghasemi M, Saeedi A, Sen TK, Majumder SK, Ghosh P. Interfacial, emulsifying, and rheological properties of an additive of a natural surfactant and polymer and its performance assessment for application in enhanced oil recovery. Energy Fuels 2021;35:4823–34.

[29] Rane JP, Pauchard V, Couzis A, Banerjee S. Interfacial rheology of asphaltenes at oil–water interfaces and interpretation of the equation of state. Langmuir 2013;29:4750–9.

[30] He L, Lin F, Li X, Sui H, Xu Z. Interfacial sciences in unconventional petroleum production: From fundamentals to applications. Chem Soc Rev 2015;44:5446–94.

[31] Wu W, Fang H, Yang F, Chen S, Zhu X, Yuan Q, Gan W. Understanding the different steps of surfactant adsorption at the oil–water interface with second harmonic generation. J Phys Chem C 2016;120:6515–23.

[32] Mondain-Monval O, Leal-Calderon F, Bibette J. Forces between emulsion droplets: Role of surface charges and excess surfactant. J Phys II 1996;6:1313–29.

[33] Evans E, Needham D. Attraction between lipid bilayer membranes in concentrated solutions of nonadsorbing polymers: comparison of mean-field theory with measurements of adhesion energy. Macromolecules 1988;21:1822–31.

[34] Vrij A. Polymers at interfaces and the interactions in colloidal dispersions. Colloid and Surface Science. Amsterdam, Netherlands: Elsevier; 1977, p. 471–83.

[35] Penfold J, Thomas R, Dong C, Tucker I, Metcalfe K, Golding S, Grillo I. Equilibrium surface adsorption behavior in complex anionic/nonionic surfactant mixtures. Langmuir 2007;23:10140–9.

[36] Thomas RK, Penfold J. Multilayering of surfactant systems at the air–dilute aqueous solution interface. Langmuir 2015;31:7440–56.

[37] Nikolov A, Wasan D. Ordered micelle structuring in thin films formed from anionic surfactant solutions: I. Experimental. J Colloid Interface Sci 1989;133:1–12.

[38] Ghosh P. Colloid and interface science. PHI Learning: New Delhi, India, 2009.

[39] Ojo OF, Farinmade A, John V, Nguyen D. A nanocomposite of halloysite/surfactant/wax to inhibit surfactant adsorption onto reservoir rock surfaces for improved oil recovery. Energy Fuels 2020;34:8074–84.

[40] Romero-Zeron L, Wadhwani D, Sethiya R. Formulation of an encapsulated surfactant system, ESS, via β-CD host–guest interactions to inhibit surfactant adsorption onto solid surfaces. Ind Eng Chem Res 2020;59:15542–55.

[41] Lakatos I, Lakatos-Szabo J. Effect of IOR/EOR chemicals on interfacial rheological properties of crude oil/water systems. SPE International Symposium on Oilfield Chemistry. 13–16 February 2001; Houston, Texas, USA.

[42] Zhou Y, Yin D, Chen W, Liu B, Zhang X. A comprehensive review of emulsion and its field application for enhanced oil recovery. Energy Sci Eng 2019;7:1046–58.

[43] Manev ED, Nguyen AV. Critical thickness of microscopic thin liquid films. Adv Colloid Interface Sci 2005;114:133–46.

[44] Valkovska DS, Danov KD, Ivanov IB. Stability of draining plane-parallel films containing surfactants. Adv Colloid Interface Sci 2002;96:101–29.

[45] Xu M-J, Li M-Y, Peng B, Wu Z-L, Lin M-Q, Guo J-X, Dong Z-X. Effects of strength of interfacial film and zeta potential on oil-in-water emulsion stability. Chin J Appl Chem 2007;6:623–7.

[46] Lin Y-J, Barman S, He P, Zhang Z, Christopher GF, Biswal SL. Combined interfacial shear rheology and microstructure visualization of asphaltenes at air–water and oil–water interfaces. J Rheol 2018;62:1–10.

[47] Vishal B, Ghosh P. Foaming in aqueous solutions of hexadecyltrimethylammonium bromide and silica nanoparticles: Measurement and analysis of rheological and interfacial properties. J Dispersion Sci Technol 2018;39:62–70.

[48] Santini E, Liggieri L, Sacca L, Clausse D, Ravera F. Interfacial rheology of Span 80 adsorbed layers at paraffin oil–water interface and correlation with the corresponding emulsion properties. Colloids Surf, A 2007;309:270–9.

[49] Anseth JW, Bialek A, Hill RM, Fuller GG. Interfacial rheology of graft-type polymeric siloxane surfactants. Langmuir 2003;19:6349–56.

[50] Larson-Smith K, Jackson A, Pozzo DC. SANS and SAXS analysis of charged nanoparticle adsorption at oil–water interfaces. Langmuir 2012;28:2493–501.

[51] Beaucage G. Small-angle scattering from polymeric mass fractals of arbitrary mass-fractal dimension. J Appl Cryst 1996;29:134–46.

[52] Cherny AY, Anitas EM, Osipov VA, Kuklin AI. The structure of deterministic mass and surface fractals: Theory and methods of analyzing small-angle scattering data. PCCP 2019;21:12748–62.

Chapter 7

Performance assessment of the natural surfactant–polymer additive under reservoir-like conditions

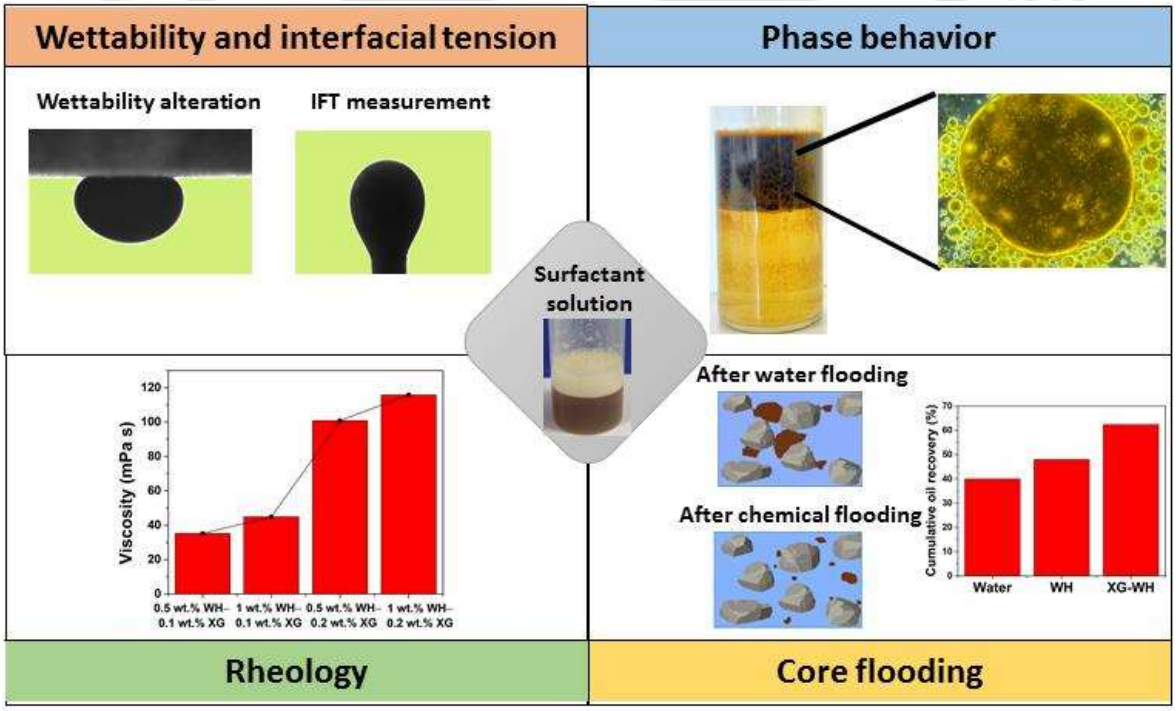

Published article: Machale J, Al-Bayati D, Almobarak M, Ghasemi M, Saeedi A, Sen TK, Majumder SK, Ghosh P. Interfacial, emulsifying, and rheological properties of an additive of a natural surfactant and polymer and its performance assessment for application in enhanced oil recovery. Energy & Fuels 2021;35:4823–34.

Performance assessment of the natural surfactant–polymer additive under reservoir-like conditions

This chapter highlights the evaluation of the synthesized natural surfactant for its potential application in the EOR under reservoir-like conditions (i.e., under high temperature and pressure). It includes the analysis of wettability alteration and IFT reduction capabilities of the synthesized surfactant. The ability of the surfactant to stabilize the oil–water emulsion was studied by the phase behavior analysis. Based on the aforesaid studies, an optimized amount of the chemical additives was selected and used in the core flooding experiments. An effective reduction of IFT and wettability, and enhancement in the oil recovery suggest that the synthesized surfactant is promising for EOR applications.

7.1 General overview

The wettability alteration and interfacial tension (IFT) reduction abilities at the reservoir-like conditions is critical inasmuch as they provide a better insight into the performance of the surfactant for enhanced oil recovery (EOR). Most studies have reported the alteration of rock from the oil-wet to the water-wet condition by saturating the rock samples in oil at a specific temperature. To the best of the authors' knowledge, the potential of the plant-based natural surfactants for wettability alteration and IFT modification under reservoir-like conditions (i.e., high temperature and pressure) has not been studied so far. Furthermore, the contact angle and IFT measurements summarized in Table 2.6 were measured under aerobic and ambient conditions. Air brings significant modifications to the interfacial properties of the liquids. Hence, it is imperative to maintain anaerobic conditions [1–3].

The present study focuses on the analysis of wettability alteration and IFT reduction at reservoir-like conditions (i.e., at high temperature and pressure, and under anaerobic condition). Based on the screening criteria established by numerous researchers for the

chemical method of EOR [4–6], primarily, two experimental conditions were adopted, i.e., (i) 298 K and 1.38 MPa, and (ii) 333 K and 13.8 MPa. The ability of the natural surfactant to stabilize the crude oil–water emulsion was studied by the phase behavior analysis. The rheological properties of xanthan gum (XG) in association with the natural surfactant were examined by steady and oscillatory shear flow tests, which highlighted the flow behavior and viscoelastic properties of the polymer–surfactant solutions. Based on the aforesaid studies, an optimal proportion of the chemical additives was determined and used in the core flooding experiments.

7.2 Results and discussion

7.2.1 Wettability alteration

The contact angle (θ) measurements were carried out to analyze the wettability alteration potential of the natural surfactant in the presence of brine. The contact angle was found to decrease with the increasing concentration of the surfactant (see Figure 7.1). At 298 K and 1.38 MPa, θ was found to decrease from 65.74 to 37.5° with the increase in surfactant concentration (i.e., 0 to 1 wt. %). On the other hand, at 333 K and 13.8 MPa, a minor reduction in θ was observed, i.e., from 60.4 to 34.5°. Under both experimental conditions, the values of θ were less than 90°, which justifies the water-wet characteristics [7]. A comparison between the values of θ at 298 and 333 K indicates that the increase in temperature led to a dominating water-wet surface. This result confirms the useful wettability alteration potential of the natural surfactant. However, pressure had a nominal influence on wettability alteration.

The water-wet characteristics was developed due to the presence of a thin film of brine (containing the surfactant) between the sandstone rock and the crude oil droplet [8]. The contact between oil, water, and rock can generally be divided into three regions, as explained in Figure 7.2 [8,9]. Generally, the wettability of rock is achievable due to the change in the repulsive

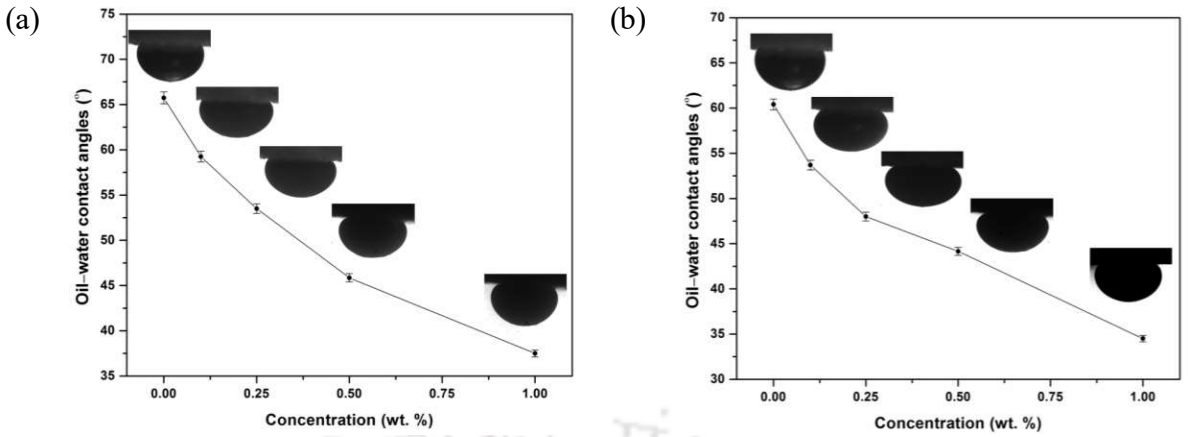

Figure 7.1. Variation of oil–water contact angle with surfactant concentration at (a) 298 K and 1.38 MPa, and (b) 333 K and 13.8 MPa.

force between the rock–water and water–oil interfaces [10]. The addition of the surfactant was responsible for governing the repulsive force at the oil–surfactant–rock interface. However, as the oil droplet comes close to the rock surface, the thin brine layer between them thins and eventually ruptures. Further, the adsorption of surfactant molecules at the oil–water interface facilitates the reduction of the tension between them, and hence the contact angle.

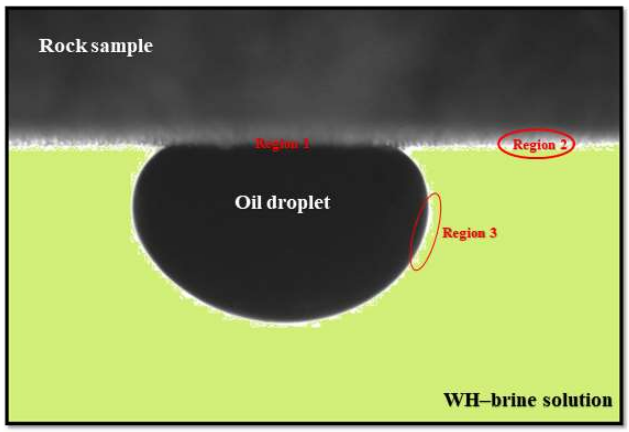

- Region 1: Thin WH–brine film between oil and rock
- Region 2: Contact region between WH–brine and rock
- Region 3: Contact region between brine and oil

Figure 7.2. Oil–water–rock contact regions.

Adsorption at the rock–oil interface (i.e., Region 1) also plays a significant role in wettability alteration due to the strong adhesion of oil to the rock surface [1]. Generally, oil components adsorb on the rock surface with their polar heads oriented toward the high-energy surface. At low temperature, the oil components do not desorb, and hence the contact angle

increases. At the higher temperatures, adsorption reduces and the oil components desorb from the rock surface. These phenomena eventually help in the reduction of contact angle, and hence the rock surface becomes more water-wet [11]. Generally, the water-wet surface initiates water upsurge through the porous rock, which further improves the displacement of the trapped oil [12].

7.2.2 Interfacial tension

The IFT between crude oil and aqueous surfactant solution was measured under high temperature and pressure. A reduction in the IFT was observed with increasing surfactant concentration (see Figure 7.3). This mainly resulted from the adsorption of the surfactant molecules at the oil–water interface. Generally, such adsorption leads to the development of a rigid film at the interface under anaerobic conditions [13]. The interaction between the polar compounds present in the crude oil (i.e., asphaltenes) and chemical additives promoted the development of this film [1]. The ionic salts accumulated at the interface alleviated the rigid film structure [14].

The tendency to develop a rigid film at the oil–water interface is reduces with increasing temperature [1]. At higher temperature, desorption of the surfactant takes place, which reduces the film at the interface. Therefore, a little increase in the IFT was observed with increasing temperature. The reduction in IFT helped to increase the microscopic displacement efficiency, which eventually enhanced the oil recovery [15]. Increase in the temperature upsurged the diffusion and adsorption velocities of the surfactant molecules at the interface [16]. Therefore, a little increase in the IFT was observed at 333 K and 13.8 MPa. However, similar to wettability alteration, a minimal impact of pressure was observed on the IFT.

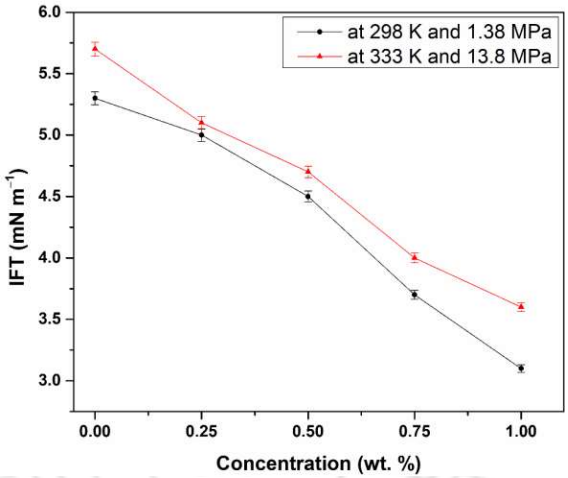

Figure 7.3. Influence of temperature and pressure on the IFT.

7.2.3 Phase behavior

Emulsion stability of the oil–surfactant system is a critical factor in evaluating the performance of the chemical additives [17]. Therefore, emulsion screening tests were carried out for the crude oil–WH system. Figure 7.4 demonstrates the emulsion stability over a wide range of surfactant concentration (i.e., 0.25–1 wt. %). It is clear from Figure 7.4 that the emulsions stabilized with WH developed dense creaming layers with increasing surfactant concentration. These systems were observed for 20 d, and the stability of emulsion improved as a result of more adsorption of the surfactant molecules on the oil droplet [18]. Besides, an oil layer was formed on top of the creaming layer. Furthermore, the adsorption of WH at the oil–water interface helped to stabilize the emulsion by generating a repulsive disjoining pressure in the thin aqueous film. Stable emulsions promote enhancement of both displacement and sweep efficiencies, resulting in a better recovery factor [19,20].

Similar to Figure 7.4, the emulsion was denser with increasing surfactant concentration, even in saline medium (see Figure 7.5). However, a minor modification at the curvature of the oil droplet was observed in the presence of brine. This is possibly due to the charge interaction between the oil, brine, and surfactant [21]. This could also be due to the coalescence of the oil

droplets in the presence of brine [22]. Generally, salt lowers the electrostatic repulsion between the oil droplets. This allows them to come closer to each other, and then coalesce.

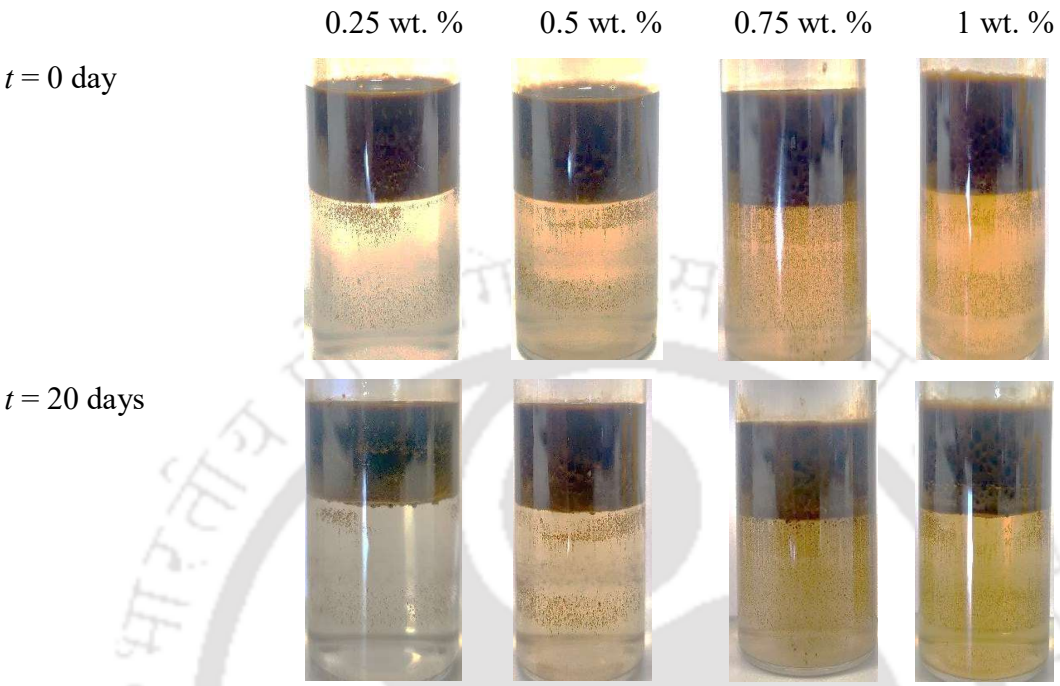

Figure 7.4. Stability of emulsions over a wide range of surfactant concentration.

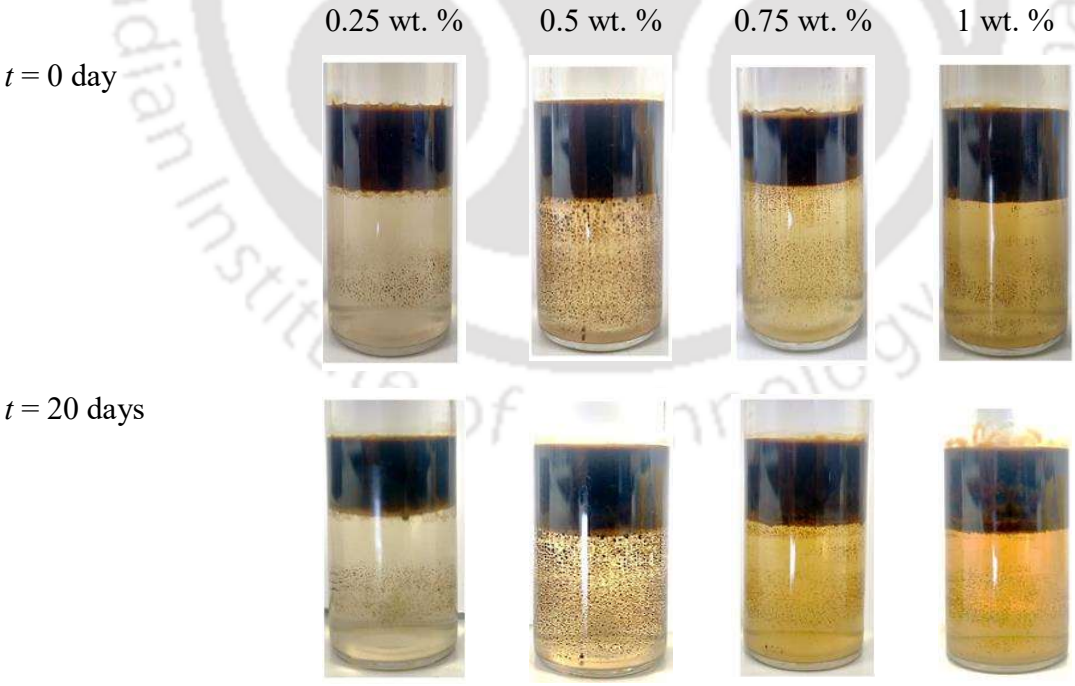

Figure 7.5. Effect of salt on the stability of the emulsions over a wide range of surfactant concentration.

The impact of surfactant concentration on the emulsion characteristics was further studied with the microscopic analysis of the emulsions (see Figure 7.6). It has been observed that the number of oil droplets increased with increasing surfactant concentration. At 0.25 wt. % WH, a small number of oil droplets was seen due to inadequate adsorption of the surfactant molecules on the surface of the oil droplets. Larger droplets were formed, which experienced fast coalescence, and the emulsion stability reduced. However, it is evident from Figure 7.6 that the number of droplets increased at the higher surfactant concentrations. This is governed by the adsorption of surfactant molecules on the drop surface. Enhancement in the number of oil droplets and emulsion stability make the removal of trapped oil possible, which leads to its superior recovery [7].

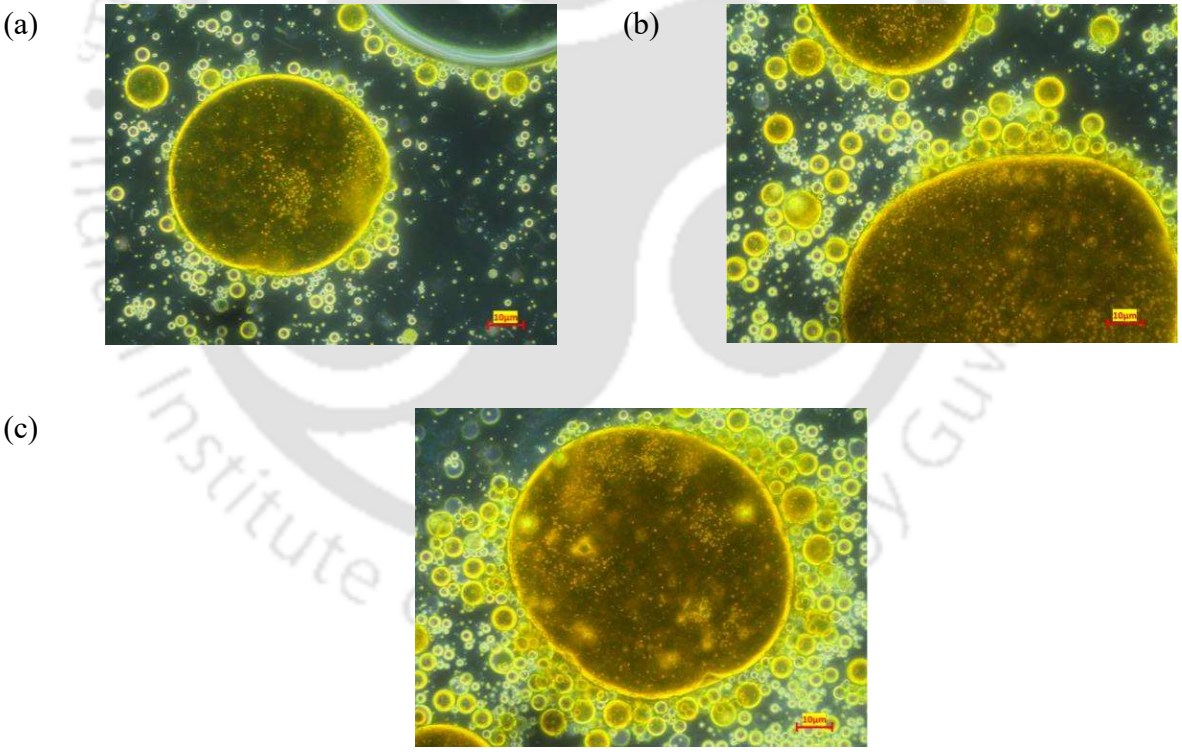

Figure 7.6. Influence of surfactant concentration on the emulsion: (a) 0.25 wt. % WH, (b) 0.5 wt. % WH, and (c) 1 wt. % WH.

7.2.4 Rheological measurement

The injection of a polymer solution to the reservoir enhances the apparent viscosity of the displacing fluid, which reduces its relative permeability in the reservoir. Figure 7.7 demonstrates the impact of surfactant concentration on the apparent viscosity of the aqueous XG solution over a wide range of shear rate. It has been observed that WH significantly increased the apparent viscosity of XG, as shown in Figure 7.7. Such improvement in the viscosity was possible because of the synergy of the WH with the hydrophobic groups of XG. This resulted in the development of an association structure between the polymer chains. Figure 7.7 also illustrates the shear-thinning behavior of the XG–WH solutions as the apparent viscosity of the solutions decreased with increasing shear rate. This is possibly due to the arrangement of the polymer chains in the course of flow, and decrease in the intermolecular interaction with the adjacent polymer chains [12,23].

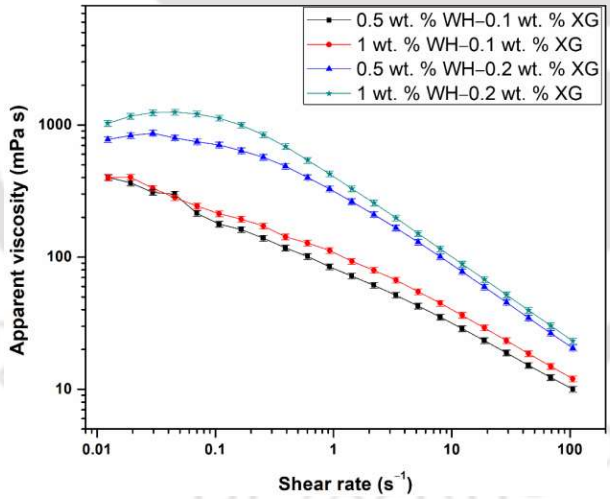

Figure 7.7. Variation of apparent viscosity of the polymeric solutions with shear rate (at 298 K).

The experimental data acquired from the analysis of flow behavior of the XG–WH solutions under shear rate were fitted by several non-Newtonian fluid models (e.g., power-law, Carreau-Yasuda, and Cross models). The details of these models are given in Table 7.1, and the

respective model fittings and parameters for the different XG–WH solutions are given in Figure 7.8 and Tables 7.2–7.4, respectively.

Table 7.1. Non-Newtonian fluid models

Model	Equation
Power-law	$\eta = K\dot{\gamma}^{n-1}$
Carreau–Yasuda	$\eta = \eta_\infty + (\eta_0 - \eta_\infty)\left[1+(\lambda\dot{\gamma})^a\right]^{\frac{n-1}{a}}$
Cross	$\frac{\eta-\eta_\infty}{\eta_0-\eta_\infty} = \frac{1}{1+(K\dot{\gamma})^n}$ Note: For shear-thinning behavior, $n<1$ For shear-thickening behavior, $n>1$

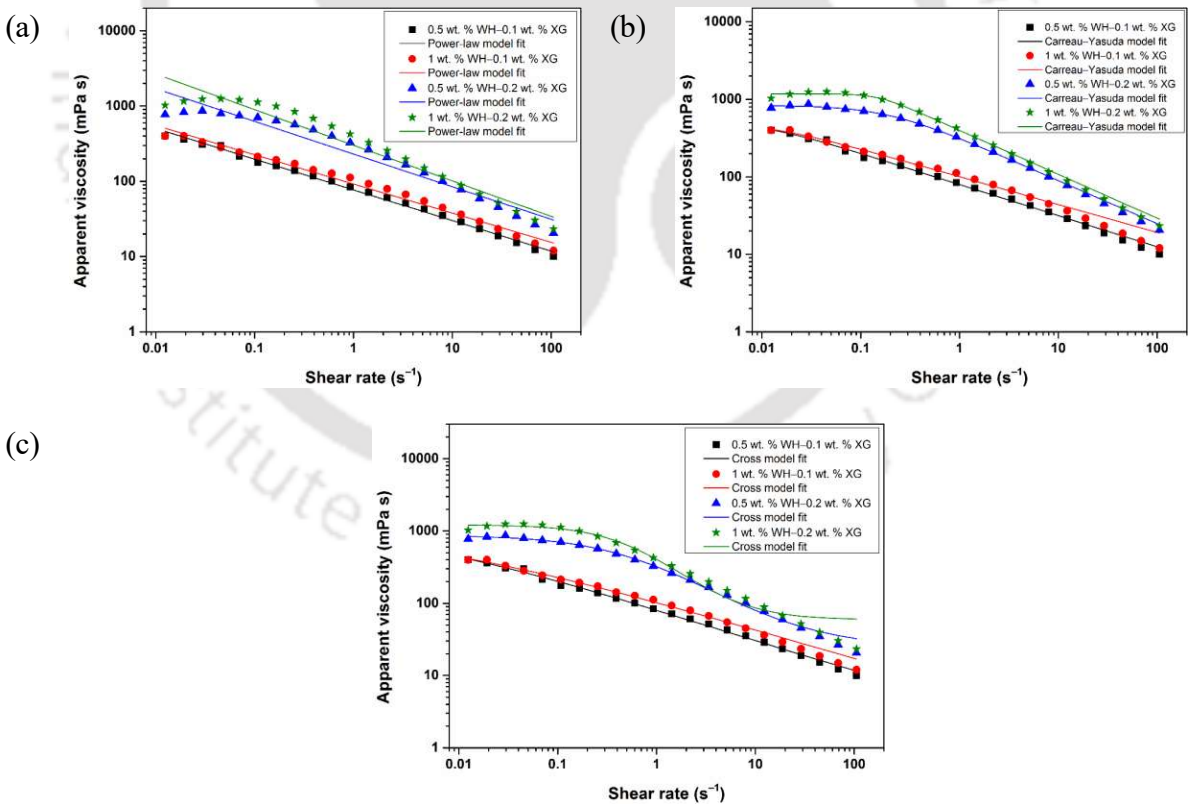

Figure 7.8. Fit of the (a) power law, (b) Carreau–Yasuda, and (c) Cross models for the surfactant–polymer systems.

Table 7.2. Power-law model parameters for the surfactant–polymer systems

Sample	n	K (mPa s)	R^2
0.5 wt. % WH–0.1 wt. % XG	0.59	77.09	0.99
1 wt. % WH–0.1 wt. % XG	0.61	92.25	0.98
0.5 wt. % WH–0.2 wt. % XG	0.56	230.67	0.96
1 wt. % WH–0.2 wt. % XG	0.53	302.00	0.95

Table 7.3. Carreau–Yasuda model parameters for the surfactant–polymer systems

Sample	η_0 (mPa s)	η_∞ (mPa s)	λ (s)	a	n	R^2
0.5 wt. % WH–0.1 wt. % XG	814.67	1×10^{-5}	92.52	1.65	0.75	0.99
1 wt. % WH–0.1 wt. % XG	645.97	1×10^{-6}	96.54	1.23	0.71	0.98
0.5 wt. % WH–0.2 wt. % XG	1144.75	0.001	5.46	1.36	0.60	0.99
1 wt. % WH–0.2 wt. % XG	4229.35	0.001	6.75	3.58	0.84	0.98

Table 7.4. Cross model parameters for the surfactant–polymer systems

Sample	η_0 (mPa s)	η_∞ (mPa s)	K (mPa s)	n	R^2
0.5 wt. % WH–0.1 wt. % XG	1223.99	1.38	367.91	0.45	0.99
1 wt. % WH–0.1 wt. % XG	1099.64	0.38	271.90	0.40	0.98
0.5 wt. % WH–0.2 wt. % XG	871.97	25.32	1.99	0.89	0.99
1 wt. % WH–0.2 wt. % XG	1216.76	59.31	1.95	0.80	0.98

The power-law model parameters for the XG–WH solutions imply a strong shear-thinning as well as gel-like behavior, as a result of the reduction in n and increment in K with increasing surfactant concentration. The value of n for all the models was less than unity. Both of these conditions confirm the shear-thinning behavior of the XG–WH solutions. Therefore, it can be concluded that the XG–WH solutions were able to reduce the water mobility and the relative permeability of water. It was also able to improve the sweep efficiency, and eventually promote additional oil recovery [24].

Figure 7.9 demonstrates the strain dependence of the storage and loss moduli for the aqueous polymeric solutions at 298 K, at a fixed frequency of 1 Hz. It can be seen that $G' > G''$ for the 0.2 wt. % XG and WH solutions throughout the strain range. Thus, under these circumstances, a solid-like behavior was observed in the material. Figure 7.9 indicates the strain-thinning characteristics of the XG–WH solutions inasmuch as G' decreased with the increase in strain amplitude. The strain-thinning characteristic is observed perhaps because of the rupture of their internal structure due to the application of the strain [25]. The 0.2 wt. % XG–WH solution was more elastic, and it was characterized by a slower relaxation mechanism [26]. However, the 0.1 wt. % XG solution, at different surfactant concentrations, demonstrated the viscoelastic liquid-like behavior as $G'' > G'$.

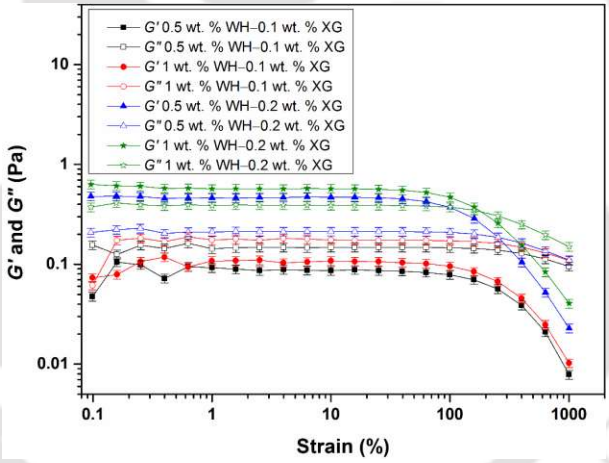

Figure 7.9. Storage modulus (G') and loss modulus (G'') for the polymeric solutions as a function of strain (i.e., 0.1–1000%) at a constant frequency (i.e., 1 Hz).

Based on the established linear viscoelastic region, the frequency sweep tests were conducted to determine the viscoelasticity of the XG–WH solutions. Figure 7.10 demonstrates that the viscoelastic nature of the 0.2 wt. % XG–1 wt. % WH solution was governed by an elastic nature inasmuch as $G' > G''$, which shows the gel-like assembly of the polymeric solutions [26]. However, the 0.1 wt. % XG–1 wt. % WH solution exhibited viscoelastic liquid-like behavior.

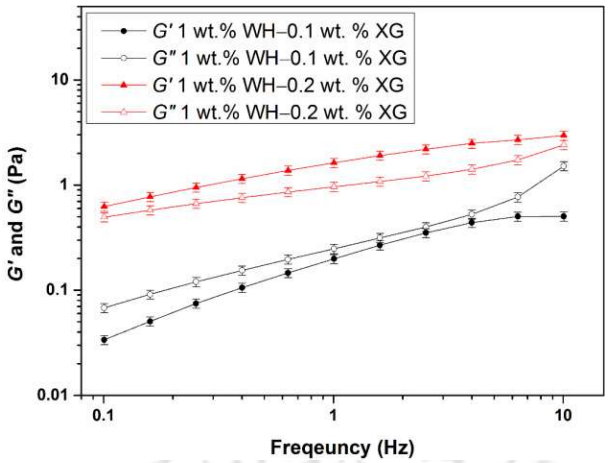

Figure 7.10. Variation of storage and loss moduli with frequency.

The slower relaxation mechanism can be verified by plotting the loss tangent $\left[\tan\delta = G''(\omega)/G'(\omega)\right]$ against frequency. The value of $\tan\delta$ should be less than unity for a solid-like behavior. If its value is greater than unity, a liquid-like nature is indicated [27]. It is clear from Figure 7.11 that $\tan\delta$ was less than unity for the 1 wt. % WH–0.2 wt. % XG solution, which signifies its solid-like viscoelastic behavior. The 1 wt. % WH–0.1 wt. % XG solution, on the other hand, demonstrated a liquid-like viscoelastic behavior (as $\tan\delta >> 1$).

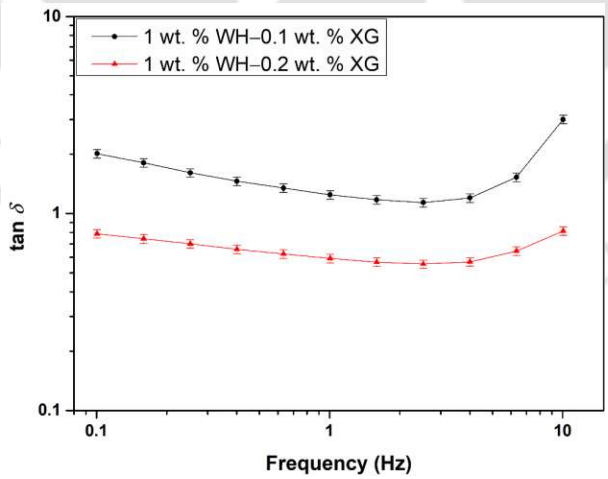

Figure 7.11. Loss tangent of the polymer–surfactant solution.

Figure 7.12a shows the influence of temperature (i.e., 298–338 K) on the apparent viscosity of XG–WH solutions at a constant 10 s^{-1} shear rate. A moderate reduction in the apparent viscosity was observed over this temperature range. Similar to Figure 7.7, the apparent

viscosity of the 1 wt. % WH–0.2 wt. % XG system was greater than the 1 wt. % WH–0.1 wt. % XG system. At 320 K, a remarkable drop in the apparent viscosity of the XG–WH solutions was observed (see Figure 7.12a). Around 45% reduction in the apparent viscosity was noticed at the end of the experiment.

A set of experiments was conducted at different temperatures (i.e., 298–338 K) at constant strain (i.e., 5%) and frequency (i.e., 1 Hz) (see Figure 7.12b). The 1 wt. % WH–0.1 wt. % XG solution was the least suitable choice for EOR as $G'' > G'$. It is also important to note that the viscoelastic properties of the 1 wt. % WH–0.1 wt. % XG solution became unstable with increasing temperature. However, injection of the 1 wt. % WH–0.2 wt. % XG solution in the reservoir could be a better option as the G' was mostly stable over the entire temperature range. This signifies a steady, well-organized, and strong structure of the 1 wt. % WH–0.2 wt. % XG system. Hence, it can be concluded that the 0.2 wt. % XG–1 wt. % WH solution was superior to the other polymer solutions.

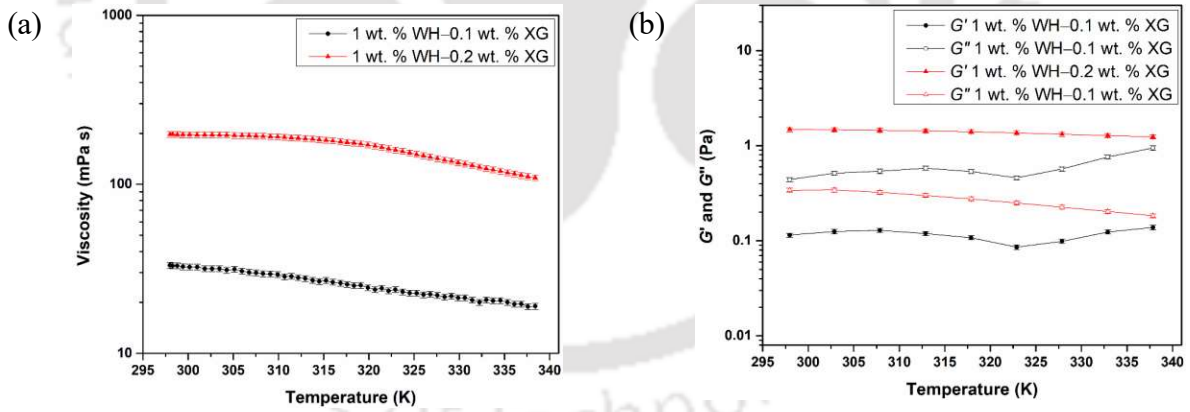

Figure 7.12. Effect of temperature on the (a) flow behavior, and (b) G' and G'' of the XG–WH solutions.

7.2.5 Core flooding measurement

Figure 7.13 shows the oil recovery using surfactant–polymer flooding. Initially, water flooding experiments were carried out, which recovered ~40% of oil. Then varying concentrations of XG (i.e., 0.05 – 0.2 wt. %) and 1 wt. % WH were injected into the core sample containing

residual oil. An additional 7 – 8% oil was recovered due to the injection of 1 wt. % WH alone. The additional oil recovery was achieved due to the wettability alteration and reduction in the IFT. These facilitate the movement of trapped oil droplets through the reservoir (discussed in Sections 1.2.1–1.2.2, 6.2.1, and 7.2.1–7.2.2) [6]. The formation of a stable oil-in-water emulsion also plays an important role in the additional oil recovery. The adsorption of the surfactant at the oil–water interface improves the strength of the interfacial film, which encapsulates the oil droplet, prevents drop coalescence, and improves the mobility ratio [19] (discussed in Sections 1.2.3, 6.2.3–6.2.4, and 7.2.3).

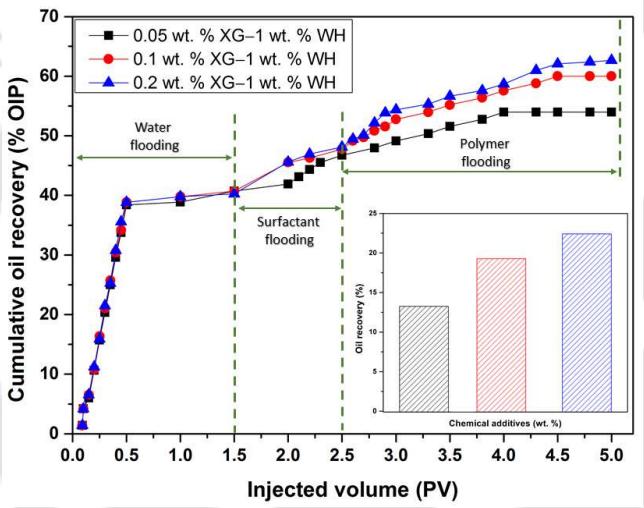

Figure 7.13. Variation of oil recovery with the injected volume at various concentrations of XG and at a fixed concentration of WH.

Polymer flooding also played a significant role in the recovery of residual oil in the core sample. Oil recovery was enhanced from 12.04% to 22.40% with increasing concentration of XG. Table 7.5 shows the oil recovery achieved using surfactant–polymer flooding. It is clear from Section 7.2.4 that the 0.1 wt. % XG–1 wt. % WH solution demonstrated liquid-like behavior as $G'' > G'$. However, it has been observed that oil recovery can be improved by the elasticity of the polymer [28]. Therefore, the dominating elastic properties of the 0.2 wt. % XG–1 wt. % WH system were able to deliver ~22.4% additional oil to the surface.

Improvement in the oil recovery depends on the elasticity of the polymer solution. Typically, the normal stress between the oil and the polymer solution becomes more governing than the shear stress due to the polymer's higher elasticity. The normal stress aids in pulling the oil from the trapped zone as well as pushing the fluid ahead [6]. This is called the "push-and-pull" mechanism [29]. The mechanism has been discussed in detail in Section 1.2.5 and the corresponding results are discussed in Section 7.2.4. The displacement efficiency can be advanced with the higher elasticity of the polymer [30].

Table 7.5. Oil recovery achieved using surfactant–polymer flooding

Test No.	Chemical composition	Water flooding (A) (% OOIP)	Surfactant flooding recovery (B) (% OOIP)	Polymer flooding recovery (C) (% OOIP)	Total tertiary recovery (D = B + C) (% OOIP)	Cumulative oil recovery (A+D) (% OOIP)
1.	0.05 wt. % XG–1 wt. % WH	41.92	7.23	4.81	12.04	53.96
2.	0.1 wt. % XG–1 wt. % WH	40.71	8.04	11.24	19.28	59.99
3.	0.2 wt. % XG–1 wt. % WH	40.24	7.86	14.56	22.42	62.66

7.3 Conclusion

Potential application of the synthesized surfactant for EOR has been investigated in reservoir-like conditions. The surfactant effectively altered the contact angle from 65.74 to 37.5° (at 298 K and 1.38 MPa), and 60.4 to 34.5° (at 333 K and 13.8 MPa). A substantial decrease in the oil–water IFT was observed in the reservoir-like conditions. An increase in temperature enhanced the wettability alteration and IFT reduction abilities of the surfactant. The adsorption of surfactant at the oil–water interface was confirmed from the phase behavior analysis. The stability of emulsion improved as the concentration of surfactant increased. A similar emulsion but with a slightly larger oil droplets was observed in the saline medium. The surfactant

improved the rheological behavior of XG. Reduction in the apparent viscosity of the XG–WH solutions depicted a shear-thinning behavior. The viscoelastic behavior of the XG–WH solutions was confirmed from the oscillation shear flow tests. A significant enhancement in the oil recovery (i.e., ~22.4%) was achieved by injecting the XG–WH solution.

Nomenclature

a	constant in the Carreau–Yasuda model equation
G'	storage modulus, Pa
G''	loss modulus, Pa
n	flow behavior index
K	consistency index, mPa s

Greek letters

$\dot{\gamma}$	shear rate, s^{-1}
η	viscosity, mPa s
η_0	zero-shear viscosity, mPa s
η_∞	infinite-shear viscosity, mPa s
λ	time constant in the Carreau–Yasuda model equation, s

Abbreviation

EOR	enhanced oil recovery
IFT	interfacial tension
WH	surfactant synthesized from *Eichhornia crassipes* (commonly known as Water Hyacinth)
XG	xanthan gum

References

[1] Hjelmeland O, Larrondo L. Experimental investigation of the effects of temperature, pressure, and crude oil composition on interfacial properties. SPE Reservoir Eng 1986;1:321–8.

[2] Pal N, Kumar N, Verma A, Ojha K, Mandal A. Performance evaluation of novel sunflower oil-based gemini surfactant(s) with different spacer lengths: application in enhanced oil recovery. Energy Fuels 2018;32:11344–61.

[3] Pal N, Saxena N, Laxmi KD, Mandal A. Interfacial behaviour, wettability alteration, and emulsification characteristics of a novel surfactant: Implications for enhanced oil recovery. Chem Eng Sci 2018;187:200–12.

[4] Lake LW, Venuto PB. A niche for enhanced oil recovery in the 1990s. Oilfield Rev J 1992;4:55–61.

[5] Olajire AA. Review of ASP EOR (alkaline surfactant polymer enhanced oil recovery) technology in the petroleum industry: Prospects and challenges. Energy 2014;77:963–82.

[6] Sheng J. Modern chemical enhanced oil recovery: Theory and practice. Gulf Professional Publishing: Massachusetts, USA, 2010.

[7] Saha R, Uppaluri RV, Tiwari P. Silica nanoparticle assisted polymer flooding of heavy crude oil: Emulsification, rheology, and wettability alteration characteristics. Ind Eng Chem Res 2018;57:6364–76.

[8] Lu Y, Najafabadi NF, Firoozabadi A. Effect of temperature on wettability of oil/brine/rock systems. Energy Fuels 2017;31:4989–95.

[9] Myint PC, Firoozabadi A. Thin liquid films in improved oil recovery from low-salinity brine. Curr Opin Colloid Interface Sci 2015;20:105–14.

[10] Ahmadi MA, Galedarzadeh M, Shadizadeh SR. Wettability alteration in carbonate rocks by implementing new derived natural surfactant: Enhanced oil recovery applications. Transp Porous Med 2015;106:645–67.

[11] Zhang Y, Zeng J, Qiao J, Feng X, Dong Y. Investigating the effect of the temperature and pressure on wettability in crude oil–brine–rock systems. Energy Fuels 2018;32:9010–9.

[12] Nedjhioui M, Moulai-Mostefa N, Canselier JP, Bensmaili A. Investigation of combined effects of xanthan gum, sodium dodecyl sulphate, and salt on some physicochemical properties of their mixtures using a response surface method. J Dispersion Sci Technol 2009;30:1333–41.

[13] Reisberg J, Doscher TM. Interfacial phenomena in crude oil-water systems. Prod Mon 1956;21:43–50.

[14] Flock D, Le T, Gibeau J. The effect of temperature on the interfacial tension of heavy crude oils using the pendent drop apparatus. J Can Pet Technol 1986;25:72–7.

[15] Machale J, Majumder SK, Ghosh P, Sen TK. Role of chemical additives and their rheological properties in enhanced oil recovery. Rev Chem Eng 2020;36:789–830.

[16] Mosayebi A, Angaji MT, Khadiv-Parsi P. The effect of temperature on the interfacial tension between crude oil and ethoxylated nonylphenols. Pet Sci Technol 2016;34:1315–22.

[17] Bera A, Ojha K, Mandal A, Kumar T. Interfacial tension and phase behavior of surfactant–brine–oil system. Colloids Surf, A 2011;383:114–9.

[18] Ghosh AK, Bandyopadhyay P. Polysaccharide-protein interactions and their relevance in food colloids. The complex world of polysaccharides. Rijeka, Croatia: InTech; 2012, 395–408.

[19] Mohyaldinn ME, Hassan AM, Ayoub MA. Application of emulsions and microemulsions in enhanced oil recovery and well stimulation. Microemulsion-A chemical nanoreactor. London, UK: IntechOpen; 2019.

[20] Wang X, Zhang J, Yuan G, Wang W, Liang Y, Wang H, Li Y. Effect of emulsification on enhanced oil recovery during surfactant/polymer flooding in the homogeneous and heterogeneous porous media. Geofluids 2021:6674185.

[21] Ahmed S, Elraies KA. Microemulsion in enhanced oil recovery. Science and Technology Behind Nanoemulsions. London, UK: IntechOpen; 2018, 145–65.

[22] Kumar MK, Mitra T, Ghosh P. Adsorption of ionic surfactants at liquid−liquid interfaces in the presence of salt: Application in binary coalescence of drops. Ind Eng Chem Res 2006;45:7135–43.

[23] Nedjhioui M, Moulai-Mostefa N, Morsli A, Bensmaili A. Combined effects of polymer/surfactant/oil/alkali on physical chemical properties. Desalination 2005;185:543–50.

[24] Sorbie KS. Polymer-improved oil recovery. CRC Press: Boca Raton, Florida 1991.

[25] Song K, Chang G, Kim C, Lee J, Paik J. Rheological characterization of aqueous poly (ethylene oxide) solutions (I): Limits of linear viscoelastic response and nonlinear behavior with large amplitude oscillatory shear deformation. J Kor Fiber Soc 1996;33:1083–93.

[26] Song KW, Kuk HY, Chang GS. Rheology of concentrated xanthan gum solutions: Oscillatory shear flow behavior. Korea-Australia Rheol J 2006;18:67–81.

[27] Ross-Murphy S, Shatwell K. Polysaccharide strong and weak gels. Biorheology 1993;30:217–27.

[28] Hou J, Liu Z, Zhang S, Yang J. The role of viscoelasticity of alkali/surfactant/polymer solutions in enhanced oil recovery. J Pet Sci Eng 2005;47:219–35.

[29] Mohammadi S, Maghzi A, Ghazanfari M, Masihi M, Mohebbi A, Kharrat R. On the control of glass micro-model characteristics developed by laser technology. Energy Sources, A 2013;35:193–201.

[30] Luo J, Liu Y, Zhu P. Polymer solution properties and displacement mechanisms. Enhanced oil recovery–polymer flooding. Beijing, China: Petroleum Industry Press; 2006, 1–72.

Chapter 8

Summary and future perspectives

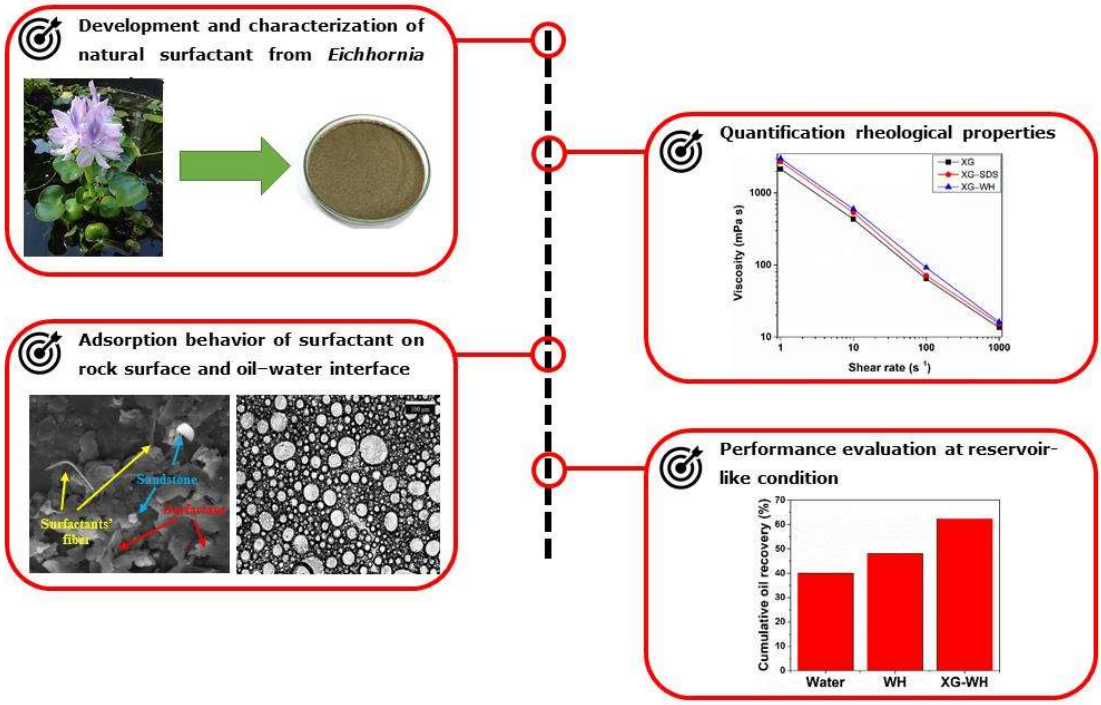

Summary and future perspectives

This chapter provides a summary of the work and provides new ideas for future research.

8.1 Summary

The present study explores the possible application of a novel anionic surfactant derived from the weed, *Eichhornia Crassipes*. The synthesis and characterization of this natural surfactant have been discussed thoroughly. The presence of fatty acids (mainly palmitic, oleic, and petroselenic), aromatic compounds, and esters have been confirmed by the GC–MS and ^{1}H NMR analyses. The composition justifies its surface-active properties. The critical micelle concentration of the synthesized natural surfactant was found to be 0.25 wt. %. The surfactant improved the rheological behavior of xanthan gum. Reduction in the apparent viscosity of the xanthan gum–surfactant solutions depicted a shear-thinning behavior. The values of the flow behavior index were found to be less than unity for the power-law and Carreau–Yasuda non-Newtonian fluid models, which corroborated the shear-thinning behavior. The viscoelastic behavior of the xanthan gum–surfactant solutions was confirmed from the oscillation shear flow tests.

The mechanism and kinetics of adsorption of the synthesized surfactant on two different adsorbents (i.e., sandstone and sand) have been studied. Based on the experimental data and model-fitting, the Langmuir adsorption isotherm and pseudo-second-order model explained the adsorption mechanism and kinetics, respectively. An increment in the surfactant adsorption on the rock surfaces was observed in the saline medium. Moreover, the adsorption of the surfactant on the rock surfaces decreased as the temperature increased, indicating that the adsorption was an exothermic process. The phase behavior and small-angle X-ray scattering analyses were performed to study the emulsion stability. Further, zeta potential and interfacial analyses were carried out to investigate the adsorption of the surfactant at the oil–water interface. The

adsorption of surfactant molecules at the oil–water interface led to an improvement in the emulsion stability and interfacial rheological properties.

The surfactant effectively altered the wettability of the rock. Moreover, a substantial reduction in the oil–water interfacial tension was observed in the reservoir-like conditions (i.e., high temperature and pressure). An increase in temperature enhanced the wettability alteration and interfacial tension reduction abilities of the surfactant. Based on the core flooding experiments, the inclusion of the surfactant resulted in an additional 7–8% oil recovery. Furthermore, 22.4% additional oil recovery was achieved by injecting the xanthan gum–surfactant solution. The synthesized natural surfactant was found to be a more cost-efficient alternative than the traditional synthetic surfactants. Depending on the aforesaid results and their interpretations, the performance of the synthesized surfactant is promising for the enhanced oil recovery applications.

8.2 Future work

Based on the scope of work covered in this Ph.D. thesis, the following research areas have been identified for consideration in the near future:

8.2.1 Examination of the performance of the synthesized natural surfactant in heterogeneous sandstone reservoir: Heterogeneity is one of the crucial aspects of the reservoir that influences crude oil recovery. Heterogeneity in a reservoir can refer to differences in porosity, permeability, and numerous geological properties. During the chemical enhanced oil recovery process, reservoir heterogeneity influences the flood and sweep patterns of the chemical additives, which results in retention of chemical additives, higher loss of surfactant, and reduction in sweep efficiency. Therefore, a systematic study assessing synthesized natural surfactant in heterogeneous sandstone reservoirs will give more insights into its applicability in enhanced oil recovery.

8.2.2 Implementation of conventionally-used synthetic polymers (such as polyacrylamide and partially-hydrolyzed polyacrylamide) in association with the synthesized natural surfactant for enhanced oil recovery: The present study observed a marginal impact of salinity on the natural surfactant–xanthan gum system. Synthetic polymers such as polyacrylamide and partially hydrolyzed polyacrylamide are extensively practiced for enhanced oil recovery. Polyacrylamide and partially hydrolyzed polyacrylamide have a greater resistance to the enzymes and are tolerant to strong mechanical and bacterial attacks. However, high salinity can noticeably reduce the performance of polyacrylamide and partially hydrolyzed polyacrylamide. Therefore, it will be interesting to study the performance of polyacrylamide and partially hydrolyzed polyacrylamide in association with the natural surfactant for enhanced oil recovery.

8.2.3 Analysis of the flooding experiments and flow visualization of the synthesized surfactant–polymer by using a 2D microfluidic micromodel: The core flooding experimental setups mimic the reservoir, and they are widely utilized to study the performance of the chemical additives in reservoir-like conditions for enhanced oil recovery. Visualization of the flow of chemical additives through the porous media can give a better insight into the displacement of trapped oil through it. This is possible by attaching the core flooding experimental setup to the x-ray micro-computed tomography setup. However, such setups are expensive and difficult to handle. To overcome such limitations, numerous researchers are utilizing the 2D microfluidic micromodels, which are cost-efficient, and easy to construct and handle as per the requirement. Therefore, it will be interesting to study flow visualization using a 2D microfluidic micromodel and further correlating the interfacial, rheological, and physicochemical properties of the surfactant–polymer solutions to oil recovery.

8.2.4 Examination of the nonlinear rheological properties of the natural surfactant–polymer system using large amplitude oscillatory shear: At high deformation, polymeric solutions exhibit nonlinear rheological behavior, which can be explored using large amplitude oscillatory shear (LAOS). In the present study, the author has studied the nonlinear rheological properties of the natural surfactant–polymer system using small amplitude oscillatory shear tests (which includes frequency and temperature sweeps). However, the utilization of LAOS can provide more insight into the nonlinear rheological properties of the natural surfactant–polymer system, which can be correlated with the fragmentation, fingering, and flow characteristics of such system in the reservoir.

Appendix A1

Compounds recognized in the crude oil by GC–MS

Appendix A1

Compounds recognized in the crude oil by GC–MS

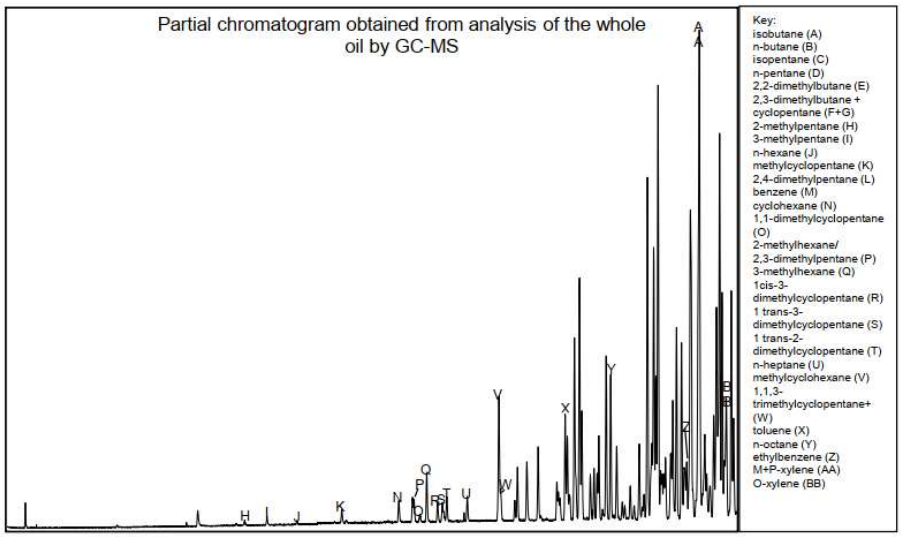

Figure A1. GC–MS spectrum of crude oil.

Table A2. Compounds recognized in the crude oil

Compound	Content (wt. %)	Compound	Content (wt. %)
Isobutane (A)	–	2-methylhexane/2,3-dimethylpentane (P)	1.5
n-butane (B)	–	3-methylhexane (Q)	4.9
Isopentane (C)	–	1 cis-3-dimethylcyclopentane (R)	1.6
n-pentane (D)	–	1 trans-3-dimethylcyclopentane (S)	1.6
2,2-dimethylbutane (E)	–	1 trans-2-dimethylcyclopentane (T)	2.4
2,3-dimethylbutane (F+G)	–	n-heptane (U)	2.5
2-methylpentane (H)	0.8	Methylcyclohexane (V)	13.7
3-methylpentane (I)	1.1	1 cis-2-dimethylcyclopentane (W)	1.7
n-hexane (J)	0.5	Toluene (X)	2.5
Methylcyclopentane (K)	2.1	n-octane (Y)	10.2
2,4-dimethylpentane (L)	–	Ethylbenzene (Z)	7.8
Benzene (M)	–	m- + p-xylene (AA)	35.7
Cyclohexane (N)	2.4	o-xylene (BB)	6.2
1,1-dimethylcyclopentane (O)	0.8		

Appendix A2

Cost estimation for surfactant production

Appendix A2: Cost Estimation for Surfactant Production

(The cost of different materials based on the present rate of the Year 2020)

Basis of calculation: 1 batch

1. Raw material

The *Eichhornia crassipes* plants were the main raw materials used in this work. They were collected from the lakes in the IIT Guwahati campus, free of cost.

2. Solvent

Ethanol: cost of 1 dm^3: ₹600

Requirement per batch: 0.25 dm^3; cost: ₹150

3. Electricity

Electricity cost = Equipment power rating × Hours of equipment use × Electricity tariff

3.1. Grinder

Electricity cost = $0.75 \times 0.17 \times 7.35$ = ₹0.94

3.2. Rotavapor

Electricity cost = $0.15 \times 6 \times 7.35$ = ₹6.62

3.3. Hot air oven

Electricity cost = $1.25 \times 12 \times 7.35$ = ₹110.25

4. Overall cost

Overall cost for a single batch = 150 + 0.94 + 6.62 + 110.25 = ₹267.81

5 g of the natural surfactant can be produced from a single batch.

Therefore, synthesis cost of 1 g of the natural surfactant under the laboratory conditions will be ₹53.56.

Research Outcomes

Publications

[1] **Machale J**, Majumder SK, Ghosh P, Sen TK. Development of a novel biosurfactant for enhanced oil recovery and its influence on the rheological properties of polymer. Fuel 2019;257:116067.

[2] **Machale J**, Majumder SK, Ghosh P, Sen TK. Role of chemical additives and their rheological properties in enhanced oil recovery. Rev Chem Eng 2020;36:789–830.

[3] **Machale J**, Al-Bayati D, Almobarak M, Ghasemi M, Saeedi A, Sen TK, Majumder SK, Ghosh P. Interfacial, emulsifying, and rheological properties of an additive of a natural surfactant and polymer and its performance assessment for application in enhanced oil recovery. Energy Fuels 2021;35:4823–34.

[4] **Machale J**, Majumder SK, Ghosh P, Sen TK, Saeedi A. Impact of mineralogy, salinity, and temperature on the adsorption characteristics of a novel natural surfactant for enhanced oil recovery. Chem Eng Commun 2022;209:143–57.

[5] **Machale J**, Majumder SK, Ghosh P, Sen TK, Saeedi A. Adsorption of a natural surfactant at oil–water interface: Interfacial structural analysis and rheology. Colloids Surf, A (*under review*)

Conferences

[1] **Machale J**, Majumder SK, Ghosh P, Sen TK. A study of the rheological properties of a biosurfactant–polysaccharide system for its application in enhanced oil recovery. International Conference on Advanced Materials, Energy, and Environmental Sustainability (ICAMEES–2018), 14–15 December 2018, University of Petroleum and Energy Studies, Dehradun, India.

[2] **Machale J**, Majumder SK, Ghosh P, Sen TK, Saeedi A. A study of the rheological properties of a biosurfactant–polysaccharide system for its application in enhanced oil recovery. Chemical Engineering megatrends and the elements (CHEMECA–2019), 29 September–02 October 2019, organized by IChemE and Engineers Australia, Sydney, Australia.

[3] **Machale J**, Majumder SK, Ghosh P, Sen TK, Saeedi A. Investigation of a novel natural surfactant–polysaccharide system for enhanced oil recovery application. Web International Conference on Accelerating Innovations in Material Science (AIMS–2020), 04–07 August 2020, organized by BMS Institute of Technology and Management, Bengaluru, India.

[4] **Machale J**, Majumder SK, Ghosh P, Sen TK, Saeedi A. Investigation of a novel natural surfactant–polysaccharide system for enhanced oil recovery application. Annual European Rheology Conference (AERC–2021), 13–15 April 2021, organized by pan-European committee.

[5] **Machale J**, Majumder SK, Ghosh P, Sen TK, Saeedi A. Performance assessment of a novel natural surfactant–polymer additive for enhanced oil recovery application: Interfacial, emulsion, and rheological approaches. Calcutta University Chemical Engineering Alumni Association 2021 Symposim, 17 – 19 December 2021, organized by Calcutta University.

Awards

[1] **Best Paper Award**, International Conference on Advance Materials, Energy, and Environmental Sustainability (ICAMEES–2018), organized by University of Petroleum and Energy Studies Dehradun, India.

[2] **Runner-up** of Joint Chemical Engineering Committee (Western Australia) Postgraduate **Research Excellence Awards** 2019, organized by Institution of Chemical Engineers (IChemE) and Engineers Australia, Perth, Australia.